Mag. Claudia Ramprecht

Toxicity of Oxidized Phospholipids in Cultured Skin Cancer Cell Lines

---

Dissertation

zur Erlangung des akademischen Grades einer
Doktorin der Naturwissenschaften
erreicht an der

Technischen Universität Graz

Betreuer: Ao.Univ.-Prof. Dr.phil. Albin Hermetter

Institut für Biochemie
Technische Universität Graz

2013

Statutory Declaration

I declare that I have authored this thesis independently, that I have not used other than the declared sources / resources, and that I have explicitly marked all material which has been quoted either literally or by content from the used sources.

....

date (signature)

Eidesstattliche Erklärung

Ich erkläre an Eides statt, dass ich die vorliegende Arbeit selbstständig verfasst, andere als die angegebenen Quellen/Hilfsmittel nicht benutzt, und die den benutzten Quellen wörtlich und inhaltlich entnommene Stellen als solche kenntlich gemacht habe.

....

Datum (Unterschrift)

Danksagung

Die vorliegende Arbeit wurde in der Zeit von April 2008 bis Dezember 2012 am Institut für Biochemie an der Technischen Universität Graz durchgeführt.

Betreuer der Arbeit war Prof. Dr. Albin Hermetter, dem ich an dieser Stelle meinen Dank dafür aussprechen möchte, dass er mir die Möglichkeit gegeben hat, meine Dissertation über dieses äußerst spannende und innovative Thema verfassen zu können. Neben seinem herausragenden fachlichen Wissen und den vielen Hilfestellungen in experimenteller Hinsicht im Labor haben vor allem auch zahlreiche private Diskussionen zu einem sehr angenehmen Arbeitsklima beigetragen.

Ich möchte mich auch bei der gesamten Arbeitsgruppe Hermetter bedanken, für den Rückhalt meiner vielen lieben Kollegen und für die zahlreichen Gespräche und Hilfestellungen sowohl im fachlichen Bereich als auch privater Natur. Ohne ihr Wissen, ohne ihre Ideen und ihre Kritik wäre mein Forschungsprojekt niemals so weit gekommen.

Hervorheben möchte ich in diesem Zusammenhang besonders die Arbeit von Hannah Jaritz, Luise Britz und Sandra Jantscher, den drei Masterstudentinnen, die ich während meiner Zeit am Institut betreuen durfte. Ihre großartige Arbeit im Labor, ihre Motivation und vor allem auch ihr Ehrgeiz haben dazu beigetragen, die Forschung an meinem eigenen Thema voranzutreiben.

Herzlich bedanken möchte ich mich bei meiner Familie, insbesondere bei meinen Eltern, für ihren großartigen Rückhalt in den vergangenen Jahren. Sie waren mir immer eine Stütze während meines Studiums und haben mich stets auch in schwierigen Situationen motiviert, mein Bestes zu geben.

Abstract

The oxidized phospholipids (oxPL) 1-palmitoyl-2-(5-oxovaleroyl)-*sn*-glycero-3-phosphocholine (POVPC) and 1-palmitoyl-2-glutaroyl-*sn*-glycero-3-phosphocholine (PGPC) are formed upon oxidation of 1-palmitoyl-2-arachidonoyl-*sn*-glycero-3-phosphocholine (PAPC) in lipoproteins and cell membranes. Both oxPL share high structural similarities: they contain a long hydrophobic chain at the *sn*-1 position, and a shortened polar chain at position *sn*-2, which is part of a very large headgroup. Therefore, PGPC and POVPC are highly amphipathic molecules and as a consequence exchange easily between cells, membranes and lipoproteins, where they perturb lipid organization and protein function.

We found for the first time that PGPC and POVPC selectively induce cell death in squamous cell carcinoma cell lines as well as in cultured human and murine melanoma cells isolated from different stages of tumor progression. Their toxicity was limited to tumorigenic cells, as primary human melanocytes and keratinocytes were much less affected. The toxicity of both compounds was associated with efficient lipid uptake into the tumor cells, activation of acid sphingomyelinase and cell line-dependent formation of the apoptotic second messenger ceramide.

In summary, these compounds show useful properties for the treatment of melanomas and non-melanoma skin tumors: their toxicity is preferentially expressed in malignant cells, they are naturally formed in the body and resistance to these compounds is not likely to occur.

Zusammenfassung

Die oxidierten Phospholipide (oxPL) 1-Palmitoyl-2-glutaroyl-*sn*-glycero-3-phosphocholin (PGPC) und 1-Palmitoyl-2-(5-oxovaleroyl)-*sn*-glycero-3-phosphocholin (POVPC) werden durch Oxidation von 1-Palmitoyl-2-arachidonoyl-*sn*-glycero-3-phosphocholin in Lipoproteinen und in Zellmembranen gebildet. Beide oxidierten Phospholipide weisen hohe strukturelle Ähnlichkeiten auf: sie besitzen eine lange hydrophobe Fettsäure an der *sn*-1 Position, und eine kurze polare Seitenkette an Position *sn*-2, die Teil einer sehr gro§en Kopfgruppe ist. Aufgrund dieser strukturellen Eigenschaften sind PGPC und POVPC hoch amphipathische Moleküle und als Konsequenz leicht zwischen Zellen, Membranen und Lipoproteinen austauschbar. Durch diese Eigenschaften können sie sowohl die Lipidorganisation von Membranen als auch Proteinfunktionen in Zellen verändern.

Wir konnten zum ersten Mal nachweisen, dass PGPC und POVPC selektiv Zelltod in Plattenepithelkarzinomzelllinien sowie in humanen und murinen Melanomzelllinien unterschiedlicher Tumorstadien auslösen. Die Toxizität dieser Substanzen ist auf Tumorzellen beschränkt und die Viabilität von primären humanen Melanozyten sowie Keratinozyten ist weit weniger beeinflusst. Die Toxizität beider Lipide ist mit effizienter Aufnahme in Tumorzellen verbunden, Aktivierung der sauren Sphingomyelinase und zelllinienabhängiger Bildung des apoptotischen sekundären Botenstoffes Ceramid.

Zusammenfassend konnten wir zeigen, dass oxidierte Lipide sehr nützliche Eigenschaften für die Therapie von Melanomen und anderen Hauttumoren besitzen: ihre Toxizität ist beschränkt auf Tumorzellen, sie werden im Körper natürlich gebildet und Resistenzen gegen diese Substanzen sind unwahrscheinlich.

Scope and aims of this study

It was the objective of this doctoral thesis to examine whether and to what extent apoptotic cell death can be induced by truncated oxidized phospholipids in cultured human melanoma cell lines (Chapter 2), murine B16-BL6 cells (Chapter 3) and squamous carcinoma cell lines (Chapter 4). For this purpose, we used the chemically defined oxidized diacyl-phospholipids PGPC and POVPC, the corresponding alkyl-acyl phospholipids E-PGPC and E-POVPC as well as the synthetic lysophospholipid analogue Edelfosine, which is known to possess anti-cancer activities. We determined the toxic effects of these compounds in several human melanoma cell lines of different malignancies (SBcl2, WM35, WM9, WM164), in the murine melanoma cell line B16-BL6, and in various squamous carcinoma cell lines (SCC12, SCC13). Toxic effects of oxPL in cancer cell lines were studied and compared to melanocytes (Fom) as well as keratinocytes (HaCaT). Here we provide evidence, that oxidized phospholipids preferentially induce apoptosis in skin cancer cells, but not in healthy cells of the skin. However, the toxicity of these compounds differed depending on cell line, lipid structure and lipid concentration.

In the first part of this doctoral thesis we investigated whether cell death, preferentially apoptosis, was elicited by oxPL in human melanoma cell lines. We found that the oxidized phospholipids efficiently killed human melanoma cells of different stages but left primary human melanocytes almost unaffected. The favored mode of cell death was always apoptosis, but not necrosis, with POVPC being more toxic than PGPC. The toxicity of PGPC and POVPC was associated with efficient uptake of these

lipids into cancer cells but not melanocytes, activation of acid sphingomyelinase and the formation of the pro-apoptotic second messenger ceramide.

The second part of the thesis was devoted to the uptake and the toxicity of oxPL, ether-oxPL and Edelfosine in murine B16-BL6 melanoma cells. The BODIPY-labeled ethanolamine phospholipids BY-PGPE and BY-POVPE were used for visualization of oxPL in live cells. Here we could show that B16-BL6 cells rapidly internalized both oxPL. Both lipids localized to the ER as proven by co-staining experiments. In addition, we could demonstrate that oxidized phospholipids, especially PGPC and POVPC, triggered different cellular responses in B16-BL6 cells depending on their concentration. Intermediate concentrations (25 µM) elicited apoptotic cell death, whereas higher amounts of oxPL (50 µM) led to necrosis. Migration of melanoma cells was inhibited by low concentrations of POVPC (5 µM). This result can be regarded as a favorable requirement for an anti-tumor agent, especially with respect to the spread of tumor cells to distant tissues and the subsequent formation of metastatic tumors.

The third part of the thesis was dedicated to the question, whether the toxic effects of oxPL previously shown in melanoma cells were also detectable in other tumor cells of the skin. For this purpose, we screened several squamous carcinoma cell lines for morphological changes induced by PGPC and POVPC. We were able to prove uptake differences in healthy and tumorigenic cells. Both oxPL were retained in the plasma membrane of HaCaT keratinocytes, whereas in SCC13 cells they were rapidly internalized and transported to the ER. Oxidized phospholipids induced apoptotic cell death in SCC13 cancer cells but not in HaCaT cells, which was accompanied by activation of aSMase and ceramide formation. In addition to toxicity studies, primary protein targets of the aldehydo phospholipid BY-POVPE in SCC13 cells were analyzed. Covalent formation of Schiff base adducts between BY-POVPE and NH_2 groups of proteins was shown to be rather a selective than a random process. The protein targets in total

cell lysates were isolated and identified by MS/MS analysis. The identified targets are involved in RNA processing and splicing (e.g. splicing factors, heterogeneous nuclear ribonucleoproteins, ribosomal proteins), membrane transport (e.g. VDAC), cellular stress response (e.g. heat shock proteins), apoptosis (e.g. Diablo homolog), cell migration, cell structure and mobility (e.g. myosin, integrin) as well as other processes.

In summary, we have shown for the first time that oxidized phospholipids possess high potential for cancer treatment, for the following reasons: First of all, their toxicity is preferentially expressed in malignant tumor cells. Secondly, they trigger more general membrane effects based on the compositional and structural differences between healthy cells and cancer cells, rather than activating/inactivating specific mutated signaling pathways. Finally, the oxPL are naturally formed in the body and resistances to these compounds are not very likely to occur.

Table of Contents

List of Figures

Figures Chapter I

Figures Chapter II

Figures Chapter III

Figures Chapter IV

List of Tables

Tables Chapter III

Tables Chapter IV

Chapter 1

General Introduction

1.1 Oxidized phospholipids

Glycerophospholipids comprise a heterogeneous group of lipids, consisting of a glycerol backbone, a polar phosphate-containing headgroup and two fatty acid residues. The residue at the *sn*-1 position of the glycerol backbone is either a saturated acyl or an alkyl residue bound via an ester or an ether bond, respectively. The latter bonding element is characteristic to saturated ether phospholipids or their unsaturated enolether counterparts (plasmalogens). Polyunsaturated fatty acids (PUFAs) at the *sn*-2 position are a major target for enzymatic or non-enzymatic oxidation processes. Lipid oxidizing enzymes include lipoxygenase (Hammarstrom, 1983), cyclooxygenase (Änggård and Samuelsson, 1965), myeloperoxidase, NADPH oxidase and cytochrome P450 (Samuelsson *et al.*, 1987). Additionally, in the absence of enzymes, lipid oxidation can occur as a consequence of free radical attack, and propagates via the classical mechanisms of lipid peroxidation chain reaction. The oxidative modification of phospholipids leads to the formation of several oxidation products with multiple biological activities, depending on the degree of unsaturation and the chain length of the fatty acid at the *sn*-2 position. These reaction products differ in the degree of modification, hydrophobicity, chemical reactivity, physical properties and biological activities (Fruhwirth *et al.*, 2007).

Most oxidized phospholipids contain a choline headgroup, as PC is the most abundant phospholipid in mammalian cells. In addition to phosphatidylcholine, other phospholipids containing different polar headgroups like phosphatidylethanolamine and phosphatidylserine can be oxidatively modified.

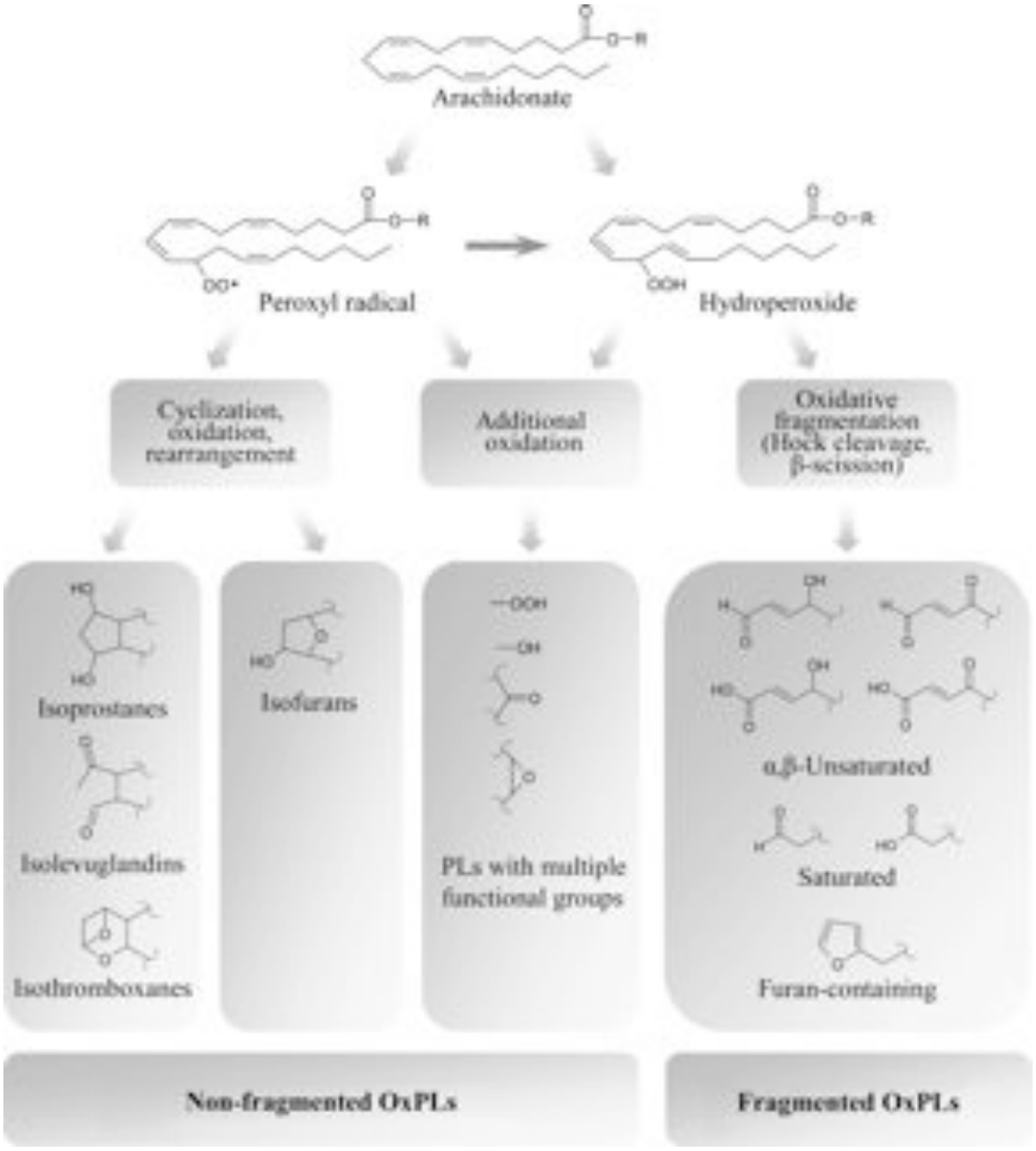

Figure 1.1. Classification of phospholipid oxidation products

Peroxidation of PL-esterified PUFAs is initiated by formation of hydroperoxides or peroxyl radicals. Further oxidation proceeds via three major pathways. First, intramolecular cyclization, rearrangement, and further oxidation can lead to the formation of isoprostanes, isolevuglandins, isothromboxanes and isofurans. The second pathway involves additional oxidation within the same PUFA generating oxPL with multiple functional groups (hydroperoxides, hydroxides, keto-groups, epoxy-groups). The third group of transformations results from several chemical reactions finally leading to fragmentation of PUFAs and generation of short residues. (Figure from Bochkov et al. (Bochkov et al., 2010))

Enzyme-catalyzed and non-enzymatic reactions lead to the formation of non-fragmented and fragmented oxidized phospholipids. The first group includes isoprostanes, isolevuglandins, isothromboxanes, isofurans and phospholipids with multiple functional groups. The latter group consists of α,β-unsaturated, saturated and furan-containing fragmented oxidized phospholipids (Figure 1.1).

Typical derivatives of fragmented phospholipids are POVPC (1-palmitoyl-2-(5-oxovaleroyl)-*sn*-glycero-3-phosphocholine) and PGPC (1-palmitoyl-2-glutaroyl-*sn*-glycero-3-phosphocholine) (Figure 1.2). These compounds share structural similarities: both contain a single long-chain carboxylic acid at the *sn*-1 position of the glycerol backbone and they only differ in their functional group at the ω-end of the truncated acyl residue at the *sn*-2 position. In PGPC, this is a carboxylate group, whereas POVPC contains a chemically highly reactive aldehyde function. The latter compound can therefore undergo Schiff base formation with NH_2 groups of proteins and aminophospholipids such as phosphatidylethanolamine and phosphatidylserine.

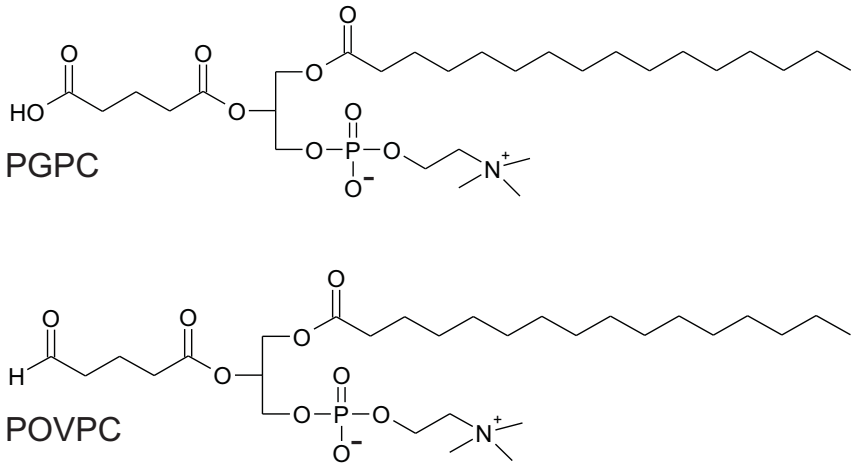

Figure 1.2. Chemical structures of the oxidized phospholipids PGPC and POVPC

1-palmitoyl-2-glutaroyl-sn-glycero-3-phosphocholine (PGPC)
1-palmitoyl-2-(5-oxovaleroyl)-sn-glycero-3-phosphocholine (POVPC)

1.1.1 Biophysical properties of oxPL

Phospholipid oxidation products can dramatically change the properties of phospholipid bilayers. Their polarity and their shape differ from the molecules they originate from. Thus, they can unspecifically alter lipid-lipid and lipid-protein interactions and as a consequence, membrane protein functions (Fruhwirth *et al.*, 2007).

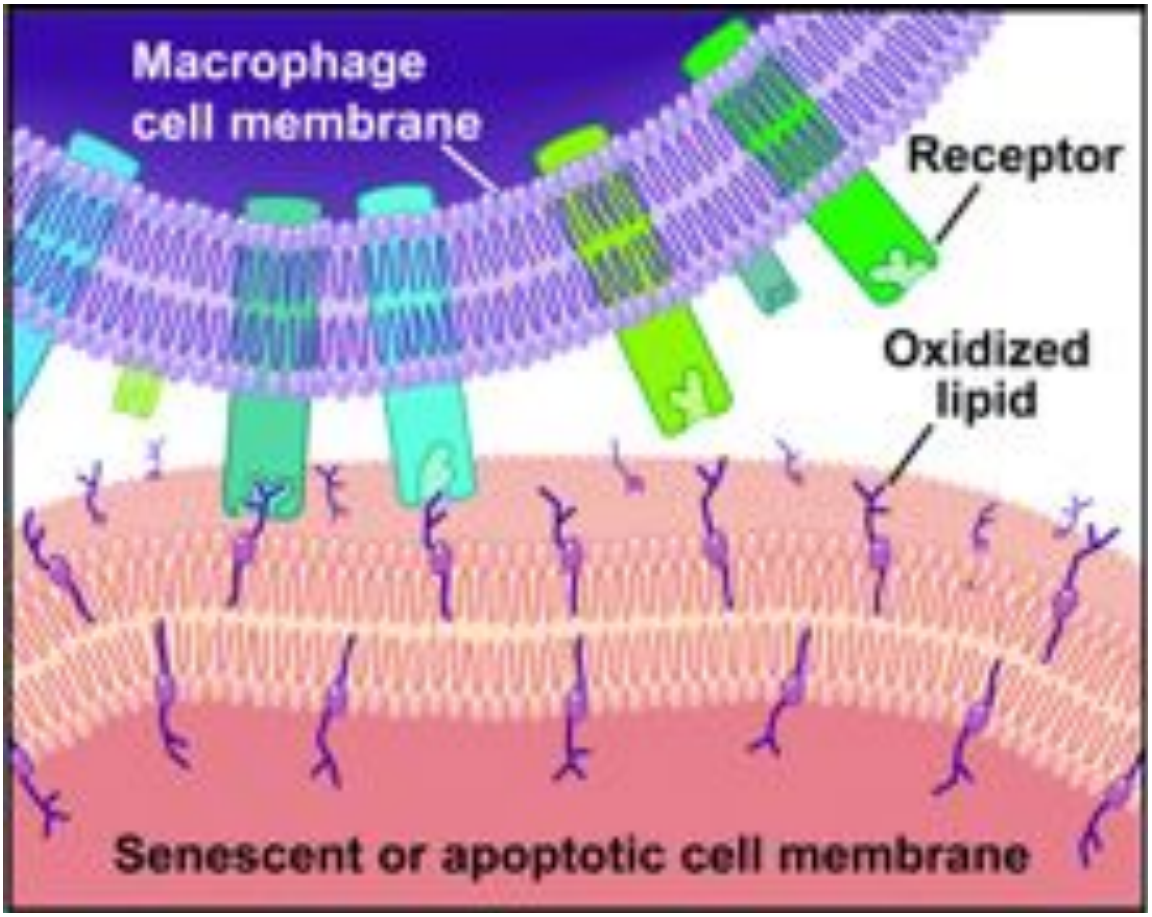

Figure 1.3. Schematic representation of the Lipid Whisker Model

Cell membranes of senescent or apoptotic cells contain oxPL with a variety of oxidized fatty acyl chains of different structures protruding into the aqueous compartment. This conformation renders them accessible to interaction with scavenger receptors and other (pattern recognition) receptors on the surface of macrophages. It may also make them more accessible for some phospholipases, promoting membrane remodeling by release of oxidized fatty acids and reacylation of the formed lysophospholipids. (Figure from Greenberg et al. (Greenberg et al., 2008)

Greenberg *et al.* were able to demonstrate that phospholipid oxidation leads to con-

formational changes of oxPL within the lipid bilayer (Greenberg *et al.*, 2008). Upon oxidation, the truncated lipid acyl chains are no longer buried within the interior of the bilayer, but they rather protrude into the aqueous compartment, forming whisker-like structures (Figure 1.3). In addition, there are no significant conformational alterations in the headgroup during the oxidation. This reorientation in the lipid bilayer enables contact between pattern recognition receptors and molecular pattern ligands, e.g. recognition of truncated oxPL by the scavenger receptor CD36 and Toll-like receptors. The oxPL on the cell surface may also bind to the PAF receptor though their binding affinities are much lower compared to PAF which is the "natural" ligand.

Finally, oxPL exert significant effects on membrane curvature and stability. Carboxy and aldehydo phospholipids induce positive membrane curvatures and consequently facilitate the formation of membrane vesicles (Stemmer and Hermetter, 2012).

1.1.2 Biochemical reactivity of oxidized phospholipids

Many oxidized phospholipids contain reactive groups including aldehyde residues, epoxide rings and double bonds conjugated to carbonyl groups. Consequently, oxPL bearing these groups can undergo chemical reactions with biological molecules (Fruhwirth *et al.*, 2007).

OxPL containing aldehyde groups (e.g. POVPC) can form Schiff bases with NH_2 groups of proteins and aminophospholipids (Figure 1.4). This covalent modification may modulate the functional properties of biomolecules, thus changing localization, net charge, conformation, state of association, enzymatic and signaling functions and biological recognition by receptors and the immune system. Interactions depend on

the localization of the functional aldehyde group, the molecular lipid mobility and the steric constraints due to lateral lipid and protein packing. Formation of covalent lipid-lipid adducts may also change membrane organization thereby affecting lateral lipid organization, local membrane curvature and lipid mobilities. This may finally affect membrane protein function, membrane stability and the tendency to release membrane vesicles (Stemmer and Hermetter, 2012).

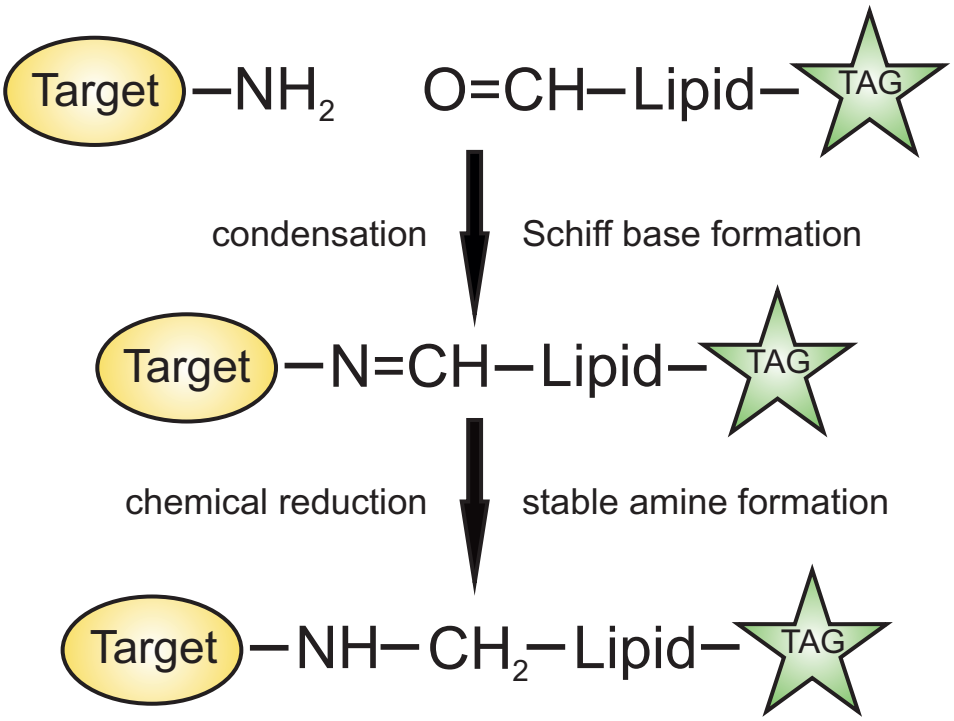

Figure 1.4. Interaction of aldehydo phospholipids and their protein and lipid targets

The aldehyde group at the sn-2 position of aldehydo phospholipids, e.g. POVPC, can chemically react with free amino groups of target proteins and lipids by forming Schiff bases. For further analysis of the formed adducts, the labile imines have to be reduced with $NaCNBH_3$ to generate stable amines. PGPC can only physically interact with its targets.

1.1.3 Pathophysiological effects of oxidized phospholipids

Oxidized phospholipids mediate many pathophysiological effects in several chronic diseases, including atherosclerosis. LDL (low density lipoprotein) is a source of cho-

lesterol for peripheral cells. PUFAs and cholesterol are easily oxidizable. The extent of lipid and LDL oxidation depends on the reactive oxygen species involved. Oxidation of LDL is known to be a key step in atherogenesis, leading to inflammation, proliferation and apoptosis of cells of the arterial wall. Highly oxidized LDL (oxLDL) is modified in both, the lipid and the protein moiety, whereas minimally modified LDL (mmLDL) mainly contains oxidized lipids. Therefore, mmLDL properties differ from LDL properties only as a consequence of lipid modification. LDL can be internalized by cells via interaction with the LDL-receptor (apoprotein B/E receptor) which recognizes the apoprotein B100 on the particle (Goldstein and Brown, 1977), whereas oxLDL is recognized by the scavenger receptor, which is not able to recognize native LDL and is expressed on macrophages and endothelial cells (Mahley *et al.*, 1979; Pitas *et al.*, 1985; Stein and Stein, 1980).

When LDL undergoes oxidation, a large variety of biologically active lipids are formed (McIntyre *et al.*, 1999; Witztum and Berliner, 1998). Among other lipid degradation products, PGPC and POVPC are present in mmLDL and they are known for their critical role in the induction and progression of atherosclerosis by mediating pro-inflammatory and toxic effects of this particle. Studies from several laboratories have shown that many biological effects triggered by mmLDL can be attributed to oxidized phospholipids (Leitinger *et al.*, 1998; Watson *et al.*, 1995; Leitinger *et al.*, 1999; Loidl *et al.*, 2003).

Atherosclerosis is a chronic disease and the major cause of heart attack and stroke. The early atherosclerotic lesion ("fatty streak") is characterized by accumulation of LDL lipids in foam cells derived predominantly from macrophages. In more ad-

vanced lesions, these foam cells are also derived from smooth muscle cells (Aqel *et al.*, 1984; Faggiotto *et al.*, 1984; Fowler *et al.*, 1979; Gerrity, 1981a,b; Schaffner *et al.*, 1980). Lipid deposition and oxidation, infiltration of inflammatory cells, and accumulation of matrix and cellular debris within the blood vessel wall lead to the development of atherosclerotic plaques (Ross, 1993; Stocker and Keaney, 2004; Chisolm and Steinberg, 2000). These atherosclerotic lesions contain high concentrations of oxidized phospholipids and during the development and progression of these lesions oxPL are continuously generated and degraded (Berliner *et al.*, 2001; Watson *et al.*, 1997). It has been shown that oxPL act on all different cell types involved in the formation of atherosclerotic lesions, including monocytes, macrophages, endothelial cells, vascular smooth muscle cells and lymphocytes.

Besides their role in atherosclerosis, phospholipid oxidation products have also been detected in different organs and pathological states. These include inflamed lung (Nakamura *et al.*, 1998; Yoshimi *et al.*, 2005), ischemia, apoptotic cells (Chang *et al.*, 2004; Huber *et al.*, 2002), virus-infected cells (Van Lenten *et al.*, 2004), multiple sclerosis (Qin *et al.*, 2007) and coronary artery disease (Tsimikas *et al.*, 2007) (Bochkov, 2007).

1.1.4 Detoxification of oxPL

Stability of oxidized phospholipids in biological systems is limited, since several processes lead to detoxification of these compounds, including hydrolytic degradation and/or enzymatic reduction of reactive groups. Cleavage of oxPL by intracellular and plasma phospholipases release oxidized *sn*-2 carboxylic acids and as a consequence lysophospholipids are formed. Such hydrolytic reactions may be due to the

activity of Platelet activating factor acetylhydrolase (PAF-AH, Lp-PLA2), which hydrolyzes PAF and truncated oxidized phospholipids including PGPC and POVPC (Chakraborti, 2003; Fruhwirth *et al.*, 2007). Finally, some oxPL are capable of forming covalent adducts with proteins, and this represents an additional pathway for their inactivation. However, adduct formation might also increase their toxicity. Coupling of oxPL to NH_2 groups of proteins might inactivate functional amino acid residues or induce polymerization of proteins. Both reactions ultimately lead to protein dysfunction.

1.1.5 Oxidized phospholipids and apoptosis

In the context of atherosclerosis, apoptotic cells represent an additional source of oxidized phospholipids and thus can actively contribute to inflammatory processes (Huber *et al.*, 2002). Apoptotic cell death is a phenomenon predominant in the late phase of atherosclerosis (Martinet and Kockx, 2001). In early lesions, apoptosis helps to reduce lesion size (Pollman *et al.*, 1998; Wang *et al.*, 1999), whereas at later stages accumulation of apoptotic cells contributes to the formation of unstable plaques (Kockx, 1998; Libby *et al.*, 1997; Fruhwirth *et al.*, 2007). Since the toxicity of oxidized phospholipids depends on their structure, it is important to use defined oxidized phospholipid species in biomedical studies.

Apoptosis as an intrinsic suicide program of the cell is an important mechanism to remove infected, transformed or damaged cells (Fadeel, 2003; Mallat and Tedgui, 2009). It is an active process, characterized by cell shrinkage, membrane blebbing, chromatin condensation with internucleosomal fragmentation of DNA, organelle relocalization, formation of discrete membrane enclosed vesicles (apoptotic bodies) and finally cell

fragmentation without leakage of cytosolic macromolecules (McConkey, 1998). In contrast, necrosis is a passive process characterized by an increase in cell volume, swelling of the mitochondria and loss of membrane integrity, resulting in cell lysis and spillage of cellular contents into the environment, that generally leads to an inflammatory response (Fruhwirth *et al.*, 2006).

Fruhwirth *et al.* showed, that PGPC and POVPC inhibit cell proliferation and induce cytotoxic effects in VSMCs under low serum conditions (Fruhwirth *et al.*, 2006). Analysis of the characteristic signs of cell death as described above led to the conclusion that apoptosis was the predominant form of cell death, POVPC being more active than PGPC. In addition, Loidl *et al.* could show that the oxidized phospholipids PGPC and POVPC activate acid sphingomyelinase in VSMCs, which participates in the very early apoptotic stress response. Downstream targets like mitogen-activated protein kinase (MAPK), c-Jun N-terminal kinase (JNK) and p35 were phosphorylated in response to stimulation with oxPL, finally leading to the activation of caspase 3. In contrast, components of survival and proliferation pathways including ERK, NF-$\varkappa$B or AKT-kinase/PKB were not activated by PGPC and POVPC (Loidl *et al.*, 2003).

The toxic lipids were efficiently incorporated by the cells although in a different manner. Moumtzi *et al.* could show, that the fluorescent oxPL BY-PGPE and BY-POVPE were rapidly transferred from the aqueous phospholipid dispersion into VSMCs. PGPC localized to the lysosomes, whereas POVPC was initially captured in the plasma membrane, most likely due to formation of covalent adducts with free amino and sulfhydryl groups of proteins and aminophospholipids (Moumtzi *et al.*, 2007).

Recent studies by Stemmer *et al.* revealed cellular toxicities of PGPC and POVPC in RAW 264.7 macrophages (Stemmer *et al.*, 2012). PGPC was rapidly taken up into RAW 264.7 macrophages, whereas POVPC was initially trapped in the plasma membrane, most likely due to covalent interaction of POVPC with amino groups of proteins and aminophospholipids and subsequent Schiff base formation. Due to their amphipathic structure, both oxPL were easily exchangeable between cells membranes and other lipid carriers such as LDL and BSA (Stemmer *et al.*, 2012).

PGPC and POVPC induced apoptosis in RAW 264.7 macrophages as well as in primary bone marrow-derived macrophages. Lipid toxicity was causally related to activation of acid sphingomyelinase. Another facet of lipid toxicity in these stimulated cells was release of oxPL-containing apoptotic blebs (Stemmer *et al.*, 2012).

1.2 Skin cancer

Cancer is a group of diseases characterized by uncontrolled cell growth, invasiveness and spread of abnormal cells. About 1.6 million new skin cancer cases are expected to be diagnosed in 2012. This makes cancer the second most common cause of death in the US, exceeded only by heart disease. Although there are various treatment options for cancer, like surgery, radiation, chemotherapy, hormone therapy and targeted therapy, the survival rates for some cancers, especially the treatment of distant metastases, often remains a challenge.

There are several requirements for malignant transformation of a cell. These requirements ("hallmarks of cancer") include self-sufficiency of growth signals (e.g. by alteration in growth signals, up-regulation of growth factor receptors, mutations in growth signaling pathways), insensitivity to antigrowth signaling, resistance towards apoptosis (e.g. by defects in the activation of FAS death signaling pathway or mutation in p53), limitless replicative potential (e.g. by maintenance of telomere length by up-regulation of telomerase activity), sustained angiogenesis and tissue invasion and metastasis (Hanahan and Weinberg, 2000).

Skin cancer is the most common type of cancer worldwide. Each year, more new cases of skin cancer are diagnosed than total number of cancers of the breast, prostate, lung and colon. Generally, skin cancers are named after the type of cells that become malignant. There are two major groups of skin cancer, melanoma and non-melanoma skin cancers. The latter group comprises basal cell carcinoma (BCC), squamous cell carcinoma (SCC) and premalignant lesions including actinic keratosis and Bowen's

disease. Melanomas account for less than 5% of skin cancer cases, but for the vast majority of skin cancer deaths. BCC is the most common type of skin cancer, but mortality of BCC and SCC is generally low when compared to other types of cancer. However, when allowed to grow, these types of skin cancer can be highly disfiguring (Center *et al.*, 2011).

1.3 Melanoma

Figure 1.5. Primary melanoma
Melanomas are characterized by asymmetry, irregular borders, variegated color, large diameter and continuous growth (Figure from Abbasi et al. (Abbasi et al., 2004)).

Unlike most other types of cancer, the rate of melanoma has almost doubled in the past 30 years in the United States. From 1970 to 2009, the incidence of melanoma increased by 800% among young women and 400% among young men (Reed *et al.*, 2012). Although better detection systems have been developed and a greater awareness of the dangers of sun and UV exposure has risen, this disease is in desperate need of new therapeutic options. Two new drugs, Ipilimumab (Yervoy) and Vemurafenib (Zelboraf), have recently been approved by the FDA and reportedly extend short-time survival in people with advanced melanoma. Despite recent successes in melanoma research, this aggressive type of skin cancer, which shows a high tendency to spread to other organs, is not curable so far.

Melanomas represent a heterogeneous group of neoplasms with variable genotypic and phenotypic characteristics depending on anatomic location, degree of sun exposure and individual susceptibility (Slipicevic and Herlyn, 2012). They arise from malignant transformation of the pigment producing melanocytes in the skin as a consequence of accumulation of genetic alterations. In addition, melanomas can also develop in the mucosal membranes, uveal tract of the eyes and leptomeninges. Melanomas usually develop from melanocytes, but they can also arise from preexisting nevi due to sequential accumulation of genetic and molecular alterations. Genetic predispositions as well as environmental factors such as sunlight contribute to its formation.

1.3.1 Architecture of the healthy skin

Human skin consists of two layers, the epidermis and the dermis, which are separated by a basement membrane (Figure 1.6). In the epidermis, keratinocytes represent a primary barrier to the outside environment. They produce a huge number of molecules for cell growth and host defense. Undifferentiated basal keratinocytes ("basal cells") proliferate and differentiate into a multilayered tissue. Melanocytes are distributed as single cells within the basal layer of the epidermis (one per 5-10 basal keratinocytes), forming an epidermal-melanin unit (Nordlund, 2007). Each melanocyte is in contact with about 36 keratinocytes and transports melanin-containing melanosomes to them through multiple dendrites. The melanin protects keratinocytes from the harmful effects of UV light. Proliferation of melanocytes is strictly controlled by keratinocytes.

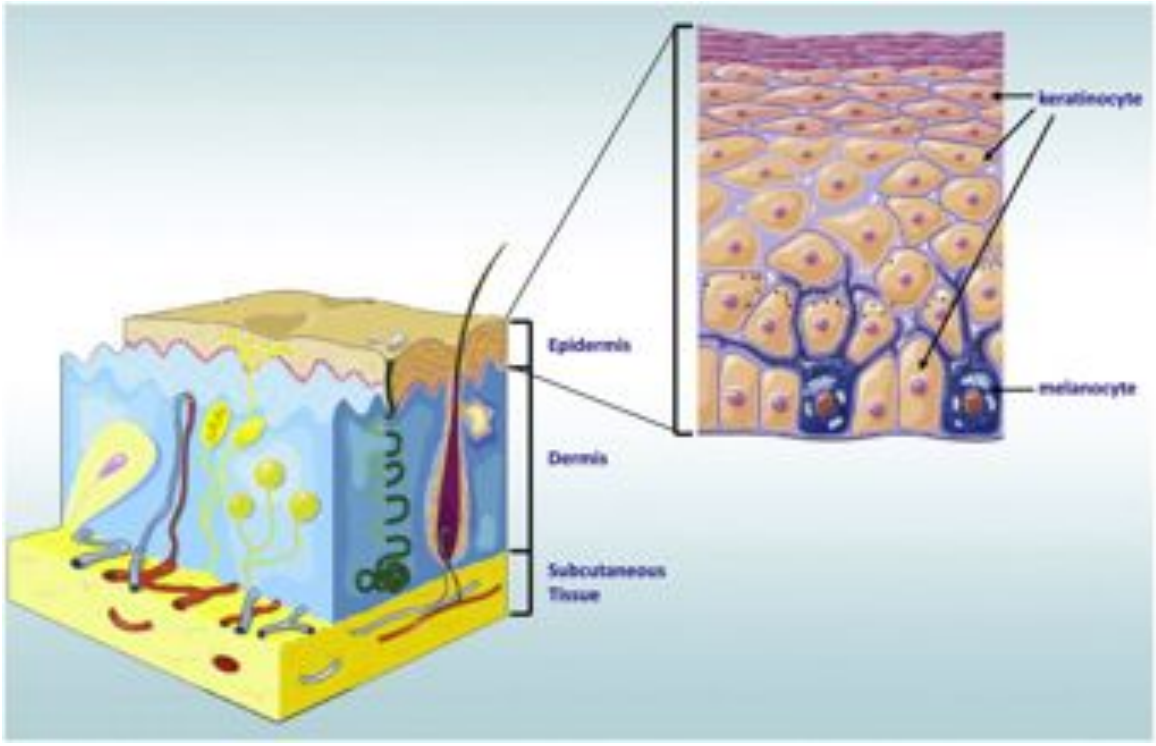

Figure 1.6. Anatomy of the skin

Skin consists of three distinct layers, epidermis, dermis and subcutaneous tissue. Melanocytes are positioned singly between basal cells at the basal layer of the epidermis. Proliferation, division and migration of melanocytes are tightly controlled by keratinocytes (Figure from Nys et al. (Nys et al., 2011))

1.3.2 Risk factors

Two major factors are important for the development of melanomas in humans: genetic predisposition and exposure to environmental factors.

Familial melanomas represent 8-12% of all melanomas (Fountain *et al.*, 1990; Goldman *et al.*, 1986; Greene, 2000; Greene *et al.*, 1983). The development of melanomas is also linked to the skin color as melanomas occur tenfold more frequently in caucasians than in blacks (Crombie, 1979). Fair-skinned people who have nevi or frequently suffer from sunburn without tanning have a higher risk of developing melanomas than people with darker skin (Gallagher *et al.*, 1990). Survivors of melanoma are about nine times as likely as the general population to develop a new melanoma (Bradford

et al., 2010).

About 86% of melanomas can be attributed to exposure to ultraviolet radiation from the sun, either causing their formation or contributing to it (Parkin *et al.*, 2011). The vast majority of mutations found in melanomas are caused by UV light (Pleasance *et al.*, 2009). Especially intensive exposure to sunlight during childhood or the use of tanning lamps are known to increase the risk of melanoma dramatically. UV radiation comprises UVA (320-400 nm), UVB (280-320 nm) and UVC (200-280 nm). The effect of UVC on the human skin can be ignored, as this radiation is absorbed by oxygen and ozone in the atmosphere. In contrast, UVA and UVB radiation can cause harmful effects on the skin, including increased DNA instability (Cifone and Fidler, 1981), inactivation of antioxidants (Fuchs and Packer, 1990) and suppression of the immune system. The role of UVB as a cause of white skin cancer and to a lesser extent of melanomas is well documented, whereas the role of UVA is still less understood. UVB radiation is absorbed mainly by the epidermis thus causing DNA damage to keratinocytes and inducing white skin cancer. It causes direct damage to the DNA thereby initiating a primary mutation in the skin. UVB induces two major types of DNA modifications: pyrimidine-pyrimidone (6-4) photoproducts (6-4PPs) can be generated between adjacent pyrimidine residues. In addition, pyrimidine and cyclobutane dimers can be formed between adjacent thymine and cytosine dimers. Pyrimidine dimers are considered to be more carcinogenic as they are formed three times more often and are less efficiently repaired. UVB can also cause C –> A and G –> T changes and DNA strand breaks. In contrast, UVA is able to penetrate deeper into the skin thus reaching more melanocytes compared to UVB. In contrast to UVB, UVA causes oxidative damage to the cells by formation of reactive oxygen species (ROS).

Thus it can induce mutations in the DNA only indirectly. UVA cannot be absorbed directly by native DNA.

Non-sunlight risk factors include exposure to ionizing radiation and chemicals. However, synergistic effects with genetic factors and UV radiation have to be taken in account in this case (Gruber *et al.*, 2008).

1.3.3 Melanoma progression and clinical staging

Major steps of tumor progression according to Clark (Clark, 1991) are defined as follows (Figure 1.7): The earliest hyperplastic melanocyte lesion is the common acquired nevus. The dysplastic nevus shows increased levels of cytological and architectural atypia. The first malignant stage is the radial growth phase (RGP) primary melanoma, in which melanoma cells are restricted to the epidermis or are only locally invasive. Vertical growth phase (VGP) melanoma lesions are characterized by infiltration into the dermis and the subcutaneous tissue. All VGP melanomas are tumorigenic, although to a different extent. Metastasis represents the most advanced step in tumor progression.

Melanomas are classified histologically based upon their location and stage of progression. The stages of melanomas are defined as follows (Balch *et al.*, 2009):

Stage 0: The melanoma involves only the top layer of the skin, also called melanoma *in situ*.

Stage I: The tumor is no more than 1 mm thick, the surface may appear broken down.

Stage II: The tumor is between 1 and 2 mm thick, the surface appears broken down.

Stage III: The melanoma cells have spread to at least one nearby lymph node.

Stage IV: Malignant cells have spread to areas of the body far away from original growth.

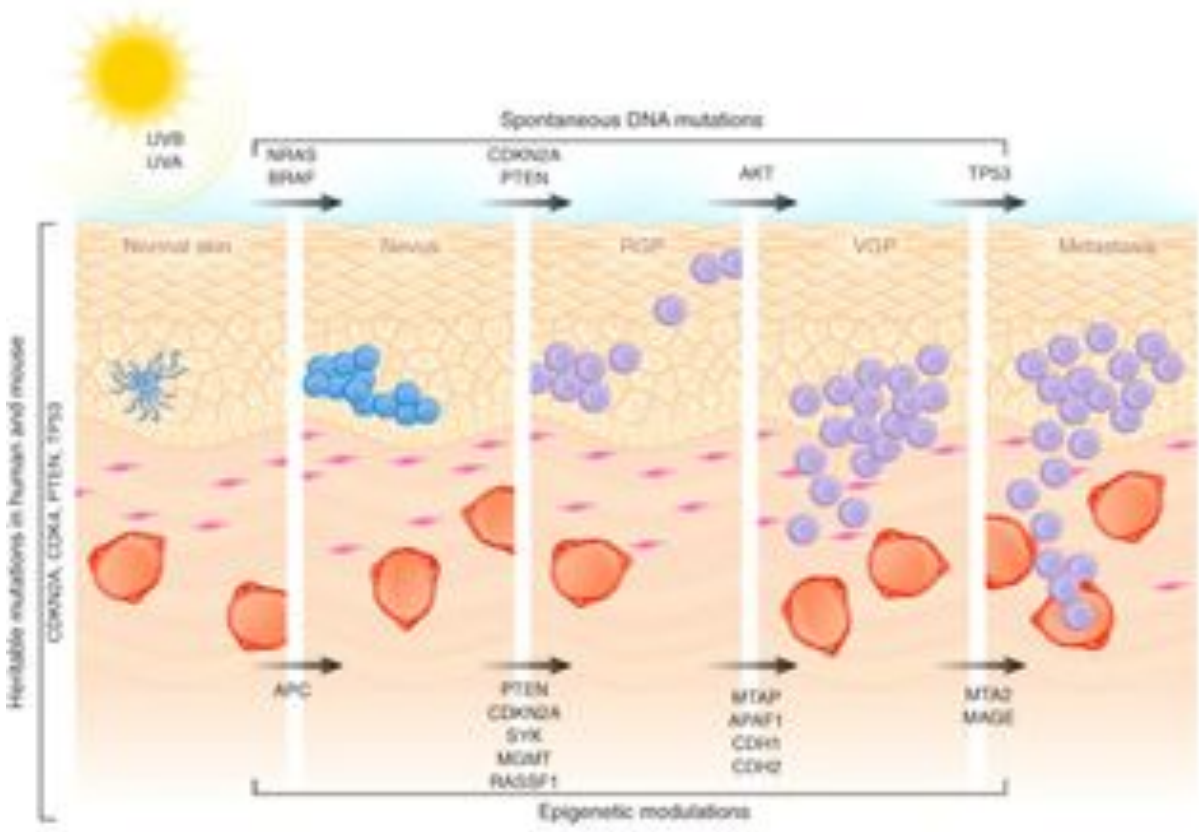

Figure 1.7. Proposed molecular alterations associated with the initiation and progression of melanoma

Human melanoma progression is associated with molecular alterations that can occur at different stages. Aberrant proliferation of normal melanocytes results in the formation of benign or dysplastic nevi. Radial growth phase (RGP) melanomas exhibit the ability to grow intra-epidermally, followed by invasion of the dermis in the vertical growth phase (VGP), and ending with metastasis. Only about half of the melanomas are known to arise from nevi, and progression can occur without going through all the stages described. (Figure from Zaidi et al. (Zaidi et al., 2008))

1.3.4 Genetic background

Mutations in two categories of genes are relevant for cancer development and growth: oncogenes and tumor suppressor genes. Proteins encoded by oncogenes contribute to

cancer formation through a dominant gain of function mutation. Tumor suppressor gene products suppress carcinogenic progression and recessive loss-of-function mutations in these genes enable cancer growth.

Multiple mutations have been detected in melanomas, as summarized in Figure 1.8. These mutations are affecting either proliferative, senescence or apoptotic pathways.

Proliferative pathways

Proliferative pathways including the MAPK-ERK pathway are involved in the control of cell growth, proliferation and migration, and play a major role in the development and progression of melanoma. They are implicated in rapid melanoma cell growth, enhanced cell survival and resistance to apoptosis (Davies *et al.*, 2002; Palmieri *et al.*, 2009).

PTEN. *PTEN* (phosphatase and tensin homologue) is a suppressor gene that encodes for a phosphatase, which regulates extracellular growth signals, cellular division, cell migration and spreading (Tamura *et al.*, 1998). Mutations lead to activation of the serine/threonine kinase AKT3 and thus promote cell cycle progression and inhibition of apoptosis. *PTEN* is inactivated in 25% to 50% of melanomas by mutation, reduced expression or deletion.

c-kit. The transmembrane tyrosine kinase receptor c-kit is activated by binding to its ligand stem cell factor, which leads to the stimulation of the mitogen-activated protein kinase (MAPK), AKT1 and JAK-STAT signaling pathway, thereby producing proliferative and survival effects. c-kit expression is up-regulated in 60% of melanomas but

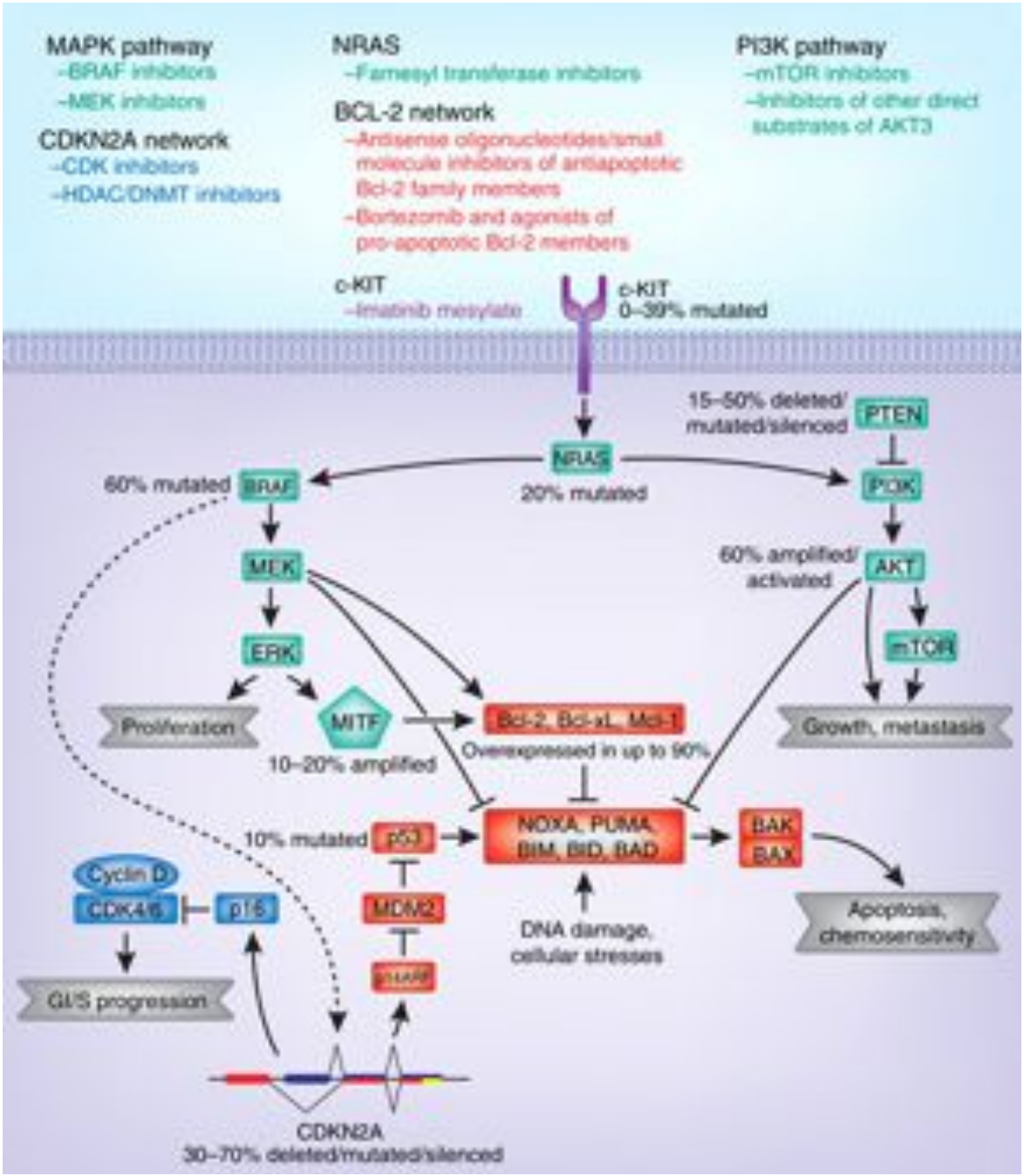

Figure 1.8. Melanoma signaling networks

Shown is a simplified diagram of three of the major genetic networks involved in melanoma tumorigenesis, survival, and senescence. Included in the NRAS signaling network (green) are the MAPK and the PI3 Kinase/AKT pathways, which have been implicated in melanoma proliferation, survival, and progression. The CDKN2A locus encodes two separate tumor suppressors, p16 and p14ARF, both of which are thought to contribute to senescence and tumor growth restriction. The p53/Bcl-2 signaling network (red) is a major contributor to melanoma apoptosis and chemosensitivity and is regulated by many of the oncogenic melanoma pathways. Shown at the top of the figure are selected therapeutic agents that target each of these genetic networks. (Figure from Hocker et al. (Hocker et al., 2008))

not in melanocytes (Curtin *et al.*, 2006; Lassam *et al.*, 1992). c-kit-alterations are found more frequently in melanomas from acral, mucosal and chronic sun-damaged sites (Nikolaou *et al.*, 2012).

NRAS. The ras signaling cascade promotes proliferation, survival and invasion through two distinct pathways, the MAPK pathway and the PI3K pathway (Hocker *et al.*, 2008). Changes in the expression of all RAS genes (*NRAS*, *HRAS* and *KRAS*) have been detected in human melanomas. Mutations in *NRAS*, leading to a constitutive activation of this gene, are present in about 20% of human melanomas and within the *RAS* gene family it is the most commonly mutated gene. *NRAS* mutations are very often found in melanomas on sun-exposed areas of the body. This suggests a strong association between mutations of this gene and UV light.

BRAF. Three highly conserved *RAF* genes are present in human cells: *ARAF*, *BRAF* and *CRAF*. *CRAF* and *ARAF* mutations are rare in human cancers (Emuss *et al.*, 2005; Lee *et al.*, 2005; Zebisch *et al.*, 2006), which might be due to the fact that oncogenic mutation in these genes requires two coexisting mutations, whereas *BRAF* can be activated by a single amino acid substitution (Beeram *et al.*, 2005; Zebisch *et al.*, 2006). Mutations in the proto-oncogene *BRAF* represent approximately 60% of mutations found in melanomas, and it is the most frequently mutated gene in this skin tumor. The most common mutation (95% of mutations of *BRAF*) within this gene is a glutamic acid-for-valine substitution at position 600 ($BRAF^{V600E}$), which is a gain-of-function mutation (Davies *et al.*, 2002). *BRAF* encodes a serine/threonine kinase in the ras signaling pathway and as a consequence, this mutation leads to constitutive activation of downstream protein kinases by phosphorylation (MEK/ERK).

Interestingly, *BRAF* mutations are necessary but not sufficient for the development of melanoma. They represent an early event in melanoma development and must be accompanied by other gene alterations (Haluska *et al.*, 2006). They are already found in nevi, which implicates that they rather influence proliferation than tumorigenesis. Activating mutations of *BRAF* alone constitutively induce up-regulation of *p16* and cell cycle arrest (Michaloglou *et al.*, 2005), therefore *in vitro* introduction of $BRAF^{V600E}$ in normal human melanocytes leads to cellular senescence (Slipicevic and Herlyn, 2012).

Mutations of *PTEN* and *BRAF* frequently occur together, whereas *NRAS* mutations and *BRAF* mutations are not present in the same melanoma (Goel *et al.*, 2006).

Senescence pathways

Cell senescence is an arrest of proliferation at the somatic level. This is induced by telomere shortening, oncogenic activation and/or cellular stress due to intense proliferative signals (Di Micco *et al.*, 2006; Mooi and Peeper, 2006; Palmieri *et al.*, 2009). During melanoma progression, expression and activity of telomerase is up-regulated (Palmieri *et al.*, 2009).

$p16^{CDKN2A}$. p16 is one of two products of the cyclin-dependent kinase inhibitor 2A (*CDKN2A*) gene, which also encodes for p14 (product of alternative splicing). As a consequence, *p16* and *p14* are simultaneously altered in many tumors. p16 is a tumor suppressor protein involved in the G1/S checkpoint of the cell cycle. It acts as an inhibitor of the cyclin-dependent kinases CDK4 and CDK6 and prevents S-phase entry

during cell cycle. Studies have shown that *CDKN2A* is mutated in 42% of malignant melanomas (Talve *et al.*, 1998), in 59% of melanoma metastases (Maelandsmo *et al.*, 1996) and in 77% of melanoma cell lines (Bartkova *et al.*, 1996). Mutations lead to ineffective inhibition of cell proliferation. Thus, they promote uncontrolled cell growth, which may increase the aggressiveness of the transformed melanocytic cells (Haluska *et al.*, 2006; Palmieri *et al.*, 2009).

Apoptotic pathways

p53. Mutations and over-expression of this gene have been found in melanomas (Stretch *et al.*, 1991; Volkenandt *et al.*, 2006), but the frequency numbers are very variable from study to study. Under normal conditions, the expression levels of the stress response protein p53 in cells are low. In response to DNA damage, p53 accumulates and prevents cell division. Inactivation of p53 by mutation results therefore in an accumulation of genetic damage, which promotes tumor formation (Levine, 1997; Palmieri *et al.*, 2009). In melanoma, this inactivation of p53 is mainly due to a functional gene silencing, as mutations in *p53* are low (Box and Terzian, 2008).

p14^{CDKN2A}. p14 is a tumor suppressor protein which acts by inhibiting the MDM2 protein. The latter protein interacts with p53 by blocking p53-mediated activities and targeting substrates for rapid degradation (Pomerantz *et al.*, 1998; Palmieri *et al.*, 2009).

It has to be emphasized that single genetic or molecular alterations are not sufficient for the induction of melanoma formation. According to Palmieri *et al.* (Palmieri *et al.*, 2009), the following alterations are needed for melanoma development and progression:

- induction of clonal expansion (mutational activation of *BRAF* or *NRAS*)
- modifications to overcome mechanisms controlling melanocyte senescence, which otherwise would halt the lesion as a benign mole (inactivation of the p16 pathway)
- suppression of apoptosis (increased expression of AKT)

1.3.5 Melanoma treatment

The median survival time for melanoma patients with metastatic disease is 8-9 months (Balch *et al.*, 2009). Despite recent successes in the treatment of melanoma, the 5-year survival rate of patients suffering from metastasized melanomas (stage III and IV) is less than 10%. This is mainly due to the aggressiveness of the tumor but also due to a lack of therapeutic approaches for treating this disease (Kuphal and Bosserhoff, 2009).

Clinical trials of chemotherapy, immunotherapy and biochemotherapy have failed to significantly improve survival rates. Recent advances have been made with new treatment strategies that target specific molecules and pathways expressed in cancer cells.

Surgery and radiation therapy. Early stage melanoma is curable through surgery. In advanced disease, surgery and radiation therapy are usually used for palliation of symptoms due to local tumor growth. Melanoma is considered a relatively radioresistant tumor and radiation therapy is used as an adjunct to the use of systemic therapy (Bhatia *et al.*, 2009).

Chemotherapy (Systemic therapy). Systemic therapies include chemotherapy with Dacarbazine (DTIC) and cytokines interleukin-2 (IL-2) and interferon-a2b (IFN-a2b). Only 5%-10% of patients respond to DTIC treatment with median response durations

of 5 to 6 months. Immunotherapy with IL-2 treatment using IFN-a2b as an adjuvant achieves a response in 10%-20% of patients. Effects are usually short-lived and associated with high toxicity (Slipicevic and Herlyn, 2012; Tsao *et al.*, 2004). The primary purpose of Dacarbazine therapy for metastatic melanoma is palliation. Nevertheless, treatment with Dacarbazine is still the "standard treatment" of metastatic melanoma (Balch *et al.*, 2009; Bhatia *et al.*, 2009; Blesa *et al.*, 2011).

Other chemotherapeutic agents used in the treatment of metastatic melanoma include alkylating agents (Temozolomide, nitrosoureas), platinum analogs (cisplatin, carboplatin), and microtubular toxins (vinca alkaloids such as vindesine and vinblastine; taxanes such as paclitaxel). These agents have been used alone or in combination. However, combinations of cytotoxic agents may yield higher response rates than Dacarbazine monotherapy, but they are also associated with greater toxicity and do not extend survival significantly (Bhatia *et al.*, 2009).

Targeting specific signaling molecules in melanomas (Targeted therapy)

RAS. Farnesyltransferase inhibitors (e.g. Tipifarnib and Lonafarnib) block RAS activation by inhibiting posttranslational farnesylation of the protein. This prevents translocation of RAS to the plasma membrane, which is required for dimerization of RAF and activation of downstream signaling pathways (Purcell and Donehower, 2002). Single-agent studies were not successful, but there is evidence, that RAS antagonism might enhance the effectiveness of other chemotherapeutic agents. As a consequence such inhibitors might be used as part of a combination treatment (Nikolaou *et al.*, 2012).

BRAF. Sorafenib is a non-selective RAF inhibitor that targets the ATP-binding site of RAF, and it abolishes MAPK signaling biochemically. Besides RAF, Sorafenib also inhibits receptor tyrosine kinases, including c-kit, platelet-derived growth factor (PDGF) receptors and vascular endothelial growth factor (VEGF). At low concentrations, it inhibits both wild-type and mutated BRAF. Comparable to farnesyltransferase inhibitors, single agent studies were not successful, and also combinations failed to prove any clinical benefit for metastatic melanoma patients (Bhatia *et al.*, 2009; Nikolaou *et al.*, 2012).

Other, more selective BRAF inhibitors are currently under investigation, including Vemurafenib. This agent has a 30fold higher selectivity for the mutated BRAF compared to wild-type BRAF. In a Phase I trial, an 80% response rate to Vemurafenib among 32 genotype-selected metastatic melanoma patients was found. In addition, progression-free survival rates were also prolonged (Flaherty *et al.*, 2010). However, there is increasing evidence, that the promising effects of Vemurafenib are associated with severe side effects.

Development of keratoacanthomas and invasive squamous cell carcinomas (SCCs) was associated with Vemurafenib, which might be due to compensatory signaling through RAS/CRAF (Heidorn *et al.*, 2010; Nikolaou *et al.*, 2012). In addition, after an initial period of response to the drug, most patients relapse and develop resistance to Vemurafenib. This resistance can be acquired through several mechanisms including activation of the serine/threonine kinase COT and RAF isoform switching (Flaherty *et al.*, 2010; Slipicevic and Herlyn, 2012; Villanueva *et al.*, 2011).

Targeting angiogenesis. Angiogenesis is an essential process in the development of melanomas (Hanahan and Weinberg, 2011). Melanoma cells produce a wide variety of angiogenic factors, including vascular endothelial growth factor (VEGF), basic fibroblast growth factor (bFGF), interleukin-8 (IL-8) and platelet-derived growth factor (PDGF). High serum levels of VEGF correlate with poor prognosis. Several inhibitors of angiogenesis have been tested so far. Anti-angiogenic agents show promising clinical activity, especially by increasing growth control (Bhatia *et al.*, 2009).

Targeting the immune system. Melanoma is one of the most immunogenic tumors. Immunological approaches have shown some activity in patients with advanced melanoma. Therapies include the use of high-dose interleukin-2 (IL-2) and IFN-α, autologous and allogeneic cellular vaccines and cytokines. In addition, multiple novel immunomodulatory agents with activity against melanoma are under development (Bhatia *et al.*, 2009; Nikolaou *et al.*, 2012).

IL-2 is a lymphokine that stimulates T-cell proliferation and function and triggers the release of cytokines such as interferon gamma and tumor necrosis factor by activated lymphocytes. However, high-dose IL-2 shows high toxicity, including fever, chills, hypotension, increased capillary permeability, rash and others.

Only recently, survival benefits were proven for treatment with Ipilimumab, a human monoclonal antibody against cytotoxic T-lymphocyte-associated antigen 4 (CTLA-4) (Hodi *et al.*, 2010), which regulates T-cell activation. Cytotoxic T-lymphocytes (CTLs) can recognize and destroy cancer cells, but this effect is abolished by an inhibitory mechanism, which is resolved by Ipilimumab. In resting T-cells, CTLA-4 is expressed

intracellularly. Upon T-cell activation, the protein is transported to the immune synapse where CTLs and the antigen-presenting dendritic cell are in physical contact. This interaction with CTLA-4 turns the cytotoxic reaction off, allowing cancer cells to survive. Monoclonal antibodies that bind to CTLA-4 can block the interaction and thus enhance immune responses, including anti-tumor immunity (Nikolaou *et al.*, 2012). In advanced stage melanoma patients, treatment with Ipilimumab resulted in 20% increased survival up to 4 years after treatment (Hodi *et al.*, 2010; Slipicevic and Herlyn, 2012).

1.3.6 Conclusions

Melanoma remains the deadliest form of skin cancer and until recently, there have been only few therapeutic options for patients with metastatic disease. Although targeted therapies were successful in the clinics in some instances, more efficient methods for treatment will be needed.

1.4 Non-melanoma skin cancer

Non-melanoma skin cancers are the most frequent tumors in the world and their incidence is increasing every year by 3-8% (Glass and Hoover, 1989; Green *et al.*, 1992). These tumors are usually associated with a low rate of death but often cause disfigurement when skin lesions are located on the head and neck (Ahmed *et al.*, 2008; Trakatelli *et al.*, 2007). Non-melanoma skin cancers comprise basal cell carcinomas (BCCs), squamous cell carcinomas (SCCs) and premalignant lesions such as actinic keratoses, Bowen's disease am keratoacanthomas, which can progress to SCCs.

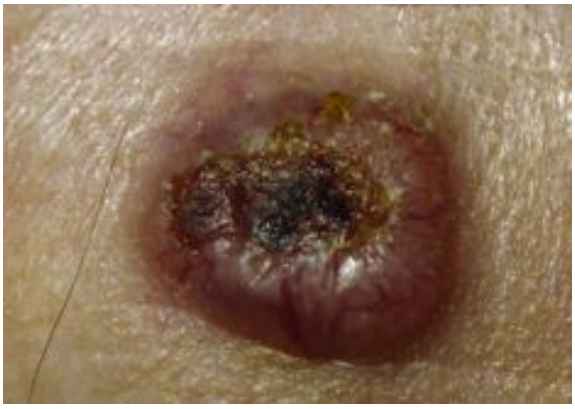

Figure 1.9. Basal cell carcinoma
Figure from Wong et al. (Wong et al., 2003)

Basal cell carcinoma (BCC). BCCs are the most common type of skin cancer, associated with a limited number of sunburns (one or more severe sunburns). They represent about 75% of all skin cancers (Ahmed et al., 2008). BCCs can be categorized into nodular (50-60%), superficial spreading (15%), micro-nodular (15%), infiltrative (7%), pigmented (2%) and sclerosing (2-3%) BCCs (Chummun and McLean, 2011). BCCs are predominantly found on the face or the neck and develop from basal keratinocytes. They are characterized by slow growth and the metastatic rate is lower than 0.1%. However, BCCs are highly invasive and locally destructive (Ahmed *et al.*, 2008).

Figure 1.10. Squamous cell carcinoma
Figure from Madan et al. (Madan et al., 2010)

Squamous cell carcinoma (SCC). SCCs occur less frequently than BCCs, but they are more aggressive. They arise from basal keratinocytes and show uncontrolled growth as they develop from the proliferative basal layer (Chummun and McLean, 2011). SCCs usually arise at sites of intensive sun exposure, that is the face, neck, back, hand, forearm and head. SCCs are associated with recurrent UV exposure (Ahmed *et al.*, 2008). About 10% of SCCs originate from actinic keratoses. Keratoacanthomas can also be regarded as precursor lesions (Burnworth *et al.*, 2006). SCCs have a metastatic rate of 1% (Boukamp, 2005), and they do not only have the capacity to metastasize to the re-

gional nodal basin, but also to the lungs, liver, brain, skin and bone (Chummun and McLean, 2011).

Figure 1.11. Actinic keratosis
Figure from Madan et al. (Madan et al., 2010)

Actinic keratosis (AK). AKs develop on chronically sun-exposed skin and usually manifest as small, scaly lesions with proliferation of atypical keratinocytes. About 25% of AKs regress spontaneously. About 65% of all SCCs and 36% of all BCCs arise in lesions that have been diagnosed as AKs before (Criscione *et al.*, 2009). However, the actual rate of progression of AKs to SCCs is unknown and ranges between 0.1 and 16% (Chummun and McLean, 2011).

Bowen's disease (SCC *in situ***).** Bowen's disease is caused by prolonged exposure to the sun; it is more common in females and found predominantly on the legs. Bowen's disease is an intraepidermal squamous cell carcinoma that is confined to the epidermis with no dermal invasion. It represents a slowly enlarging, well defined erythematous scaly plaque and is regularly mistaken by non-dermatologists for eczema or psoriasis (Ogden and Telfer, 2009). The rate of progression to invasive SCCs ranges between 3 and 5% (Chummun and McLean, 2011).

Figure 1.12. Bowen's disease
Figure from Ogden and Telfer (Ogden and Telfer, 2009)

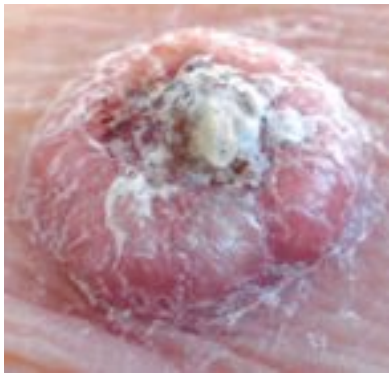

Figure 1.13. Keratoacanthoma
Figure from Madan et al. (Madan et al., 2010)

Keratoacanthoma (KA). Keratoacanthomas represent self-limiting tumors that tend to occur on sun-exposed sites. Clinically and histologically, these tumors are very often difficult to distinguish from SCCs. They are structurally characterized by a nodule with a central keratin plug. Spontaneous involution occurs usually within a few weeks, leaving a ragged scar (Ogden and Telfer, 2009).

1.4.1 Development of non-melanoma skin cancer lesions

The risk of developing non-melanoma skin cancer depends on genotype, phenotype, and environmental factors. It is highest in people with light skin, eye and hair color and in people with benign sun-related skin disorders such as actinic keratosis or Bowen's disease (Madan *et al.*, 2010). Sunlight (English *et al.*, 1997; Neale *et al.*, 2007), viral infections (Asgari *et al.*, 2008; Harwood *et al.*, 2000; Karagas *et al.*, 2006), diet and immunosuppression in organ transplant recipients can increase the risk of the formation of non-melanoma skin cancers (Ahmed *et al.*, 2008). In addition, exposure to carcinogens, such as pesticides, arsenic (Kennedy *et al.*, 2005), hydrocarbons and betel leaves, ionizing radiation (Lichter *et al.*, 2000), tobacco smoking (Odenbro *et al.*, 2005) and photosensitizing drugs (Karagas *et al.*, 2007) can lead to the development SCCs and BCCs (Chummun and McLean, 2011).

General risk factors

Ultraviolet radiation. UV radiation is a major risk factor for non-melanoma skin cancers. It may act as a primary carcinogen or as a promoter of tumor formation (Ahmed *et al.*, 2008; Molho-Pessach *et al.*, 2007). For detailed information on the mechanism of how UVA and UVB induce DNA damage in skin cells, see above. Cumulative sun exposure during a lifetime strongly correlates with the development with SCC, whereas intermittent sun exposure and exposure during childhood are more important for BCC development (Madan *et al.*, 2010). Major targets of UV radiation are the *p53* gene in SCC and BCC, and the patched gene (*PTCH*) in BCC. Inactivation of these genes by mutation leads to uncontrolled cell proliferation (Lacour, 2002).

Viral infection. Viral infections due to the human papilloma virus (HPV) correlate with the simultaneous occurrence of non-melanoma skin cancers. In this context, UV-induced DNA damage and other factors such as immunosuppression lead to increased HPV replication and as a consequence to persistent viral infections. Furthermore, additional DNA mutations accumulate, apoptosis is prevented and DNA repair is impaired. Thus, it is suggested that HPV is indirectly involved in the pathogenesis of non-melanoma skin cancers (Ahmed *et al.*, 2008; Nindl *et al.*, 2007).

Diet. Several studies support the assumption that higher intake of meat and fat increase the risk of developing SCC. In addition, consumption of high amounts of unmodified dairy, such as whole milk and cheese may increase the risk of SCC in susceptible individuals (Ahmed *et al.*, 2008; Hughes *et al.*, 2006; Ibiebele *et al.*, 2007).

Immunosuppresion. In transplant recipients, the risk of developing SCC is increased 65 to 250 fold and the risk of developing BCC is increased 10 to 16 fold compared

with non-transplanted individuals (Madan *et al.*, 2010).

Genetic aberrations

SCC. There is evidence that SCC development is a multistep process (Figure 1.14). This hypothesis is supported by the fact that these skin tumors develop as a consequence of cumulative UV damage. Actinic keratoses are believed to be precursor lesions of SCCs, whereas BCCs are thought to develop *de novo*. *p53* mutations can already be detected in unsuspicious epidermis. Their frequency increases with age and therefore it has been suggested that *p53* mutations represent an early if not initial event in the formation of squamous cell carcinomas. *p53* mutations are found in about 90% of SCCs (Madan *et al.*, 2010). In addition, changes in glutathione peroxidase activity lead to increased peroxide levels in cells causing increased cell damage (Walshe *et al.*, 2007). Advanced stages in the development of SCCs are associated with up-regulation of the cell cycle regulator cyclin D1 and loss of expression of the cell cycle inhibitor p16 due to genetic or epigenetic silencing (Burnworth *et al.*, 2007, 2006; Utikal *et al.*, 2005).

BCC. BCCs show a high frequency of *p53* mutations (50%), but also other pathways are frequently mutated, especially the sonic hedgehog (SHH) pathway (Figure 1.14) (Madan *et al.*, 2010). This pathway regulates cell growth and differentiation. Activation of the SHH pathway involves the binding of the sonic hedgehog (SHH) protein to a cell membrane receptor complex consisting of patched (PTCH)1 protein and smoothened (SMO) protein. *PTCH1* gene mutations prevent PTCH1 from binding to SMO. As a consequence, unbound SMO allows unregulated cell growth through activation of the transcription factors GLI1 and GLI2, activation of cell proliferation genes (including cyclin D, cyclin E and myc), and activation of regulators of angiogenesis.

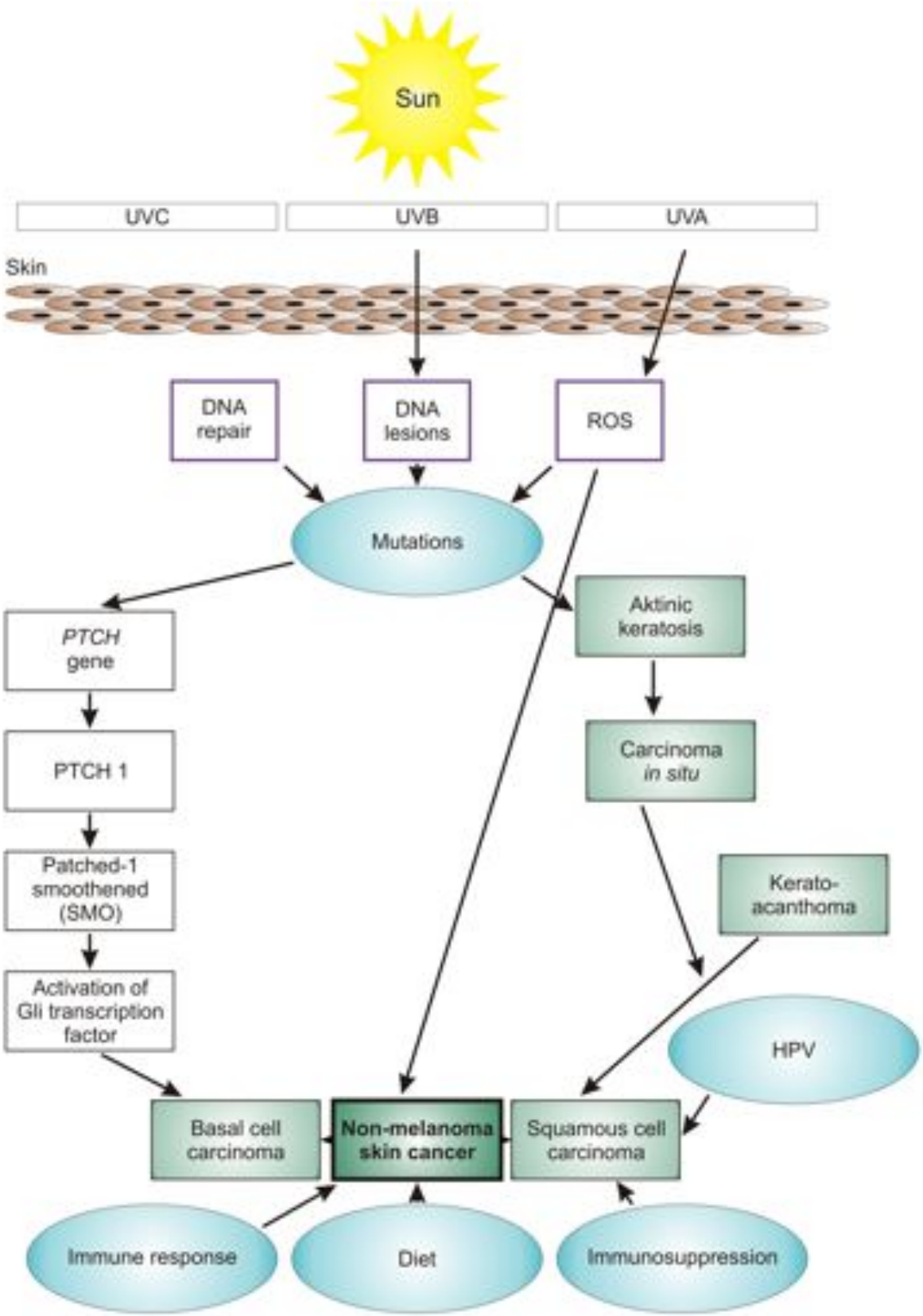

Continued on the following page

Figure 1.14. Development of SCCs and BCCs

Solar UVB and UVA radiation are thought to induce non-melanoma skin cancers. Squamous cell carcinoma development is a multistep process, which involves precursor lesions including actinic keratoses, keratoacanthomas and Bowen's disease. In contrast, basal cell carcinomas develop de novo. Immunosuppression, diet, HPV viral infections and immune responses contribute to the formation of non-melanoma skin cancers. Original figure adapted from Ahmed et al. (Ahmed et al., 2008)

1.4.2 Treatment of non-melanoma skin cancer

The treatment of non-melanoma skin cancer aims to remove the tumor, achieve high cure rates, preserve as much local tissue as possible and achieve an optimum cosmetic result (Chummun and McLean, 2011).

Prevention. If possible, prevention is the method of choice. Thus, agents like sunscreens and antioxidants are highly recommended. In addition, several substances have been suggested for potential prevention. The respective products include isotretinoin (vitamin A-derived retinoid) (Chakraborti, 2003), COX-2 inhibitors (COX-2 expression is increased by UV light exposure and may play a role in the formation of non-melanoma skin cancers) (An *et al.*, 2002; Buckman *et al.*, 1998), therapeutic vaccines against HPV infections (Lowy *et al.*, 2006) and silibinin (Singh and Agarwal, 2005). The latter compound has been proven to elicit several favorable effects, including inhibition of skin inflammation, DNA damage, epithelial cell proliferation and sunburns, alteration of mitogenic, apoptotic and survival signaling, activation of p53, induction of cell cycle arrest, and enhanced repair of DNA damage (Ahmed *et al.*, 2008; Singh and Agarwal, 2005).

Surgical options include surgical excision of the lesion, Mohs micrographic surgery and curettage and electrodessication. Non-surgical options are preferred if the risk

of disfigurement and functional impairment is high. The latter treatments include radiation therapy, cryosurgery, topical chemotherapeutic agents, modifier of biological immune response and photodynamic therapy.

Excisional surgery. Surgery is the most common treatment option for non-melanoma skin cancers and it is widely used for low-risk tumors. Cure rates are acceptable and combined with low costs. Furthermore, it allows full histological analysis of the tumor.

Mohs micrographic surgery (MMS). MMS involves several excisions of the tumor (horizontal sections). These sections are microscopically analyzed and re-excision is performed until the whole tumor is removed. MMS allows complete removal of the tumor and is more accurate compared to standard surgery, leading to recurrence rates of only 1% for BCC and 3% for SCC, compared to 5.3% and 8% recurrence in standard surgery (Chummun and McLean, 2011; Neville *et al.*, 2007; Thissen *et al.*, 1999).

Curettage and electrodessication. Superficial non-melanoma skin cancers are curetted down to normal looking tissue, followed by electrodessication of the basal skin layer to induce necrotic cell death. Cure rates of up to 93% have been achieved with this method, however, it should not be considered for treatment of recurrent or ill-defined tumors (Rowe *et al.*, 1989; Telfer *et al.*, 2008; Madan *et al.*, 2010).

Radiation therapy. This treatment option is successful in the management of primary and recurrent BCCs. It can be used as adjuvant therapy of aggressive SCCs showing invasion and metastasis (Voss and Kim-Sing, 1998). Furthermore, it is used as a palliative modality to improve quality of life for patients with advanced or incurable

disease (Veness, 2008; Madan *et al.*, 2010).

Liquid nitrogen cryosurgery. Tumor cells of low-risk primary basal cell and squamous cell carcinomas can be destroyed by liquid nitrogen. However, this treatment is only suggested for selected cases, and cosmetic results are worse compared to most standard surgical treatment options (Mallon *et al.*, 1996; Telfer *et al.*, 2008; Thissen *et al.*, 2001; Madan *et al.*, 2010).

Topical chemotherapy. 5-fluorouracil (5-FU) is the most commonly used topic agent in the treatment of non-melanoma skin cancers. It induces tumor cell death because it interferes with DNA and RNA synthesis by inhibiting the enzyme thymidylate synthetase, thereby preventing purine and pyrimidine from becoming incorporated into DNA during the S-phase of the cell cycle. 5-FU has been established as a drug for topical treatment of actinic keratosis and Bowen's disease but is rarely used to treat BCCs. Treatment of SCCs with 5-FU is not recommended. Drawbacks of 5-FU are side effects including inflammation and blistering, as well as the inability of the compound to penetrate into the dermis. Thus, its use is limited to the treatment of superficially growing skin cancers (Gross *et al.*, 2007; Sloan *et al.*, 1990; Madan *et al.*, 2010).

Biological immune-response modifier. Imiquimod is a synthetic immune response modifier belonging to the imidazoquinolone family. It stimulates innate and cell-mediated immune responses via stimulation of the Toll-like receptor 7. This effect leads to increased production and release of cytokines and chemokines and subsequent activation of TH-1 cell-mediated immunity (Chummun and McLean, 2011; Dummer *et al.*, 2003; Madan *et al.*, 2010).

Injection of interferons or cytostatic agents into the tumor. IFN induces apoptosis in BCC cells through the release of IL-2 and IL-10. Intralesional IFN is used for patients with BCC where surgery would lead to disfigurement. Cure rates vary between 50% and 80% (Chummun and McLean, 2011; Neville *et al.*, 2007).

Photodynamic therapy. This treatment option involves the topic or systemic application of photosensitizing agents and preferential accumulation of these compounds in tumor cells. Activation by a light source leads to production of reactive oxygen, induction of apoptosis or necrosis and selective damage to the tumor cells (Zeitouni *et al.*, 2003; Madan *et al.*, 2010).

1.4.3 Summary

Non-melanoma skin cancers are the most common type of cancer. Their incidence is rising every year. Treatment options are mainly limited to surgery and topical application of cytostatic agents. However, disfigurement, recurrence of the tumor and low drug efficiency are current limitations in the treatment of non-melanoma skin cancers. The development of more powerful therapeutic agents that preferentially kill tumor cells and show only low toxicity in healthy skin cells is still a challenge in the treatment of this disease.

References Chapter I

Abbasi, N., H. Shaw, D. Rigel, R. Friedman, W. McCarthy, I. Osman, A. Kopf, and D. Polsky (2004). Early diagnosis of cutaneous melanoma. *JAMA: the journal of the American Medical Association 292*(22), 2771–2776.

Ahmed, A., H. Soyer, N. Saunders, P. Boukamp, and M. Roberts (2008). Non-melanoma skin cancers. *Drug Discovery Today: Disease Mechanisms 5*(1), e55–e62.

An, K., M. Athar, X. Tang, S. Katiyar, J. Russo, J. Beech, M. Aszterbaum, L. Kopelovich, E. Epstein, H. Mukhtar, and D. Bickers (2002). Cyclooxygenase-2 expression in murine and human nonmelanoma skin cancers: Implications for therapeutic approaches. *Photochem Photobiol 76*(1), 73–80.

Änggård, E. and B. Samuelsson (1965). Biosynthesis of prostaglandins from arachidonic acid in guinea pig lung. *Journal of Biological Chemistry 240*(9), 3518–3521.

Aqel, N., R. Ball, H. Waldmann, and M. Mitchinson (1984). Monocytic origin of foam cells in human atherosclerotic plaques. *Atherosclerosis 53*(3), 265–271.

Asgari, M., N. Kiviat, C. Critchlow, J. Stern, Z. Argenyi, G. Raugi, D. Berg, P. Odland, S. Hawes, and E. de Villiers (2008). Detection of human papillomavirus dna in cutaneous squamous cell carcinoma among immunocompetent individuals. *Journal of Investigative Dermatology 128*(6), 1409–1417.

Balch, C., J. Gershenwald, S. Soong, J. Thompson, M. Atkins, D. Byrd, A. Buzaid, A. Cochran, D. Coit, S. Ding, *et al.* (2009). Final version of 2009 ajcc melanoma staging and classification. *Journal of Clinical Oncology 27*(36), 6199–6206.

Bartkova, J., J. Lukas, P. Guldberg, J. Alsner, A. Kirkin, J. Zeuthen, and J. Bartek (1996).

The p16-cyclin d/cdk4-prb pathway as a functional unit frequently altered in melanoma pathogenesis. *Cancer research 56*(23), 5475–5483.

Beeram, M., A. Patnaik, and E. Rowinsky (2005). Raf: a strategic target for therapeutic development against cancer. *Journal of clinical oncology 23*(27), 6771–6790.

Berliner, J., G. Subbanagounder, N. Leitinger, A. Watson, D. Vora, *et al.* (2001). Evidence for a role of phospholipid oxidation products in atherogenesis. *Trends in cardiovascular medicine 11*(3-4), 142.

Bhatia, S., S. Tykodi, and J. Thompson (2009). Treatment of metastatic melanoma: an overview. *Oncology (Williston Park, NY) 23*(6), 488.

Blesa, J., E. Pulido, V. Candel, and M. Pulla (2011). Melanoma: from darkness to promise. *American Journal of Clinical Oncology 34*(2), 179.

Bochkov, V. (2007). Inflammatory profile of oxidized phospholipids. *Thrombosis and Haemostasis-Stuttgart- 97*(3), 348.

Bochkov, V., O. Oskolkova, K. Birukov, A. Levonen, C. Binder, and J. Stöckl (2010). Generation and biological activities of oxidized phospholipids. *Antioxidants & redox signaling 12*(8), 1009–1059.

Boukamp, P. (2005). Uv-induced skin cancer: Similarities–variations. *JDDG: Journal der Deutschen Dermatologischen Gesellschaft 3*(7), 493–503.

Box, N. and T. Terzian (2008). The role of p53 in pigmentation, tanning and melanoma. *Pigment cell & melanoma research 21*(5), 525–533.

Bradford, P., D. Freedman, A. Goldstein, and M. Tucker (2010). Increased risk of second primary cancers after a diagnosis of melanoma. *Archives of dermatology 146*(3), 265.

Buckman, S., A. Gresham, P. Hale, G. Hruza, J. Anast, J. Masferrer, and A. Pentland (1998). Cox-2 expression is induced by uvb exposure in human skin: implications for the development of skin cancer. *Carcinogenesis 19*(5), 723–729.

Burnworth, B., S. Arendt, S. Muffler, V. Steinkraus, E. Bröcker, C. Birek, W. Hartschuh, A. Jauch, and P. Boukamp (2007). The multi-step process of human skin carcinogenesis: a role for p53, cyclin d1, htert, p16, and tsp-1. *European journal of cell biology 86*(11), 763–780.

Burnworth, B., S. Popp, H. Stark, V. Steinkraus, E. Bröcker, W. Hartschuh, C. Birek, and P. Boukamp (2006). Gain of 11q/cyclin d1 overexpression is an essential early step in skin cancer development and causes abnormal tissue organization and differentiation. *Oncogene 25*(32), 4399–4412.

Center, M., R. Siegel, and A. Jemal (2011). American cancer society global cancer: Facts and figures.

Chakraborti, S. (2003). Phospholipase a2 isoforms: a perspective. *Cellular signalling 15*(7), 637–665.

Chang, M., C. Binder, Y. Miller, G. Subbanagounder, G. Silverman, J. Berliner, and J. Witztum (2004). Apoptotic cells with oxidation-specific epitopes are immunogenic and proinflammatory. *The Journal of experimental medicine 200*(11), 1359–1370.

Chisolm, G. and D. Steinberg (2000). The oxidative modification hypothesis of atherogenesis: an overview. *Free radical biology and medicine 28*(12), 1815–1826.

Chummun, S. and N. McLean (2011). Management of malignant skin cancers. *Surgery (Oxford) 29*(10), 529–533.

Cifone, M. and I. Fidler (1981). Increasing metastatic potential is associated with increasing genetic instability of clones isolated from murine neoplasms. *Proceedings of the National Academy of Sciences 78*(11), 6949–6952.

Clark, W. (1991). Tumour progression and the nature of cancer. *British journal of cancer 64*(4), 631.

Criscione, V., M. Weinstock, M. Naylor, C. Luque, M. Eide, and S. Bingham (2009). Actinic keratoses. *Cancer 115*(11), 2523–2530.

Crombie, I. (1979). Racial differences in melanoma incidence. *British journal of cancer 40*(2), 185.

Curtin, J., K. Busam, D. Pinkel, and B. Bastian (2006). Somatic activation of kit in distinct subtypes of melanoma. *Journal of clinical oncology 24*(26), 4340–4346.

Davies, H., G. Bignell, C. Cox, P. Stephens, S. Edkins, S. Clegg, J. Teague, H. Woffendin, M. Garnett, W. Bottomley, *et al.* (2002). Mutations of the braf gene in human cancer. *Nature 417*(6892), 949–954.

Di Micco, R., M. Fumagalli, A. Cicalese, S. Piccinin, P. Gasparini, C. Luise, C. Schurra, M. Garre, P. Nuciforo, A. Bensimon, *et al.* (2006). Oncogene-induced senescence is a dna damage response triggered by dna hyper-replication. *Nature 444*(7119), 638–642.

Dummer, R., M. Urosevic, W. Kempf, K. Hoek, J. Hafner, and G. Burg (2003). Imiquimod in basal cell carcinoma: how does it work? *British Journal of Dermatology 149*(s66), 57–58.

Emuss, V., M. Garnett, C. Mason, R. Marais, *et al.* (2005). Mutations of c-raf are rare in human cancer because c-raf has a low basal kinase activity compared with b-raf. *Cancer research 65*(21), 9719–9726.

English, D., B. Armstrong, A. Kricker, and C. Fleming (1997). Sunlight and cancer. *Cancer Causes and Control 8*(3), 271–283.

Fadeel, B. (2003). Programmed cell clearance. *Cellular and molecular life sciences 60*(12), 2575–2585.

Faggiotto, A., R. Ross, and L. Harker (1984). Studies of hypercholesterolemia in the nonhuman primate. i. changes that lead to fatty streak formation. *Arteriosclerosis, Thrombosis, and Vascular Biology 4*(4), 323–340.

Flaherty, K., I. Puzanov, K. Kim, A. Ribas, G. McArthur, J. Sosman, P. O'Dwyer, R. Lee, J. Grippo, K. Nolop, *et al.* (2010). Inhibition of mutated, activated braf in metastatic melanoma. *New England Journal of Medicine 363*(9), 809–819.

Fountain, J., S. Bale, D. Housman, N. Dracopoli, *et al.* (1990). Genetics of melanoma. *Cancer surveys 9*(4), 645.

Fowler, S., H. Shio, and N. Haley (1979). Characterization of lipid-laden aortic cells from cholesterol-fed rabbits. iv. investigation of macrophage-like properties of aortic cell populations. *Laboratory investigation; a journal of technical methods and pathology 41*(4), 372.

Fruhwirth, G., A. Loidl, and A. Hermetter (2007). Oxidized phospholipids: from molecular properties to disease. *Biochimica et Biophysica Acta (BBA)-Molecular Basis of Disease 1772*(7), 718–736.

Fruhwirth, G., A. Moumtzi, A. Loidl, E. Ingolic, and A. Hermetter (2006). The oxidized phospholipids povpc and pgpc inhibit growth and induce apoptosis in vascular smooth muscle cells. *Biochimica et Biophysica Acta (BBA)-Molecular and Cell Biology of Lipids 1761*(9), 1060–1069.

Fuchs, J. and L. Packer (1990). Ultraviolet irradiation and the skin antioxidant system. *Photodermatology 7*(2), 90–92.

Gallagher, R., D. McLean, C. Yang, A. Coldman, H. Silver, J. Spinelli, and M. Beagrie (1990). Suntan, sunburn, and pigmentation factors and the frequency of acquired melanocytic nevi in children: similarities to melanoma: the vancouver mole study. *Archives of dermatology 126*(6), 770.

Gerrity, R. (1981a). The role of the monocyte in atherogenesis: I. transition of blood-borne monocytes into foam cells in fatty lesions. *The American journal of pathology 103*(2), 181.

Gerrity, R. (1981b). The role of the monocyte in atherogenesis: Ii. migration of foam cells from atherosclerotic lesions. *The American journal of pathology 103*(2), 191.

Glass, A. and R. Hoover (1989). The emerging epidemic of melanoma and squamous cell skin cancer. *JAMA: the journal of the American Medical Association 262*(15), 2097–2100.

Goel, V., A. Lazar, C. Warneke, M. Redston, and F. Haluska (2006). Examination of mutations in braf, nras, and pten in primary cutaneous melanoma. *Journal of investigative dermatology 126*(1), 154–160.

Goldman, L., D. Elder, W. Clark Jr, M. Mastrangelo, and J. Stennett (1986). Assessment of survival rates with metastatic malignant melanomas. *Surgery, gynecology & obstetrics 162*(3), 199–203.

Goldstein, L. and S. Brown (1977). The low-density lipoprotein pathway and its relation to atherosclerosis. *Annual review of biochemistry 46*(1), 897–930.

Green, A. *et al.* (1992). Changing patterns in incidence of non-melanoma skin cancer. *Epithelial cell biology 1*(1), 47.

Greenberg, M., X. Li, B. Gugiu, X. Gu, J. Qin, R. Salomon, and S. Hazen (2008). The lipid whisker model of the structure of oxidized cell membranes. *Journal of Biological Chemistry 283*(4), 2385.

Greene, M. (2000). The genetics of hereditary melanoma and nevi. *Cancer 86*(S11), 2464–2477.

Greene, M., R. Sanders, F. Chu, W. Clark Jr, D. Elder, D. Cogan, *et al.* (1983). The familial occurrence of cutaneous melanoma, intraocular melanoma, and the dysplastic nevus syndrome. *American journal of ophthalmology 96*(2), 238.

Gross, K., L. Kircik, and G. Kricorian (2007). 5% 5-fluorouracil cream for the treatment of small superficial basal cell carcinoma: Efficacy, tolerability, cosmetic outcome, and patient satisfaction. *Dermatologic surgery 33*(4), 433–440.

Gruber, F., M. Kaštelan, I. Brajac, M. Saftić, V. Peharda, L. Čabrijan, Z. Stanić Žgombić, and E. Simonić (2008). Molecular and genetic mechanisms in melanoma. *Collegium antropologicum 32*(2), 147–152.

Haluska, F., H. Tsao, H. Wu, F. Haluska, A. Lazar, and V. Goel (2006). Genetic alterations in signaling pathways in melanoma. *Clinical cancer research 12*(7), 2301s–2307s.

Hammarstrom, S. (1983). Leukotrienes. *Annual review of biochemistry 52*(1), 355–377.

Hanahan, D. and R. Weinberg (2000). The hallmarks of cancer. *cell 100*(1), 57–70.

Hanahan, D. and R. Weinberg (2011). Hallmarks of cancer: the next generation. *Cell 144*(5), 646–674.

Harwood, C., T. Surentheran, J. McGregor, P. Spink, I. Leigh, J. Breuer, and C. Proby (2000). Human papillomavirus infection and non-melanoma skin cancer in immunosuppressed and immunocompetent individuals. *Journal of medical virology 61*(3), 289–297.

Heidorn, S., C. Milagre, S. Whittaker, A. Nourry, I. Niculescu-Duvas, N. Dhomen, J. Hussain, J. Reis-Filho, C. Springer, C. Pritchard, *et al.* (2010). Kinase-dead braf and oncogenic ras cooperate to drive tumor progression through craf. *Cell 140*(2), 209–221.

Hocker, T., M. Singh, and H. Tsao (2008). Melanoma genetics and therapeutic approaches in the 21st century: moving from the benchside to the bedside. *Journal of Investigative Dermatology 128*(11), 2575–2595.

Hodi, F., S. O'Day, D. McDermott, R. Weber, J. Sosman, J. Haanen, R. Gonzalez, C. Robert, D. Schadendorf, J. Hassel, *et al.* (2010). Improved survival with ipilimumab in patients with metastatic melanoma. *New England Journal of Medicine 363*(8), 711–723.

Huber, J., A. Vales, G. Mitulovic, M. Blumer, R. Schmid, J. Witztum, B. Binder, and N. Leitinger (2002). Oxidized membrane vesicles and blebs from apoptotic cells contain biologically active oxidized phospholipids that induce monocyte-endothelial interactions. *Arteriosclerosis, thrombosis, and vascular biology 22*(1), 101–107.

Hughes, M., J. Van Der Pols, G. Marks, and A. Green (2006). Food intake and risk of squamous cell carcinoma of the skin in a community: the nambour skin cancer cohort study. *International journal of cancer 119*(8), 1953–1960.

Ibiebele, T., J. van der Pols, M. Hughes, G. Marks, G. Williams, and A. Green (2007). Dietary pattern in association with squamous cell carcinoma of the skin: a prospective study. *The American journal of clinical nutrition 85*(5), 1401–1408.

Karagas, M., H. Nelson, P. Sehr, T. Waterboer, T. Stukel, A. Andrew, A. Green, J. Bavinck, A. Perry, S. Spencer, *et al.* (2006). Human papillomavirus infection and incidence of squamous cell and basal cell carcinomas of the skin. *Journal of the National Cancer Institute 98*(6), 389–395.

Karagas, M., T. Stukel, V. Umland, M. Tsoukas, L. Mott, H. Sorensen, A. Jensen, H. Nelson, S. Spencer, A. Perry, *et al.* (2007). Reported use of photosensitizing medications and basal cell and squamous cell carcinoma of the skin: results of a population-based case–control study. *Journal of Investigative Dermatology 127*(12), 2901–2903.

Kennedy, C., C. Bajdik, R. Willemze, and J. Bouwes Bavinck (2005). Chemical exposures other than arsenic are probably not important risk factors for squamous cell carcinoma, basal cell carcinoma and malignant melanoma of the skin. *British Journal of Dermatology 152*(1), 194–197.

Kockx, M. (1998). Apoptosis in the atherosclerotic plaque quantitative and qualitative aspects. *Arteriosclerosis, thrombosis, and vascular biology 18*(10), 1519–1522.

Kuphal, S. and A. Bosserhoff (2009). Recent progress in understanding the pathology of malignant melanoma. *The Journal of pathology 219*(4), 400–409.

Lacour, J. (2002). Carcinogenesis of basal cell carcinomas: genetics and molecular mechanisms. *British Journal of Dermatology 146*(s61), 17–19.

Lassam, N., S. Bickford, *et al.* (1992). Loss of c-kit expression in cultured melanoma cells. *Oncogene 7*(1), 51.

Lee, J., Y. Soung, S. Kim, W. Park, S. Nam, W. Min, S. Kim, J. Lee, N. Yoo, and S. Lee (2005). Mutational analysis of the araf gene in human cancers. *Apmis 113*(1), 54–7.

Leitinger, N., T. Tyner, L. Oslund, C. Rizza, G. Subbanagounder, H. Lee, P. Shih, N. Mackman, G. Tigyi, M. Territo, *et al.* (1999). Structurally similar oxidized phospholipids differentially regulate endothelial binding of monocytes and neutrophils. *Proceedings of the National Academy of Sciences 96*(21), 12010.

Leitinger, N., A. Watson, K. Faull, A. Fogelman, and J. Berliner (1998). *Monocyte binding to endothelial cells induced by oxidized phospholipids present in minimally oxidized low density lipoprotein is inhibited by a platelet activating factor receptor antagonist In*. Plenum Press, New York.

Levine, A. (1997). p53, the cellular gatekeeper review for growth and division. *Cell 88*, 323–331.

Libby, P., Y. GENG, G. Sukhova, D. Simon, and R. Lee (1997). Molecular determinants of atherosclerotic plaque vulnerabilitya. *Annals of the New York Academy of Sciences 811*(1), 134–145.

Lichter, M., M. Karagas, L. Mott, S. Spencer, T. Stukel, E. Greenberg, *et al.* (2000). Therapeutic ionizing radiation and the incidence of basal cell carcinoma and squamous cell carcinoma. *Archives of dermatology 136*(8), 1007.

Loidl, A., E. Sevcsik, G. Riesenhuber, H. Deigner, and A. Hermetter (2003). Oxidized phospholipids in mmldl induce apoptotic signaling via activation of acid sphingomyelinase in arterial smooth muscle cells. *Journal of Biological Chemistry 278*(35), 32921.

Lowy, D., J. Schiller, *et al.* (2006). Prophylactic human papillomavirus vaccines. *Journal of Clinical Investigation 116*(5), 1167.

Madan, V., J. Lear, and R. Szeimies (2010). Non-melanoma skin cancer. *The Lancet 375*(9715), 673–685.

Maelandsmo, G., V. Flørenes, E. Hovig, T. Oyjord, O. Engebraaten, R. Holm, A. Børresen, and O. Fodstad (1996). Involvement of the prb/p16/cdk4/cyclin d1 pathway in the tumorigenesis of sporadic malignant melanomas. *British journal of cancer 73*(8), 909.

Mahley, R., T. Innerarity, K. Weisgraber, and S. Oh (1979). Altered metabolism (in vivo and in vitro) of plasma lipoproteins after selective chemical modification of lysine residues of the apoproteins. *Journal of Clinical Investigation 64*(3), 743.

Mallat, Z. and A. Tedgui (2009). Apoptosis in the vasculature: mechanisms and functional importance. *British journal of pharmacology 130*(5), 947–962.

Mallon, E., R. Dawber, *et al.* (1996). Cryosurgery in the treatment of basal cell carcinoma. assessment of one and two freeze-thaw cycle schedules. *Dermatologic surgery: official publication for American Society for Dermatologic Surgery [et al.] 22*(10), 854.

Martinet, W. and M. Kockx (2001). Apoptosis in atherosclerosis: focus on oxidized lipids and inflammation. *Current opinion in lipidology 12*(5), 535–541.

McConkey, D. (1998). Biochemical determinants of apoptosis and necrosis. *Toxicology letters 99*(3), 157–168.

McIntyre, T., G. Zimmerman, and S. Prescott (1999). Biologically active oxidized phospholipids. *Journal of Biological Chemistry 274*(36), 25189–25192.

Michaloglou, C., L. Vredeveld, M. Soengas, C. Denoyelle, T. Kuilman, C. van der Horst, D. Majoor, J. Shay, W. Mooi, and D. Peeper (2005). Brafe600-associated senescence-like cell cycle arrest of human naevi. *Nature 436*(7051), 720–724.

Molho-Pessach, V., M. Lotem, *et al.* (2007). Ultraviolet radiation and cutaneous carcinogenesis. *Current Problems In Dermatology 35*, 14.

Mooi, W. and D. Peeper (2006). Oncogene-induced cell senescence halting on the road to cancer. *New England Journal of Medicine 355*(10), 1037–1046.

Moumtzi, A., M. Trenker, K. Flicker, E. Zenzmaier, R. Saf, and A. Hermetter (2007). Import and fate of fluorescent analogs of oxidized phospholipids in vascular smooth muscle cells. *Journal of lipid research 48*(3), 565–582.

Nakamura, T., P. Henson, and R. Murphy (1998). Occurrence of oxidized metabolites

of arachidonic acid esterified to phospholipids in murine lung tissue. *Analytical biochemistry 262*(1), 23–32.

Neale, R., M. Davis, N. Pandeya, D. Whiteman, A. Green, *et al.* (2007). Basal cell carcinoma on the trunk is associated with excessive sun exposure. *Journal of the American Academy of Dermatology 56*(3), 380.

Neville, J., E. Welch, and D. Leffell (2007). Management of nonmelanoma skin cancer in 2007. *Nature Clinical Practice Oncology 4*(8), 462–469.

Nikolaou, V., A. Stratigos, K. Flaherty, and H. Tsao (2012). Melanoma: new insights and new therapies. *Journal of Investigative Dermatology 132*, 854–863.

Nindl, I., M. Gottschling, and E. Stockfleth (2007). Human papillomaviruses and non-melanoma skin cancer: basic virology and clinical manifestations. *Disease markers 23*(4), 247–259.

Nordlund, J. (2007). The melanocyte and the epidermal melanin unit: an expanded concept. *Dermatologic clinics 25*(3), 271–281.

Nys, K., H. Maes, A. Dudek, and P. Agostinis (2011). Uncovering the role of hypoxia inducible factor-1α in skin carcinogenesis. *Biochimica et Biophysica Acta (BBA)-Reviews on Cancer 1816*(1), 1–12.

Odenbro, Å., R. Bellocco, P. Boffetta, B. Lindelöf, and J. Adami (2005). Tobacco smoking, snuff dipping and the risk of cutaneous squamous cell carcinoma: a nationwide cohort study in sweden. *British journal of cancer 92*(7), 1326–1328.

Ogden, S. and N. Telfer (2009). Skin cancer. *Medicine 37*(6), 305–308.

Palmieri, G., M. Capone, M. Ascierto, G. Gentilcore, D. Stroncek, M. Casula, M. Sini, M. Palla, N. Mozzillo, and P. Ascierto (2009). Main roads to melanoma. *Journal of translational medicine 7*(1), 86.

Parkin, D., D. Mesher, and P. Sasieni (2011). 13. cancers attributable to solar (ultraviolet) radiation exposure in the uk in 2010. *British journal of cancer 105*, S66–S69.

Pitas, R., J. Boyles, R. Mahley, D. Bissell, *et al.* (1985). Uptake of chemically modified low density lipoproteins in vivo is mediated by specific endothelial cells. *J Cell Biol 100*(1), 103–117.

Pleasance, E., R. Cheetham, P. Stephens, D. McBride, S. Humphray, C. Greenman, I. Varela, M. Lin, G. Ordóñez, G. Bignell, *et al.* (2009). A comprehensive catalogue of somatic mutations from a human cancer genome. *Nature 463*(7278), 191–196.

Pollman, M., J. Hall, M. Mann, L. Zhang, and G. Gibbons (1998). Inhibition of neointimal cell bcl-x expression induces apoptosis and regression of vascular disease. *Nature medicine 4*(2), 222–227.

Pomerantz, J., N. Schreiber-Agus, N. Liégeois, A. Silverman, L. Alland, L. Chin, J. Potes, K. Chen, I. Orlow, H. Lee, *et al.* (1998). The ink4a tumor suppressor gene product, p19 arf, interacts with mdm2 and neutralizes mdm2's inhibition of p53. *Cell 92*(6), 713–723.

Purcell, W. and R. Donehower (2002). Evolving therapies: farnesyltransferase inhibitors. *Current oncology reports 4*(1), 29–36.

Qin, J., R. Goswami, R. Balabanov, and G. Dawson (2007). Oxidized phosphatidylcholine is a marker for neuroinflammation in multiple sclerosis brain. *Journal of neuroscience research 85*(5), 977–984.

Reed, K., J. Brewer, C. Lohse, K. Bringe, C. Pruitt, and L. Gibson (2012). Increasing incidence of melanoma among young adults: An epidemiological study in olmsted county, minnesota. In *Mayo Clinic Proceedings*, Volume 87, pp. 328–334. Elsevier.

Ross, R. (1993). The pathogenesis of atherosclerosis: a perspective for the 1990s. *Nature 362*, 801.

Rowe, D., R. Carroll, C. Day Jr, *et al.* (1989). Long-term recurrence rates in previously untreated (primary) basal cell carcinoma: implications for patient follow-up. *The Journal of dermatologic surgery and oncology 15*(3), 315.

Samuelsson, B., S. Dahlen, J. Lindgren, C. Rouzer, C. Serhan, *et al.* (1987). Leukotrienes and lipoxins: structures, biosynthesis, and biological effects. *Science (New York, NY) 237*(4819), 1171.

Schaffner, T., K. Taylor, E. Bartucci, K. Fischer-Dzoga, J. Beeson, S. Glagov, and R. Wissler (1980). Arterial foam cells with distinctive immunomorphologic and histochemical features of macrophages. *The American journal of pathology 100*(1), 57.

Singh, R. and R. Agarwal (2005). Mechanisms and preclinical efficacy of silibinin in preventing skin cancer. *European Journal of Cancer 41*(13), 1969–1979.

Slipicevic, A. and M. Herlyn (2012). Narrowing the knowledge gaps for melanoma. *Upsala Journal of Medical Sciences 117*(2), 237–243.

Sloan, K., E. Sherertz, and R. McTiernan (1990). The effect of 5-fluorouracil on inhibition of epidermal dna synthesis in vivo: a comparison of the effect of formulations and a prodrug of 5-fu. *Archives of dermatological research 282*(7), 484–486.

Stein, O. and Y. Stein (1980). Bovine aortic endothelial cells display macrophage-like properties towards acetylated 125 i-labelled low density lipoprotein. *Biochimica et Biophysica Acta (BBA)-Lipids and Lipid Metabolism 620*(3), 631–635.

Stemmer, U., Z. Dunai, D. Koller, G. Pürstinger, E. Zenzmaier, H. Deigner, E. Aflaki, D. Kratky, and A. Hermetter (2012). Toxicity of oxidized phospholipids in cultured macrophages. *Lipids in Health and Disease 11*(1), 110.

Stemmer, U. and A. Hermetter (2012). Protein modification by aldehydophospholipids and its functional consequences. *Biochimica et Biophysica Acta (BBA)-Biomembranes*.

Stemmer, U., C. Ramprecht, E. Zenzmaier, B. Stojčić, G. Rechberger, M. Kollroser, and A. Hermetter (2012). Uptake and protein targeting of fluorescent oxidized phospholipids in cultured raw 264.7 macrophages. *Biochimica et Biophysica Acta (BBA)-Molecular and Cell Biology of Lipids*.

Stocker, R. and J. Keaney (2004). Role of oxidative modifications in atherosclerosis. *Physiological reviews 84*(4), 1381–1478.

Stretch, J., K. Gatter, E. Ralfkiaer, D. Lane, and A. Harris (1991). Expression of mutant p53 in melanoma. *Cancer research 51*(21), 5976–5979.

Talve, L., I. Sauroja, Y. Collan, K. Punnonen, and T. Ekfors (1998). Loss of expression of the p16ink4/cdkn2 gene in cutaneous malignant melanoma correlates with tumor cell proliferation and invasive stage. *International journal of cancer 74*(3), 255–259.

Tamura, M., J. Gu, K. Matsumoto, S. Aota, R. Parsons, and K. Yamada (1998). Inhibition of cell migration, spreading, and focal adhesions by tumor suppressor pten. *Science 280*(5369), 1614–1617.

Telfer, N., G. Colver, and C. Morton (2008). Guidelines for the management of basal cell carcinoma. *British Journal of Dermatology 159*(1), 35–48.

Thissen, M., M. Neumann, and L. Schouten (1999). A systematic review of treatment modalities for primary basal cell carcinomas. *Archives of dermatology 135*(10), 1177.

Thissen, M., F. Nieman, A. Ideler, P. Berretty, and H. Neumann (2001). Cosmetic results of cryosurgery versus surgical excision for primary uncomplicated basal cell carcinomas of the head and neck. *Dermatologic surgery 26*(8), 759–764.

Trakatelli, M., C. Ulrich, V. Del Marmol, S. Euvrard, E. Stockfleth, and D. Abeni (2007). Epidemiology of nonmelanoma skin cancer (nmsc) in europe: accurate and comparable data are needed for effective public health monitoring and interventions. *British Journal of Dermatology 156*(s3), 1–7.

Tsao, H., M. Atkins, and A. Sober (2004). Management of cutaneous melanoma. *New England Journal of Medicine 351*(10), 998–1012.

Tsimikas, S., E. Brilakis, R. Lennon, E. Miller, J. Witztum, J. McConnell, K. Kornman, and P. Berger (2007). Relationship of igg and igm autoantibodies to oxidized

low density lipoprotein with coronary artery disease and cardiovascular events. *Journal of lipid research 48*(2), 425–433.

Utikal, J., M. Udart, U. Leiter, P. Kaskel, R. Peter, and G. Krähn (2005). Numerical abnormalities of the cyclin d1 gene locus on chromosome 11q13 in non-melanoma skin cancer. *Cancer letters 219*(2), 197–204.

Van Lenten, B., A. Wagner, M. Navab, G. Anantharamaiah, E. Hui, D. Nayak, and A. Fogelman (2004). D-4f, an apolipoprotein ai mimetic peptide, inhibits the inflammatory response induced by influenza a infection of human type ii pneumocytes. *Circulation 110*(20), 3252–3258.

Veness, M. (2008). The important role of radiotherapy in patients with non-melanoma skin cancer and other cutaneous entities. *Journal of medical imaging and radiation oncology 52*(3), 278–286.

Villanueva, J., A. Vultur, and M. Herlyn (2011). Resistance to braf inhibitors: unraveling mechanisms and future treatment options. *Cancer research 71*(23), 7137–7140.

Volkenandt, M., U. Schlegel, D. Nanus, and A. Albino (2006). Mutational analysis of the human p53 gene in malignant melanoma. *Pigment cell research 4*(1), 35–40.

Voss, N. and C. Kim-Sing (1998). Radiotherapy in the treatment of dermatologic malignancies. *Dermatologic clinics 16*(2), 313–20.

Walshe, J., M. Serewko-Auret, N. Teakle, S. Cameron, K. Minto, L. Smith, P. Burcham, T. Russell, G. Strutton, A. Griffin, *et al.* (2007). Inactivation of glutathione peroxidase activity contributes to uv-induced squamous cell carcinoma formation. *Cancer research 67*(10), 4751–4758.

Wang, B., H. Ho, P. Lin, S. Schwarzacher, M. Pollman, G. Gibbons, P. Tsao, and J. Cooke (1999). Regression of atherosclerosis role of nitric oxide and apoptosis. *Circulation 99*(9), 1236–1241.

Watson, A., N. Leitinger, M. Navab, K. Faull, S. Hörkkö, J. Witztum, W. Palinski, D. Schwenke, R. Salomon, W. Sha, *et al.* (1997). Structural identification by

mass spectrometry of oxidized phospholipids in minimally oxidized low density lipoprotein that induce monocyte/endothelial interactions and evidence for their presence in vivo. *Journal of Biological Chemistry 272*(21), 13597–13607.

Watson, A., M. Navab, S. Hama, A. Sevanian, S. Prescott, D. Stafforini, T. McIntyre, B. Du, A. Fogelman, and J. Berliner (1995). Effect of platelet activating factor-acetylhydrolase on the formation and action of minimally oxidized low density lipoprotein. *Journal of Clinical Investigation 95*(2), 774.

Witztum, J. and J. Berliner (1998). Oxidized phospholipids and isoprostanes in atherosclerosis. *Current opinion in lipidology 9*(5), 441–448.

Wong, C., R. Strange, and J. Lear (2003). Basal cell carcinoma. *BMJ: British Medical Journal 327*(7418), 794.

Yoshimi, N., Y. Ikura, Y. Sugama, S. Kayo, M. Ohsawa, S. Yamamoto, Y. Inoue, K. Hirata, H. Itabe, J. Yoshikawa, *et al.* (2005). Oxidized phosphatidylcholine in alveolarmacrophages in idiopathic interstitial pneumonias. *Lung 183*(2), 109–121.

Zaidi, M., C. Day, and G. Merlino (2008). From uvs to metastases: modeling melanoma initiation and progression in the mouse. *Journal of Investigative Dermatology 128*(10), 2381–2391.

Zebisch, A., P. Staber, A. Delavar, C. Bodner, K. Hiden, K. Fischereder, M. Janakiraman, W. Linkesch, H. Auner, W. Emberger, *et al.* (2006). Two transforming c-raf germ-line mutations identified in patients with therapy-related acute myeloid leukemia. *Cancer research 66*(7), 3401–3408.

Zeitouni, N., A. Oseroff, and S. Shieh (2003). Photodynamic therapy for nonmelanoma skin cancers: current review and update. *Molecular immunology 39*(17), 1133–1136.

Chapter 2

Oxidized Phospholipids Preferentially Induce Apoptosis in Human Melanoma Cells but not Primary Human Melanocytes

Oxidized Phospholipids Preferentially Induce Apoptosis in Human Melanoma Cells but not Primary Human Melanocytes

Claudia Ramprecht[1], Hannah Jaritz[1], Ingo Streith[2], Elfriede Zenzmaier[1], Harald Köfeler[3], Helmut Schaider[4] and Albin Hermetter[1]

[1] *Department of Biochemistry, Graz University of Technology, Graz, Austria*

[2] *Institute of Molecular Biosciences, Karl-Franzens University Graz, Graz, Austria*

[3] *Core Facility for Mass Spectrometry, Center for Medical Research, Medical University of Graz, Austria*

[4] *Cancer Biology Unit, Department of Dermatology, Medical University Graz, Graz, Austria and Center for Medical Research (ZMF), Medical University Graz, Grau, Austria*

2.1 Abstract

The oxidized phospholipids (oxPL) 1-palmitoyl-2-glutaroyl-*sn*-glycero-3-phosphocholine (PGPC) and 1-palmitoyl-2-(5-oxovaleroyl)-*sn*-glycero-3-phosphocholine (POVPC) are formed upon oxidation of 1-palmitoyl-2-arachidonoyl-phosphatidylcholine in lipoproteins and cell membranes. Both oxPL share high structural similarities: they contain a long hydrophobic chain at the *sn*-1 position, and a shortened polar chain at position *sn*-2 which is part of a very large headgroup. Therefore, PGPC and POVPC are highly amphipathic molecules and as a consequence exchange easily between cells, membranes and lipoproteins, where they perturb lipid organization and protein function.

We found that PGPC and POVPC selectively induce cell death in human melanoma cells isolated from different stages of tumor progression but leave primary human melanocytes almost unaffected. The toxicity of both compounds was associated with efficient lipid uptake into the tumor cells, activation of acid sphingomyelinase and cell line-dependent formation of the apoptotic second messenger ceramide. In summary, both compounds show useful properties. First of all, their toxicity is preferentially expressed in malignant cells. Secondly, they are naturally formed in the body and resistance to these compounds is not likely to occur.

2.2 Introduction

Melanomas are highly heterogeneous as are most tumor cells within one lesion (Quintana *et al.*, 2010; Shackleton *et al.*, 2009). There are hundreds of different genetic al-

terations that drive cancer cells to grow, migrate, invade and survive (Palmieri *et al.*, 2009; Sauter *et al.*, 1998). As a consequence blocking just a single signaling pathway by an inhibitor is not sufficient to kill all tumor cells. Malignant cells within one tumor often differently respond to therapy, some may even be completely unaffected. For instance, some sub-populations may have more efficient efflux pumps for drug removal (Luo *et al.*, 2012), whereas some do not proliferate at all. Many of these properties make them inaccessible to most of the currently used drugs, which are proliferation antagonists. Thus, recent therapeutic strategies are based on the combination of multiple pathway inhibitors, and new concepts have evolved such as individualized therapies and combination therapies (Nikolaou *et al.*, 2012). However, the required identification of mutations for each patient receiving signal transduction inhibitors is time-consuming and costly. For these reasons, there is a need for a general approach for the treatment of melanomas, aiming at targeting all cancer cells within a tumor independent of individual differences in their genetic background.

Here we describe an approach, which is based on oxidized phospholipids, which are major components of oxidized LDL. The respective compounds are the choline phospholipids 1-palmitoyl-2-glutaroyl-*sn*-glycero-3-phosphocholine (PGPC) and 1-palmitoyl-2-(5-oxovaleroyl)- *sn*-glycero-3-phosphocholine (POVPC). Next to a variety of other products, these compounds are oxidative modifications of arachidonic acid in position *sn*-2 of phosphatidylcholine in lipoproteins and cell membranes (Fruhwirth *et al.*, 2007). Both oxPL share high structural similarities: they contain a long hydrophobic chain at the *sn*-1 position, and a shortened polar chain at position *sn*-2, which is part of a very large headgroup. As a consequence, PGPC and POVPC are highly amphipathic molecules and exchange easily between cells, membranes and

lipoproteins, where they perturb lipid organization (Stemmer *et al.*, 2012).

Here, we present a novel, generalized strategy that can be the basis for the treatment of skin cancer and other types of cancer irrespective of their genetic background. It makes use of a subclass of oxidized phospholipids that are formed endogenously in the human body under oxidative stress. The respective compounds are the truncated phosphatidylcholines PGPC and POVPC (see Figure 2.1) which contain a long fatty acid and a short carboxylic acid in positions *sn*-1 and -2 of the phospholipid, respectively. We provide evidence that these oxidized phospholipids preferentially kill skin cancer cells in culture but leave primary human melanocytes almost unaffected. In this context, we investigated the toxicity, uptake and target interactions of the cytotoxic compounds in cultured human melanoma cells of different stages. The basis for our study was the observation, that truncated oxPL which are components of oxidized low density lipoprotein (oxLDL) and minimally modified low density lipoprotein (mmLDL) are cytotoxic in cells of the arterial wall thus playing an important role in the development and progression of atherosclerosis. The toxic lipid effects include inflammation, proliferation and under sustained exposure programmed cell death (apoptosis).

It was the aim of this study to find out whether such toxic effects, especially apoptosis, are also elicited by oxPL in cancer cells. We found that the oxidized phospholipids efficiently kill human melanoma cells of different stages but leave primary human melanocytes almost unaffected. The toxicity of PGPC and POVPC was associated with efficient uptake of these lipids into the cells, activation of aSMase and the formation of the apoptotic second messenger ceramide. Several evidences support the

assumption that the truncated oxidized phospholipids may possess high potential for cancer treatment. First of all, their toxicity is preferentially expressed in malignant cells. Secondly, they are naturally formed in the body and resistances to these compounds are not very likely to occur.

2.3 Experimental Procedures

2.3.1 Materials

Oxidized phospholipids (PGPC and POVPC) and their fluorescent analogues (BY-PGPE and BY-POVPE) were synthesized in our laboratory as previously described (Moumtzi *et al.*, 2007). 1-Palmitoyl-2-oleoyl-*sn*-glycero-3-phosphocholine (POPC) was synthesized according to the method of Hermetter *et al*. (Hermetter *et al.*, 1989). 1-Palmitoyl-*sn*-glyero-3-phosphocholine (PLPC) was purchased from Bachem (Bubendorf, Switzerland). Tissue culture dishes and flasks were obtained from Sarstedt (Nürmbrecht, Germany) or Greiner (Kremsmünster, Austria). RPMI-1640 medium with or without Phenol red, fetal calf serum (FCS) and Trypsin were purchased from Gibco (Carlsbad, CA), Melanocyte Growth Medium (MGM) with or without Phenol red were obtained from Promo Cell (Heidelberg, Germany). Phosphate buffered saline (PBS) and all supplements for cell culture were purchased from PAA Laboratories (Linz, Austria), unless otherwise indicated. Chemicals for gel electrophoreses were obtained from Bio-Rad Laboratories (Hercules, CA, USA). Vybrant® apoptosis assay kit#2 (V-132451) and staurosporine were from Invitrogen (Leek, Netherlands). Flow cytometry fluids and FACS tubes were from BD Bioscience (Heidelberg, Germany). Organic solvents and all other standard chemicals were purchased from Carl

Roth (Karlsruhe, Germany) or Sigma-Aldrich (Vienna, Austria), unless otherwise indicated.

2.3.2 Cell culture and incubation with oxidized phospholipids

Human primary melanoma cell lines (SBcl2, WM35) and metastatic melanoma cell lines (WM9, WM164) were cultured in RPMI-1640 medium supplemented with 2% FCS, 200 units/ml penicillin/streptomycin and 4 mM L-glutamine. The melanocytic cell lines were kindly provided by Dr. Meenhard Herlyn (The Wistar Institute, Philadelphia, PA, USA). Human melanocytes (Fom), derived from human foreskin, were cultured in Melanocyte Growth Medium (MGM). All cells were routinely grown at 37°C in humidified CO_2 (5%) atmosphere.

For all experiments, ethanolic solutions of lipids containing the indicated lipid concentration were prepared using the ethanol injection method (Batzri and Korn, 1973). The final concentration of EtOH was always kept below 1% (v/v). Incubation medium for all experiments was RPMI-1640 culture medium containing 0.1% FCS without Phenol red unless otherwise indicated. Control experiments were carried out with incubation medium containing 0.1% FCS and the same amount of EtOH but without lipids.

2.3.3 Time-dependent stability of PGPC and POVPC in serum containing media

Stability of oxidized phospholipids in RPMI-1640 media supplemented with 0.1% or 2% FCS was determined as previously described (Fruhwirth *et al.*, 2006). In detail, lipid dispersions containing 100 µM PGPC or POVPC in media supplemented with

varying concentrations of FCS were prepared and incubated at 37°C under shaking (550 rpm) for different times. After incubation, phospholipids were extracted with $CHCl_3$/MeOH 2:1 (v/v) under short intense mixing. Extraction was repeated once, the organic phases were combined and the solvent was removed under a gentle stream of nitrogen.

The lipids were dissolved in $CHCl_3$/MeOH 2:1 (v/v) and analyzed by thin layer chromatography on silica plates. For the separation of POVPC and its degradation product PLPC, the mobile phase was $CHCl_3$/MeOH/H_2O 30:50:10 (v/v/v). PGPC and PLPC were separated using an acidic mobile phase containing $CHCl_3$/MeOH/ acetone/glacial acetic acid/H_2O (20:40:10:10:10 per vol.). After separation, lipid spots were detected using molybdenum blue reagent which specifically stains phospholipids (Vaskovsky and Kostetsky, 1968). Different phospholipids were identified by comparison with pure reference compounds.

2.3.4 Fluorescence microscopy

Cells were grown to 70% confluency on Chamber slides (Nunc, Nalgene, Rochester USA). Cells were incubated with dispersions of 5 µM oxPL in incubation medium for 5 and 30 minutes. After incubation, cells were washed with medium and observed with an Axiovert 35 inverted fluorescence microscope equipped with a mercury-arc lamp and a CCD camera, driven by AxioVision software package (Carl Zeiss, Germany). BODIPY fluorescence (Ex 505 nm, Em 510 nm) was detected using the following filter set: Excitation filter BP 450-490 nm, Beam splitter 510 nm and barrier filter LP 520 nm. Unlabelled cells were used as a reference to examine autofluorescence.

2.3.5 Flow cytometric analysis of apoptotic and necrotic cells

For the determination of apoptotic and necrotic cell populations, the Vybrant® apoptosis assay kit#2 was used according to a slightly modified manufacturer's protocol. Cells were seeded into 24-well plates and grown to 80% confluency. Cells were incubated with 400 µl lipid dispersion in incubation medium (final lipid concentrations were 25 µM or 50 µM) for 6 hours. Controls were cells incubated with medium containing 1 vol.% EtOH. Medium containing H_2O_2 was used as a positive control (necrosis).

After incubation, the supernatant was removed, the cells were harvested after treatment with accutase, and the wells were washed twice to collect any remaining cells. All fractions were combined. Cells were isolated by centrifugation followed by washing with PBS containing 2 mg/ml glucose and resuspension in 100 µl Annexin Binding Buffer. The cell suspension was mixed with 5 µl AlexaFluor®488 Annexin V, 5.5 µl of an aqueous solution of propidium iodide (final concentration 1 mg/ml) and incubated in the dark at RT for 15 minutes. Subsequently, samples were diluted with 400 µl PBS containing 2 mg/ml glucose, gently mixed and kept on ice until analysis.

Stained samples were analyzed immediately using a FACS Calibur flow cytometer (BD Bioscience, NJ). The green fluorescence emission at 530 nm and the red fluorescence emission above 575 nm were detected upon excitation at 488 nm. Cell populations were separated into three groups: apoptotic cells were only stained by green fluorescent AlexaFluor®488 Annexin V. Necrotic cells showed red fluorescence due to binding of PI to DNA or double staining due to binding of both fluorescence markers. Intact cells were not stained. Each experiment was carried out three times and

each sample was done in parallel. The percentage of apoptotic and necrotic cells was calculated using WinMDI 2.8 software.

2.3.6 Morphological studies

Cells were grown to 60-70% confluency in chamber slides (Nunc, Nalgene, Rochester, USA) and incubated with oxPL or 1% EtOH (v/v) in media without Phenol red under low serum conditions. After incubation, the cells were washed twice with medium and observed with an Axiovert 35 inverted microscope equipped with a charged coupled device camera, driven by AxioVision software package (Carl Zeiss, Germany).

2.3.7 Labelling of cell proteins with BY-POVPE

WM9 metastatic melanoma cells were grown in RPMI-1640 medium to 80% confluency in Petri dishes (60 mm) and washed twice with RPMI-1640 (0.1% FCS) prior to stimulation. Cells were incubated in the dark for 30 minutes with 3 ml of a 10 µM BY-POVPE dispersion or the same amount of incubation medium containing 1% EtOH (v/v) as a negative control. After treatment, cells were washed twice with ice-cold PBS and scraped into 3 ml of washing solution (PBS supplemented with 100 mg/l $CaCl_2$, 100 mg/l $MgCl_2$ x 6 H_2O, 1 mM PMSF and 10 mM $NaCNBH_3$). The following steps were performed at 4°C. Cells were pelleted at 300 g for 3 minutes followed by lysis in 150 µl of neutral cell lysis buffer for one hour on ice (20 mM HEPES, 2 mM EDTA, 1% Triton X-100, pH 7.4, 10 mM $NaCNBH_3$, 5 mM DTT, 1 mM PMSF, 10 µg/ml SBTI, 10 µg/ml leupeptin; stock solutions of soybean Trypsin inhibitor, leupeptin and $NaCNBH_3$ were added directly before use). The suspension was shaken vigorously every 15 minutes. To remove nuclei and cell debris, the lysate was centrifuged at 1000

g for 5 minutes. After reduction of formed Schiff bases at 37°C for 2 hours, samples were stored at -20°C. Measurements of cell protein content were performed using a microtiter plate assay based on the method of Bradford (Bradford, 1976).

2.3.8 One-dimensional gel electrophoresis of labelled proteins

For one-dimensional SDS-PAGE, 60 µg of protein per sample were precipitated with 10% trichloroacetic acid on ice for 1 hour and collected by centrifugation at 4°C and 14.000 g for 15 minutes. The pellet was washed once with ice-cold acetone and re-suspended in sample buffer for 1-D SDS-PAGE (20 mM KH_2PO_4, 6 mM EDTA, 60 mg/ml SDS, 100 mg/ml glycerol, 0.5 mg/ml Bromophenol blue, 20 µl/ml mercaptoethanol, pH 6.8). Prior to loading onto the gel, the samples were heated to 95°C for 5 minutes. Proteins were separated by SDS-PAGE (4.5% stacking gel, 10% resolving gel) (Fling and Gregerson, 1986). After electrophoresis, gels were fixed in aqueous solution containing 10 vol.% EtOH and 7 vol.% AcOH for 2 hours. Fluorescence of BODIPY-labelled proteins was detected using a BioRad laser scanner (Ex 488 nm, Em 530/30). Total protein patterns were visualized by SYPRO Ruby Protein Gel Stain (Molecular Probes) according to the manufacturer's protocol (Ex 488 nm, Em 605 nm).

2.3.9 Labelling of cell phospholipids with BY-POVPE and two-dimensional TLC separation of labelled cellular lipid extracts

Melanocytes and melanoma cells were grown in 100 mm Petri dishes to 80% confluency. After washing twice with SFM, cells were treated with 6 ml SFM containing 1 µM BY-POVPE or BY-PGPE for various time points at 37°C. Control cells were treated with 1 vol.% EtOH in SFM under the same conditions. After discarding the supernatant, cells were rinsed with PBS twice and lipids were extracted by a modified

procedure of Folch *et al.* (Folch *et al.*, 1957). In detail, cells were scraped into 10 ml of PBS and transferred into 15 ml pyrex tubes. The mixture was incubated with 10 µM $NaCNBH_3$ for 10 minutes at RT to reduce the formed Schiff bases to stable amines. After harvesting of the cells by centrifugation (2500 g, 3 min), the cell pellet was resuspended in 3 ml of $CHCl_3$/MeOH 2:1 (v/v), $NaCNBH_3$ was added to reach a final concentration of 10 mM, and the suspension was shaken vigorously for one hour at 4°C. After washing with 700 µl of a $MgCl_2$ solution (0.036% in water w/v) and centrifugation at 2500 g for 2 minutes at RT, the lower chloroform phase was collected and evaporated to dryness under a nitrogen stream.

The extracted lipids were dissolved in $CHCl_3$/MeOH 2:1 (v/v) and subjected to two-dimensional TLC (silica gel 60, Merck) using $CHCl_3$/MeOH/25% NH_3 (65:25:5 per vol.) and $CHCl_3$/acetone/MeOH/glacial AcOH/H_2O (50:20:10:10:5 per vol.) as solvents in the first and the second dimension, respectively. Total lipids were visualized by iodine vapour after detection of fluorescent spots with a charge-coupled device camera (Herolab, Vienna, Austria) at an excitation wavelength of 365 nm using EasyWin® software for data acquisition.

2.3.10 Analysis of phospholipid composition

Cells were grown to 80% confluency on Petri dishes (100 mm) in full growth medium. Total lipids of all cell lines were extracted with $CHCl_3$/MeOH 2:1 (v/v) according to the procedure of Folch *et al.* (Folch *et al.*, 1957). The supernatant medium was discarded, cells were rinsed with PBS twice and scraped into 10 ml of PBS. Cells were harvested by centrifugation (2500 g, 3 min), the cell pellet was resuspended in 3 ml of $CHCl_3$/MeOH 2:1 (v/v) and the suspension was shaken vigorously for one hour

at 4°C. After washing with 700 µl of a $MgCl_2$ solution (0.036% in water w/v) and centrifugation at 2500 g for 2 minutes at RT to separate the aqueous phase from the organic phase, the lower chloroform phase was collected and evaporated to dryness under a nitrogen stream.

Phospholipid composition was analyzed by normal-phase HPLC (high-pressure liquid chromatography), using an Agilent 1100 HPLC system (Agilent Technologies, Waldbronn, Germany) which was equipped with an evaporative light scattering detector (PL-ELS 1000, Polymer Labs, Amherst, Massachusetts). The stationary phase was an YMC-Pack™Diol column (250x4.6 mm, 5 µm). The elution gradient was based on a previously reported method (Sas *et al.*, 1999), ranging changed from acetone to acetone/MeOH (46.2/53.8 v/v). Elution time was 32 minutes at a flow rate of 0.4 ml/min. Both solvents contained a constant amount of hexane (7% v/v), acetic acid (1.9% w/w) and triethylamine (1.6% w/w). Quantification of phosphatidylethanolamine and phosphatidylcholine levels was achieved by external standardization using standards from Avanti Polar Lipids Inc. (Alabaster, Alabama). HPLC grade solvents were purchased from Carl Roth GesmbH (Karlsruhe, Germany), acetic acid and triethylamine were purchased from Merck (Darmstadt, Germany).

2.3.11 Determination of acid sphingomyelinase activity

Human melanocytes (Fom), primary melanoma cells (SBcl2, WM35) and metastatic melanoma cells (WM9, WM164) were grown on 60 mm Petri dishes to 80% confluency in full growth medium. Prior to stimulation with the oxPL, cells were washed twice with medium containing 0.1% FCS to remove excess serum. Cells were subsequently incubated with 2 ml of a 50 µM oxPL dispersion in RPMI-1640 medium (0.1%

FCS) or MGM, or the same medium containing 1 vol.% EtOH (negative control) for 5 minutes or 15 minutes.

After incubation, cells were washed with ice-cold PBS, scraped, harvested by centrifugation (1500 rpm, 10 min, 4°C) and lysed by incubation with acid lysis buffer (250 mM sodium acetate, 0.2% Triton X-100, pH 5.0). The protein content of the samples was determined by the method of Bradford (Bradford, 1976). Aliquots of cell lysates containing 15 µg of protein were used for the determination of acid sphingomyelinase activity using a fluorescent sphingomyelin substrate as described previously (Loidl *et al.*, 2002). Fluorescent sphingomyelin was separated from fluorescent ceramide by thin layer chromatography (mobile phase was $CHCl_3$:MeOH:H_2O 65:25:4 v/v/v). The labelled fluorescent lipid spots were quantified with a charged coupled device camera (Herolab, Vienna) at an excitation wavelength of 365 nm using EasyWin software.

2.3.12 Identification and quantification of ceramide and sphingomyelin species

All cell lines were grown in 100 mm Petri dishes to 80% confluency in full growth media. Prior to stimulation with the oxPL, cells were washed twice with medium containing 0.1% FCS to remove excess serum. Cells were subsequently incubated with 4.5 ml of a 50 µM oxPL dispersion in either RPMI-1640 (0.1% FCS) or in MGM for 6 hours. 1 vol.% EtOH in the respective media was used as a negative control. After incubation, cells were washed with ice-cold PBS, scraped into PBS and harvested by centrifugation (1500 rpm, 5 min, 4°C). Cells were resuspended in 1 ml PBS and 100 µl aliquots were used for measuring sample protein concentrations. For this purpose, cells were harvested by centrifugation (640 g, 5 min, 4°C) and lysed in 70

µl of neutral lysis buffer for one hour on ice (20 mM HEPES, 10 mM $MgCl_2$, 2 mM EDTA, 5 mM DTT, 0.1 mM Na_2MoO_4, 1 mM PMSF, 1 mg/ml 4-aminobenzamidine dihydrochloride, 1 mM NaF, 0.2% Triton X-100, pH 7.5; stock solutions of DTT, PMSF and 4-ABA were added just before use). The suspension was shaken vigorously every 15 minutes. To remove nuclei and cell debris, the lysate was centrifuged for 5 minutes at 1000 g. Aliquots of the lysate were used to determine the protein concentration by the method of Bradford (Bradford, 1976).

The remaining 900 µl cell suspension was centrifuged under the conditions described above and cells were resuspended in 3 ml $CHCl_3$/MeOH 2:1 (v/v). The suspension was shaken vigorously for 1 hour at 4°C. The organic phase was washed with 700 µl of a $MgCl_2$ solution (0.036% in water w/v) for 15 minutes and centrifuged at 300 g for 2 minutes at RT to separate the aqueous phase from the organic phase. The lower chloroform phase was collected and evaporated to dryness under a nitrogen stream.

For mild alkaline hydrolysis, 400 µl of $CHCl_3$/MeOH/H_2O (16/16/5 per vol.) were added to the solvent-free lipid extracts and the solution was shaken vigorously. After addition of 400 µl 0.2 M NaOH in MeOH, the samples were incubated at RT for 45 minutes. Following addition of 400 µl 0.5 M EDTA and 150 µl CH_3COOH and vigorous shaking, 1 ml $CHCl_3$ was added to extract the lipids. Extracts were shaken for 5 minutes and centrifuged for 3 minutes at 300 g to facilitate phase separation. The chloroform phase was transferred to a new vial and the solvent was removed under a nitrogen stream. Solvent-free lipid extracts were dissolved in 100 µl $CHCl_3$/MeOH (1:1 v/v) containing 100 pmol CER 12:0, CER 25:0 and SM 12:0 each as internal standards. Lipids were separated by Accela HPLC (Thermo Scientific) on

a Thermo Hypersil GOLD C18, 100x1 mm, 1.9 µm column. Solvent A was an aqueous solution of 1% ammonium acetate (v/v) and 0.1% formic acid (v/v). Solvent B was acetonitrile/2-propanol (5:2, v/v) supplemented with 1% ammonium acetate (v/v) and 0.1% formic acid (v/v), respectively. The gradient was run from 35% to 70%. Elution time was 4 minutes. Finally, elution was continued with 100% B for 16 minutes with a subsequent hold at 100% for 10 minutes. The flow rate was 250 µl/min. Sphingolipid species were determined using a TSQ Quantum Ultra (Thermo Scientific) triple quadrupole instrument in positive ESI mode. Spray voltage and capillary voltage were set 5000 V and 35 V, respectively. SM and CER species were detected in positive ionization by precursor ion scan at m/z 184, 35 eV and at m/z 264, 30 eV, respectively as described previously (Bielawski *et al.*, 2009; Brügger *et al.*, 1997). CER and SM peak areas were calculated by QuanBrowser for all lipid species and quantification was performed by correlation to internal standards.

2.3.13 Statistical analysis

Data are expressed as means $\pm$ standard deviation (SD). Two-tailed unpaired Student's t-test was used to determine the significance of the differences. A p-value $\leq$ 0.05 was considered significant.

2.4 Results

2.4.1 Stability of PGPC and POVPC in culture medium containing fetal calf serum

PGPC and POVPC contain a single hydrophobic fatty acid at the *sn*-1 position. They only differ in their short polar fatty acyl chains in position 2 of glycerol (Figure 2.1).

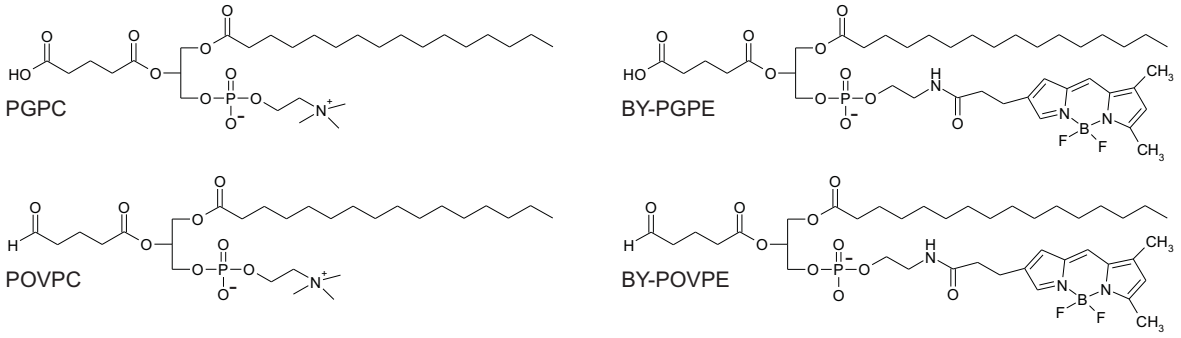

Figure 2.1. Chemical structures of oxidized phospholipids

1-palmitoyl-2-glutaroyl-sn-glycero-3-phosphocholine (PGPC)
1-palmitoyl-2-(5-oxovaleroyl)-sn-glycero-3-phosphocholine (POVPC)
N-BY-1-palmitoyl-2-glutaroyl-sn-glycero-3-phosphoethanolamine (BY-PGPE)
N-BY-1-palmitoyl-2-(5-oxovaleroyl)-sn-glycero-3-phosphoethanolamine (BY-POVPE)

The residue at the *sn*-2 position of PGPC contains an ω-carboxyl function. In contrast, the *sn*-2 acyl residue of POVPC contains a highly reactive ω-aldehydo group that allows the molecule to interact chemically with its targets by Schiff base formation. The uptake and intracellular partitioning of oxidized phospholipids in the cells, as well as the interaction of these compounds with the cellular proteins and lipids was studied using BODIPY-labelled analogues of PGPC and POVPC (Figure 2.1). In forgoing experiments we showed that these BODIPY-labelled oxidized phospholipids are reliable

analogues of their unlabelled counterparts (Moumtzi *et al.*, 2007) with respect to biophysical and biochemical properties.

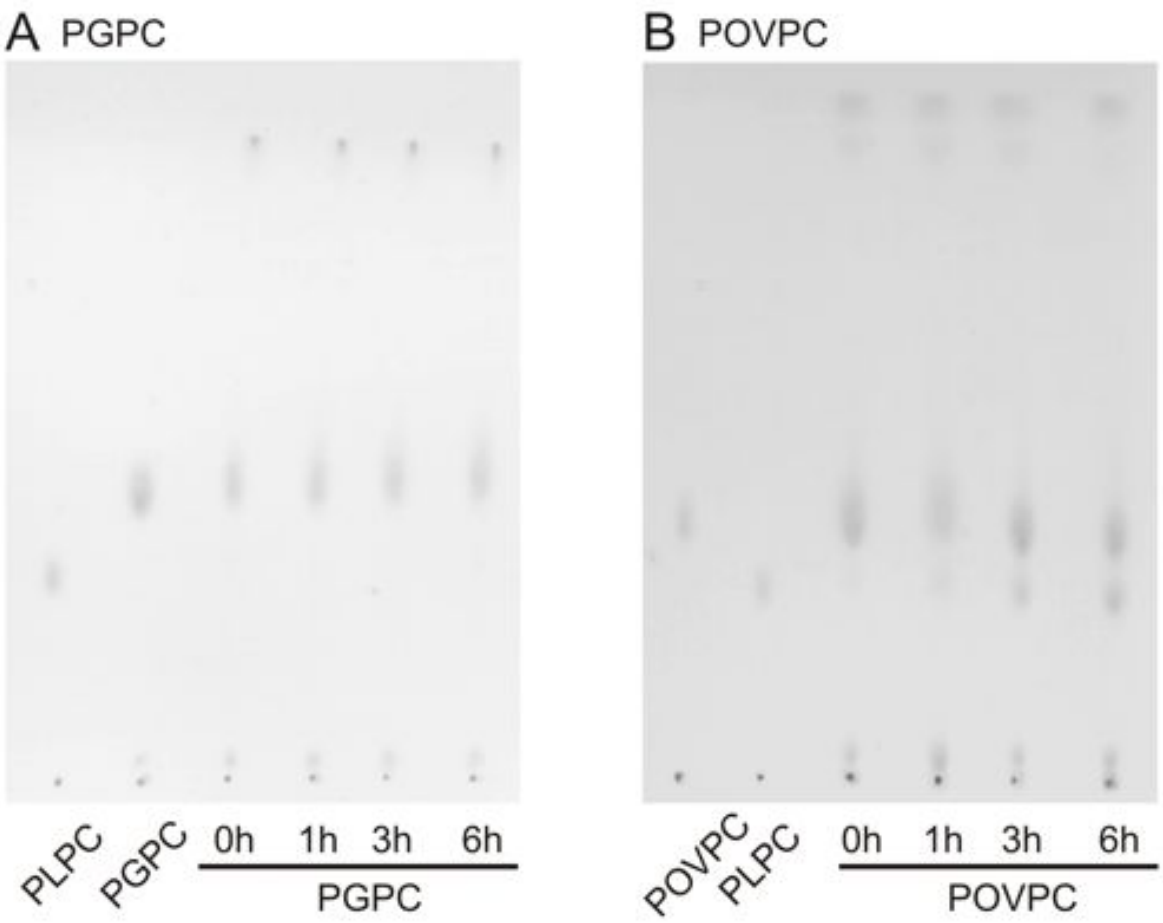

Figure 2.2. Time dependent hydrolysis of PGPC and POVPC under low serum conditions

Oxidized phospholipids were incubated in RPMI-1640 medium supplemented with 0.1% FCS for various times. After incubation, lipids were extracted with organic solvents and separated by thin-layer chromatography. For separation of POVPC (RF=0.38) and PLPC (RF=0.26) from other phospholipids, a neutral mobile phase was used, whereas for separation of PGPC (RF=0.41) and PLPC (RF=0.30) an acidic mobile phase was applied (see Experimental Procedures.

Under high serum conditions, hydrolysis of both oxPL starts after 3 hours (data not shown). However, under low serum conditions, PGPC is stable for at least 6 hours ***(A)****, whereas degradation of POVPC begins after 3 hours and is still ongoing at 6 hours of incubation* ***(B)****. For all experiments, a significant amount of oxPL remains intact over the entire incubation time period (n = 3).*

Previous studies showed that the cytotoxic effects of oxidized phospholipids on vascular smooth muscle cells in DMEM were abolished under high serum conditions

(10% FCS) (Fruhwirth *et al.*, 2006). In order to find out, if the oxidized phospholipids PGPC and POVPC are stable in the culture media under different serum conditions used in this study, we incubated the oxPL in RPMI-1640 growth media supplemented with 0.1% FCS or 2% FCS, extracted and analyzed the lipids by TLC. In medium containing 2% FCS, hydrolytic cleavage of the oxidized *sn*-2 chain of PGPC and POVPC starts after 3 hours of incubation and is still ongoing after 6 hours (data not shown). However, at low serum conditions, PGPC is stable for at least 6 hours and no degradation products are detectable. In case of POVPC, hydrolysis starts after 3 hours, leading to the formation of PLPC (Figure 2.2). After 20 hours of incubation, about 50% of the intact oxPL are still detectable (data not shown).

2.4.2 Import and intracellular distribution of fluorescent PGPC and POVPC analogues

To study the import and intracellular distribution of oxPL in melanoma cells, we used the fluorescent oxPL analogues BY-PGPE and BY-POVPE. These experiments were performed in culture medium supplemented with 0.1% FCS (except for FOM melanocytes, which were cultured in full growth medium) to avoid degradation of the oxidized phospholipids by lipolytic enzymes (see above).

In all cell lines, the fluorescent oxidized phospholipids are internalized rapidly. However, intracellular localization is different depending on the lipid and the cell line (Figure 2.3).

After 5 minutes of incubation, both BY-POVPE and BY-PGPE are distributed quite uniformly in all cell lines, except for SBcl2 cells. In the latter cell line, both lipids are

internalized rapidly and localize to just one single area within the cell, most likely the endoplasmic reticulum.

After 30 minutes of incubation, all cell lines show nearly the same fluorescence pattern. Both lipids are concentrated near the nucleus, but can also be found in the cytoplasm. The amounts of BY-POVPE and BY-PGPE within these areas vary widely between the cell lines. Even after longer incubation times, more BY-POVPE than BY-PGPE is seen in the plasma membrane.

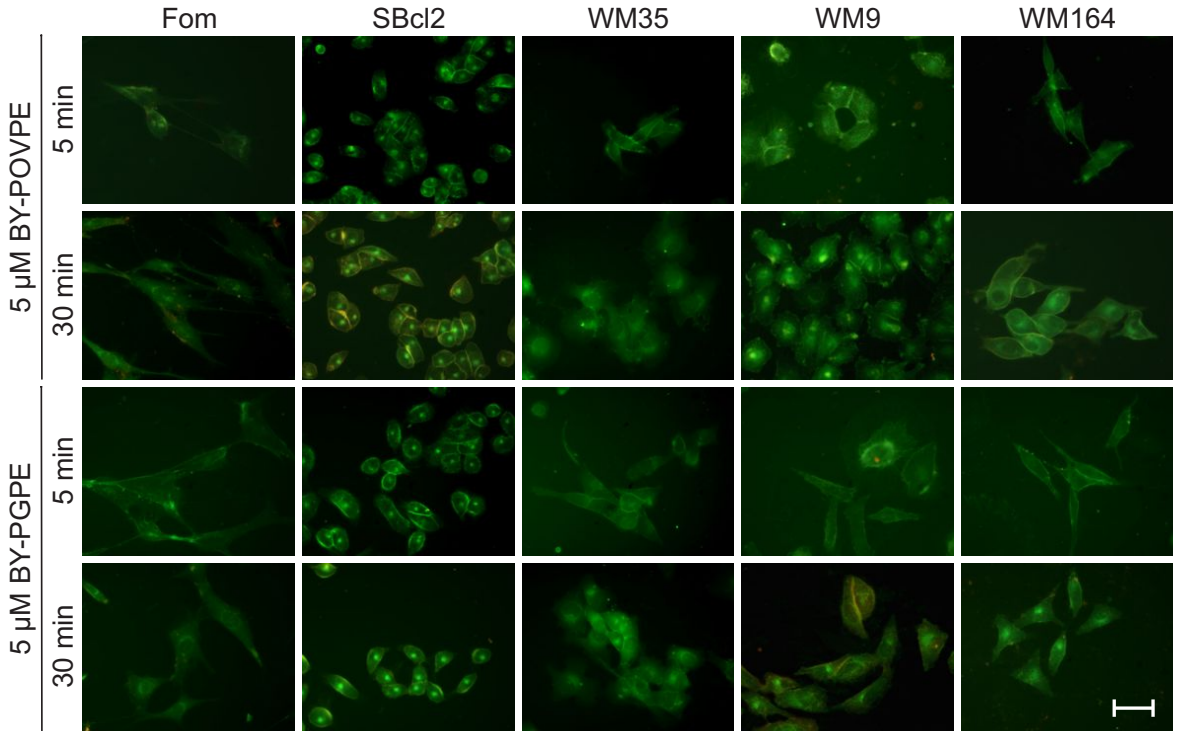

Figure 2.3. Time-dependent cellular uptake of fluorescent oxidized phospholipids

Cells (Fom, SBcl2, WM35, WM9, WM164) were incubated with 5 µM BY-POVPE or 5 µM BY-PGPE in Phenol red-free Melanocyte Growth Medium (Fom) or Phenol red-free RPMI-1640 medium supplemented with 0.1% FCS (melanoma cell lines) for 5 minutes or 30 minutes at 37°C. Cells were observed by fluorescence microscopy (320x magnification). The fluorescent oxidized phospholipids are rapidly internalized by all cell lines. However, localization of lipids is cell line dependent. Scale bar = 50 µm (n = 3)

2.4.3 Oxidized phospholipids induce apoptosis in human melanoma cells

We determined the effects of PGPC and POVPC on cell viability and identified the mode of cell death using FACS (fluorescence-activated cell sorting) to analyze cell staining by green fluorescent AlexaFluor488® Annexin V, which binds to PS at the cell's outer plasma membrane leaflet (apoptosis marker) and the red fluorescent PI, which binds to the DNA of permeable cells (necrosis marker).

Typically, Fom melanocytes, primary melanoma cells (SBcl2, WM35) or metastatic melanoma cells (WM9, WM164) were exposed to PGPC or POVPC (25 µM, 50 µM) for 6 hours and the percentage of apoptotic and necrotic cells was determined and compared to untreated control cells (Figure 2.4). These effects largely depend on the lipid and the cell line used with the aldehyde-containing lipid POVPC being more cytotoxic than PGPC at low concentrations.

Both, 25 µM or 50 µM PGPC induce apoptosis in SBcl2 cells. In contrast, all other cell lines used in this study are unaffected by PGPC. 50 µM POVPC is apoptotic in all cell lines with the Fom melanocytes being least affected. The metastatic cell lines WM9 and WM164 show the highest sensitivity. 25 µM POVPC induce apoptosis only in SBcl2 cells, whereas 50 µM concentrations of this lipid are apoptotic in all cells under investigation. In control FACS experiments, necrosis was induces in all cells by H_2O_2. Staurosporine, an inducer of apoptosis did not show any detectable effect on all cancer cell lines used.

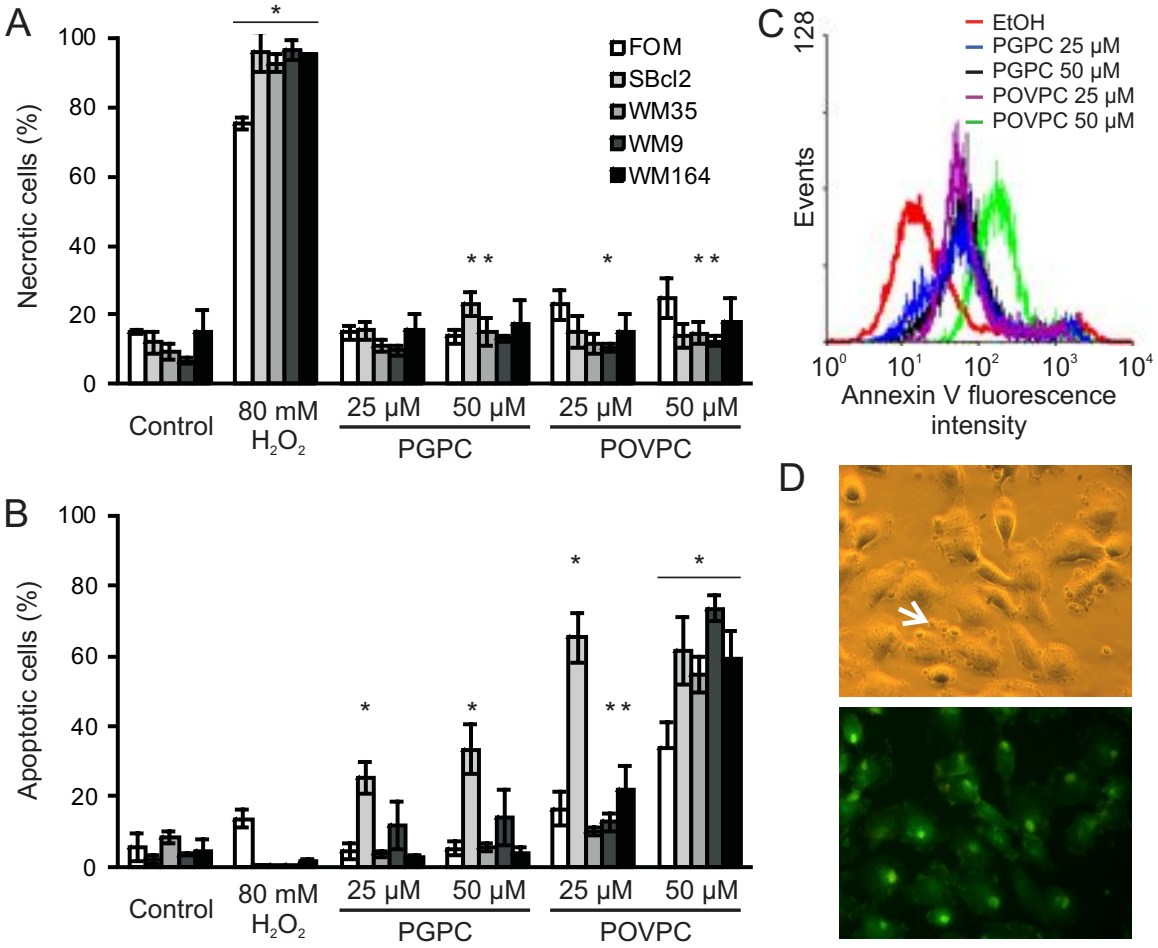

Figure 2.4. FACS analysis of cell death induced by oxidized phospholipids

Cells were incubated with the indicated concentrations of oxPL for 6 hours in incubation medium. Control cells were treated with H_2O_2 (positive control for necrosis) or 1% (v/v) EtOH (negative control). Cells were stained with Annexin and PI and cell populations were analyzed by flow cytometry (for details see Experimental Procedures).

Panel A: *Neither PGPC nor POVPC induce necrosis under the described experimental conditions.*
Panel B: *POVPC and PGPC induce apoptosis melanoma cell lines but not in Fom cells.*
Panel C: *FL1 overlay histogram of WM9 cells, stained by fluorescent Annexin V.*
Panel D: *Formation of apoptotic blebs (arrows) in WM9 cells stained with BY-POVPE for 30 minutes.*

*Results were obtained from 2 replicates of at least three independent experiments. Values represent means ± SD *P<0.05 compared with control ($n \geq 3$).*

2.4.4 POVPC covalently interacts with protein and lipid targets

The aldehydophospholipid POVPC covalently binds to free amino groups of proteins and phospholipids by Schiff base formation (Stemmer and Hermetter, 2012; Stemmer *et al.*, 2012) (Figure 2.5).

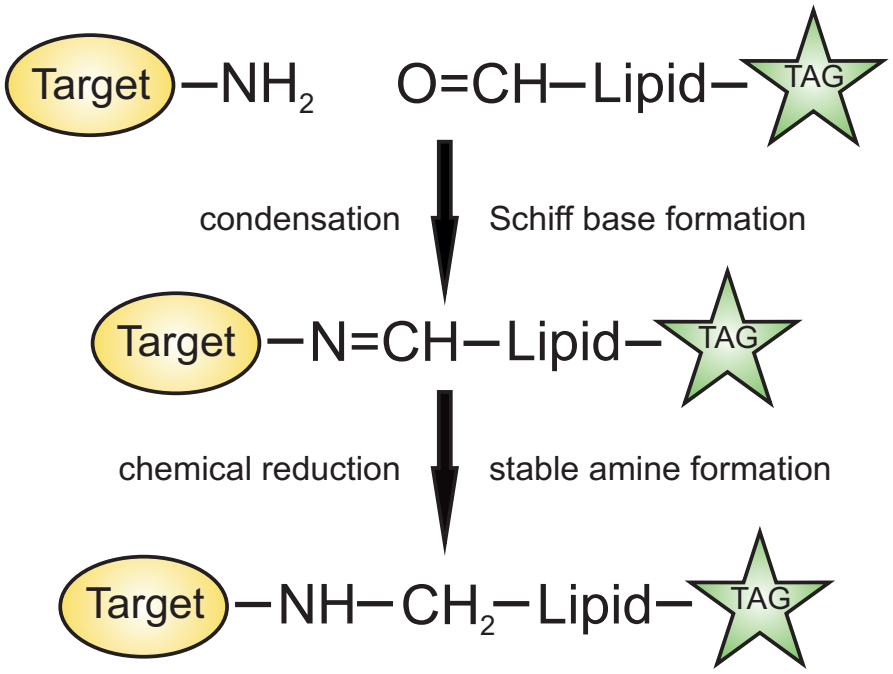

Figure 2.5. Interaction of POVPC with its targets

The aldehyde group at the sn-2 position of POVPC can chemically react with free amino groups of target proteins and lipids by forming Schiff bases. For further analysis of the formed adducts, labile imines have to be reduced with $NaCNBH_3$ to generate stable amines. PGPC can only physically interact with its targets.

However, the lipid-protein and lipid-lipid adducts cannot be isolated directly since they are unstable. Before isolation, they have to be stabilized by chemical reduction with $NaCNBH_3$ leading to the formation of the respective amines. For detection of POVPC-proteins adducts, cells were incubated with 10 µM fluorescent BY-POVPE for 30 minutes, followed by protein isolation, chemical reduction of the formed Schiff

base adducts and separation of the proteins by 1-D gel electrophoresis.

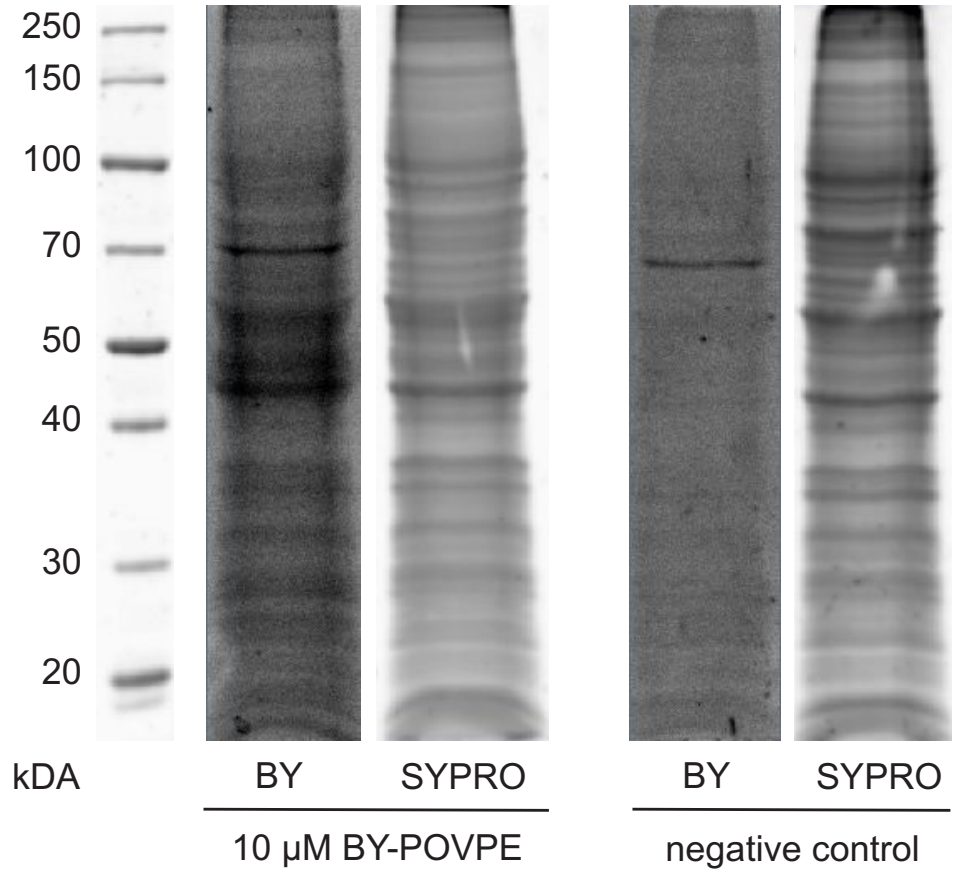

Figure 2.6. Detection of primary protein targets of BY-POVPE in the human melanoma cell line WM9

Cells were incubated with 10 µM BY-POVPE for 30 minutes and lysed in lysis buffer under reductive conditions with $NaCNBH_3$ to stabilize the formed lipid-protein complexes. Proteins were precipitated and separated by one-dimensional SDS gel electrophoresis. Protein adducts with the fluorescent lipid were detected using a fluorescence laser scanner (for details see Experimental Procedures). The BODIPY stain represents proteins that are covalently labelled by BY-POVPE. The SYPRO Ruby Protein gel stain represents the full proteome.

Figure 2.6 shows a representative 1-D electrophoresis gel of labelled proteins which were isolated from the metastatic cell line WM9. Multiple fluorescent protein spots can be detected that reflect covalently labelled protein targets. It is remarkable that the number of the lipid stained proteins is much smaller than the number of total

proteins that can be stained by SYPRO Ruby.

In addition to the interaction of POVPC with target proteins, this oxidized phospholipid can also interact with free amino groups of lipids. Candidate aminophospholipids are phosphatidylserine (PS) and phosphatidylethanolamine (PE). To identify lipid-lipid adducts, cells were incubated with 1 µM BY-POVPE for 30 minutes. Formed Schiff bases were stabilized by chemical reduction, lipids were extracted with organic solvents and separated by 2-D TLC. After fluorescence imaging, two spots can be detected in addition to the spot of the substrate BY-POVPE in all melanoma cells, but not in melanocytes (Figure 2.7). RF-values of the newly formed fluorescent spots indicate that they are less polar than BY-POVPE. The quantity of these new spots is cell line-dependent but is not influenced by incubation times or BY-POVPE concentration (data not shown). Currently, the putative adducts of BY-POVPE with phosphatidylserine or phosphatidylethanolamine are chemically synthesized as reference compounds for identification of the cellular lipid products of BY-POVPE by NMR and MS/MS analysis.

Differences between the different cell lines in lipid-lipid adduct formation can in part be explained by the localization of PS in the plasma membrane of the cells. The absolute amounts of phosphatidylethanolamine and phosphatidylserine in the different cell lines are almost the same (Figure 2.8). However, PS in Fom melanocytes localizes to the cytoplasmic leaflet of the plasma membrane, whereas it is exposed on the outer leaflet of the PM of cancer cells (Riedl *et al.*, 2011). Therefore, the accessibility of this PL is much better in melanoma cells and as a consequence, more "lipid adducts" are formed.

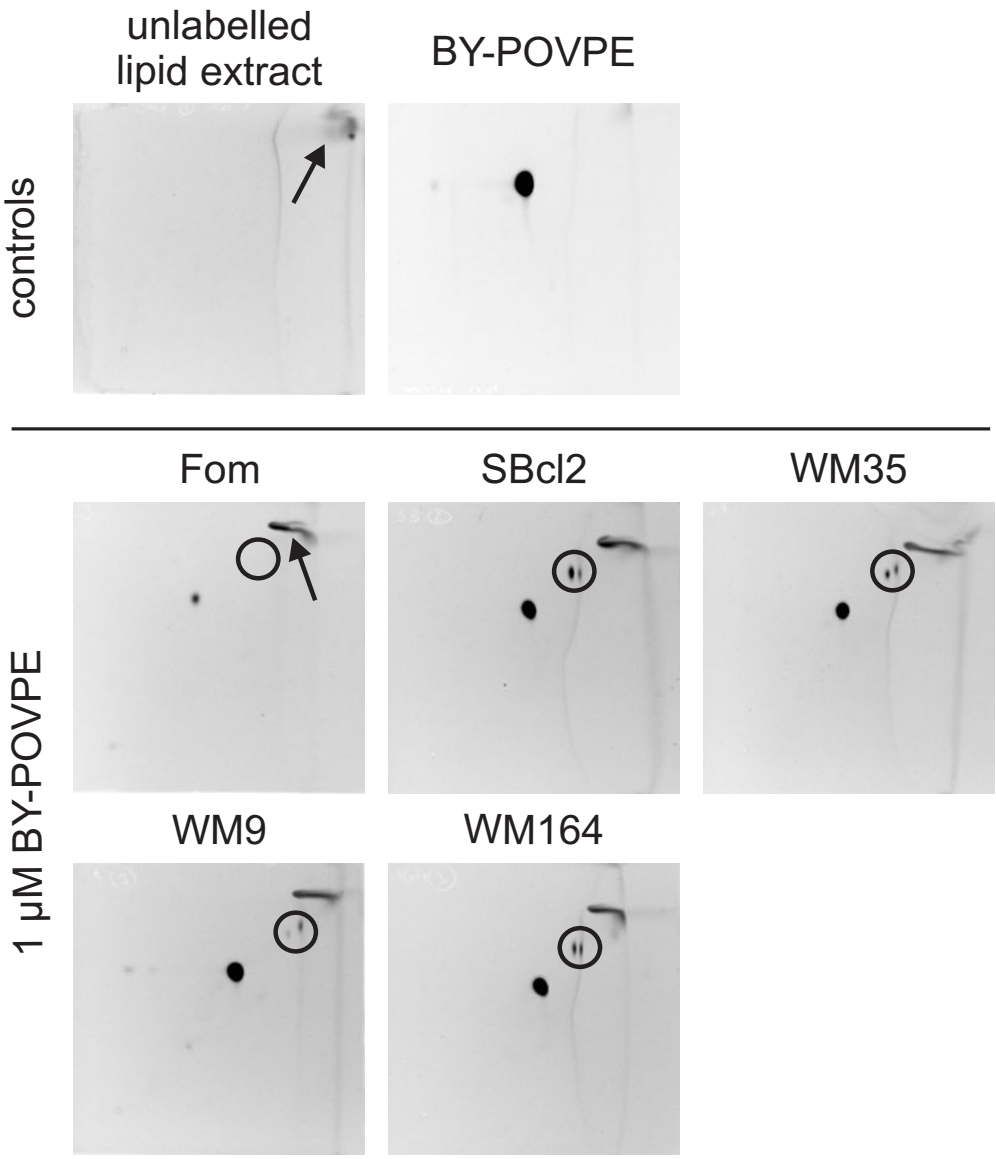

Figure 2.7. Detection of covalent BY-POVPE lipid adducts in cultured melanocytes and melanoma cells

Cells were incubated with 1 µM BY-POVPE for 30 minutes in RPMI-1640 medium supplemented with 0.1% FBS (SBcl2, WM35, WM9, WM164) or in Melanocyte Growth Medium (Fom). After lipid extraction and reduction of formed Schiff bases with 50 µM $NaCNBH_3$, lipids were separated by two-dimensional TLC using $CHCl_3$/MeOH/25% NH_3 (65:25:5 v/v/v) and $CHCl_3$/acetone/MeOH/glacial AcOH/H_2O (50:20:10:10:5 per vol.) in the first and second dimension, respectively. Lipid adducts of the fluorescent oxPL were detected with a charge-coupled device camera (see Experimental Procedures). Circles mark lipid products that are likely to be adducts formed between BY-POVPE and phosphatidylserine or phosphatidylethanolamine. Arrows mark autofluorescent impurities. No adducts were observed when cells were incubated with BY-PGPE (data not shown) (n = 3).

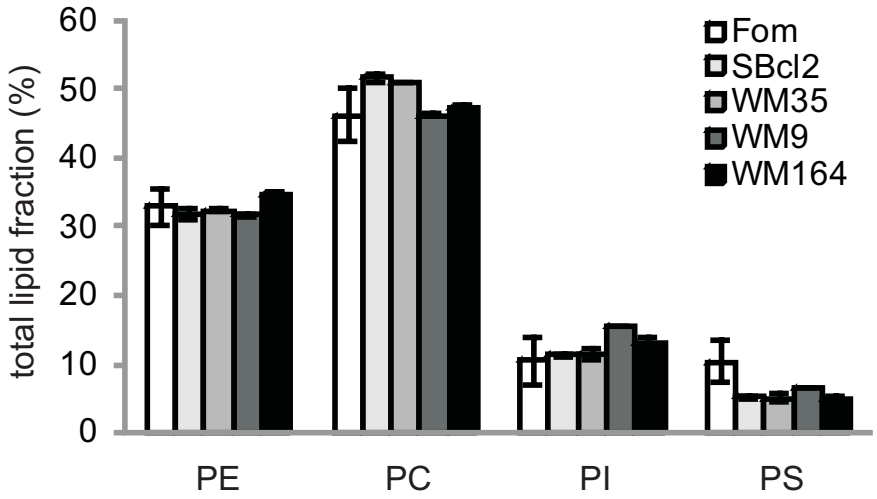

Figure 2.8. Phospholipid composition of melanocytes and melanoma cell lines

Total lipids of all cell lines were extracted with $CHCl_3$/MeOH 2:1 (v/v) according to Folch et al. (Folch et al., 1957) and analyzed by normal-phase HPLC (for details see Experimental Procedures). No significant differences in the relative amounts of phosphatidylethanolamine (PE), phosphatidylcholine (PE) and phosphatidylinositol (PI) can be observed between melanocytes and melanoma cell lines. The absolute amount of phosphatidylserine (PS) is highest in Fom melanocytes. However, it has to be emphasized that most of the PS found in Fom melanocytes localizes to the inner cytoplasmic leaflet. In contrast, the major fraction of PS of melanomas localizes to the outside of the plasma membrane (Riedl et al., 2011). Therefore it is a potential target for the interaction with POVPC. All data are means $\pm$ SD ($n \geq 3$).

2.4.5 PGPC and POVPC activate acid sphingomyelinase

Sphingomyelinases are central elements of stress-induced signal transduction. They catalyze the hydrolysis of sphingomyelin, thus generating the second messenger ceramide which is a key upstream component of apoptotic signaling. In previous studies it has been shown that PGPC and POVPC activate acid sphingomyelinase in vascular smooth muscle cells (Loidl *et al.*, 2003).

Figure 2.9 shows the activity of sphingomyelinase in response to stimulation by 50 µM POVPC or PGPC for 5 minutes and 15 minutes. In primary human melanocytes,

POVPC and PGPC only show minor effects on the activation level of acid sphingomyelinase activity within 15 minutes (Figure 2.9 B). In contrast, stimulation of the melanoma cells by the same compounds induces a substantial increase in aSMase activity. This activation is dependent on cell line, the oxPL and the incubation time. All melanoma cell lines show a significant increase of aSMase activity after stimulation with PGPC or POVPC for 15 minutes. However, the extent of activation differs widely between the cell lines, the SBcl2 cells (Figure 2.9 C) and WM9 cells (Figure 2.9 E) showing the highest activation of aSMase. Incubation of WM35 cells (Figure 2.9 D) and WM164 cells (Figure 2.9 F) with oxPL leads to a significant but less substantial activation of aSMase. In all cell lines, aSMase activities return to control levels after 60 minutes of stimulation (data not shown).

2.4.6 PGPC and POVPC elicit the formation of distinct ceramide species in melanoma cells

Sphingomyelinases catalyze the conversion of sphingomyelin to ceramide. Figure 2.10 summarizes the oxPL dependent formation of different ceramide species and the sphingomyelin patterns in melanocytes and melanoma cells. OxPL did not affect ceramide and sphingomyelin composition in melanocytes (Figure 2.10 A), in primary melanoma cells WM35 (Figure 2.10 C) and the metastatic melanoma cells WM164 (Figure 2.10 E). In contrast, activation of acid sphingomyelinase in SBcl2 cells and WM9 cells by POVPC correlates with an increase in ceramide levels. C16:0 ceramide, C18:2 ceramide and C24:2 ceramide are significantly increased in both SBcl2 cells and WM9 cells after incubation with POVPC for 6 hours (Figure 2.10 B and Figure 2.10 D). In addition, C24:0 ceramide and C24:1 ceramide are also elevated in SBcl2 cells, but not in the other cell lines used in this study.

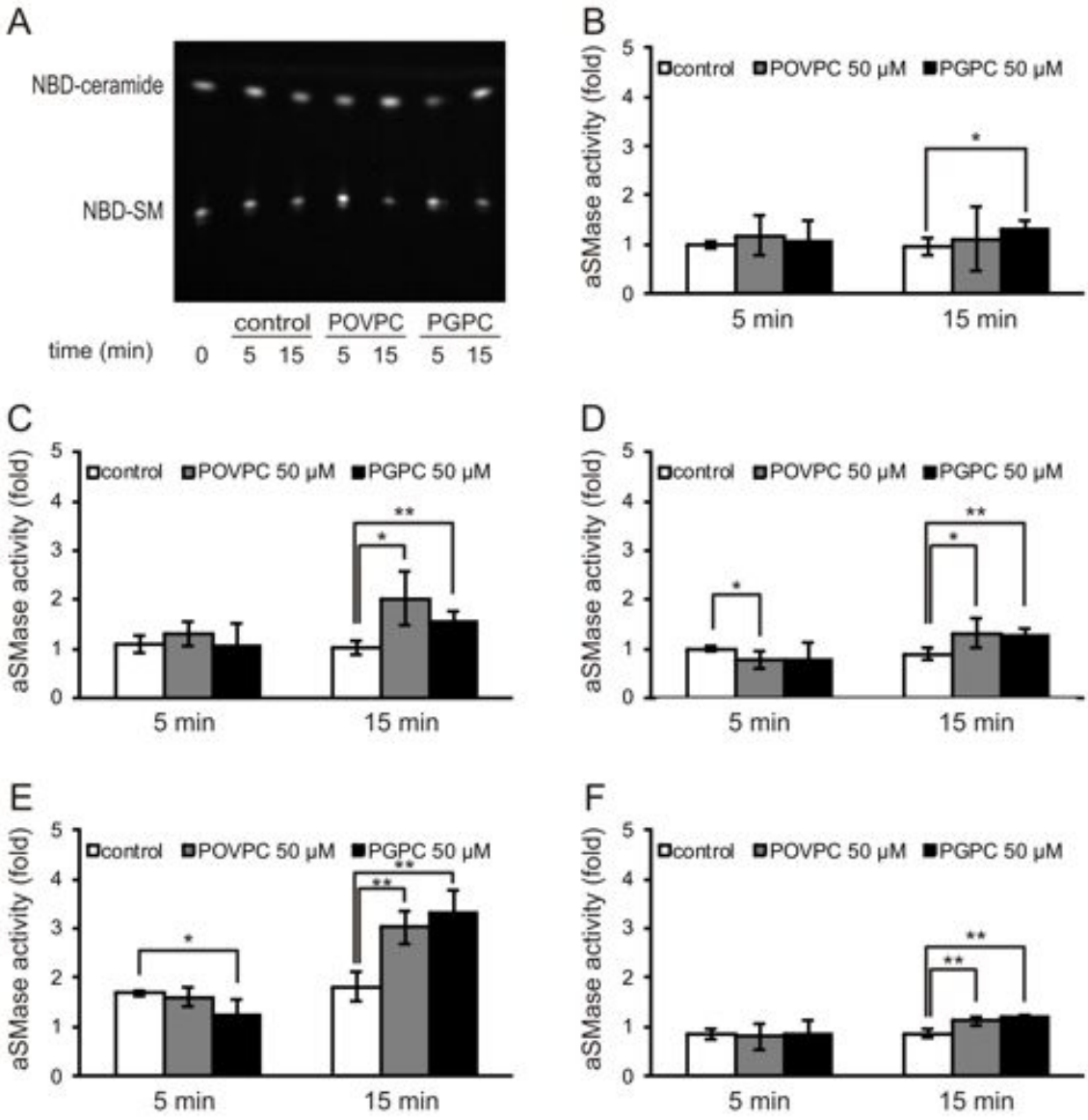

Figure 2.9. Effect of oxPL on aSMase activity

Human melanocytes (Fom) and melanoma cell lines were incubated with 50 µM oxPL or 1% (v/v) EtOH as a control for 5 and 15 minutes. Cells were harvested and lysed in lysis buffer (see Experimental Procedures). Enzyme activities were determined as described previously (Loidl et al., 2002) using NBD-labelled sphingomyelin as substrate. The ratio of NBD-ceramide to total NBD lipid (Cer+SM) was determined and expressed as fold of control at time point zero. **A:** *Representative TLC of lipids from the cell line SBcl2 after treatment with 50 µM oxPL or EtOH (1% v/v),* **B-F:** *Relative aSMase activities in Fom melanocytes* **(B)**, *and melanoma cells: SBcl2* **(C)**, *WM35* **(D)**, *WM9* **(E)**, *WM164* **(F)**. *Data are expressed as means ± SD ($n \geq 4$). *P < 0.05 compared with control. **P < 0.005 compared with control.*

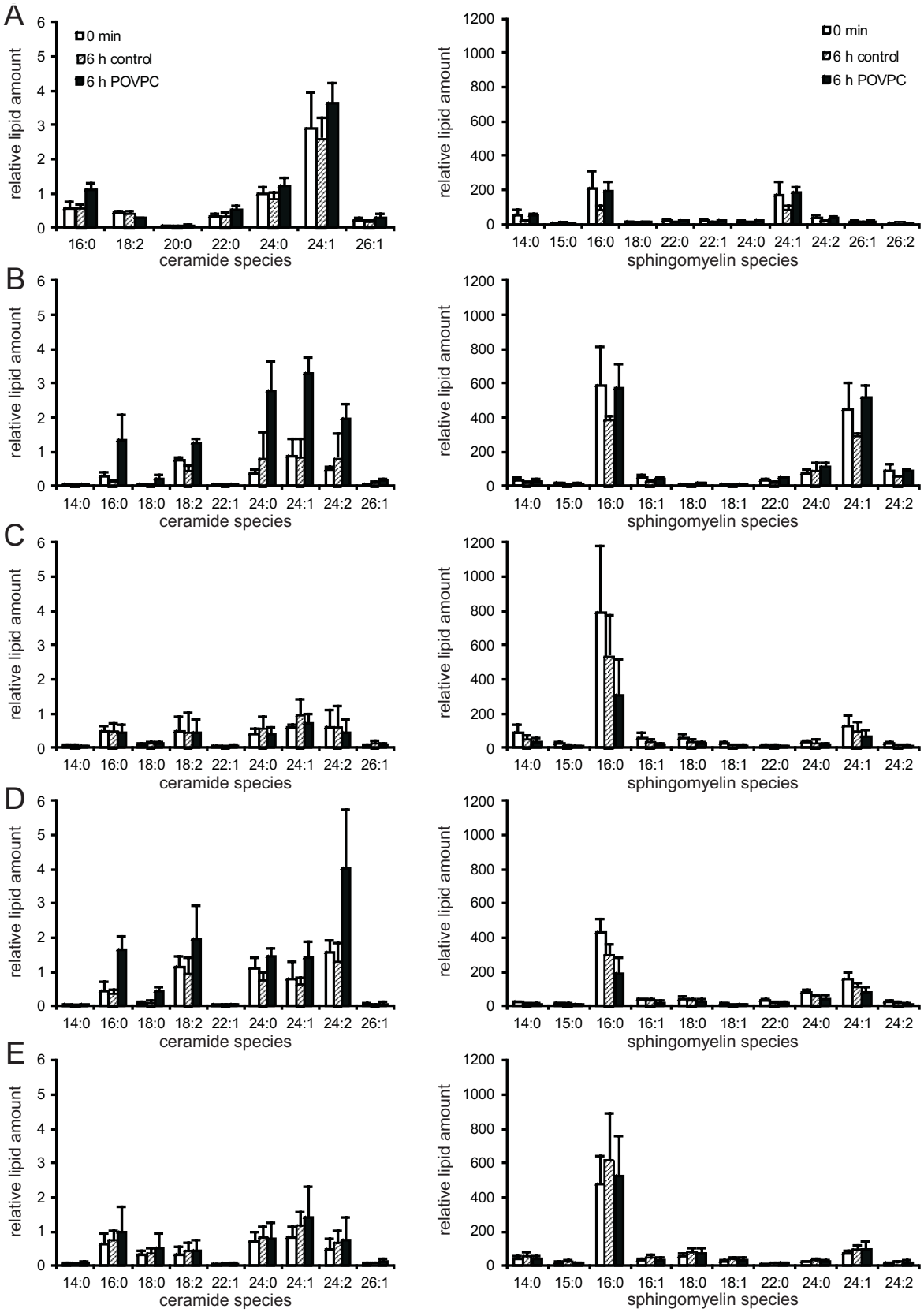

Continued on the following page

Figure 2.10. Effect of oxPL on cellular ceramide and sphingomyelin patterns

Cells were incubated with 50 µM oxPL for 6 hours. Lipids were extracted and ceramide and sphingomyelin species were analyzed as described. Relative lipid amounts were obtained by referencing measured lipid amounts to an internal standard and the cellular protein content. **Panels A-E:** *Relative amounts of ceramide species (left column) and sphingomyelin species (right column) after stimulation with 50 µM POVPC or 50 µM PGPC for 6 hours.* **A***: Fom melanocytes,* **B***: primary melanoma cell line SBcl2,* **C***: primary melanoma cell line WM35,* **D***:: metastatic melanoma cell line WM9,* **E***: metastatic melanoma cell line WM164. Values represent means ± SD (n = 3).*

2.5 Discussion

In the present study, we report on the cytotoxicity of the truncated oxidized phospholipids PGPC and POVPC in different human melanoma cell lines in vitro. PGPC and POVPC are characterized by a long hydrophobic chain at the *sn*-1 position, a shortened polar chain at position *sn*-2 and a very large polar headgroup. These truncated oxidized phospholipids are amphipathic molecules and thus highly exchangeable between cells, membranes and lipoproteins (Stemmer *et al.*, 2012).

PGPC and POVPC are components of oxidized low density lipoprotein (oxLDL). They elicit cytotoxic effects on vascular cells (Fruhwirth *et al.*, 2006; Loidl *et al.*, 2003) and they play a fundamental role in the development and progression of atherosclerosis (Chisolm and Steinberg, 2000; Parthasarathy and Rankin, 1992; Steinberg, 2009; Steinbrecher *et al.*, 1990). Depending on lipid concentrations and exposure time, oxPL may induce inflammation, cell proliferation or apoptotic cell death in the vascular wall (Bochkov, 2007; Leitinger, 2005).

We found for the first time that PGPC and POVPC are also capable of inducing cell death in cancer cells. We found that PGPC and POVPC preferentially induced apop-

totic cell death in these cells in a concentration- and time-dependent manner (Figure 3.5). However, the cytotoxicity of the oxidized phospholipids depended on the tested cell lines. At low lipid concentrations (25 µM), SBcl2 cells were most sensitive to both oxidized phospholipids, which is in line with the very fast uptake of the lipids in this cell line. Higher concentrations of the oxPL (50 µM) were required to induce apoptosis in all other melanoma cell lines (WM35, WM9, WM164). In primary human melanocytes, both oxidized phospholipids were much less toxic compared to the cancer cells.

We provide evidence that the observed cellular effects on the viability of cancer cells were due to the intact oxPL within the first three hours. After longer incubation times POVPC is degraded by serum components in the culture medium, leading to the formation of PLPC, which is also cytotoxic (data not shown). As a consequence, the observed effects are likely to be caused by a complex reaction mixture containing the intact lipid and the degradation products.

OxPL are recognized by different receptors (Leitinger *et al.*, 1999; Subbanagounder *et al.*, 1999). However, it has to be emphasized that apart from receptor-mediated pathways, many other modes of interaction between oxPL and their target cells are effective. For instance, aldehydo oxPL (POVPC) interact with proteins and lipids by Schiff base formation. In addition, oxPL may elicit general membrane effects modulating physical membrane properties (Stemmer *et al.*, 2012) and as a consequence membrane protein functions.

According to the Lipid Whisker model of Greenberg *et al.* (Greenberg *et al.*, 2008), the short polar side chains at the *sn*-2 position of the oxPL become part of an en-

larged headgroup and protrude into the aqueous compartment thus giving rise to activation of cell (receptor) binding to these motifs. Since oxidized phospholipids are easily exchangeable between cells, target lipids and proteins (Stemmer *et al.*, 2012), their biological interactions may be observed far distant from the site of their origin or application.

We used fluorescently labelled derivates of PGPC and POVPC to study the time-dependent uptake of oxPL in cells and the interaction of these truncated phospholipids with proteins and lipids. In previous studies, we found that the uptake of oxPL labelled with different fluorophores always led to the same fluorescence pattern irrespective of the attached fluorophore indicating that the label does not affect lipid properties. This assumption is supported by the observation that labelled oxidized phospholipids elicited the same intracellular signaling compared to the unlabelled counterparts (Moumtzi *et al.*, 2007; Stemmer *et al.*, 2012).

In vascular smooth muscle cells BY-PGPE and BY-POVPE were rapidly taken up by the cells (within minutes). BY-PGPE finally localized to the lysosomes, whereas BY-POVPE stained the plasma membrane due to covalent reaction with amino and other groups in lipids and proteins (Moumtzi *et al.*, 2007). Similar effects were observed for both fluorescent lipids in RAW 264.7 macrophages (Stemmer *et al.*, 2012).

Contrarily to these earlier findings, the uptake of BY-POVPE and BY-PGPE in human melanoma cells led to entirely different fluorescence patterns (Figure 2.3). The uptake of both oxidized phospholipids into melanoma cells was very fast. Surprisingly, only little BY-POVPE fluorescence was detectable in the plasma membrane. Both fluorescent lipids mainly localized to the endoplasmic reticulum, which was co-stained

with an organelle-specific marker (data not shown). Uptake in the primary melanoma cell line SBcl2 and the metastatic melanoma cell line WM9 were particularly efficient. Most of the fluorescent lipid concentrated around the nucleus in those cells. The high amount of PS in the plasma membrane's outer leaflet (Riedl *et al.*, 2011) may lead to a differing polarity of the plasma membrane which could explain the rapid uptake of these amphipatic molecules into melanoma cells but not into Fom melanocytes.

The mechanism of the efficient BY-PGPE uptake can be elucidated on the basis of previous findings (Rhode *et al.*, 2004). Immediately after insertion into the plasma membrane, this compound forms clusters that are rapidly endocytosed. This effect can be explained in terms of the conical molecular lipid shape favoring high membrane curvature and membrane blebbing.

At present, we can only speculate about the unusually fast uptake of BY-POVPE by the cancer cells. This phospholipid aldehyde is initially enriched due to chemical complexation with lipids and proteins in the plasma membrane of vascular cells, followed by slow internalization. The surface of cancer cells contains the aminophospholipids phosphatidylethanolamine and phosphatidylserine (Riedl *et al.*, 2011). If BY-POVPE reacts with these phospholipids, large amounts of lipid-lipid Schiff bases containing three hydrophobic chains and a relatively small headgroup are formed. Such products could destabilize the bilayer and favor release of non-bilayer aggregates. Obviously, reaction of BY-POVPE with PS must play a specific role in fast lipid uptake by cancer cells because PS does not localize to the surface of healthy cells. In addition, the total lipid patterns including PE in control melanocytes and melanoma cells are very similar (Figure 2.8). We have preliminary results indicating that fluorescently labelled

BY-POVPE forms covalent lipid-lipid adducts with PE and PS (Figure 2.7). This new compound is currently being isolated for identification by NMR and mass spectrometry. In addition, we are synthesizing the putative Schiff bases to test this hypothesis in artificial membranes.

Whereas POVPC can covalently react with primary NH_2 groups of proteins and aminophospholipids by Schiff base formation (Stemmer and Hermetter, 2012), PGPC can only physically interact with its targets on the cell surface and within the cell. Stemmer *et al.* identified the primary protein targets of POVPC in RAW 264.7 macrophages (Stemmer *et al.*, 2012).The respective candidates include proteins involved in cell death and survival, stress response, transport and lipid metabolism. Here, we provide evidence that POVPC also forms covalent Schiff bases with a defined subset of proteins in the human melanoma cell line WM9 (Figure 2.6). Cellular protein targeting by POVPC is selective (Stemmer and Hermetter, 2012) as the fluorescence pattern of the labelled proteins is less complex compared to the total proteins. The identification of these protein targets and the associated signaling pathways in melanoma cells is currently subject to a separate study. The total lipid patterns of the melanoma cancer cell lines in this study and the control melanocytes are very similar (Figure 2.8). However, the outside-inside lipid asymmetry is different. Riedl *et al.* found that cancer cells unlike melanocytes contain exceptionally high PS concentrations on the cell surface (see above) (Riedl *et al.*, 2011).

OxPL induced apoptosis in VSMC (Fruhwirth *et al.*, 2006) and in RAW 264.7 macrophages (Stemmer *et al.*, 2012) is associated with activation of acid sphingomyelinase and formation of ceramide. However, higher concentrations of oxPL are needed to

elicit cell death in these cells compared to melanoma cells. Increased ceramide levels have also been observed in tumor cells as a consequence of treatment with chemotherapeutic agents (Senchenkov *et al.*, 2001). The reported drugs induced ceramide formation by *de novo* synthesis, activation of sphingomyelinase and/or by blocking glucosylceramide formation. Ceramide-based therapies that stimulate the generation of ceramide and inhibit ceramide catabolism or metabolism have been discussed as potential cancer therapies (Reynolds *et al.*, 2004). In this context, preclinical studies suggest that induction of ceramide generation and inhibition of ceramide degradation might be a useful new approach for killing cancer cells with tolerable toxicity to normal healthy cells.

Both oxPL elicited fast activation of acid sphingomyelinase in two of the tested cell lines within minutes (SBcl2, WM9) (Figure 2.9). This effect correlated with higher rates of apoptosis, fast uptake of the lipids, and the formation of distinct ceramide species after stimulation with POVPC. The highest amounts of ceramide were found 6 hours after stimulation by the oxPL (Figure 2.10). Thus, we conclude from these findings that the observed activation of aSMase cannot be solely responsible for the ceramide formation. It seems as if this enzyme was only important for the initiation of apoptosis. We have evidence from studies on vascular cells, that oxPL activate *de novo* enzymes of ceramide synthesis after longer incubation times. We speculate that this second wave of the sphingolipid formation is required for the execution phase of programmed cell death e.g. by membrane destabilization. OxPL-induced apoptosis seems to be ceramide-independent in the melanoma cell lines WM35 and WM9. Thus, further studies will aim at identifying the mechanisms of cell death in melanomas under the influence of oxidized phospholipids.

In summary, toxicity of oxPL in cancer cells is mediated by lipid and membrane effects. Interactions of oxPL with PS are specific for cancer cells which in contrast to healthy cells express large amounts of this lipid on the outer leaflet of their plasma membrane. Such membrane effects of oxPL are primarily independent of the genetic background of the cells, which makes oxPL potentially useful anti-cancer drugs. In contrast to pathway-directed treatments aiming at activating or inactivating specifically mutated pathways, the oxPL-based approach could be the basis of a general "membrane therapy" for the treatment of melanoma and other skin cancers. Our study provides the first evidence that oxidized phospholipids can be used for such purposes. Meanwhile we have sound evidence that the oxidized phospholipids preferentially affect skin tumor cells but leave melanocytes and keratinocytes almost unaffected. All these properties can be considered very favorable conditions for employing oxPL as therapeutics for topical and perhaps systemic treatment of skin cancer.

2.6 Acknowledgements

We gratefully acknowledge financial support of the PhD thesis of Claudia Ramprecht by TU Graz.

References Chapter II

Batzri, S. and E. Korn (1973). Single bilayer liposomes prepared without sonication. *Biochimica et Biophysica Acta 298*(4), 1015–1019.

Bielawski, J., J. Pierce, J. Snider, B. Rembiesa, Z. Szulc, and A. Bielawska (2009). Comprehensive quantitative analysis of bioactive sphingolipids by high-performance liquid chromatography-tandem mass spectrometry. *Methods Mol Biol 579*, 443–467.

Bochkov, V. (2007). Inflammatory profile of oxidized phospholipids. *Thrombosis and Haemostasis-Stuttgart- 97*(3), 348.

Bradford, M. (1976). A rapid and sensitive method for the quantization of microgram quantities of protein utilizing the principle of protein-dye binding. *Anal Biochem 72*(1-2), 248–54.

Brügger, B., G. Erben, R. Sandhoff, F. Wieland, and W. Lehmann (1997). Quantitative analysis of biological membrane lipids at the low picomole level by nano-electrospray ionization tandem mass spectrometry. *Proceedings of the National Academy of Sciences 94*(6), 2339.

Chisolm, G. and D. Steinberg (2000). The oxidative modification hypothesis of atherogenesis: an overview. *Free radical biology and medicine 28*(12), 1815–1826.

Fling, S. and D. Gregerson (1986). Peptide and protein molecular weight determination by electrophoresis using a high-molarity tris buffer system without urea. *Analytical biochemistry 155*(1), 83–88.

Folch, J., M. Lees, G. Sloane-Stanley, *et al.* (1957). A simple method for the isolation and purification of total lipids from animal tissues. *J. biol. Chem 226*(1), 497–509.

Fruhwirth, G., A. Loidl, and A. Hermetter (2007). Oxidized phospholipids: from molecular properties to disease. *Biochimica et Biophysica Acta (BBA)-Molecular Basis of Disease 1772*(7), 718–736.

Fruhwirth, G., A. Moumtzi, A. Loidl, E. Ingolic, and A. Hermetter (2006). The oxidized phospholipids povpc and pgpc inhibit growth and induce apoptosis in vascular smooth muscle cells. *Biochimica et Biophysica Acta (BBA)-Molecular and Cell Biology of Lipids 1761*(9), 1060–1069.

Greenberg, M., X. Li, B. Gugiu, X. Gu, J. Qin, R. Salomon, and S. Hazen (2008). The lipid whisker model of the structure of oxidized cell membranes. *Journal of Biological Chemistry 283*(4), 2385.

Hermetter, A., H. Stütz, R. Franzmair, and F. Paltauf (1989). 1-o-trityl-sn-glycero-3-phosphocholine: a new intermediate for the facile preparation of mixed-acid 1, 2-diacylglycerophosphocholines. *Chemistry and physics of lipids 50*(1), 57–62.

Leitinger, N. (2005). Oxidized phospholipids as triggers of inflammation in atherosclerosis. *Molecular nutrition & food research 49*(11), 1063–1071.

Leitinger, N., T. Tyner, L. Oslund, C. Rizza, G. Subbanagounder, H. Lee, P. Shih, N. Mackman, G. Tigyi, M. Territo, *et al.* (1999). Structurally similar oxidized phospholipids differentially regulate endothelial binding of monocytes and neutrophils. *Proceedings of the National Academy of Sciences 96*(21), 12010.

Loidl, A., R. Claus, H. Deigner, and A. Hermetter (2002). High-precision fluorescence assay for sphingomyelinase activity of isolated enzymes and cell lysates. *Journal of lipid research 43*(5), 815–823.

Loidl, A., E. Sevcsik, G. Riesenhuber, H. Deigner, and A. Hermetter (2003). Oxidized phospholipids in mmldl induce apoptotic signaling via activation of acid sphingomyelinase in arterial smooth muscle cells. *Journal of Biological Chemistry 278*(35), 32921.

Luo, Y., L. Ellis, K. Dallaglio, M. Takeda, W. Robinson, S. Robinson, W. Liu, K. Lewis, M. McCarter, R. Gonzalez, *et al.* (2012). Side population cells from human melanoma tumors reveal diverse mechanisms for chemoresistance. *Journal of Investigative Dermatology*.

Moumtzi, A., M. Trenker, K. Flicker, E. Zenzmaier, R. Saf, and A. Hermetter (2007). Import and fate of fluorescent analogs of oxidized phospholipids in vascular smooth muscle cells. *Journal of lipid research 48*(3), 565–582.

Nikolaou, V., A. Stratigos, K. Flaherty, and H. Tsao (2012). Melanoma: new insights and new therapies. *Journal of Investigative Dermatology 132*, 854–863.

Palmieri, G., M. Capone, M. Ascierto, G. Gentilcore, D. Stroncek, M. Casula, M. Sini, M. Palla, N. Mozzillo, and P. Ascierto (2009). Main roads to melanoma. *Journal of translational medicine 7*(1), 86.

Parthasarathy, S. and S. Rankin (1992). Role of oxidized low density lipoprotein in atherogenesis. *Progress in lipid research 31*(2), 127–143.

Quintana, E., M. Shackleton, H. Foster, D. Fullen, M. Sabel, T. Johnson, and S. Morrison (2010). Phenotypic heterogeneity among tumorigenic melanoma cells from patients that is reversible and not hierarchically organized. *Cancer Cell 18*(5), 510–523.

Reynolds, C., B. Maurer, and R. Kolesnick (2004). Ceramide synthesis and metabolism as a target for cancer therapy. *Cancer letters 206*(2), 169–180.

Rhode, S., A. Breuer, J. Hesse, M. Sonnleitner, T. Pagler, M. Doringer, G. Schütz, and H. Stangl (2004). Visualization of the uptake of individual hdl particles in living cells via the scavenger receptor class b type i. *Cell biochemistry and biophysics 41*(3), 343–356.

Riedl, S., B. Rinner, M. Asslaber, H. Schaider, S. Walzer, A. Novak, K. Lohner, and D. Zweytick (2011). In search of a novel target–phosphatidylserine exposed by non-apoptotic tumor cells and metastases of malignancies with poor treatment efficacy. *Biochimica et Biophysica Acta (BBA)-Biomembranes 1808*(11), 2638–2645.

Sas, B., E. Peys, and M. Helsen (1999). Efficient method for (lyso) phospholipid class separation by high-performance liquid chromatography using an evaporative light-scattering detector. *Journal of Chromatography A 864*(1), 179–182.

Sauter, E., M. Herlyn, *et al.* (1998). Molecular biology of human melanoma development and progression. *Molecular carcinogenesis 23*(3), 132–143.

Senchenkov, A., D. Litvak, and M. Cabot (2001). Targeting ceramide metabolism - a strategy for overcoming drug resistance. *Journal of the National Cancer Institute 93*(5), 347–357.

Shackleton, M., E. Quintana, E. Fearon, and S. Morrison (2009). Heterogeneity in cancer: cancer stem cells versus clonal evolution. *Cell 138*(5), 822–829.

Steinberg, D. (2009). The ldl modification hypothesis of atherogenesis: an update. *Journal of lipid research 50*(Supplement), S376–S381.

Steinbrecher, U., H. Zhang, and M. Lougheed (1990). Role of oxidatively modified ldl in atherosclerosis. *Free Radical Biology and Medicine 9*(2), 155–168.

Stemmer, U. and A. Hermetter (2012). Protein modification by aldehydophospholipids and its functional consequences. *Biochimica et Biophysica Acta (BBA)-Biomembranes*.

Stemmer, U., C. Ramprecht, E. Zenzmaier, B. Stojčić, G. Rechberger, M. Kollroser, and A. Hermetter (2012). Uptake and protein targeting of fluorescent oxidized phospholipids in cultured raw 264.7 macrophages. *Biochimica et Biophysica Acta (BBA)-Molecular and Cell Biology of Lipids*.

Subbanagounder, G., N. Leitinger, P. Shih, K. Faull, J. Berliner, *et al.* (1999). Evidence that phospholipid oxidation products and/or platelet-activating factor play an important role in early atherogenesis: in vitro and in vivo inhibition by web 2086. *Circulation research 85*(4), 311.

Vaskovsky, V. and E. Kostetsky (1968). Modified spray for the detection of phospholipids on thin-layer chromatograms. *Journal of lipid research 9*(3), 396–396.

Chapter 3

Oxidized Phospholipids Efficiently Induce Cell Death in Mouse Melanoma Cells

Oxidized Phospholipids Efficiently Induce Cell Death in Mouse Melanoma Cells

C. Ramprecht[1], L. Britz[1], E. Zenzmaier[1], H. Köfeler[2], H. Schaider[3,4] and A. Hermetter[1]

[1] *Department of Biochemistry, University of Technology, Graz, Austria*

[2] *Core Facility for Mass Spectrometry, Center for Medical Research, Medical University of Graz, Graz, Austria*

[3] *Cancer Biology Unit, Department of Dermatology, Medical University Graz, Graz, Austria*

[4] *Center for Medical Research (ZMF), Medical University Graz, Graz, Austria*

3.1 Abstract

The truncated phospholipids 1-palmitoyl-2-(5-oxovaleroyl)-*sn*-glycero-3-phosphocholine (POVPC) and 1-palmitoyl-2-glutaroyl-*sn*-glycero-3-phosphocholine (PGPC) as well as their ether analogues 1-O-hexadecyl-2-glutaroyl-*sn*-glycero-3-phosphocholine (E-PGPC) and 1-O-hexadecyl-2-(5-oxovaleroyl)-*sn*-glycero-3-phosphocholine (E-POVPC) are generated under conditions of oxidative stress from polyunsaturated diacyl- and alkylacyl-glycero-phosphocholines, respectively. These lipids share high structural similarities: they contain a long hydrophobic chain at the *sn*-1 position, and a shortened polar chain at position *sn*-2 which is part of a very large headgroup. As a consequence, they are highly amphipathic molecules and exchange easily between cells, membranes and lipoproteins, where they perturb lipid organization and protein function. We found that B16-BL6 melanoma cells efficiently incorporated oxidized phospholipids. Oxidized diacyl and alkylacyl phospholipids induced apoptosis or necrosis in a concentration-dependent manner. Lipid-induced cell death was associated with activation of acid sphingomyelinase and an increase of distinct ceramide species. The latter observation is important insofar, as ceramide has been recognized as a mediator of cell death in cancer cells. The results of this study may be considered a useful basis for testing the therapeutic potential of oxidized phospholipids in mouse models.

3.2 Introduction

Malignant melanoma is a highly aggressive type of skin cancer that is characterized by high metastatic potential, poor survival rates associated with advanced stages of

this disease, resistance to chemotherapy and poor response to most standard therapies (Hoang *et al.*, 2000; MacKie *et al.*, 2009). Surgery remains the best treatment option for earlier stages. However, metastatic melanoma is incurable in most affected patients. Thus, there is an urgent need to develop new therapeutic compounds for the treatment of melanoma, selectively inducing cytotoxic effects in the tumor but not in differentiated cells of the skin.

Recent studies in our laboratory led to the discovery that the truncated oxidized phospholipids 1-palmitoyl-2-glutaroyl-*sn*-glycero-3-phosphocholine (PGPC) and 1-palmitoyl-2-(5-oxovaleroyl)-*sn*-glycero-3-phosphocholine (POVPC) are cytotoxic to cultured melanoma cells. Both compounds preferentially induced apoptosis but not necrosis in tumor cells of different stages while melanocytes were almost unaffected (Ramprecht *et al.*, unpublished data). The toxicities of PGPC and POVPC were associated with efficient uptake of the lipids into the cells, activation of acid sphingomyelinase and the formation of the apoptotic second messenger ceramide in a cell- and lipid-specific manner.

PGPC and POVPC as well as their ether analogues E-PGPC and E-POVPC are generated under conditions of oxidative stress from polyunsaturated diacyl- and alkylacyl-glycero-phosphocholines, respectively (Bochkov *et al.*, 2010; Fruhwirth *et al.*, 2007; Marathe *et al.*, 2000). PGPC and POVPC share high structural similarities (Figure 3.1). They are characterized by a long hydrophobic chain at the *sn*-1 position, a truncated fatty acyl chain at position *sn*-2 and a very large polar head group. These truncated lipids are amphipathic molecules and thus highly exchangeable between cells, membranes and lipoproteins (Stemmer *et al.*, 2012).

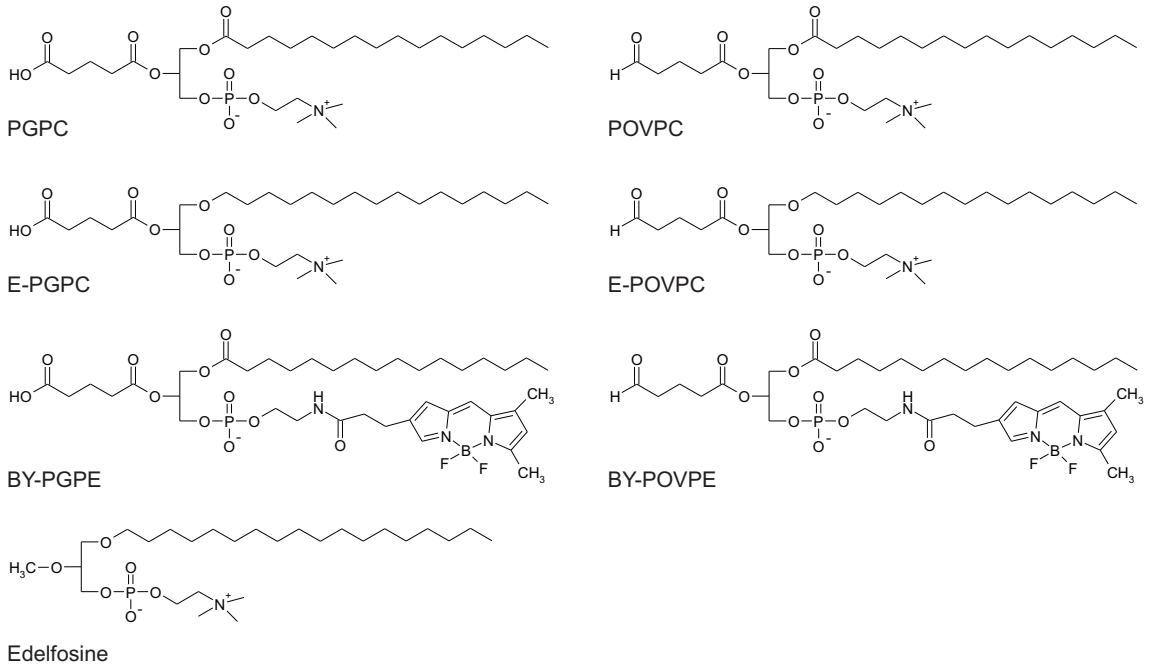

Figure 3.1. Chemical structures of oxidized phospholipids and ether analogues

1-palmitoyl-2-glutaroyl-sn-glycero-3-phosphocholine (PGPC)
1-palmitoyl-2-(5-oxovaleroyl)-sn-glycero-3-phosphocholine (POVPC)
1-O-hexadecyl-2-glutaroyl-sn-glycero-3-phosphocholine (E-PGPC)
1-O-hexadecyl-2-(5-oxovaleroyl)-sn-glycero-3-phosphocholine (E-POVPC)
N-BY-1-palmitoyl-2-glutaroyl-sn-glycero-3-phosphoethanolamine (BY-PGPE)
N-BY-1-palmitoyl-2-(5-oxovaleroyl)-sn-glycero-3-phosphoethanolamine (BY-POVPE)
1-octadecyl-2-O-methyl-sn-glycero-3-phosphocholine (Edelfosine)

The 1-O-alkyl ether phospholipid analogues E-PGPC and E-POVPC are structurally very similar to their respective diacyl counterparts PGPC and POVPC, except that their *sn*-1 hydrocarbon chains are linked to the glycerol backbone via an ether bond. Small amounts of 1-O-alk(en)yl lipids can be found in LDL, whereas large amounts of ether choline (and ethanolamine) phospholipids are found in cell membranes of animals and humans (except for the liver) (Schmid and Takahashi, 1968). These oxidized phospholipids are cytotoxic in cells of the vascular wall (Fruhwirth *et al.*, 2006; Loidl *et al.*, 2003; Stemmer *et al.*, 2012) hence playing a fundamental role in the development and progression of atherosclerosis (Chisolm and Steinberg, 2000; Parthasarathy and

Rankin, 1992; Steinberg, 2009; Steinbrecher *et al.*, 1990). Depending on lipid concentration and exposure time, PGPC and POVPC may induce inflammation, cell proliferation and, under sustained exposure, programmed cell death (apoptosis) (Bochkov, 2007; Leitinger, 2005; Fruhwirth and Hermetter, 2008; Fruhwirth *et al.*, 2007; Loidl *et al.*, 2004, 2003). We found that very low lipid concentrations were sufficient to induce apoptotic cell death in melanoma cells.

Anti-proliferative properties of synthetic alkyl-lysophospholipids and ether phospholipids on tumor cells have already been studied for decades (Ruiter *et al.*, 2001). Edelfosine is such a typical compound. It contains a long hydrophobic alkyl chain at the *sn*-1 position that is connected to the glycerol backbone via an ether bond, and an ether-linked methyl group in the *sn*-2 position (Figure 3.1). Its cytotoxic potential has been shown in several tumor cells, e.g. human leukemic cells (Gajate and Mollinedo, 2002; Gajate *et al.*, 2000) or myelomas (Gajate and Mollinedo, 2007).

Considering a potential therapeutic application of oxPL for the treatment of skin cancer, the ability of PGPC and POVPC to efficiently induce apoptosis in murine melanoma cells has to be proven in *in vitro* cell culture experiments, before testing these compounds in animal models. For this reason, the murine melanoma cell line B16-BL6 was chosen to investigate toxic effects of oxidatively modified phospholipids.

It was the aim of this study to examine if the oxidized phospholipids PGPC and POVPC and their ether analogues E-PGPC and E-POVPC are cytotoxic in the murine melanoma cell line B16-BL6. Edelfosine was used in this study as a reference compound. In addition, we determined the uptake of fluorescently labelled oxPL into the

cells, the activation of sphingomyelinase and the formation of ceramide in response to the toxic compounds. We found that the melanoma cells efficiently incorporated oxidized phospholipids. Oxidized diacyl and alkylacyl phospholipids induced apoptosis or necrosis in a concentration-dependent manner. Lipid-induced cell death was associated with activation of acid sphingomyelinase and an increase of distinct ceramide species. The latter observation is important insofar, as ceramide has been recognized as a mediator of cell death in cancer cells (Wymann and Schneiter, 2008). The results of this study may be considered as useful basis for testing the therapeutic potential of oxidized phospholipids in mouse models.

3.3 Experimental Procedures

3.3.1 Materials

PGPC (1-palmitoyl-2-glutaroyl-*sn*-glycero-3-phosphocholine) and POVPC (1-palmitoyl-2-(5-oxovaleroyl)-*sn*-glycero-3-phosphocholine) as well as their fluorescent analogues (BY-PGPE and BY-POVPE) were either synthesized in our laboratory as previously described (Moumtzi *et al.*, 2007) or purchased from Avanti Polar Lipids, Inc. (Alabaster, AL). POPC (1-palmitoyl-2-oleoyl-*sn*-glycero-3-phosphocholine) was synthesized according to the method of Hermetter *et al.* (Hermetter *et al.*, 1989). PLPC (1-palmitoyl-*sn*-glycero-3-phosphocholine) was purchased from Bachem (Bubendorf, Switzerland). Edelfosine (1-octadecyl-2-O-methyl-*sn*-glycero-3-phosphocholine), E-PGPC (1-O-hexadecyl-2-glutaroyl-*sn*-glycero-3-phosphocholine) and E-POVPC (1-O-hexadecyl-2-(5-oxovaleroyl)-*sn*-glycero-3-phosphocholine) were synthesized in our laboratory (Hermetter *et al.*, 1989; Stemmer *et al.*, 2012).

Tissue culture dishes and flasks were purchased from Sarstedt (Nürmbrecht, Germany) or Greiner (Kremsmünster, Austria). DMEM with or without Phenol red, fetal bovine serum (FCS) and Trypsin were purchased from Gibco (Carlsbad, CA). Phosphate buffered saline (PBS) and all other supplements for cell culture were from PAA Laboratories (Linz, Austria), unless otherwise indicated. Vybrant® MTT Cell proliferation Assay kit (V-13154), Vybrant® apoptosis assay kit#2 (V-132451) and staurosporine were from Invitrogen (Leek, Netherlands). Flow cytometry fluids and FACS tubes were from BD Bioscience (Heidelberg, Germany). Culture-inserts for self-insertion were from Ibidi GmbH (Munich, Germany). Organic solvents and all other standard chemicals were obtained from Carl Roth (Karlsruhe, Germany) or Sigma-Aldrich (Vienna, Austria), unless otherwise indicated.

3.3.2 Cell culture and incubation of cells with lipids

B16-BL6 murine melanoma cells were from Dr. Yasuhisa Matsui (Cell Resource Center for Biomedical Research, Institue of Development, Aging and Cancer, Tohoku University, Sendai, Japan). B16-BL6 cells were routinely grown in DMEM (4.5 g/l glucose, 25 mM HEPES, 4 mM L-glutamine, without sodium pyruvate) supplemented with 2% fetal bovine serum and 200 units/ml penicillin/streptomycin at 37°C in humidified CO_2 (5%) atmosphere.

For all experiments, aqueous lipid suspensions containing the indicated lipid concentrations were prepared using the ethanol injection method (Batzri and Korn, 1973). The final ethanol concentration in the incubation medium did not exceed 1% (v/v). Incubation medium for all experiments was DMEM without Phenol red supplemented with only 0.1% FCS to minimize degradation of the oxidized phospholipids by serum

components. Control experiments were carried out with incubation medium containing 0.1% FCS and the same amount of EtOH without lipids.

3.3.3 Fluorescence microscopy

For microscopy experiments, monolayer cultures of B16-BL6 cells were grown to 60-70% confluency in Chamber slides (Imaging Chambers CG8 Cover Glass Bottom from MoBiTec, Göttingen, Germany). Fluorescence of the individual probes was observed with an Axiovert 35 inverted fluorescence microscope equipped with a mercury-arc lamp (HBO® 50W/AC; OSRAM, Munich, Germany) and a charge-coupled device digital camera system (AxioCam HR), driven by AxioVision software 3.1 package (Carl Zeiss Vision GmbH, Germany). Unlabeled cells were used as a reference to examine autofluorescence. Table 3.1 summarizes the filter sets used. For comparative studies, all photomicrographs were taken and processed under identical conditions for a given fluorophore.

Colocalization experiments. To identify the subcellular localization of BY-PGPE or BY-POVPE, cells were stained with specific organelle markers localizing to the endoplasmic reticulum (ER-Tracker™Red dye from Invitrogen, 1 µM final concentration) or mitochondria (MitoTracker® Red CM-XRos from Invitrogen, 0.3 µM final concentration). For this purpose, cells were pre-treated with the respective probe for 20 min in incubation medium (DMEM without Phenol red supplemented with 0.1% FCS) followed by two washing steps with medium and incubation with 5 µM fluorescently labelled oxPL for 5 or 30 min at 37°C. After rinsing the cells twice with medium, cells were viewed under the fluorescence microscope. Fluorescence images of both the

BODIPY lipid and the organelle-specific marker were recorded from the same cells and used to produce overlay images using CorelDRAW X4 software.

Table 3.1. Excitation and emission maxima of fluorescence probes and optical instrument settings for fluorescence microscopy

Samples were observed with an Axiovert 35 inverted fluorescence microscope equipped with a mercury-arc lamp.

Fluorophore (Invitrogen)	Excitation Maxima [nm]	Emission Maxima [nm]	Excitation Filter Beam Splitter Barrier Filter
BODIPY	505	510	BP 450-490 FT 510 LP 520
DAPI Nucleic Acid Stain	358	461	BP 365 FT 395 LP 397
MitoTracker® Red CM-XRos	579	599	BP 510-560 FT 580 LP 590
ER-Tracker™ Red	587	615	BP 575-625 FT 665 LP 666-710

For colocalization studies of BY-PGPE or BY-POVPE and the nucleic acid specific probe DAPI (DAPI nucleic acid stain from Invitrogen, 0.3 µM final concentration), cells were first incubated with 5 µM labelled lipid for 5 or 30 min at 37°C as described above. After incubation, cells were carefully rinsed with media, fixed by incubation with 300 µl 3.7% formaldehyde solution (v/v in PBS) for 10 min at RT, washed and incubated with the indicated amount of the DAPI stain for 5 min at RT. Fixing of the cells with formaldehyde did not change the localization of BY-PGPE or BY-POVPE (data not shown).

3.3.4 MTT viability assay

To investigate the cytotoxic effects of PGPC, POVPC and Edelfosine on murine B16-BL6 melanoma cells, the Vybrant® MTT Cell proliferation assay was used according to the manufacturer's protocol with slight modification. This assay is based on the conversion of water soluble MTT to insoluble formazan by living cells (Liu *et al.*, 1997). The formed purple formazan is solubilised by the addition of SDS and the optical density is measured at 595 nm; low absorbance values reflect low viability of cells and *vice versa*. In brief, cells were seeded in DMEM (supplemented with 2% FCS) in 96-well-plates and allowed to reach 80% confluency. The medium was replaced by the lipid dispersion containing the indicated lipid (5 to 250 µM) or just organic solvent (1% EtOH (v/v) or 1% DMSO (v/v)) as negative controls. Cells were also incubated with 2.5 mM H_2O_2 or 10 µM staurosporine, which served as controls for necrosis and apoptosis, respectively. Following incubation, the lipid containing medium was replaced by 100 µl fresh medium (0.1% FCS) and 10 µl MTT solution (2.5 mg/ml) in PBS prior to cell incubation at 37°C for 4 hours. Subsequently, 100 µL 10% SDS (w/v) in 0.01% HCl (v/v) were added and the cells were incubated for another 4 hours under the same conditions. After incubation, the heterogenous mixture was resuspended carefully and optical density was measured at 595 nm using an Anthos plate reader driven by WinRead 2.3 software (Anthos Labotec, Salzburg, Austria). Data were obtained from 2 replicates of three or more independent experiments. Values are means $\pm$ SD ($n \geq 3$).

3.3.5 Flow cytometric analysis of apoptotic and necrotic cells

The Vybrant® apoptosis assay kit#2 was used for FACS analysis of cell death according to the manufacturer's instructions with slight modifications. Cells were seeded into

24 well plates and allowed to reach 80% confluency. After washing with DMEM containing 0.1% FCS, cells were incubated with 400 µl of a dispersion of 25 µM or 50 µM lipid (PGPC, POVPC, E-PGPC, E-POVPC or Edelfosine) in DMEM (0.1% FCS), or 400 µl incubation medium containing 1% EtOH (v/v) (control), 10 mM H_2O_2 (induces necrosis), 10 µM STS (apoptosis inducer) or 1% DMSO (v/v) (control) for 6 hours. Following incubation, the supernatant was collected and the cells were harvested after treatment with accutase. Wells were washed twice with DMEM to collect residual cells and all fractions were combined. After centrifugation, cells were washed with PBS containing 2% glucose and resuspended in 100 µl Annexin Binding Buffer. 5 µl AlexaFluor®488 Annexin V solution and 5.5 µl of an aqueous solution of PI (final concentration 1 mg/ml) were added to each sample and incubated in the dark at room temperature for 15 minutes. Samples were diluted with 400 µl PBS containing 2% glucose, gently mixed and kept on ice until analysis. Stained samples were analyzed using a FACS Calibur flow cytometer (BD Bioscience, NJ). The green fluorescence emission was measured at 530 nm and the red fluorescence emission was determined at 575 nm. Excitation wavelength was 488 nm. Three cell populations were identified: living cells were unstained; cells stained by PI only or cells double stained by PI and Annexin V were considered necrotic; cells showing only the green AlexaFluor®488 Annexin V fluorescence were considered apoptotic cells. The percentage of apoptotic and necrotic cells was calculated using the WinMDI 2.8 software package. Data were obtained from 2 replicates of three or more independent experiments. Values are means $\pm$ SD ($n \geq 3$).

3.3.6 Microscopic analysis of apoptotic and necrotic cells

Prior to harvesting cells for FACS analysis of apoptotic and necrotic cells, cells were observed in the transmission mode with an Axiovert 35 inverted microscope equipped with a charge-coupled device camera, driven by AxioVision software package (Carl Zeiss Vision GmbH, Germany) to detect morphological changes induced by oxPL.

3.3.7 Determination of acid sphingomyelinase activity

Murine B6-BL6 melanoma cells were grown on 60 mm Petri dishes to 70-80% confluency in DMEM (supplemented with 2% FCS) over night. Prior to stimulation with oxPL, the cells were washed once with medium containing 0.1% FCS. Cells were incubated with 3 ml of a 25 µM aqueous lipid dispersion or 3 ml medium containing 0.1% EtOH (v/v) as a negative control for 15 min, 30 min or 60 min. Following incubation, cells were rinsed with ice-cold PBS, scraped and harvested by centrifugation (300 g, 10 min, 4°C). Cells were lysed in 50 µl lysis buffer (250 mM sodium acetate, 0.2% Triton X-100, pH 5.0) for one hour on ice. The suspension was shaken vigorously every 15 minutes. Cell debris and unlysed cells were removed by centrifugation (1000 g, 5 min, 4°C) and the protein content of the samples was determined according to the method of Bradford (Bradford, 1976). Aliquots of cell lysates containing 15 µg of protein were incubated with 2 nmol NBD-sphingomyelin in acid reaction buffer for 30 minutes to determine acid sphingomyelinase activity as previously described (Loidl *et al.*, 2002). Fluorescent NBD-sphingomyelin was separated from formed NBD-ceramide by thin-layer chromatography on silica gel (mobile phase was $CHCl_3$:MeOH:H_2O 65:24:4 per vol.). The fluorescent spots were quantified with a charge-coupled device camera (Herolab, Vienna) at an excitation wavelength of 365 nm using EasyWin software.

The ratio of NBD-ceramide to total NBD lipid (Cer+SM) was determined and data (relative aSMase activity) were expressed as means $\pm$ SD ($n \geq 3$).

3.3.8 Determination of ceramide and sphingomyelin species

Murine B16-BL6 melanoma cells were grown on 100 mm Petri dishes to 70-80% confluency in DMEM (supplemented with 10% FCS) over night. Prior to incubation, cells were rinsed once with media containing 0.1% FCS to remove excess serum and incubated with 4 ml of 25 µM lipid dispersion in DMEM without Phenol red (0.1% FCS) or control medium containing 1% EtOH (v/v) for 6 hours. Following incubation, cells were rinsed once with ice cold PBS, scraped into PBS and harvested by centrifugation (300 g, 10 min, 4°C). Cells were suspended in 1 ml PBS and 100 µl aliquots were taken for measuring sample protein concentration. For this purpose, cells were harvested by centrifugation, resuspended in 0.5 ml buffer (50 mM Tris/HCl, pH 7.4) and lysed by sonication (5 pulses, 10 sec). To remove cell debris, the lysate was centrifuged (1000 g, 5 min, 4°C) and the protein content was determined according to the method of Bradford (Bradford, 1976).

The remaining 900 µl cell suspension were centrifuged under the conditions described above and cells were suspended in 3 ml $CHCl_3$:MeOH (2:1 v/v). The mixture was shaken for 1 h at 4°C. After addition of 700 µl $MgCl_2$ solution (0.036% in H_2O w/v) for 15 min, the upper aqueous phase was removed and the solvent was removed from the lower chloroform phase under a gentle stream of nitrogen.

Mild alkaline hydrolysis of lipid esters and detection of ceramide and sphingomyelin species by HPLC-MS were performed as previously described (Ramprecht *et al.* un-

published data). Results were obtained from three independent experiments and data represent means ± SD (n = 3).

3.3.9 Determination of cell migration using a scratch assay

Cells were seeded into 24 well plates covered with culture-inserts (Ibidi, Planegg/ Martinsried, Germany) containing full growth medium. Cell were grown over night and allowed to reach 100% confluency. After cell attachment, the culture-inserts were removed leaving a cell-free gap of approximately 500 µm width. The remaining cells were washed with medium five times to reduce the number of floating cells that could reattach to the cell-free zone during further incubation. Cells were incubated with 5 µM or 10 µM oxPL in DMEM (2% FCS) or 1% (v/v) EtOH in DMEM (2% FCS). Cell migration into the cell-free zone under the influence of oxidized phospholipids was followed over a 48 h time period. Micrographs of the scratch were taken after the indicated incubation times using an Axiovert 35 inverted microscope equipped with a charge-coupled device camera, driven by AxioVision software package (Carl Zeiss Vision GmbH, Germany). The microscopy images were always taken from the identical scratch area within one well. The width of the cell-free zone was measured using ImageJ software (Abràmoff *et al.*, 2004) and the migration rate was calculated and expressed as percentage of the initial width of the gap. Results were obtained from replicates of three or more independent experiments and data represent means ± SD ($n \geq 3$).

3.3.10 Statistical analysis

Data are expressed as means ± standard deviation (SD). Two-tailed unpaired Student's t-test was used to determine the significance of the differences. A p-value ≤

0.05 was considered significant.

3.4 Results

To understand the toxicity of oxidized phosholipids in the murine cell line B16-BL6, we determined the effects of these lipids on cell viability, cell death, activation of acid sphingomyelinase and ceramide formation and studied the cellular uptake of fluorescent oxPL analogues into these cells.

To ensure that any observed cellular effects of oxPL are exclusively the result of incubation with intact lipids and not elicited by degradation products, all experiments were performed in DMEM supplemented with 0.1% FCS. Under high serum conditions (10% FCS) the stability of oxPL is decreased due to serum lipases, which cleave the oxidized fatty acid at the *sn*-2 position. The so generated PLPC is cytotoxic as well (Fruhwirth *et al.*, 2006; Stemmer *et al.*, 2012).

3.4.1 Import and localization of fluorescent PGPC and POVPC analogues

We performed microscopic studies to examine the uptake and the intracellular distribution of the fluorescent PGPC and POVPE analogues BY-PGPE and BY-POVPE, respectively, in murine B16-BL6 melanoma cells. For this purpose, cells were incubated with the corresponding lipid followed by staining with an organelle specific marker in serum-free medium to avoid degradation of the lipids by lipases in the serum.

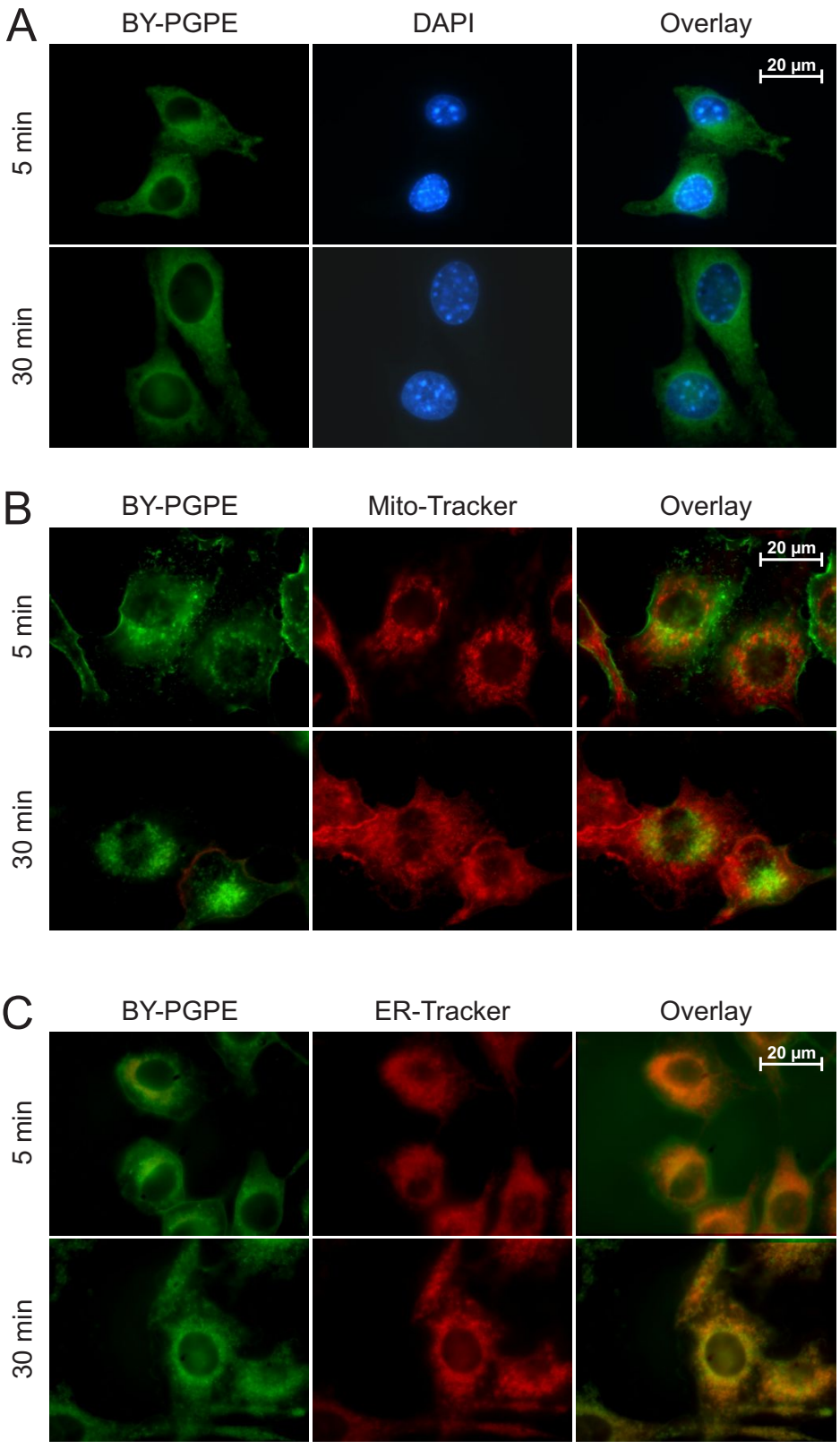

Continued on the following page

Figure 3.2. Uptake and subcellular localization of BY-PGPE in B16-BL6 murine melanoma cells

Cells were incubated with 5 µM BY-PGPE in Phenol red-free medium supplemented with 0.1% FCS for the indicated times at 37°C and fixed with formaldehyde-solution. Nuclei were stained with DAPI Nucleic Acid Stain (0.3 µM) as described in Experimental Procedures ***(A)****. Alternatively, cells were pretreated with MitoTracker® Red CM-XRos (0.3 µM)* ***(B)*** *or ER-Tracker™Red dye (1 µM)* ***(C)****, followed by incubation with 5 µM BY-PGPE in Phenol red-free medium (0.1% FCS) for 5 or 30 minutes at 37°C. Fluorescence images of both the BODIPY lipid and the organelle-specific marker were recorded from the same cells and images were overlaid using CorelDRAW X4 software. In control experiments, no crossover between green (BODIPY-PGPE), blue (DAPI Nucleic Acid Stain), and red (MitoTracker® Red CM-XRos, ER-Tracker™Red dye) fluorescence was detected at the concentrations indicated above. No background fluorescence was detected (data not shown). Brightness and contrast were adjusted to the same levels in all images using CorelDRAW X4 software. Photographs shown are representative for three or more independent experiments.*

Both fluorescent oxidized phospholipids are rapidly internalized by B16-BL6 cells. BY-PGPE is transferred to the endoplasmatic reticulum (ER) within 5 minutes, where it remains at least for 30 minutes. This oxPL does not localize to mitochondria and the nucleus under our experimental conditions, as determined by double staining experiments (Figure 3.2).

Fluorescent BY-POVPE is also rapidly internalized by B16-BL6 cells, and partial delivery of the fluorescently labelled lipid to the ER can be observed after 30 minutes of incubation. No colocalization with the mitochondria-specific probe MitoTracker® Red CM-XRos or the nucleic acid specific probe DAPI was found (Figure 3.3).

These data are at variance to earlier studies on vascular smooth muscle cells (Moumtzi *et al.*, 2007) and RAW 264.7 macrophages (Stemmer *et al.*, 2012). In these cells, BY-POVPE localized to the plasma membrane, whereas BY-PGPE localized to intracellular membranes.

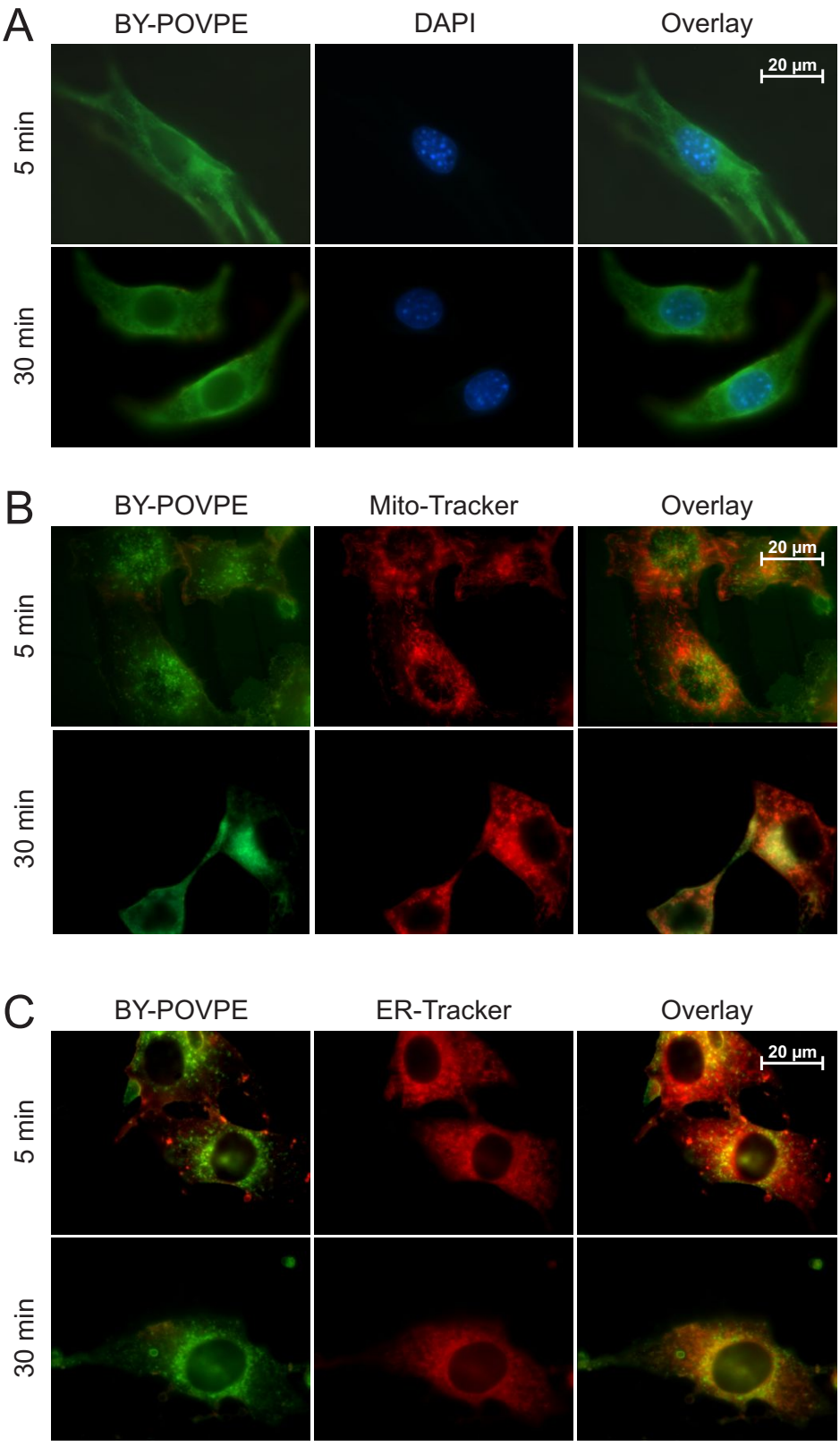

Figure 3.3. Uptake and subcellular localization of fluorescent BY-POVPE in murine B16-BL6 melanoma cells

A-C: *Cells were incubated with the fluorescent BY-POVPE and organelle specific stains and fluorescence images were obtained as described for BY-PGPE (Figure 3.2).*

3.4.2 OxPL reduce viability of B16-BL6 mouse melanoma cells in a time- and concentration dependent manner

We used the photometric Vybrant® MTT Cell Viability assay to determine time- and concentration-dependent effects of oxPL on cell viability. For this purpose, B16-BL6 cells were incubated with different concentrations (5-250 µM) of the synthetic lipids for varying times. POPC and PLPC were used as natural reference phospholipids. H_2O_2 and staurosporine were used as positive controls for the induction of necrosis and apoptosis, respectively.

We found that all oxidized lipids used in this study induce a time- and concentration-dependent decrease in cell viability, but the extent of cell death is dependent on the individual lipid (Figure 3.4). Independent of the incubation time, Edelfosine is the most toxic lipid. 50 µM concentrations of this compound are sufficient to decrease cell viability by 70% after 2 hours. Longer incubation times lead to a complete loss of cell viability. If cells are exposed to 50 µM PGPC and POVPC, cell death is already detectable after 2 hours. Independent of the incubation time, PGPC is in all cases more toxic to B16-BL6 cells than POVPC. The non-oxidized phospholipid POPC does not affect cell viability at all. Toxicity of 50 µM PLPC is comparable to Edelfosine, almost completely killing B16-BL6 cells after short incubation times.

3.4.3 Low concentrations of oxPL preferentially induce apoptosis in murine melanoma cells

MTT experiments revealed that incubation of B16-BL6 mouse melanoma cells with oxPL is associated with decreased cell viability (Figure 3.4). To find out whether oxidized phospholipid-induced cell death is due to apoptosis and necrosis, we stained

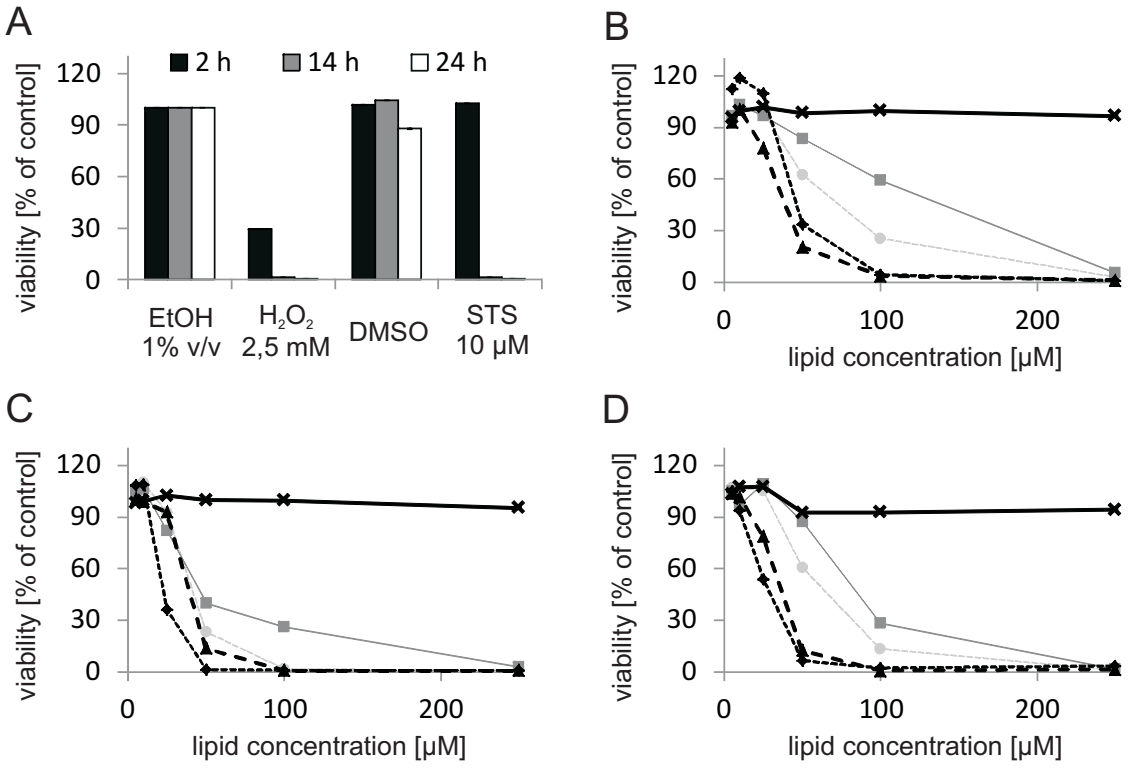

Figure 3.4. Effect of oxPL on viability of B16-BL6 murine melanoma cells

Viability of B16-BL6 murine melanoma cells was analyzed using the MTT photometric assay (for details see Experimental Procedures). Cells were incubated with different concentrations of PGPC (●), POVPC (■) or Edelfosine (♦) in DMEM supplemented with 0.1% FCS for 2 h ***(panel B)****, 14 h* ***(panel C)*** *or 24 h* ***(panel D)****. POPC (×) was used as a reference phospholipid. PLPC (▲) served as a positive control for the induction of cell death. Results were obtained from 2 replicates of three or more independent experiments and values represent means ± SD ($n \geq 3$).*

the cells with specific fluorescence markers followed by FACS analysis: AlexaFluor488® Annexin V binds to phosphatidylserine on the cell surface which is indicative for apoptosis. Red fluorescent propidium iodide (PI) crosses the permeabilized membrane of necrotic cells and stains their DNA. Labelled cells were counted and spectroscopically identified by FACS. Cells stained by PI or double stained cells were defined as necrotic cells, cells showing only the green Annexin V fluorescence were considered apoptotic. Intact cells were not stained by either fluorescence dye. Staurosporine and H_2O_2 were used as control reagents that induce apoptosis and necrosis.

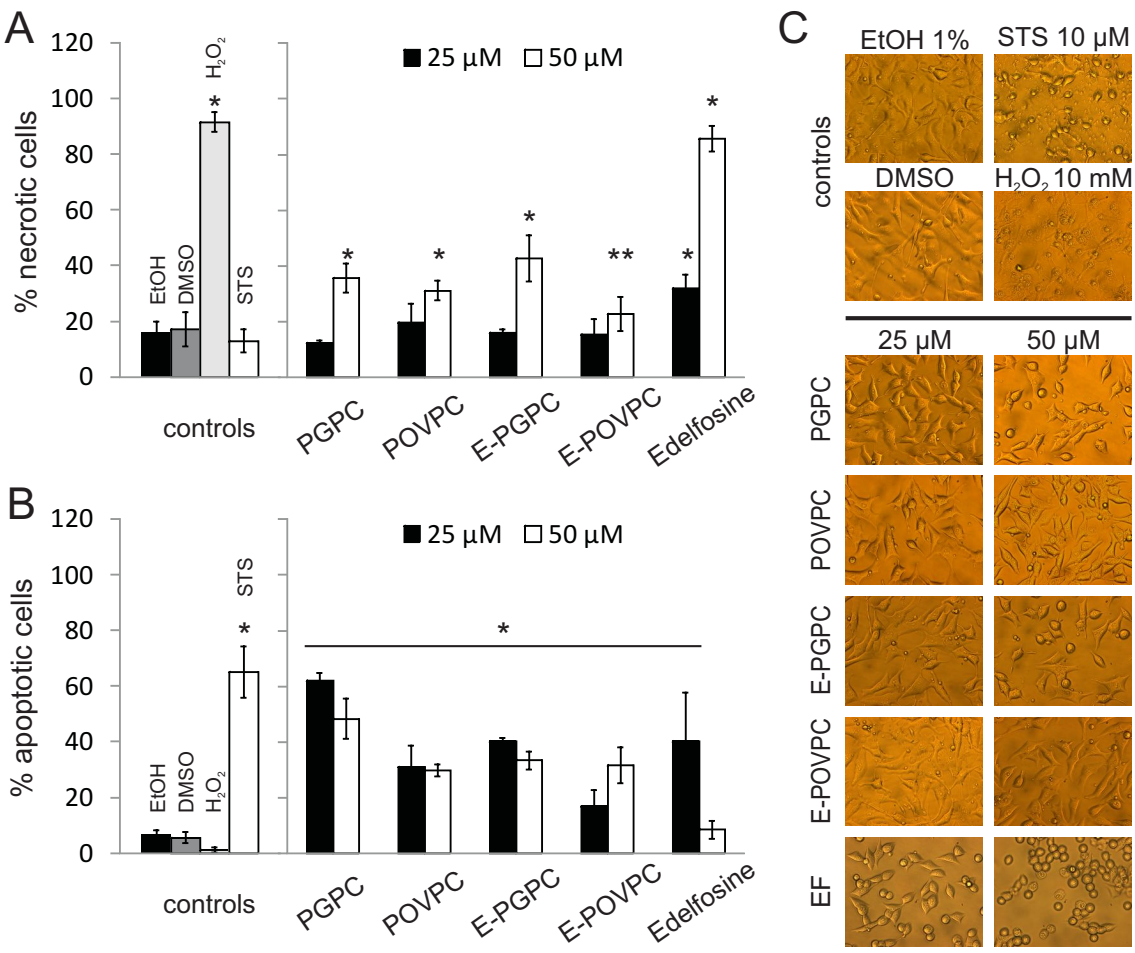

Figure 3.5. Apoptosis and necrosis of cultured B16-BL6 murine melanoma cells in response to oxidized phospholipids

B16-BL6 cells were incubated with 25 or 50 µM lipid for 6 hours in DMEM (0.1% FCS). Control cells were treated with EtOH (1% v/v) (negative control), 10 µM STS (positive control for apoptosis) or 10 mM H_2O_2 (positive control for necrosis). After fluorescence staining, cells were analyzed by flow cytometry (for details see Experimental Procedures) to determine the fractions of apoptotic and necrotic cells. Apoptotic cells were stained by green fluorescent AlexaFluor488® Annexin V. Necrotic cells were stained by fluorescent Annexin V and propidium iodide. ***Panel A:*** *Stimulation of necrosis.* ***Panel B:*** *Stimulation of apoptosis.* ***Panel C:*** *Morphological changes after incubation with the same lipids and control media. Results shown in panels A and B were obtained from 2 replicates of three or more independent experiments and values represent means ± SD (*P < 0.05 compared with control; **P < 0.005 compared with control; $n \geq 3$)*

At low concentrations (25 µM) all tested lipids significantly induce apoptosis in B16-BL6 mouse melanoma cells (Figure 3.5 B). The amount of necrosis is comparable in stimulated and unstimulated cells (Figure 3.5 A). The sensitivity of the cells towards

the toxic compounds is highly dependent on lipid structure and concentration. PGPC is the most toxic oxPL, which is in line with the results from the MTT assay. The oxidized diacyl phospholipids PGPC and POVPC elicit more severe apoptotic effects as compared to their alkylacyl counterparts. Raising the lipid concentration to 50 µM leads to both an increase in the fractions of apoptotic and necrotic cells.

In addition to FACS measurements for the discrimination of apoptotic and necrotic cell death, we assessed morphological changes associated with apoptosis (Figure 3.5 C). Early phase programmed cell death is characterized by cell shrinkage, condensation of chromatin, membrane blebbing and formation of apoptotic blebs (Elmore, 2007). Typical signs of necrosis are an increase in cell volume caused by loss of plasma membrane integrity and thus a disturbance of the osmotic balance and the formation of cytoplasmic vesicles (Elmore, 2007). These morphological changes were observed in cells treated with staurosporine or hydrogen peroxide for the induction of apoptosis and necrosis, respectively. Upon treatment of the cells with higher concentrations of oxPL (50 µM), cell shrinkage as well as cell rounding were visible. These effects were more pronounced if cells were exposed to PGPC, E-PGPC and Edelfosine. Latter lipid showed characteristic signs of necrosis in cells treated with 50 µM Edelfosine, confirming the FACS results.

3.4.4 Activation of acid sphingomyelinase by PGPC and POVPC

Ceramide mediates the cellular response to various stress stimuli. Specifically, it is a key upstream component in many apoptotic signaling pathways. It can be generated by different pathways including the degradation of sphingomyelin by sphingomyelinases, *de novo* formation from sphinganine by ceramide synthases and the formation

of ceramide from sphingosine in the salvage pathway utilizing sphingosine for reacylation by ceramide synthase.

Recently, we found that aSMase activity and ceramide formation were stimulated by oxPL in human melanoma cells (Ramprecht *et al.*, unpublished data). According to the present study, acid sphingomyelinase activity is activated by oxPL in murine B16-BL6 melanoma cells, too. Specifically, cells were stimulated with 25 µM PGPC or POVPC for different times and the rise in aSMase activity was measured (Figure 3.6) as described in Experimental Procedures.

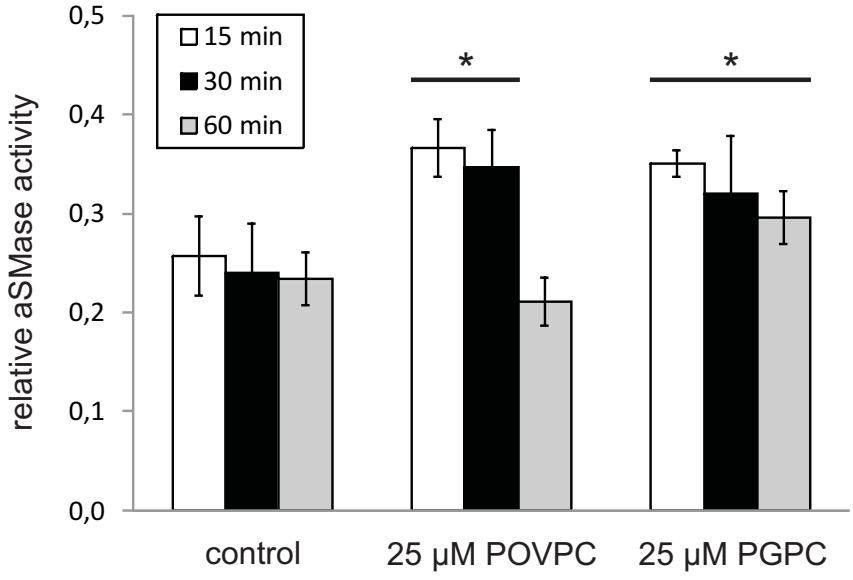

Figure 3.6. Effects of oxPL on acid sphingomyelinase activity in B16-BL6 melanoma cells

*Murine B16-BL6 melanoma cells were incubated with 25 µM oxPL or 1% (v/v) EtOH as a control in DMEM (0.1% FCS) without Phenol red for the indicated times. Cells were harvested and lysed in acid lysis buffer for assaying acid sphingomyelinase activity according to the method of Loidl et al. (Loidl et al., 2002). Enzyme activities were determined using NBD-labelled sphingomyelin as a substrate. The fluorescent NBD-ceramide product was separated from the remaining sphingomyelin substrate by thin-layer chromatography on silica plates using $CHCl_3$:MeOH:H_2O (65:24:4, per vol.) as solvent. Fluorescence intensities were analyzed using a CCD camera, and the ratio of NBD-ceramide to total NBD lipid (Cer + SM) was determined. Results represent means ± SD (*P < 0.05 compared with control, n ≥ 3)*

The enzyme was activated by both PGPC and POVPC within minutes and the efficiency of stimulation was similar in both cases. However, at prolonged incubation time (60 min), aSMase returned to control levels in POVPC-treated cells, whereas the enzyme remained active in PGPC-treated cells. This finding is very unusual compared to other cell lines insofar as aSMase activities in vascular cells (vascular smooth muscle cells and macrophages) returned to control levels after one hour (Loidl *et al.*, 2003; Stemmer *et al.*, 2012).

3.4.5 OxPL affect ceramide and sphingomyelin species in B16-BL6 mouse melanoma cells

Earlier studies demonstrated that ceramide was formed in cultured human melanoma cells upon exposure to POVPC (Ramprecht *et al.*, unpublished data). Here, we provide evidence that both PGPC and POVPC lead to a significant rise in total ceramide content after 6 hours (Figure 3.7 B). PGPC preferentially stimulated formation of C24:0 as well as C24:1 ceramide, whereas POVPC only triggered the formation of C24:0 ceramide (Figure 3.7 A). However, the oxPL-induced formation of ceramide is not associated with significant changes in apparent sphingomyelin patterns. Total sphingomyelin contents remain constant independent of the stimulus, and no significant changes in the amounts of the individual sphingomyelin species can be detected (Figure 6, panels C and D).

3.4.6 POVPC decreases undirected cell movement (chemokinesis)

Cancer cells spread from the initial site of tumor growth into surrounding tissues and the vasculature. Preventing metastasis represents an important therapeutic approach to cancer treatment. OxLDL, which contains significant amounts of PGPC and

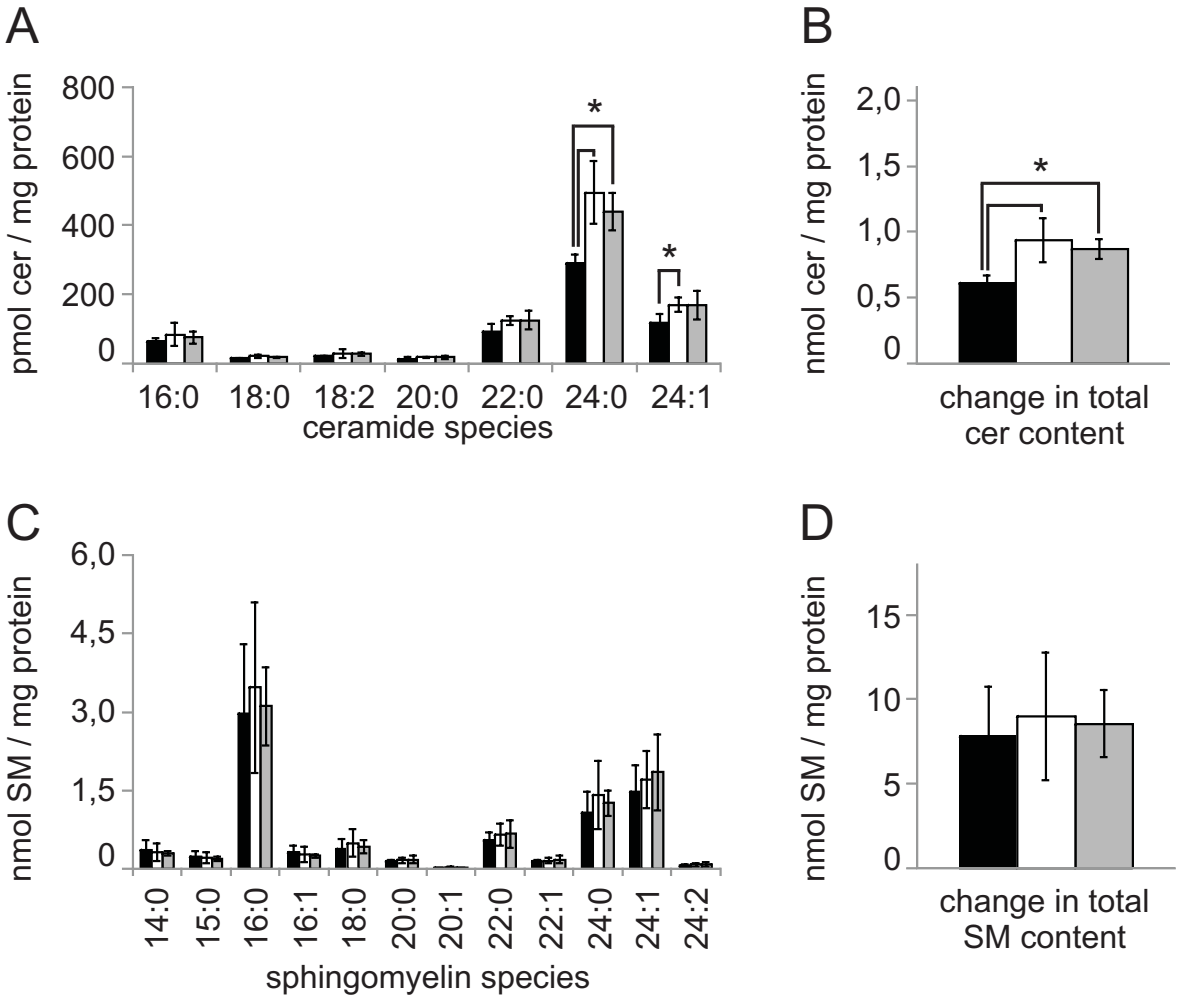

Figure 3.7. Effect of oxPL on ceramide and sphingomyelin patterns in B16-BL6 murine melanoma cells

Cells were incubated with 25 µM PGPC (□), POVPC (■) or 1% EtOH (v/v) (negative control) (■) for 6 hours in DMEM supplemented with 0.1% FCS. Lipids were extracted and analyzed by MS as described in Experimental Procedures. ***Panels A+C:*** *Lipid-protein ratios of ceramide (A) and sphingomyelin (C) species characterized by the N-acyl residues indicated on the abscissa.* ***Panels B+D:*** *Lipid-protein ratios of total ceramide (B) and sphingomyelin (D) content. Values represent means ± SD (*P < 0.05 compared with control, n = 3)*

POVPC, has already been known to induce different responses (proliferation or cell death) in vascular cells depending on concentration, incubation time and extent of particle oxidation (Han *et al.*, 1999). Thus, we further investigated the effects of lower (5 µM or 10 µM) oxPL concentrations on proliferation and migration of murine B16-BL6 melanoma cells.

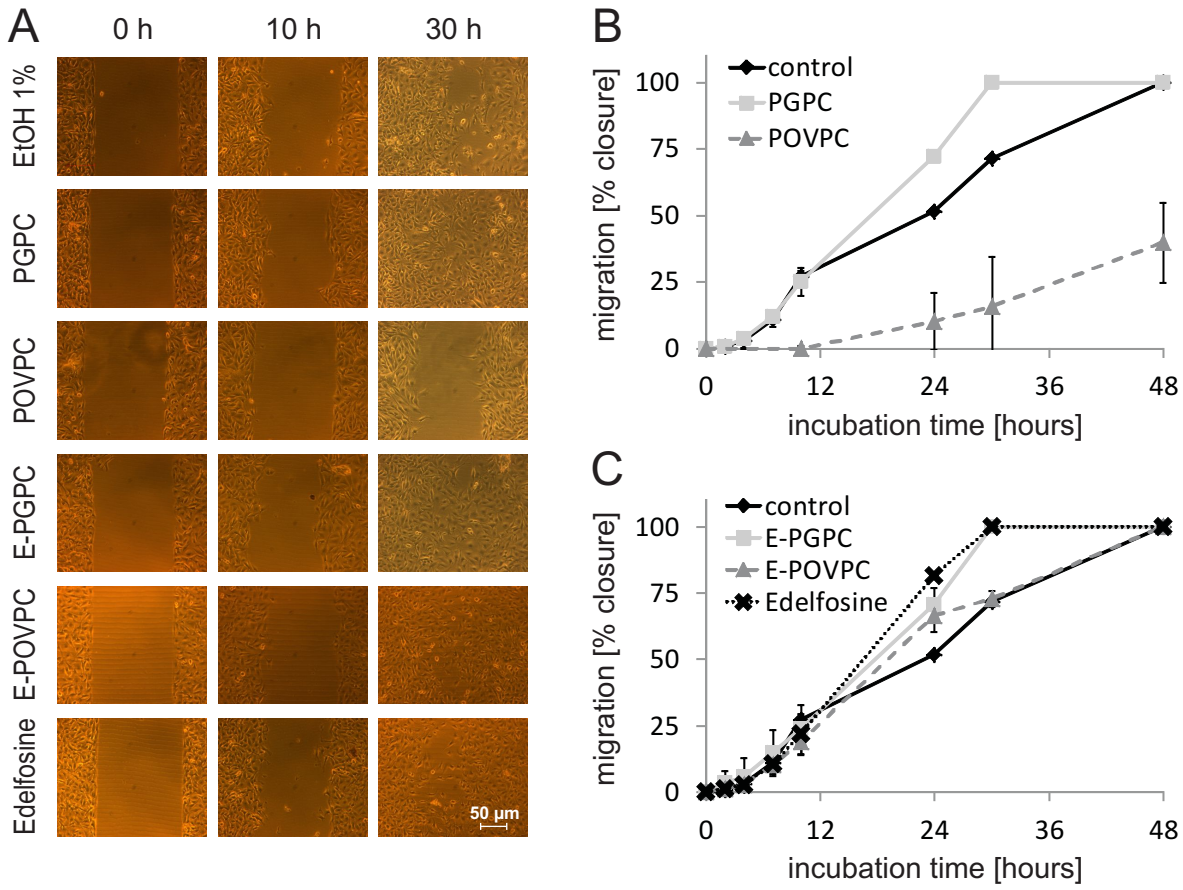

Figure 3.8. Effects of oxPL on migration of cultured murine B16-BL6 melanoma cells

Cultured B16-BL6 melanoma cells were analyzed for their potential to migrate into a cell-free scratch region under the influence of 5 µM oxPL (see Experimental Procedures). ***Panel A:*** *Microscopy images of cells after 0 h, 10 h and 30 h incubation with oxPL. The % width of the cell-free scratches relative to control cells are expressed as reciprocal values (% closure) in panels B and C.* ***Panel B:*** *Effects of 5 µM PGPC or POVPC or 1% (v/v) EtOH (negative control).* ***Panel C:*** *Effects of 5 µM oxidized ether-phospholipids E-PGPC or E-POVPC, in comparison to untreated control cells. Data are expressed as means ± SD ($n \geq 3$).*

Figure 3.8 A shows phase-contrast optical micrographs of melanoma cells migrating across a cell free zone after incubation with 5 µM oxPL for 0 h, 10 h and 30 h. Depending on the oxPL used, cells show a different tendency to migrate into this cell free zone over 48 hours. Cells preincubated with the ether-oxPL show the same migration rate compared with control cells (Figure 3.8 C). Treatment of B16-BL6 cells with PGPC leads to an increased motility leading to complete gap closure within 30 hours, whereas incubation with POVPC significantly inhibits cell migration. Most interestingly, higher concentrations of oxPL (10 µM) do not show any effects on cell migration. If in contact with POVPC, the cells would even die. They show cell shrinkage, membrane blebbing and detachment from the plate surface (data not shown).

3.5 Discussion

In the present study we report on the cytotoxicity of oxidized phospholipids in murine melanoma cells. We found that these compounds induce cell death in B16-BL6 cells. Fluorescent analogues of PGPC and POVPC are rapidly taken up by the cells and localize to the ER. Cell death is associated with activation of acid sphingomyelinase and increased levels of distinct ceramide species. Activity patterns of PGPC, POVPC and their respective ether analogues are different, because POVPC is chemically reactive and PGPC is not.

Efficient uptake of a drug by its target cells is a prerequisite for its cellular activity. Thus, we used fluorescently labelled derivates of PGPC and POVPC to investigate the uptake and intracellular localization of these lipids in B16-BL6 cells. In vascular smooth muscle cells, BY-PGPE was rapidly taken up by the cells, finally localizing to

the lysosomes. In contrast, BY-POVPE stained the plasma membrane, most likely due to covalent Schiff base formation with NH_2 groups of lipids and proteins (Moumtzi *et al.*, 2007). Similar uptake patterns were observed in RAW 264.7 macrophages (Stemmer *et al.*, 2012). Our laboratory showed for the first time a different uptake scheme for oxPL in cancer cells. In human melanoma cells, both oxPL were rapidly internalized without retention in the plasma membrane (Ramprecht *et al.*, unpublished data). Co-localization studies in B16-BL6 cells revealed similar fluorescence patterns compared to human melanoma cells. Both, BY-PGPE and BY-POVPE were internalized within minutes and at least in part localized in a nucleus near region of the ER (Figure 3.2, Figure 3.3).

The toxic effects of oxidized phospholipids in mouse melanoma cells are in line with previous results from our laboratory obtained with human melanoma cell lines. Interestingly, the mode of cell death depends on oxPL concentrations. Exposure of cells to 25 µM oxPL led to apoptosis, whereas higher lipid concentrations induced necrosis (Figure 3.5). According to Zeiss, both apoptosis and necrosis are not completely independent processes. Cellular ATP-concentrations, Ca^{2+} concentration and ROS levels determine the outcome of a death signal that is apoptosis or necrosis. A change in one of these critical parameters induced e.g. by cellular stress may lead to a switch in the cell death program (McConkey, 1998; Zeiss, 2003). Our studies on oxPL-induced toxicity in B16-BL6 cells suggest such a concentration-dependent balance between apoptotic and necrotic cell death.

Toxic effects of oxidized phospholipids depend on both their biochemical and biophysical properties. The structural differences between POVPC and PGPC are very

small. However, their biological activities differ to a large extent, depending mainly on the oxidized *sn*-2 acyl chain. The polar phospholipid headgroup plays only a minor role (Subbanagounder *et al.*, 2000). Greenberg *et al.* suggested that the modified *sn*-2 carboxylic acids of PGPC and POVPC protrude from the plasma membrane into the aqueous environment forming whisker like structures (Greenberg *et al.*, 2008). These structural elements can be recognized by macrophages and other phagocytes. Within the cell membranes the oxPL can undergo specific interactions with other biomolecules, induce changes in membrane organization and membrane curvature thus influencing the functional membrane-associated molecules (Stemmer and Hermetter, 2012). Last but not least oxidized phospholipids can give rise to a loss in membrane asymmetry, which in turn may have fundamental consequences for cellular signaling networks (Stemmer and Hermetter, 2012)(Kinnunen *et al.*, 2012).

It is interesting to note that the ether analogues of PGPC and POVPC exhibit similar toxicities as compared to their diacyl counterparts. Whereas the stability of the latter lipid subclass mostly depends on their susceptibility towards lipid hydrolases, alkyl-acyl phospholipids require oxidative enzymes for full degradation that is removal of the *sn*-2 acyl chains by lipolysis and removal of the 1-O-alkyl residue by an oxidative step. Therefore, it is likely that both lipid subclasses may undergo similar molecular interactions at least during a limited lifetime.

A fundamental difference between (E-)PGPC and (E-)POVPC activities is based on the chemical reactivity of POVPC. This lipid covalently forms Schiff bases with NH_2 groups of proteins and lipids due to its aldehyde group at the ω-position of the truncated *sn*-2 fatty acyl chain (Stemmer and Hermetter, 2012; Stemmer *et al.*, 2012).

First of all, this covalent binding can influence the functional properties of the target biomolecules. In addition, the resultant lipid-lipid or lipid-protein adducts may serve as signaling platforms and influence downstream signaling cascades. Basically, such effects can also be elicited by PGPC. However, this compound can only interact physically with other biomolecules and therefore it is likely, that the molecular targets and consequences are different.

Stemmer *et al.* were able to identify a large number of potential protein targets of POVPC in RAW 264.7 macrophages (Stemmer *et al.*, 2012). The respective proteins were involved in cellular stress response, apoptosis and lipid metabolism. Thus, the toxicity of the oxPL in cells is due to the combination of different pathways, the outcome depending on the individual experimental or biological conditions.

Edelfosine was used as a cytotoxic reference in this study. It is known that Edelfosine and many of its analogues selectively induce apoptosis in various tumor cell lines (Ruiter *et al.*, 2001). Toxic effects are due to modulation of membrane properties and activation of pro-apoptotic signaling pathways (Gajate and Mollinedo, 2007). This lipid accumulates in lipid rafts of the plasma membrane of cancer cells, leading to rearrangement and reorganisation of (signaling) proteins and lipids within these domains. As a consequence of the altered biophysical environment, their activities are changed and apoptosis is induced (Ausili *et al.*, 2008; Mollinedo *et al.*, 1997). In addition, Edelfosine accumulates in the ER of cells of solid tumors. It triggers an ER-dependent stress response which results in the activation of the mitochondrial apoptosis pathway, the perturbation of the outer mitochondrial membrane, cytochrome c release and the activation of caspase-3 (Huang *et al.*, 2011; Mollinedo *et al.*, 2011). In

contrast to these studies, we found that Edelfosine preferentially induced necrosis in B16-BL6 cells already at very low concentrations. The mechanism of this effect is yet to be elucidated.

A key feature of phospholipid organization in the plasma membrane of animal cells is the asymmetric distribution of these compounds in the bilayer. The aminophospholipids phosphatidylserine and phosphatidylethanolamine are enriched in the inner leaflet of the plasma membrane (Zwaal *et al.*, 2005). In apoptotic cells this asymmetry is lost. PS is translocated to the outer leaflet of the plasma membrane. Several studies provide evidence that cancer cells expose *a priori* a large fraction of phosphatidylserine on the plasma membrane surface. According to Riedl *et al.*, the malignancy of melanomas correlates with the amount of exposed PS. It is highest in late stage and metastatic melanomas (Riedl *et al.*, 2011). Why and how cancer cells expose PS, and how they can escape recognition by phagocytes is currently not known. The surface-exposed aminophospholipids may be considered as likely targets of oxPL. POVPC would even be capable of forming covalent lipid-lipid adducts (Stemmer *et al.*, 2012). Reaction of POVPC with PE or PS could lead to the formation of Schiff bases containing three hydrophobic chains and a relatively small headgroup. Such a molecular geometry could destabilize the lipid bilayer, reduce membrane stability, activate cellular stress responses and as a result induce cell death.

Activation of aSMase and ceramide formation is a hallmark of apoptosis induced by oxPL in VSMC (Loidl *et al.*, 2003) and RAW 264.7 macrophages (Stemmer *et al.*, 2012) as well as in some human melanoma cell lines (Ramprecht *et al.*, unpublished data). Such effects have also been observed in other tumor cells under the influence

of chemotherapeutic agents (Senchenkov *et al.*, 2001). Ceramide-based therapies have been discussed as potential cancer therapies (Reynolds *et al.*, 2004). Results from preclinical studies also suggest that induction of ceramide formation and/or inhibition of ceramide breakdown might be useful new approaches for killing cancer cells. Because of its apoptosis-inducing effects in cancer cells, ceramide has been termed a "tumor suppressor lipip" (Hannun and Linardic, 1993).

In this study, we provide evidence that oxPL dependent cell death of mouse melanoma cells is also associated with aSMase activation and ceramide formation. Whether ceramide is formed under oxPL stress by the *de novo* pathway or sphingosine recycling still has to be demonstrated. The molecular mechanisms of ceramide signaling and activity are complex. Ceramide participates in the regulation of various cellular processes such as apoptosis (Pettus *et al.*, 2002), cell aging (Venable *et al.*, 1995), cell growth arrest (Jayadev *et al.*, 1995) and differentiation (Bielawska *et al.*, 1992) depending on stimulus and cell type. It represents a structural membrane component and a functional modulator of membrane proteins by influencing lateral membrane organization curvature. Ceramide triggers the formation of rigid membrane domains, so-called rafts, which give rise to aggregation and clustering of activated receptor molecules that finally propagate apoptotic signals into the cell (Gulbins, 2003; Gulbins and Grassmé, 2002; Schenck *et al.*, 2007).

Acid sphingomyelinase acts as an upstream signaling component of the early phase of cellular stress response. It converts sphingomyelin to ceramide at the plasma membrane (Hannun and Obeid, 2008) in response to various stimuli (Andrieu-Abadie *et al.*, 2001). We found that aSMase was rapidly stimulated by PGPC and POVPC in B16-

BL6 cells within minutes (Figure 3.6) by POVPC whereas activation by PGPC was slower. Concomitantly, total cellular ceramide levels and in particular, distinct ceramide species were elevated in response to stimulation with PGPC and POVPC (Figure 3.7). The initial rise in ceramide may be due to activation of aSMase, whereas the persistently elevated ceramide levels must be due to another pathway e.g. *de novo* synthesis. We have evidence that such a pathway is responsible for persistent ceramide formation in cultured macrophages under the influence of oxPL (unpublished).

The involvement of de novo ceramide synthesis in oxPL-induced melanoma cell death would be in line with the subcellular localization of the oxPL in mouse melanoma cells (Figure 3.2, Figure 3.3). Fluorescence microscopic analysis showed co-localization of BY-POVPE and BY-PGPE with the ER. In this organelle oxPL could induce ER stress possibly stimulating the enzymes of *de novo* ceramide synthesis. The slow cumulative increase in ceramide might play a role in the effector phase of apoptosis because of its biophysical membrane effects (Van Blitterswijk *et al.*, 2003). Ceramide can be transferred from the ER to the mitochondria where it elicits cytochrome c efflux and caspase-3 activation (Stiban *et al.*, 2008). The cellular sphingomyelin content did not change very much in the presence of the oxPL. Degradation of this lipid by aSMase in the plasma membrane and formation of ceramide are small compared to the total cellular lipid amount. The quantitative sphingolipid/ceramide balance would require lipid analysis of the isolated plasma membrane.

Cell mobility and migration are crucial for cancer cell metastasis. OxPL effect these properties in a specific fashion. At low concentrations (5 µM) POVPC inhibited cell growth, whereas PGPC stimulated it (Figure 3.8). E-PGPC and E-POVPC showed

marginal growth stimulating effects only after 24 hours stimulation. These results seem to be in conflict with FACS measurements, where PGPC had a more pronounced pro-apoptotic effect. However, pro-apoptotic and anti-proliferative effects of oxPL are strongly concentration dependent.

In summary, the oxidized phospholipids PGPC and POVPC, as well as their ether analogues E-PGPC and E-POVPC induce different cellular responses in B16-BL6 cells in a concentration-dependent manner. They can trigger apoptosis, necrosis or even show anti-proliferative effects. The knowledge of these effects is important for potential therapeutic applications. The results obtained in this study are the basis for further experiments using animal models to exploit the potential of oxidized phospholipids for the topic and systemic treatment of melanomas.

3.6 Acknowledgements

We gratefully acknowledge financial support of the PhD thesis of Claudia Ramprecht by TU Graz and by the project I308-B12.

References Chapter III

Abràmoff, M., P. Magalhães, and S. Ram (2004). Image processing with imagej. *Biophotonics international 11*(7), 36–42.

Andrieu-Abadie, N., V. Gouazé, R. Salvayre, and T. Levade (2001). Ceramide in apoptosis signaling: relationship with oxidative stress. *Free Radical Biology and Medicine 31*(6), 717–728.

Ausili, A., A. Torrecillas, F. Aranda, F. Mollinedo, C. Gajate, S. Corbala n Garci a, A. de Godos, and J. Go mez Ferna ndez (2008). Edelfosine is incorporated into rafts and alters their organization. *The Journal of Physical Chemistry B 112*(37), 11643–11654.

Batzri, S. and E. Korn (1973). Single bilayer liposomes prepared without sonication. *Biochimica et Biophysica Acta 298*(4), 1015–1019.

Bielawska, A., C. Linardic, and Y. Hannun (1992). Modulation of cell growth and differentiation by ceramide. *FEBS letters 307*(2), 211–214.

Bochkov, V. (2007). Inflammatory profile of oxidized phospholipids. *Thrombosis and Haemostasis-Stuttgart- 97*(3), 348.

Bochkov, V., O. Oskolkova, K. Birukov, A. Levonen, C. Binder, and J. Stöckl (2010). Generation and biological activities of oxidized phospholipids. *Antioxidants & redox signaling 12*(8), 1009–1059.

Bradford, M. (1976). A rapid and sensitive method for the quantization of microgram quantities of protein utilizing the principle of protein-dye binding. *Anal Biochem 72*(1-2), 248–54.

Chisolm, G. and D. Steinberg (2000). The oxidative modification hypothesis of atherogenesis: an overview. *Free radical biology and medicine 28*(12), 1815–1826.

Elmore, S. (2007). Apoptosis: a review of programmed cell death. *Toxicologic pathology 35*(4), 495–516.

Fruhwirth, G. and A. Hermetter (2008). Mediation of apoptosis by oxidized phospholipids. *Lipids in Health and Disease 49*, 351–367.

Fruhwirth, G., A. Loidl, and A. Hermetter (2007). Oxidized phospholipids: from molecular properties to disease. *Biochimica et Biophysica Acta (BBA)-Molecular Basis of Disease 1772*(7), 718–736.

Fruhwirth, G., A. Moumtzi, A. Loidl, E. Ingolic, and A. Hermetter (2006). The oxidized phospholipids povpc and pgpc inhibit growth and induce apoptosis in vascular smooth muscle cells. *Biochimica et Biophysica Acta (BBA)-Molecular and Cell Biology of Lipids 1761*(9), 1060–1069.

Gajate, C. and F. Mollinedo (2002). Biological activities, mechanisms of action and biomedical prospect of the antitumor ether phospholipid et-18-och3 (edelfosine), a proapoptotic agent in tumor cells. *Current drug metabolism 3*(5), 491–525.

Gajate, C. and F. Mollinedo (2007). Edelfosine and perifosine induce selective apoptosis in multiple myeloma by recruitment of death receptors and downstream signaling molecules into lipid rafts. *Blood 109*(2), 711–719.

Gajate, C., A. Santos-Beneit, A. Macho, M. Lazaro, A. Hernandez-De Rojas, M. Modolell, E. Muñoz, and F. Mollinedo (2000). Involvement of mitochondria and caspase-3 in et-18-och3-induced apoptosis of human leukemic cells. *International journal of cancer 86*(2), 208–218.

Greenberg, M., X. Li, B. Gugiu, X. Gu, J. Qin, R. Salomon, and S. Hazen (2008). The lipid whisker model of the structure of oxidized cell membranes. *Journal of Biological Chemistry 283*(4), 2385.

Gulbins, E. (2003). Regulation of death receptor signaling and apoptosis by ceramide.

Pharmacological research 47(5), 393–399.

Gulbins, E. and H. Grassmé (2002). Ceramide and cell death receptor clustering. *Biochimica et Biophysica Acta (BBA)-Molecular and Cell Biology of Lipids 1585*(2), 139–145.

Han, C., Y. Pak, *et al.* (1999). Oxidation-dependent effects of oxidized ldl: proliferation or cell death. *Exp Mol Med 31*(4), 165–173.

Hannun, Y. and C. Linardic (1993). Sphingolipid breakdown products: anti-proliferative and tumor-suppressor lipids. *Biochimica et Biophysica Acta-Biomembranes-Including Reviews on Biomembranes 1154*(3), 223–236.

Hannun, Y. and L. Obeid (2008). Principles of bioactive lipid signalling: lessons from sphingolipids. *Nature Reviews Molecular Cell Biology 9*(2), 139–150.

Hermetter, A., H. Stütz, R. Franzmair, and F. Paltauf (1989). 1-o-trityl-sn-glycero-3-phosphocholine: a new intermediate for the facile preparation of mixed-acid 1, 2-diacylglycerophosphocholines. *Chemistry and physics of lipids 50*(1), 57–62.

Hoang, M., L. Eichenfield, *et al.* (2000). The rising incidence of melanoma in children and adolescents. *Dermatology nursing/Dermatology Nurses' Association 12*(3), 188.

Huang, W., C. Chen, Y. Lin, and C. Lin (2011). Apoptotic sphingolipid ceramide in cancer therapy. *Journal of lipids 2011*.

Jayadev, S., B. Liu, A. Bielawska, J. Lee, F. Nazaire, M. Pushkareva, L. Obeid, and Y. Hannun (1995). Role for ceramide in cell cycle arrest. *Journal of Biological Chemistry 270*(5), 2047–2052.

Kinnunen, P., K. Kaarniranta, and A. Mahalka (2012). Protein-oxidized phospholipid interactions in cellular signalling for cell death: From biophysics to clinical correlations. *Biochimica et Biophysica Acta (BBA)-Biomembranes*.

Leitinger, N. (2005). Oxidized phospholipids as triggers of inflammation in atherosclerosis. *Molecular nutrition & food research 49*(11), 1063–1071.

Liu, Y., D. Peterson, H. Kimura, and D. Schubert (1997). Mechanism of cellular 3-(4, 5-dimethylthiazol-2-yl)-2, 5-diphenyltetrazolium bromide (mtt) reduction. *Journal of neurochemistry 69*(2), 581–593.

Loidl, A., R. Claus, H. Deigner, and A. Hermetter (2002). High-precision fluorescence assay for sphingomyelinase activity of isolated enzymes and cell lysates. *Journal of lipid research 43*(5), 815–823.

Loidl, A., R. Claus, E. Ingolic, H. Deigner, and A. Hermetter (2004). Role of ceramide in activation of stress-associated map kinases by minimally modified ldl in vascular smooth muscle cells. *Biochimica et Biophysica Acta (BBA)-Molecular Basis of Disease 1690*(2), 150–158.

Loidl, A., E. Sevcsik, G. Riesenhuber, H. Deigner, and A. Hermetter (2003). Oxidized phospholipids in mmldl induce apoptotic signaling via activation of acid sphingomyelinase in arterial smooth muscle cells. *Journal of Biological Chemistry 278*(35), 32921.

MacKie, R., A. Hauschild, and A. Eggermont (2009). Epidemiology of invasive cutaneous melanoma. *Annals of Oncology 20*(suppl 6), vi1–vi7.

Marathe, G., K. Harrison, R. Murphy, S. Prescott, G. Zimmerman, T. McIntyre, *et al.* (2000). Bioactive phospholipid oxidation products. *Free radical biology & medicine 28*(12), 1762.

McConkey, D. (1998). Biochemical determinants of apoptosis and necrosis. *Toxicology letters 99*(3), 157–168.

Mollinedo, F., M. Fernández, V. Hornillos, J. Delgado, F. Amat-Guerri, A. Acuña, T. Nieto-Miguel, J. Villa-Pulgarín, C. González-García, V. Ceña, *et al.* (2011). Involvement of lipid rafts in the localization and dysfunction effect of the antitumor ether phospholipid edelfosine in mitochondria. *Cell Death & Disease 2*(5), e158.

Mollinedo, F., J. Fernández-Luna, C. Gajate, B. Martín-Martín, A. Benito, R. Martínez-Dalmau, and M. Modolell (1997). Selective induction of apoptosis in cancer

cells by the ether lipid et-18-och3 (edelfosine): molecular structure requirements, cellular uptake, and protection by bcl-2 and bcl-xl. *Cancer research 57*(7), 1320–1328.

Moumtzi, A., M. Trenker, K. Flicker, E. Zenzmaier, R. Saf, and A. Hermetter (2007). Import and fate of fluorescent analogs of oxidized phospholipids in vascular smooth muscle cells. *Journal of lipid research 48*(3), 565–582.

Parthasarathy, S. and S. Rankin (1992). Role of oxidized low density lipoprotein in atherogenesis. *Progress in lipid research 31*(2), 127–143.

Pettus, B., C. Chalfant, and Y. Hannun (2002). Ceramide in apoptosis: an overview and current perspectives. *Biochimica et Biophysica Acta (BBA)-Molecular and Cell Biology of Lipids 1585*(2), 114–125.

Reynolds, C., B. Maurer, and R. Kolesnick (2004). Ceramide synthesis and metabolism as a target for cancer therapy. *Cancer letters 206*(2), 169–180.

Riedl, S., B. Rinner, M. Asslaber, H. Schaider, S. Walzer, A. Novak, K. Lohner, and D. Zweytick (2011). In search of a novel target–phosphatidylserine exposed by non-apoptotic tumor cells and metastases of malignancies with poor treatment efficacy. *Biochimica et Biophysica Acta (BBA)-Biomembranes 1808*(11), 2638–2645.

Ruiter, G., M. Verheij, S. Zerp, and W. van Blitterswijk (2001). Alkyl-lysophospholipids as anticancer agents and enhancers of radiation-induced apoptosis. *International Journal of Radiation Oncology* Biology* Physics 49*(2), 415–419.

Schenck, M., A. Carpinteiro, H. Grassmé, F. Lang, and E. Gulbins (2007). Ceramide: physiological and pathophysiological aspects. *Archives of biochemistry and biophysics 462*(2), 171–175.

Schmid, H. and T. Takahashi (1968). The alk-i-enyl ether and alkyl ether lipids of bovine heart muscle. *Biochimica et Biophysica Acta (BBA)-Lipids and Lipid Metabolism 164*(2), 141–147.

Senchenkov, A., D. Litvak, and M. Cabot (2001). Targeting ceramide metabolism -

a strategy for overcoming drug resistance. *Journal of the National Cancer Institute 93*(5), 347–357.

Steinberg, D. (2009). The ldl modification hypothesis of atherogenesis: an update. *Journal of lipid research 50*(Supplement), S376–S381.

Steinbrecher, U., H. Zhang, and M. Lougheed (1990). Role of oxidatively modified ldl in atherosclerosis. *Free Radical Biology and Medicine 9*(2), 155–168.

Stemmer, U., Z. Dunai, D. Koller, G. Pürstinger, E. Zenzmaier, H. Deigner, E. Aflaki, D. Kratky, and A. Hermetter (2012). Toxicity of oxidized phospholipids in cultured macrophages. *Lipids in Health and Disease 11*(1), 110.

Stemmer, U. and A. Hermetter (2012). Protein modification by aldehydophospholipids and its functional consequences. *Biochimica et Biophysica Acta (BBA)-Biomembranes*.

Stemmer, U., C. Ramprecht, E. Zenzmaier, B. Stojčić, G. Rechberger, M. Kollroser, and A. Hermetter (2012). Uptake and protein targeting of fluorescent oxidized phospholipids in cultured raw 264.7 macrophages. *Biochimica et Biophysica Acta (BBA)-Molecular and Cell Biology of Lipids*.

Stiban, J., L. Caputo, and M. Colombini (2008). Ceramide synthesis in the endoplasmic reticulum can permeabilize mitochondria to proapoptotic proteins. *Journal of lipid research 49*(3), 625–634.

Subbanagounder, G., N. Leitinger, D. Schwenke, J. Wong, H. Lee, C. Rizza, A. Watson, K. Faull, A. Fogelman, and J. Berliner (2000). Determinants of bioactivity of oxidized phospholipids specific oxidized fatty acyl groups at the sn-2 position. *Arteriosclerosis, thrombosis, and vascular biology 20*(10), 2248–2254.

Van Blitterswijk, W., A. Van Der Luit, R. Veldman, M. Verheij, and J. Borst (2003). Ceramide: second messenger or modulator of membrane structure and dynamics? *Biochemical Journal 369*(Pt 2), 199.

Venable, M., J. Lee, M. Smyth, A. Bielawska, and L. Obeid (1995). Role of ceramide in

cellular senescence. *Journal of Biological Chemistry 270*(51), 30701–30708.

Wymann, M. and R. Schneiter (2008). Lipid signalling in disease. *Nature Reviews Molecular Cell Biology 9*(2), 162–176.

Zeiss, C. (2003). The apoptosis-necrosis continuum: insights from genetically altered mice. *Veterinary Pathology Online 40*(5), 481–495.

Zwaal, R., P. Comfurius, and E. Bevers (2005). Surface exposure of phosphatidylserine in pathological cells. *Cellular and molecular life sciences 62*(9), 971–988.

Chapter 4

Toxicity of Oxidized Phospholipids in Non-Melanoma Skin Cancer Cell Lines

Toxicity of Oxidized Phospholipids in Non-Melanoma Skin Cancer Cell Lines

C. Ramprecht[1], S. Jantscher[1], L. Britz[1], E. Zenzmaier[1], G. Rechberger[2], M. Kollroser[3], H. Schaider[4,5] and A. Hermetter[1]

[1] *Department of Biochemistry, Graz University of Technology, Graz, Austria*

[2] *Institute of Molecular Biosciences, Karl-Franzens-University Graz, Graz, Austria*

[3] *Institute of Forensic Medicine, Center for Theoretical-Clinical Medicine, Medical University Graz, Graz, Austria*

[4] *Cancer Biology Unit, Department of Dermatology, Medical University Graz, Graz, Austria*

[5] *Center for Medical Research (ZMF), Medical University Graz, Graz, Austria*

4.1 Abstract

The incidence of skin cancers (melanoma and non-melanoma skin tumors) is rising worldwide every year. In contrast to melanoma, death from non-melanoma skin cancers is uncommon. A number of options is available for treating these tumors. Surgical excision is the mainstay of treatment for most squamous and basal cell carcinomas, but disfiguring cosmetic side effects have to be considered. Besides established treatments for specific subtypes of basal cell carcinoma, like photodynamic therapy and topical imiquimod, the search for more effective and tissue-salvaging therapies continues. For this reason, new non-invasive chemopreventive and chemotherapeutic agents for efficient treatment are needed, which selectively induce cell death in tumor but not in differentiated cells of the skin.

It was the aim of this study to determine the toxic effects of short-chain oxidized phospholipids in different human squamous carcinoma cell lines in comparison to human keratinocytes. These compounds are generated under conditions of oxidative stress. They are toxic in the cells of the vascular wall and are involved in the initiation and progression of atherosclerosis. Recently, we found that they are also toxic in cultured cancer cells and induce apoptosis in melanoma cells whereas they show much less activity in "healthy" melanocytes.

We investigated the effects of oxidized diacyl and alkylacyl phospholipids on cell viability and apoptosis and found that the oxPL preferentially induced apoptosis in squamous carcinoma cell lines, whereas keratinocytes were almost unaffected. Toxicities of all tested lipids were similar under the chosen experimental conditions. Flu-

orescent oxPL analogues were rapidly internalized by the cancer cells. In addition, they induced apoptosis in these cells, which was associated with changes in cellular ceramide levels and aSMase activity. Furthermore, primary protein targets of POVPC were identified. OxPL containing reactive aldehyde groups formed Schiff base adducts with their primary protein targets which were isolated and identified by MS/MS. In summary, the results of this study may be considered a first useful basis for testing and understanding the therapeutic potential of oxPL for the treatment of non-melanoma skin tumors.

4.2 Introduction

Chronic exposure of the skin to ultraviolet radiation is one of the major causes for the development of skin cancers. The incidences of skin cancer (melanoma and non-melanoma skin tumours) are rising worldwide every year. Non-melanoma skin cancers, including squamous cell carcinoma, basal cell carcinoma and precursors such as actinic keratosis, is the most common type of cancer in Western countries (Diepgen *et al.*, 2012; Housman *et al.*, 2003), with an incidence of 100 per 100.000 individuals in Europe (Madan *et al.*, 2010; Trakatelli *et al.*, 2007). In contrast to melanoma, death from non-melanoma skin cancers is very rare. A number of options are available for treating these tumors. Surgical excision is the mainstay of treatment for most squamous and basal cell carcinomas, but disfiguring cosmetic side effects have to be considered. Besides established treatments for specific subtypes of basal cell carcinoma, like photodynamic therapy and topical imiquimod, the search for more effective and tissue-salvaging therapies continues. For this reason, new non-invasive chemopreventive and chemotherapeutic agents for efficient treatment are needed, which selectively

induce cell death in tumor but not in differentiated cells of the skin.

Here we report on the toxic effects of short-chain oxPL on cultured squamous carcinoma cell lines. These compounds are generated under conditions of oxidative stress from polyunsaturated diacyl- and alkylacyl-glycero-phosphocholines, respectively (Bochkov *et al.*, 2010; Fruhwirth *et al.*, 2007; Marathe *et al.*, 2000). As components of oxLDL they are involved in the initiation and progression of atherosclerosis (Berliner *et al.*, 2009). Depending on lipid concentration and exposure time, oxidized phospholipids may induce inflammation, cell proliferation and, under sustained exposure, programmed cell death (apoptosis) (Fruhwirth and Hermetter, 2008; Fruhwirth *et al.*, 2007; Greenberg *et al.*, 2008; Loidl *et al.*, 2004, 2003).

Specifically, these oxidized phospholipids are responsible for the harmful effects of oxLDL in vascular smooth muscle cells (Fruhwirth *et al.*, 2006) and RAW 264.7 macrophages (Stemmer *et al.*, 2012). In these cells, their toxicity is causally related to the activation of aSMase which generates the apoptotic messenger ceramide (Loidl *et al.*, 2003). In a recent study we found that short-chain oxPL are also toxic to cultured human and murine melanoma cell lines (Ramprecht *et al.*, unpublished data, Ramprecht, Britz *et al.*, unpublished data). These compounds preferentially induced apoptosis in cancer cells, but healthy melanocytes remained almost unaffected. Remarkably, lipid concentrations eliciting apoptosis in tumor cells were much lower compared to toxic concentrations required for vascular cells.

In this study we screened the toxic effects of 1-palmitoyl-2-glutaroyl-*sn*-glycero-3-phosphocholine (PGPC) and 1-palmitoyl-2-(5-oxovaleroyl)-*sn*-glycero-3-phosphocho-

line (POVPC) as well as their ether analogues 1-O-hexadecyl-2-glutaroyl-*sn*-glycero-3-phosphocholine (E-PGPC) and 1-O-hexadecyl-2-(5-oxovaleroyl)-*sn*-glycero-3-phosphocholine (E-POVPC). PGPC and POVPC share similar structural features (Figure 4.1).

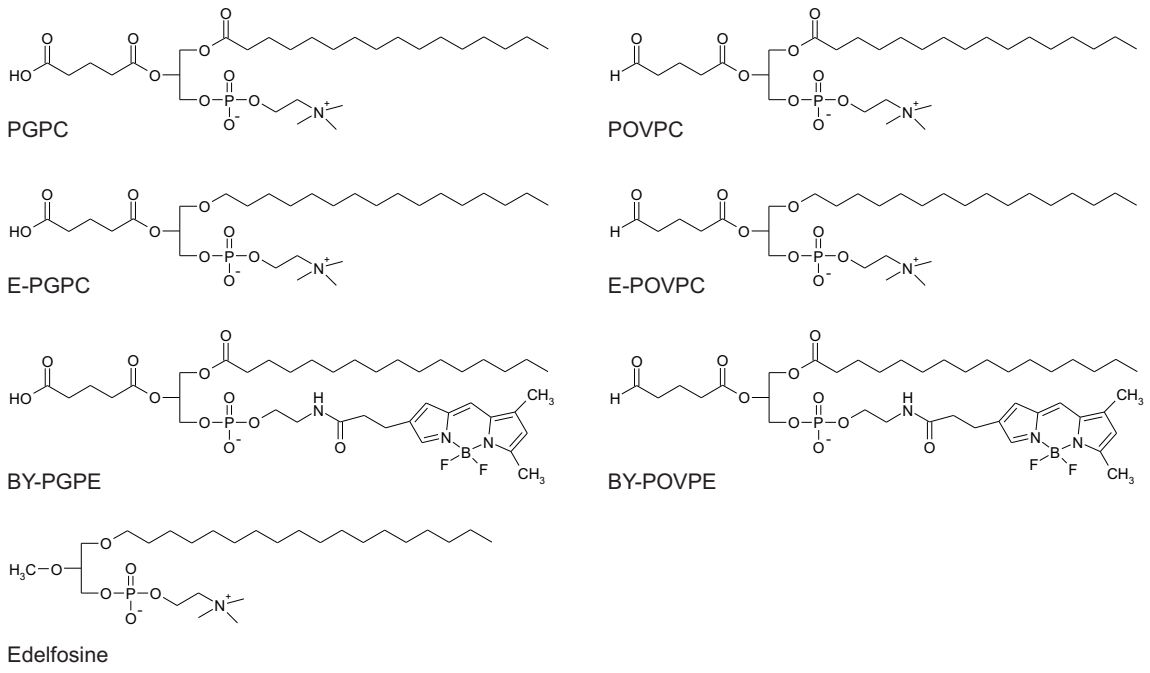

Figure 4.1. Chemical structures of oxidized phospholipids and ether analogues

1-palmitoyl-2-glutaroyl-sn-glycero-3-phosphocholine (PGPC)
1-palmitoyl-2-(5-oxovaleroyl)-sn-glycero-3-phosphocholine (POVPC)
1-O-hexadecyl-2-glutaroyl-sn-glycero-3-phosphocholine (E-PGPC)
1-O-hexadecyl-2-(5-oxovaleroyl)-sn-glycero-3-phosphocholine (E-POVPC)
1-palmitoyl-2-glutaroyl-sn-glycero-3-phospho-N-(3-BODIPY-propionyl)-ethanolamine (BY-PGPE)
1-palmitoyl-2-(5-oxovaleroyl)-sn-glycero-3-phospho-N-(3-BODIPY-propionyl)-ethanolamine (BY-POVPE)
1-octadecyl-2-O-methyl-sn-glycero-3-phosphocholine (Edelfosine)

Both oxPL contain the same long-chain fatty acid at the *sn*-1 position, but differ in their short polar fatty acyl chain at the *sn*-2 position of glycerol. POVPC contains a highly reactive ω-aldehyde group in the *sn*-2 acyl substituent that allows the molecule to interact chemically with its targets by undergoing Schiff base formation. In con-

trast, PGPC contains a carboxylic acid function at the same position. These truncated lipids are amphipathic molecules and thus highly exchangeable between cells, membranes and lipoproteins, as they contain only one long hydrophobic *sn*-1 acyl chain (Stemmer *et al.*, 2012). The 1-O-alkyl ether phospholipids E-PGPC and E-POVPC are structurally related to their diacyl counterparts PGPC and POVPC, respectively, except that their hydrophobic chains at the *sn*-1 position are linked to the glycerol backbone via an ether bond. Small amounts of 1-O-alk(en)yl lipids can be found in LDL, whereas large amounts of ether choline (and ethanolamine) phospholipids are found in cell membranes of animals and humans (except for the liver) (Schmid and Takahashi, 1968).

We compared the toxicities of the oxPL with the effects of Edelfosine. The latter compound is a synthetic alkyl-lysophospholipid analogue with a long hydrophobic substituent and a methyl group connected to the *sn*-1 and the *sn*-2 position of the glycerol backbone by an ether bond, respectively (Figure 4.1). Edelfosine has been identified as an efficient anti-tumor agent in many cancer cells (Gajate and Mollinedo, 2002, 2007; Gajate *et al.*, 2000; Ruiter *et al.*, 2001).

In the present study, we determined the toxic effects of oxPL in human squamous carcinoma cell lines in comparison to human keratinocytes. To understand the mechanism of their activities, we studied the uptake of fluorescently labelled oxPL into the cells, the activation of sphingomyelinase and the consecutive formation of the apoptotic messenger ceramide in response to the toxic compounds. Last but not least, we identified the protein targets of the aldehydo phospholipid POVPC that may serve as primary signaling platforms of the oxPL. The results of this study may be considered

as useful basis for further testing and an understanding of the therapeutic potential of oxPL for the treatment of non-melanoma skin tumors.

4.3 Experimental Procedures

4.3.1 Materials

PGPC (1-palmitoyl-2-glutaroyl-*sn*-glycero-3-phosphocholine) and POVPC (1-palmitoyl-2-(5-oxovaleroyl)-*sn*-glycero-3-phosphocholine) were either synthesized in our laboratory as previously described (Moumtzi *et al.*, 2007) or purchased from Avanti Polar Lipids, Inc. (Alabaster, AL). POPC was synthesized according to the method of Hermetter *et al.* (Hermetter *et al.*, 1989), PLPC was purchased from Bachem (Bubendorf, Switherland). Edelfosine (1-octadecyl-2-O-methyl-*sn*-glycero-3-phosphocholine), E-PGPC (1-O-hexadecyl-2-glutaroyl-*sn*-glycero-3-phosphocholine) and E-POVPC (1-O-hexadecyl-2-(5-oxovaleroyl)-*sn*-glycero-3-phosphocholine) were synthesized in our laboratory (Stemmer *et al.*, 2012). RPMI-1640 media and DMEM with or without Phenol red, Fetal Calf Serum (FCS) and Trypsin were purchased from Gibco (Carlsbad, CA). Phosphate buffered saline (PBS) and all other supplements for cell culture were from PAA Laboratories (Linz, Austria), unless otherwise indicated. Tissue culture dishes and flasks were obtained from Sarstedt (Nürmbrecht, Germany) or Greiner (Kremsmünster, Austria). Vybrant® MTT Cell proliferation Assay kit (V-13154), Vybrant® apoptosis assay kit#2 (V-132451) and staurosporine were from Invitrogen (Leek, Netherlands). Flow cytometry fluids and FACS tubes were from BD bioscience (Heidelberg, Germany). Cell culture inserts were from Ibidi GmbH (Munich, Germany). Organic solvents and all other standard chemicals were from Carl

Roth (Karlsruhe, Germany) or Sigma-Aldrich (Vienna, Austria), unless otherwise indicated.

4.3.2 Cell culture and lipid incubation

HaCaT human keratinocytes were from Dr. Helmut Schaider (Cancer Biology Unit, Department of Dermatology, Medical University Graz, Austria) (Boukamp *et al.*, 1988). SCC12 and SCC13 cells were provided by Dr. James G. Rheinwald (Department of Dermatology, Brigham and Women's Hospital, Harvard Medical School, Boston, Massachusetts) (Rheinwald and Beckett, 1981).

Table 4.1. Characterization and origin of keratinocytes and squamous skin cancer cell lines
SCC: squamous cell carcinoma; HaCaT: human adult low calcium high temperature keratinocytes

Cell line	Origin	Ref.
HaCaT	Spontaneously immortalized human skin keratinocytes (*in vitro* immortalized)	(Boukamp *et al.*, 1988)
SCC12	SCC, from the facial epidermis of squamous cell carcinoma (tumor derived)	(Rheinwald and Beckett, 1981)
SCC13	SCC, from the facial epidermis of squamous cell carcinoma (tumor derived)	(Rheinwald and Beckett, 1981)

HaCaT cells were cultured in DMEM (4.5 g/l glucose, 25 mM HEPES, 4 mM L-glutamine, without sodium pyruvate) supplemented with 10% FCS and 100 units/ml penicillin/streptomycin. SCC12 and SCC13 cells were grown in RPMI-1640 medium (supplemented with 10% FCS, 10 units/ml penicillin/streptomycin, 4 mM L-glutamine). All cell lines were routinely grown at 37°C in humidified CO_2 (5%) atmosphere.

All experiments were carried out in RPMI-1640 medium or DMEM without Phenol red (see above) supplemented with 0.1% FCS to minimize degradation of the oxidized phospholipids by lipases under high serum conditions (Fruhwirth *et al.*, 2006). For all experiments, aqueous lipid suspensions were prepared using the ethanol injection method (Batzri and Korn, 1973). The total ethanol concentration was always kept below 1% (v/v). Control experiments were performed using incubation medium containing the same amount of ethanol without the lipids.

4.3.3 Effects of oxPL on cell morphology

75.000 cells were seeded into 24 well plates containing full growth medium and allowed to grow over night. Cells were washed twice with serum-free medium (SFM) to remove floating cells, followed by incubation with different oxPL concentrations. For this purpose, aqueous suspensions containing the indicated concentrations of PGPC or POVPC in medium (0.1% FCS) were prepared as described above. Control cells were incubated with 1% (v/v) EtOH (negative control) or H_2O_2 (necrosis control) in the same medium. Cells were observed with an Axiovert 35 inverted microscope after 6 h, 12 h and 24 h.

4.3.4 Uptake and localization of fluorescent BY-POVPE and BY-PGPE

Cells were grown to 70% confluency in Chamber slides with a cover glass bottom (Imaging Chambers CG8 Cover Glass Bottom from MoBiTec, Göttingen, Germany). Cells were washed once, followed by incubation with medium containing 5 µM fluorescently labelled oxPL for 5 or 30 minutes. After incubation, cells were rinsed

carefully with SFM and observed with an Axiovert 35 inverted fluorescence microscope equipped with a mercury-arc lamp (HBO® 50W/AC; OSRAM, Munich, Germany) and a CCD camera (AxioCam HR), driven by AxioVision software package (Carl Zeiss, Germany).

Table 4.2. Spectral parameters and instrument settings for microscopy of fluorescent probes
Instrument settings refer to a Zeiss Axiovert 35 inverted fluorescence microscope. Excitation and emission maxima are indicated for fluorophore solutions in DMEM or RPMI-1640 medium supplemented with 0.1% FCS.

Fluorophore (Invitrogen)	Excitation Maxima [nm]	Emission Maxima [nm]	Excitation Filter Beam Splitter Barrier Filter
BODIPY	505	510	BP 450-490 FT 510 LP 520
MitoTracker® Red CM-XRos	579	599	BP 510-560 FT 580 LP 590
ER-Tracker™ Red	587	615	BP 575-625 FT 665 LP 666-710
CellMask™ Deep Red	649	666	BP 575-625 FT 665 LP 666-710

For costaining experiments, cells were preincubated with an organelle-specific marker followed by incubation with the BODIPY-labelled lipid. For this purpose, cells were either pre-treated with 1 µM ER-Tracker™Red dye (Invitrogen) or with 0.3 µM MitoTracker® Red CM-XRos (Invitrogen) for 20 minutes followed by two washing steps and incubation with 5 µM BY-oxPL as described above. Optical settings of the microscope as well as emission and excitation maxima of all used probes are summarized in Table 4.2. All images were processed identically to adjust brightness and contrast using CorelDRAW X4 software. In control experiments, no crossover between green BODIPY fluorescence and red organelle specific probe fluorescence was detectable.

No background could be detected in untreated cells if the same optical settings were used (data not shown).

4.3.5 MTT viability assay

The cytotoxic effects of PGPC, POVPC, E-PGPC, E-POVPC and Edelfosine on HaCaT keratinocytes and SCC13 cells were determined using the Vybrant® MTT Cell proliferation assay according to the manufacturer's protocol with slight modifications. The assay is based on the formation of insoluble formazan from water soluble MTT by living cells, and the subsequent solubilization of the purple formazan crystals by the addition of SDS (Berridge *et al.*, 2005, 1993). Cells were seeded in 96-well-plates using fully supplemented growth medium and allowed to reach 80% confluency. The medium was replaced by fresh medium containing 0.1% FCS and ethanolic solutions of the lipids (concentration range: 5-250 µM) or medium containing 1% (v/v) EtOH or DMSO (controls). 2.5 mM H_2O_2 or 10 µM staurosporine were added to the medium as positive controls for necrosis or apoptosis, respectively. After incubation at 37°C for 2 hours, the incubation medium was replaced by 100 µl fresh medium (0.1% FCS) and 10 µl MTT solution (2.5 mg/ml in PBS) and incubated for another 4 hours. Following the addition of 100 µl SDS (10% (w/v) in 0.01 % HCl (v/v)) and cell lysis for 4 hours, the heterogeneous mixture was resuspended carefully and the optical density was measured at 595 nm using the Anthos plate reader driven by WinRead 2.3 software. The decrease in the optical density was determined as a measure for the decrease in cell viability due to a loss of ER and mitochondrial functions. Results represent means $\pm$ SD of two replicates from three or more independent experiments ($n \geq 3$).

4.3.6 Flow cytometric analysis of apoptotic and necrotic cell death

Cells were incubated with 400 µl incubation medium containing different oxPL concentrations (25 µM to 200 µM) for 6 h or 24 h. Control cells were incubated with medium containing 1% (v/v) EtOH (negative control), 30 mM H_2O_2 (induces necrosis) or 20 µM staurosporine (apoptosis inducer). Following incubation, the supernatant was collected and cells were treated with accutase at 37°C for 2-3 min to detach the cells from the plate's surface. Wells were washed twice to collect any detached cells and all fractions were combined. After centrifugation, cells were washed once with ice-cold PBS containing 2% glucose (w/v) and resuspended in 100 µl Annexin Binding Buffer. For staining, 5 µl AlexaFluor®488 Annexin V solution and 5.5 µl propidium iodide (final concentration 1 mg/ml) were added and the mixture was incubated in the dark at RT for 15 minutes. Samples were diluted with 400 µl PBS (2% glucose) and FACS analysis of stained cells was performed using a FACS Calibur flow cytometer (BD Bioscience, Heidelberg, Germany). Cells were identified in the side scatter and forward scatter with linear scale. The fluorescence signals were shown and analyzed in logarithmic scale. Green (Annexin V) and red (PI) fluorescence emission were measured at 530 nm and 575 nm, respectively, upon excitation at 488 nm. Three cell populations were identified: Intact cells were unstained, apoptotic cells were stained with green AlexaFluor®488 Annexin V only, and necrotic cells were either stained by PI only or double stained by PI and Annexin V. The percentage of apoptotic and necrotic cells was calculated using WinMDI 2.8 software package. Results were obtained from three or more independent experiments and values represent means $\pm$ SD ($n \geq 3$).

4.3.7 Determination of acid sphingomyelinase activity

Cultured SCC13 cells (60 mm Petri dishes, full growth medium, 80% confluency) were washed twice with SFM to remove excess FCS. Subsequently, cells were incubated with 2 ml of 50 µM aqueous oxPL dispersion in SFM at 37°C in a humidified 5% CO_2 atmosphere for 15 min, 30 min or 60 min. Control cells were incubated with SFM containing 1 vol.% EtOH under the same conditions. Following incubation, cells were washed with 3 ml ice-cold PBS, scraped, harvested by centrifugation (1500 rpm, 10 min, 4°C) and lysed by incubation with acid lysis buffer (250 mM sodium acetate, 0.2% Triton X-100, pH 5.0). The protein content of the samples was determined using the method of Bradford (Bradford, 1976).

Aliquots of cell lysates containing 20 µg protein were used for determination of aSMase activity using fluorescent NBD-SM as a substrate as described previously (Loidl *et al.*, 2002). Briefly, cell lysates were incubated with 2 nmol fluorescent NBD-SM in 200 µl acid reaction buffer (250 mM sodium acetate, 1 mM EDTA, pH 5.0) at 37°C for 30 min, followed by lipid extraction with 300 µl $CHCl_3$:MeOH (2:1 v/v). NBD-SM was separated from the formed NBD-Cer by thin-layer chromatography on silica gel (mobile phase was $CHCl_3$:MeOH:H_2O 65:25:4 v/v/v).

Fluorescent spots were quantified with a CCD camera (Herolab, Vienna) (excitation wavelength 365 nm) using EasyWin software. The ratio of NBD-CER to total NBD-lipid (SM+Cer) was calculated and data (relative aSMase activity) were expressed as means $\pm$ SD. Results were obtained from three or more independent experiments (n $\geq$ 3).

4.3.8 Identification and quantification of total ceramide and sphingomyelin

Cultured SCC13 cells (100 mm Petri dishes, full growth medium, 80% confluency) were washed twice with SFM to remove excess serum. Subsequently, cells were incubated with 4 ml of a 50 µM oxPL dispersion in SFM at 37°C in humidified 5% CO_2 atmosphere for 6 hours. Cells incubated with the same amount of SFM containing 1 vol.% EtOH were used as negative controls. Following incubation, cells were washed with ice-cold PBS, scraped into PBS and harvested by centrifugation (1500 rpm, 5 min, 4°C). Cells were resuspended in 1 ml PBS and 100 µl aliquots were taken for the determination of sample protein concentrations by the method of Bradford (Bradford, 1976) as previously described (Ramprecht, Britz *et al.*, unpublished data).

The remaining 900 µl cell suspension was centrifuged under the conditions described above. Cells were resuspended in 3 ml $CHCl_3$/MeOH 2:1 (v/v) and internal standard (5 µg Cer 17:0 dissolved in MeOH) was added. The suspension was shaken vigorously at 4°C for 1 hour. The organic phase was washed with 700 µl of $MgCl_2$ solution (0.036% in water w/v) for 15 minutes and centrifuged to facilitate phase separation (300 g, 2 min, RT). The lower chloroform phase was collected and evaporated to dryness under a nitrogen stream.

For mild alkaline hydrolysis, 400 µl of $CHCl_3$/MeOH/H_2O (16:16:5 per vol.) were added to the solvent-free lipid extracts and the solution was shaken vigorously. After addition of 400 µl 0.2 M NaOH in MeOH, the samples were incubated at RT for 45 minutes. Following addition of 400 µl 0.5 M EDTA and 150 µl CH_3COOH and vigorous shaking, 1 ml $CHCl_3$ was added to extract the lipids. Extracts were shaken for

5 minutes and centrifuged for 3 minutes at 300 g to facilitate phase separation. The chloroform phase was transferred to a new vial and the solvent was removed under a nitrogen stream.

Evaporated lipid extracts were resuspended in 1 ml $CHCl_3$:MeOH (2:1, v/v) and diluted 1:5 with isopropanol. The AQUITY-UPLC system (Waters, Manchester, UK) equipped with a BEH-C18-column, 2.1x150 mm, 1.7 µm (Waters) was used. For chromatographic separation a binary gradient was applied. Solvent A consisted of H_2O/MeOH (1:1, v/v), solvent B was 2-propanol. Both solvents contained phosphoric acid (8 µM), ammonium acetate (10 mM) and formic acid (0.1 vol%). The column compartment was kept at 50°C. A SYNAPT™G1 qTOF HD mass spectrometer (Waters) equipped with an ESI source was used for analysis. Leucine-Enkephaline [MH+] (m/z 556.2771) was used as reference substance in the lock-spray. Data acquisition was done by the MassLynx 4.1 software (Waters), for lipid analysis the Lipid Data analyzer software was used (Hartler *et al.*, 2011). Results were obtained from 5 independent experiments and data represent means ± SD (n = 5).

4.3.9 Determination of cell migration using a scratch assay

Cells were seeded into 24 well plates covered with culture-inserts (Ibidi, Planegg/ Martiensried, Germany) containing full growth medium over night and allowed to reach 100% confluency. Culture-inserts were carefully removed, leaving a cell-free gap of about 500 µm width. Subsequently, remaining cells were rinsed with medium several times to reduce the number of floating cells that could reattach to the cell-free zone during further incubation. Following incubation with different oxPL concentrations in DMEM or RPMI-1640 medium (2% FCS), or 1% (v/v) EtOH in the same media

(negative controls), cell migration into the cell-free zone was observed. Micrographs of the scratch were taken after the indicated incubation times using an Axiovert 35 inverted microscope equipped with a CCD camera, driven by AxioVision software package (Carl Zeiss Vision GmbH, Germany). All images were taken from the identical scratch areas within one well. The width of the cell-free zone was measured using ImageJ software (Abràmoff *et al.*, 2004). The migration rate was calculated and expressed as % of the initial width of the gap. Results were obtained from replicates of three or more independent experiments and data represent means $\pm$ SD ($n \geq 3$).

4.3.10 Determination of protein targets of BY-POVPE

Labelling of cell proteins with BY-POVPE

SCC13 cells were grown to 80% confluency in 21 cm^2 tissue culture dishes over night in full growth medium. Cells were washed once with SFM and subsequently incubated with 3.5 ml BY-POVPE dispersion (1 µM to 10 µM concentration range) in incubation medium or 3.5 ml SFM containing 1% (v/v) EtOH as a negative control. Following incubation, cells were washed once with ice-cold PBS, scraped into 3 ml PBS (containing 10 mM $NaCNBH_3$ for stabilization and reduction of formed Schiff bases) and harvested by centrifugation (4°C, 5 min, 300 g). The supernatant was discarded, cells were suspended in 1 ml ice-cold PBS (+ 10 mM $NaCNBH_3$) and sonicated for 15 seconds. Cell debris were removed by centrifugation (4°C, 10 min, 1000 g). $NaCNBH_3$ was added to the supernatant (final concentration 20 mM) and the solution was incubated under stirring at RT for 30 min. Following the reduction of formed Schiff bases with $NaCNBH_3$, the protein concentration of the sample was determined using

the method of Bradford (Bradford, 1976). For gel electrophoresis, proteins were precipitated from defined sample aliquots using acetone. For this purpose, ten volumes of ice-cold acetone were added to the aqueous samples which were kept overnight at -20°C. After centrifugation (4°C, 30 min, 20.000 g), the supernatant was removed, the pellet was air-dried, solubilized in sample buffer for gel electrophoresis and stored at -20°C.

Separation of proteins by 1-D gel electrophoresis

SDS-PAGE was performed according to the method of Fling and Gregerson (Fling and Gregerson, 1986) in a Tris/glycine buffer system. Samples containing 100 µg protein per lane were dissolved in 50 µl loading buffer and applied onto a 20x20 cm SDS gel prepared and separated according to the PROTEAN II xi cell protocol provided by BioRad (4.5% stacking gel, 10% resolving gel). Gels were fixed over night in aqueous solutions containing 7 vol.% acetic acid and 10 vol.% ethanol. BY-fluorescence was detected using a BioRad laser scanner (Ex 488 nm, Em 530/30 BP). For visualization of the whole protein, gels were stained with SYPRO Ruby™according to the manufacturer's instructions (Molecular Probes) and scanned at 605 nm upon excitation at 488 nm.

2-D gel electrophoresis

For 2-D gel electrophoresis, samples containing 70 µg protein per gel were precipitated as described above. The protein pellet was solubilized in 135 µl rehydration buffer, containing 7 M urea, 2 M thiourea, 4% Chaps, 0.002% bromphenol blue and 2% Pharmalyte™3-10, at 37°C for 30 min. Isoelectric focusing and subsequent SDS-PAGE were performed according to the method of Görg *et al.* (Görg *et al.*, 2005). In detail, proteins were separated in the first dimension by isoelectric focusing in 7

cm immobilized nonlinear pH 3-10 gradients (Immobiline™Dry Strip Gel strips; GE Healthcare, Germany) using Multiphor II (GE Healthcare). A discontinuous voltage gradient was used starting at 0 V and increasing to 200 V within the first minute. Subsequently, the voltage was further increased to 3.500 V during the following 1.5 h and held at this level for another 1.5 h. In the second dimension, proteins were separated by 10% SDS-PAGE on 7 cm gels at 20 mA constant current. Fluorescence of formed BY-POVPE-protein complexes and SYPRO Ruby™fluorescence representing the full proteome were visualized as described above.

Tryptic digest and LC-MS/MS analysis

Fluorescent BY-POVPE-protein complexes of 1-D and 2-D gels were cut out from the acrylamide gels and tryptically digested according to the method of Shevchenko *et al.* (Shevchenko *et al.*, 1996). Peptide extracts were dissolved in 0.1% formic acid and separated by a nano-HPLC-system (ULTIMATE™3000 nanoLC system, Dionex, Amsterdam, The Netherlands) as described (Birner-Gruenberger and Hermetter, 2007), except for the following gradient: solvent A: water, 0.3% formic acid; solvent B: acetonitrile/water 80:20 (v/v), 0.3% formic acid; 0-5 min: 4% B, after 40 min 55% B, then for 5 min 90% B, and 47 min reequilibration at 4% B. The peptides were ionized in a Finnigan nano-ESI source equipped with Nanospray tips (PicoTip™Emitter; New Objective, Woburn, MA) and analyzed in a Thermo-Finnigan LTQ linear iontrap mass spectrometer (Thermo, San Jose, CA). The MS/MS data were analyzed by searching the NCBI nonredundant public database with SpektrumMill Rev.03.03.084 (Agilent, Darmstadt, Germany) software. Acceptance parameters were two or more identified distinct peptides according to Carr *et al.* (Carr *et al.*, 2004). Identified protein sequences were subjected to identification by SwissProt database to search for protein

target candidates.

Functional classification of identified BY-POVPE-protein adducts

Identified proteins were subjected to the high-throughput enrichment tool DAVID (Database for Annotation, Visualization, and Integrated Discovery) for functional analysis (Sherman *et al.*, 2009). Analysis was restricted to annotation terms referred to biological processes, using "GOTERM_BP_ALL" and "PANTHER_BP_AL" as data sources. Clusters of enriched annotation terms from the gene list obtained from the protein database search were generated with medium classification stringency. As a result, similar enriched annotation terms, part of similar or the same biological responses, were grouped in clusters, reflecting a biological theme (e.g. "GO:0042981 regulation of apoptosis", "GO:0033554 cellular response to stress"). Clusters sharing very similar annotation terms were pooled and these groups were interpreted reflecting biological processes.

4.3.11 Statistical analysis

Data are expressed as means $\pm$ standard deviation (SD). Two-tailed unpaired Student's t-test was used to determine the significance of the differences. p-values ≤ 0.05 were considered significant.

4.4 Results

To investigate the toxicity of oxidized phospholipids in non-melanoma skin cancer cell lines (SCC12, SCC13), we determined the effects of these lipids on cell viability, cell death, activation of acid sphingomyelinase and ceramide formation and compared

these effects to the keratinocyte cell line HaCaT. We studied the cellular uptake of fluorescent oxPL analogues into two cell lines (HaCaT, SCC13) and identified primary protein targets of BY-POVPE in SCC13 cells.

To ensure that any observed cellular effects of oxPL are exclusively the result of incubation with intact lipids and not elicited by degradation products, all experiments were performed in DMEM supplemented with 0.1% FCS. Under high serum conditions (10% FCS) the stability of oxPL is decreased due to serum lipases, which cleave the oxidized fatty acid at the *sn*-2 position. The so generated PLPC is cytotoxic as well (Fruhwirth *et al.*, 2006; Stemmer *et al.*, 2012).

4.4.1 Effects of oxPL on morphology/integrity of skin cancer cell lines

Oxidized phospholipids preferentially induce apoptosis in human melanoma cell lines but not in melanocytes (Ramprecht *et al.*, unpublished data). The same toxic effects of PGPC and POVPC were found in murine B16-BL6 melanoma cells (Ramprecht, Britz *et al.*, unpublished data). Here we show that oxPL can induce apoptotic cell death in SCC cell lines. In detail, cells were incubated with different lipid concentrations for 24 h. Microscopic images were taken after the indicated times to document morphological changes induced by oxPL. Figure 4.2 summarizes the effects of oxPL on the morphology of HaCaT cells (Figure 4.2 A), SCC12 (Figure 4.2 B) and SCC13 carcinoma cells (Figure 4.2 C). The observed morphological effects are highly dependent on cell type, lipid structure and lipid concentration. All carcinoma cell lines are highly sensitive towards the treatment with oxPL. At high lipid concentrations, cells are completely lysed. In contrast, HaCaT keratinocytes are only morphologically influenced by incubation with 200 µM oxPL.

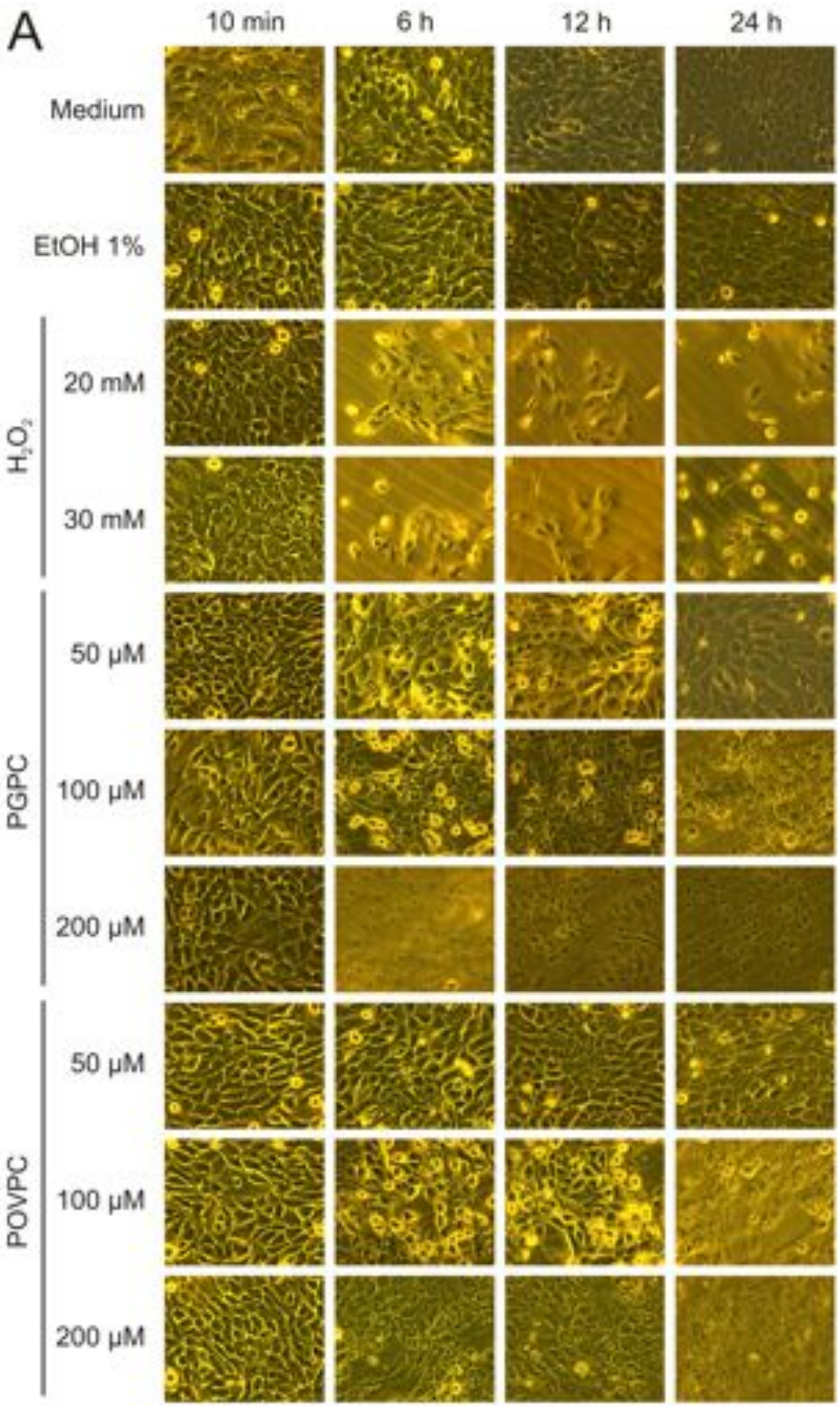
A
10 min
6 h
12 h
24 h
Medium
EtOH 1%
H_2O_2
20 mM
30 mM
PGPC
50 µM
100 µM
200 µM
POVPC
50 µM
100 µM
200 µM

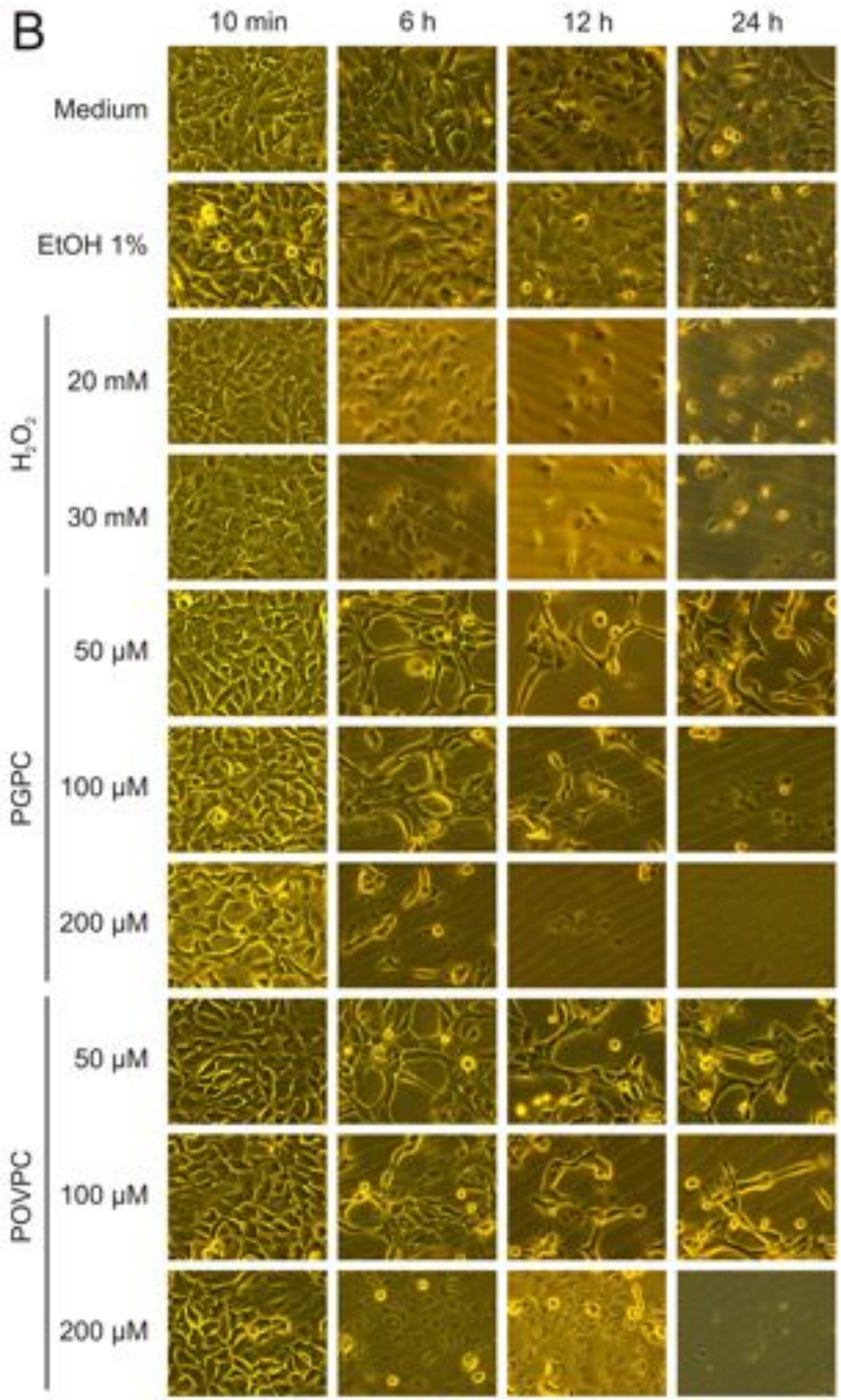
B
10 min
6 h
12 h
24 h
Medium
EtOH 1%
H_2O_2
20 mM
30 mM
PGPC
50 µM
100 µM
200 µM
POVPC
50 µM
100 µM
200 µM

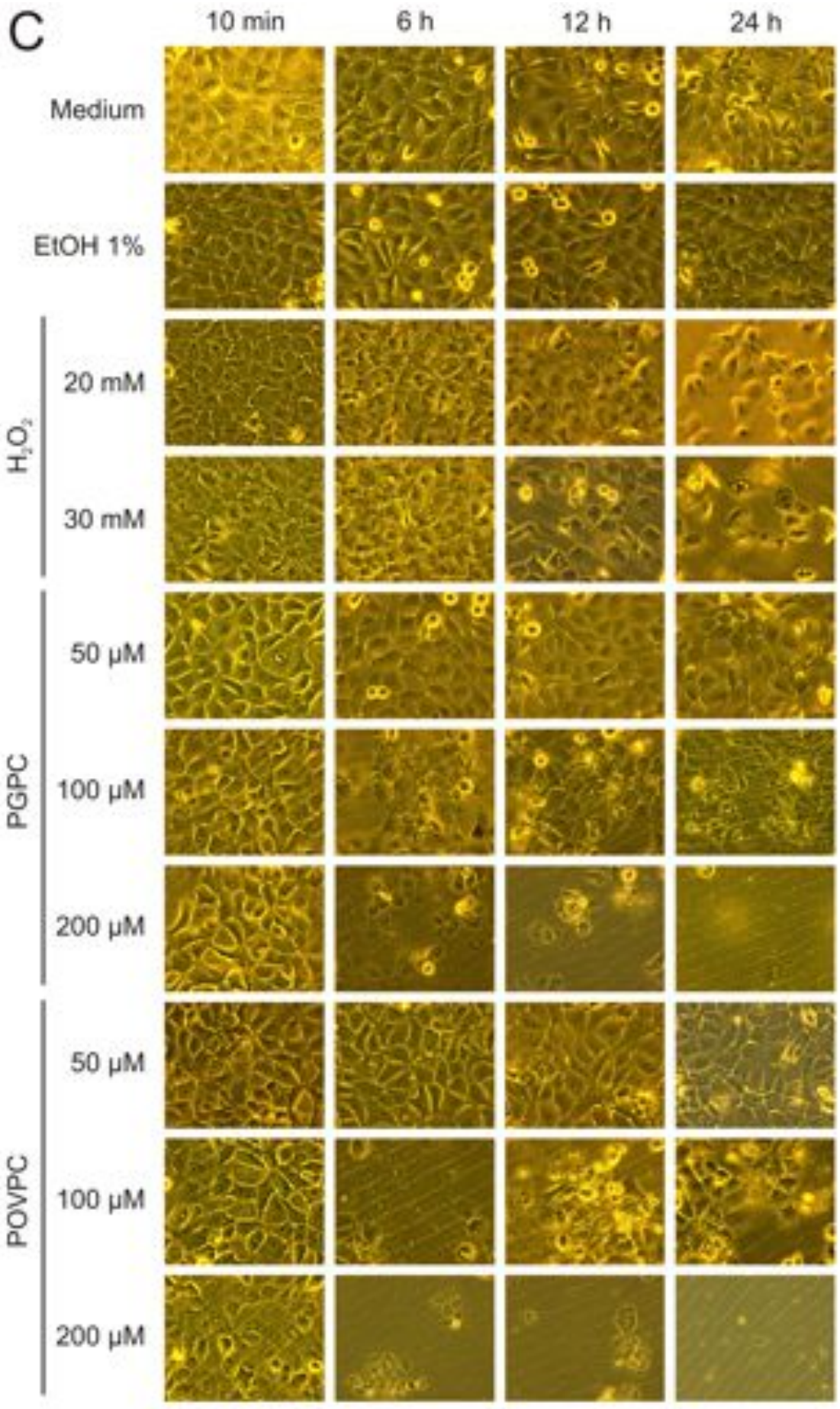

Continued on the following page

Figure 4.2. Effects of oxPL on cell morphology/integrity

Cells were seeded into 24 well plates in full growth medium and allowed to attach to the surface over night. Following several washing steps to remove floating cells, cells were incubated with different concentrations of PGPC or POVPC in medium containing 0.1 % FCS. Control cells were incubated with EtOH (1% v/v) or medium (negative controls) or with H_2O_2 (necrosis control). Microscopic images were taken after the indicated incubation times. Representative results are shown for HaCaT keratinocytes ***(A)****, SCC12* ***(B)*** *and SCC13* ***(C)*** *cell lines.*

4.4.2 Intracellular localization of BY-PGPE and BY-POVPE in HaCaT and SCC13 cells

We performed microscopic studies to examine the uptake of oxPL into various cancer cell lines. For this purpose, we used the fluorescently labelled oxPL analogues BY-PGPE and BY-POVPE. Remarkably, the localization of BY-PGPE and BY-POVPE differs significantly between HaCaT cells and SCC13 cells. In HaCaT keratinocytes, both lipids remain localized to the plasma membrane for at least 30 min as proven by double staining experiments with the plasma membrane-specific dye CellMask™Deep Red (Figure 4.3). In case of BY-POVPE, this finding is consistent with earlier localization experiments in vascular smooth muscle cells (Moumtzi *et al.*, 2007) and in RAW 264.7 macrophages (Stemmer *et al.*, 2012). The retention of the aldehyde phospholipid in the plasma membrane is most likely due to covalent Schiff base formation with amino groups of proteins and lipids. However, the prolonged localization of BY-PGPE to the PM of HaCaT cells is surprising. In several other cancer and non-cancer cell lines, the latter lipid has always been internalized quickly.

In contrast, SCC13 cells efficiently internalized both BODIPY-labelled lipids within 30 min (Figure 4.4), which is in agreement with the fast uptake of these compounds in human melanoma cells (Ramprecht *et al.*, unpublished data) and in murine B16-BL6 cells (Ramprecht, Britz *et al.*, unpublished data). In addition, the subcellular

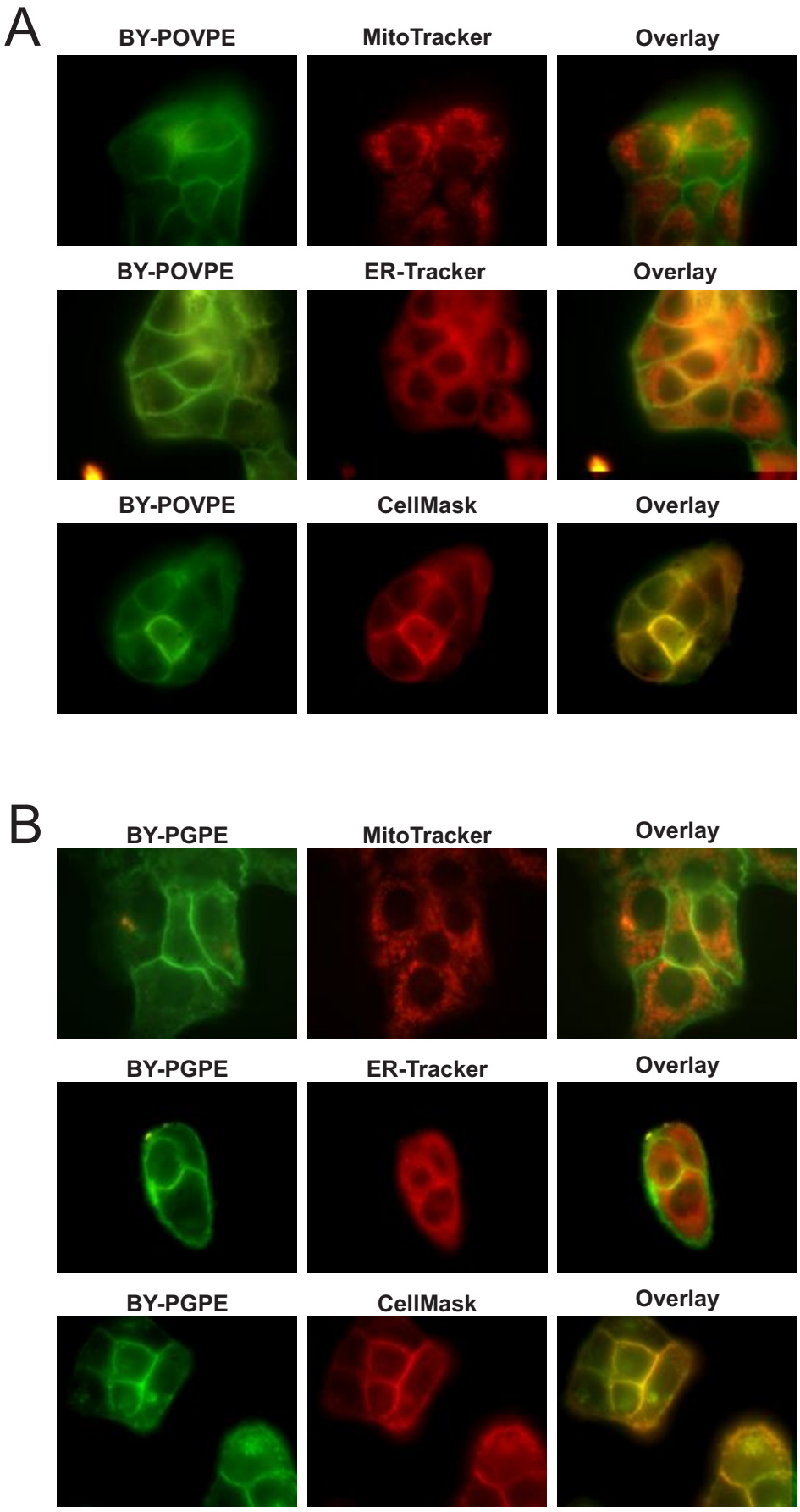

Continued on the following page

Figure 4.3. Uptake and subcellular localization of fluorescent BY-POVPE and BY-PGPE in HaCaT keratinocytes

Cells were pretreated with MitoTracker® Red CM-XRos (0.3 µM), ER-Tracker™Red dye (1 µM) or CellMask™Deep Red (5 µg/ml) followed by incubation with 5 µM BY-POVPE ***(A)*** *or 5 µM BY-PGPE* ***(B)*** *in Phenol red-free medium (0.1% FCS) at 37°C for 30 minutes. Fluorescence images of both the BODIPY lipid and the organelle-specific marker were recorded from the same cells and superimposed using CorelDRAW X4 software. Both BY-PGPE and BY-POVPE localize to the plasma membrane after 30 min in HaCaT keratinocytes. In control experiments no crossover between green (BODIPY) and red (MitoTracker® Red CM-XRos, ER-Tracker™Red dye or CellMask™Deep Reed) fluorescence was detected under the indicated experimental conditions. No autofluorescence was detected in unlabelled control cells using the optical settings indicated in Table 4.2,. Brightness and contrast were adjusted identically in all images. Photographs are representatives for two or more independent experiments.*

localization of both lipids in SCC13 and in the melanoma cell lines mentioned above is identical. They become enriched in the ER. No colocalization of the labelled oxPL and the mitochondria-specific probe MitoTracker™ Red CM-XRos was seen in SCC13 or in melanoma cells.

4.4.3 Effects of oxidized phospholipids on cell viability

Figure 4.5 shows the oxPL induced effects on cell viability which were measured using the photometric MTT assay. All lipids under investigation show a concentration-dependent effect of oxPL on the viability of HaCaT cells after 2 hours incubation, Edelfosine being the most toxic compound in this cell line (Figure 4.5 A). This is surprising insofar as the same cell line is not susceptible to lipid-induced apoptosis (see FACS results, Figure 4.6). In contrast, the effects of oxPL on SCC13 cell viability were less pronounced (Figure 4.5 B). POPC, which was used as a natural reference phospholipid, did not affect cell viability in any of the cell lines.

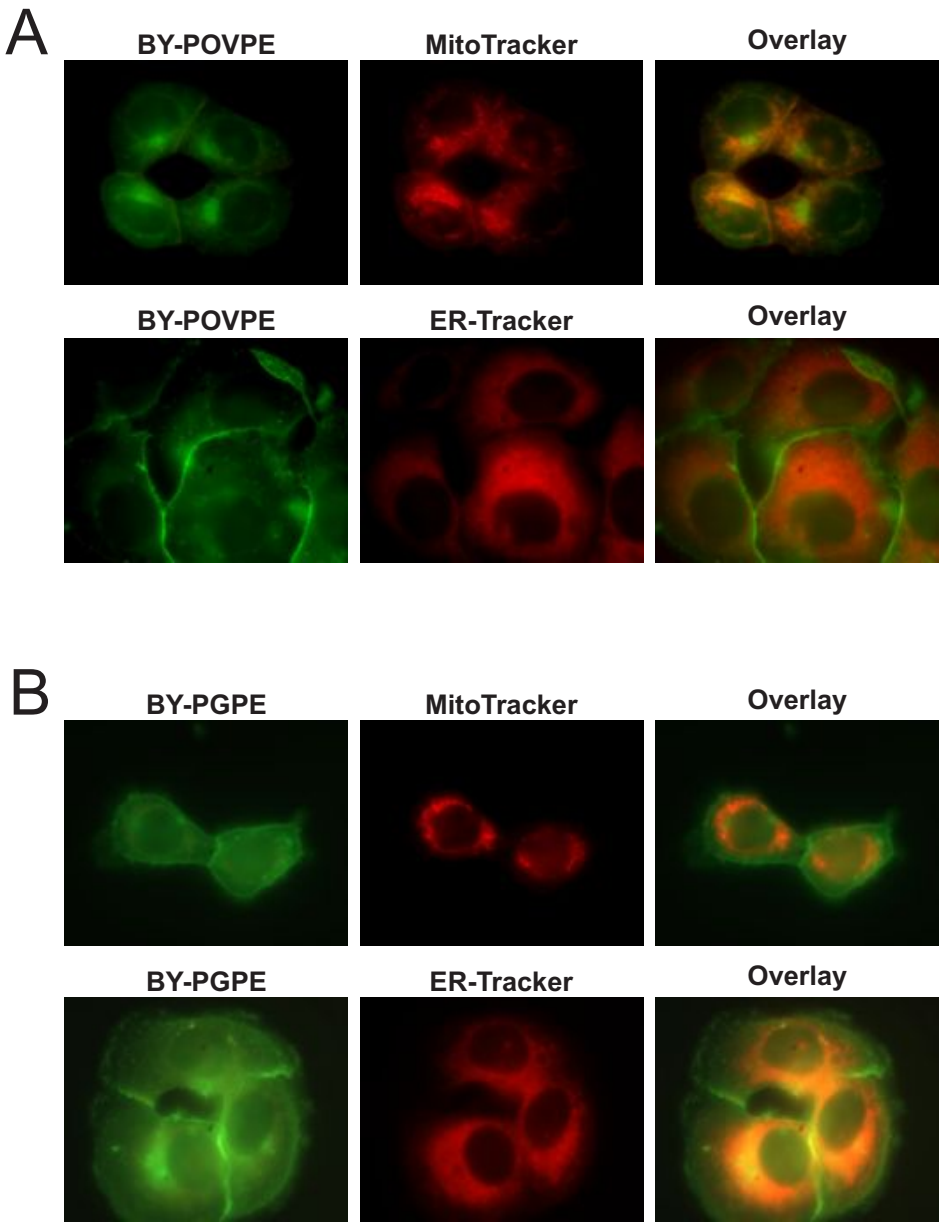

Figure 4.4. Uptake and subcellular localization of fluorescent BY-POVPE and BY-PGPE in SCC13 cells

Cells were prestained with MitoTracker® Red CM-XRos (0.3 µM) or ER-Tracker™Red dye (1 µM) followed by incubation with 5 µM BY-POVPE ***(A)*** *or 5 µM BY-PGPE* ***(B)*** *in Phenol red-free medium (0.1% FCS) at 37°C for 30 minutes. In contrast to HaCaT keratinocytes, both fluorescent oxPL are rapidly internalized by SCC13 cells. Photographs are representative for two or more independent experiments. Experimental conditions were as described in the legend to Figure 4.3.*

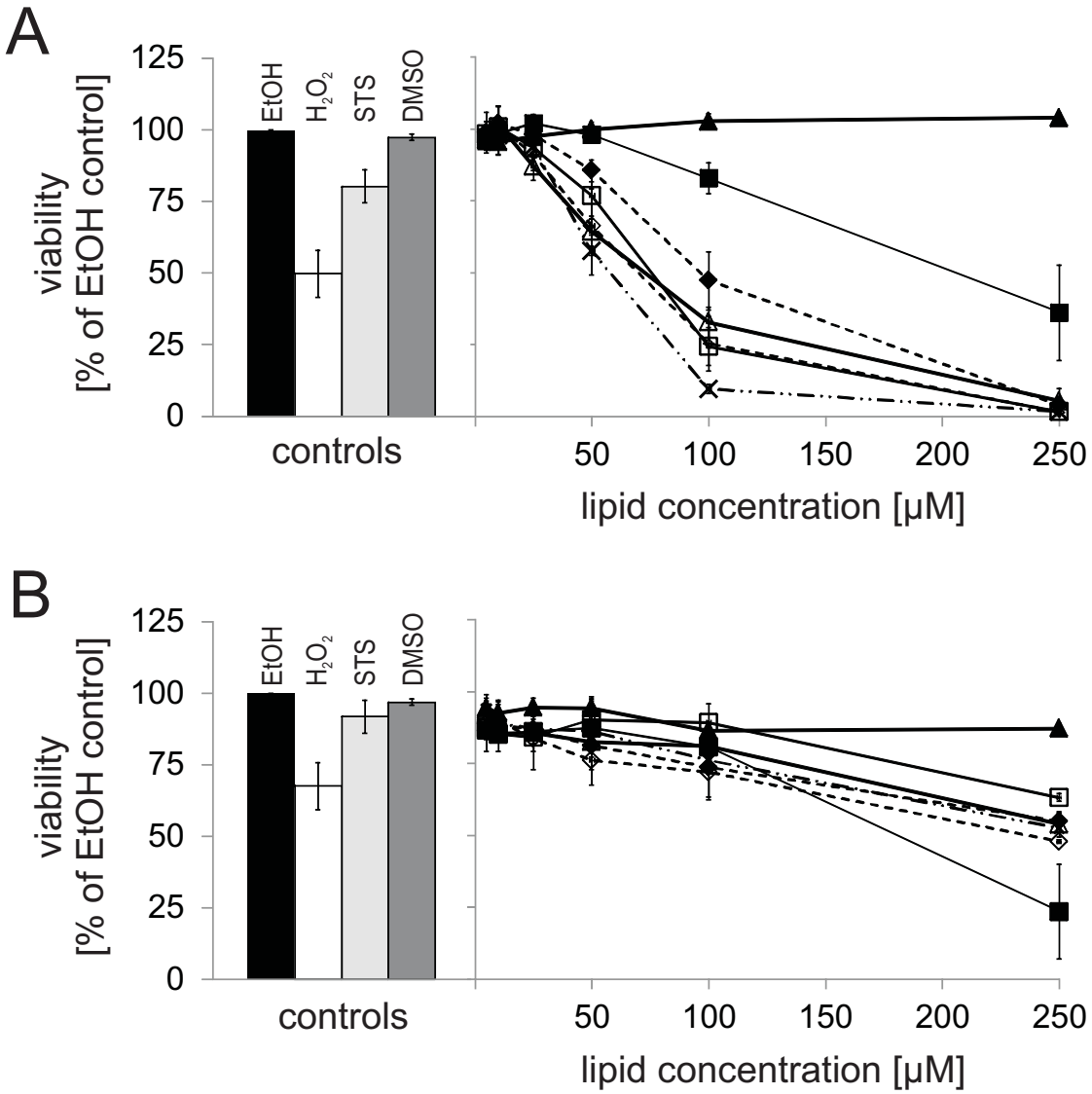

Figure 4.5. Effect of oxidized phospholipids and ether phospholipids on the viability of HaCaT keratinocytes and SCC13 squamous carcinoma cells after 2 hours

HaCaT keratinocytes ***(Panel A)*** *and SCC13 cells* ***(Panel B)*** *were incubated with different lipid concentrations in low serum medium (0.1% FCS) for 2 hours (PGPC (◊), POVPC (♦), E-PGPC (□), E-POVPC (■), Edelfosine (×), PLPC (△), POPC (▲)). Media containing EtOH and DMSO (1% (v/v)) were used as negative controls. H_2O_2 and STS represent positive controls for induction of necrosis and apoptosis, respectively. Cell viabilities were determined using the MTT viability assay (for details see Experimental Procedures). Viability of control cells (EtOH) was set to 100% and all other values represent % viabilities relative to the control. Results were obtained from three or more independent experiments and values represent means ± SD ($n \geq 3$).*

4.4.4 Effects of oxidized phospholipids on cell death

To determine the oxPL capacity of inducing cell death, both cell lines were exposed to 25 µM or 50 µM oxPL for 6 hours. Apoptotic and necrotic cell populations were identified and analyzed by FACS as described in Experimental Procedures. Staurosporine and hydrogen peroxide were used as control agents to induce apoptosis and necrosis, respectively. 50 µM PGPC, POVPC and the respective alkyl ether analogues efficiently induced apoptosis in SCC13 cells, whereas HaCaT cells were almost unaffected (Figure 4.6). In contrast, the synthetic compound Edelfosine preferentially induced necrosis already at low concentrations (25 µM) and higher amounts of this lipid led to complete lysis of the cells.

4.4.5 OxPL-induced formation of sphingomyelin and ceramide

Incubation of SCC13 cells with 50 µM oxPL for 6 hours is associated with induction of apoptosis. In previous studies it was found that oxPL-induced apoptosis was mediated by an increase in ceramide production in VSMCs (Loidl *et al.*, 2003). This rise in ceramide was also found in cultured human melanoma cells (Ramprecht *et al.*, unpublished data) and murine B16-BL6 melanoma cells (Ramprecht, Britz *et al.*, unpublished data). The second messenger ceramide propagates apoptotic signaling and can be formed via several pathways, including *de novo* synthesis, degradation of sphingomyelin and reutilization of sphingosine (salvage pathway). To find out, if apoptosis in SCC13 cells was associated with a rise in cellular ceramide concentrations, cells were stimulated with 50 µM PGPC or POVPC for 6 hours and total ceramide was determined as described in Experimental Procedures.

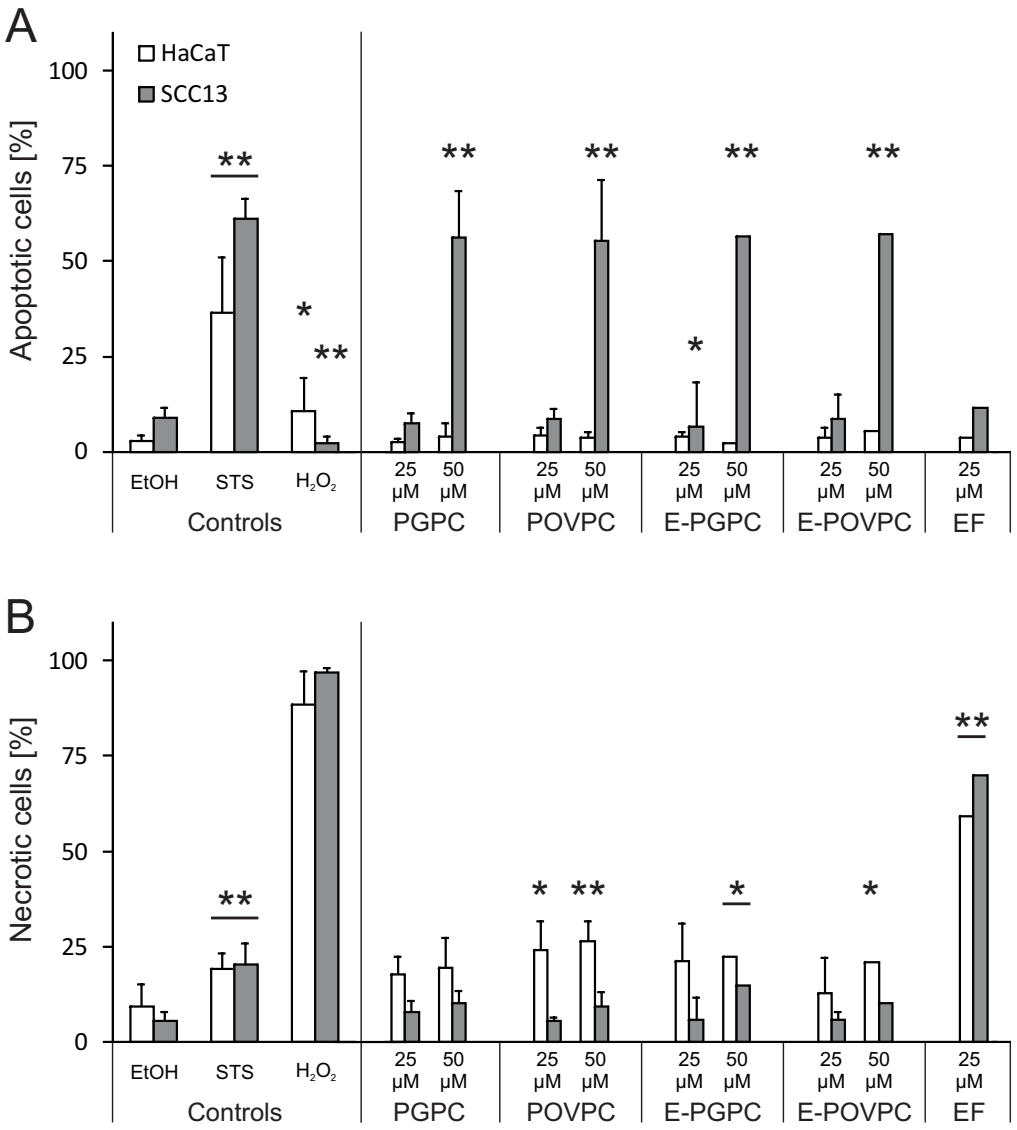

Figure 4.6. Effects of oxPL on apoptosis and necrosis of cancer cells

HaCat cells and SCC13 cells were incubated with different concentrations of oxPL for 6 h in low serum medium (0.1% FCS). Control cells were incubated with medium containing 1% (v/v) EtOH. Cells were incubated with 20 µM STS or 30 mM H_2O_2 as positive controls for apoptosis and necrosis, respectively. After stimulation, cells were harvested and, after staining with propidium iodide (PI) and Annexin V, analyzed by flow cytometry. Intact cells were unstained. Cells stained by PI or both dyes were considered necrotic. Cells stained by Annexin V were considered apoptotic. ***Panel A:*** *Apoptotic cells. No apoptosis can be detected in HaCaT keratinocytes, whereas all oxPL induce apoptosis in a concentration- and lipid-dependent manner in SCC13 cells.* ***Panel B:*** *Necrotic cells. In HaCaT cells, oxPL lead to a slight increase of necrosis, whereas no necrosis can be found in SCC13 cells. Results are expressed as means ± SD ($n \geq 3$).*

PGPC does not change ceramide and sphingomyelin levels in SCC13 cells significantly. In contrast, incubation with POVPC leads to a significant rise in total ceramide and also in total sphingomyelin after 6 hours stimulation (Figure 4.7).

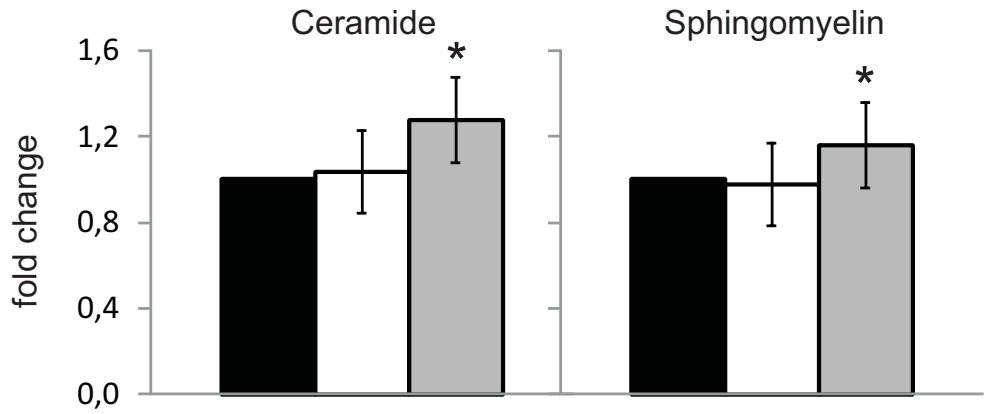

Figure 4.7. Effects of oxPL on total ceramide and sphingomyelin levels in SCC13 cells

*SCC13 cells were incubated with 50 µM PGPC (□), POVPC (■) or 1% EtOH (v/v) (■) (negative control) in RPMI-1640 medium (0.1% FCS) for 6 hours. Cells were harvested, lipids were extracted, and total amounts of ceramide and sphingomyelin were determined as described in Experimental Procedures. PGPC does not change total ceramide and sphingomyelin levels in SCC13 cells. In contrast, POVPC leads to a significant increase in total ceramide and sphingomyelin. Data are expressed as means ± SD. Significances were determined by Student's t-test (two tailed, unpaired). * $P \leq 0.05$ compared with control.*

4.4.6 Stimulation of aSMase activity in SCC13 cells

OxPL-induced apoptosis in SCC13 cells is in part associated with an increase in total ceramide (Figure 4.7). This effect may be due to activation of acid sphingomyelinase. The same phenomenon was observed in vascular cells (VSMCs and RAW 264.7 macrophage) (Loidl *et al.*, 2003; Stemmer *et al.*, 2012) as well as in cultured human melanoma cells and murine B16-BL6 cells (Ramprecht *et al.*, unpublished data, Ramprecht, Britz *et al.*, unpublished data). The detailed effects of 50 µM PGPC and POVPC

on aSMase activity in SCC13 cells are illustrated in Figure 4.8. PGPC induces a significant rise in aSMase activity already after 15 minutes. This activation is lost after 60 min. Surprisingly, POVPC does not activate aSMase in SCC13 cells, although this oxPL stimulates the formation of ceramide (Figure 4.7). To date we do not know whether the POVPC-induced change in ceramide levels is due to *de novo* synthesis or the salvage pathway.

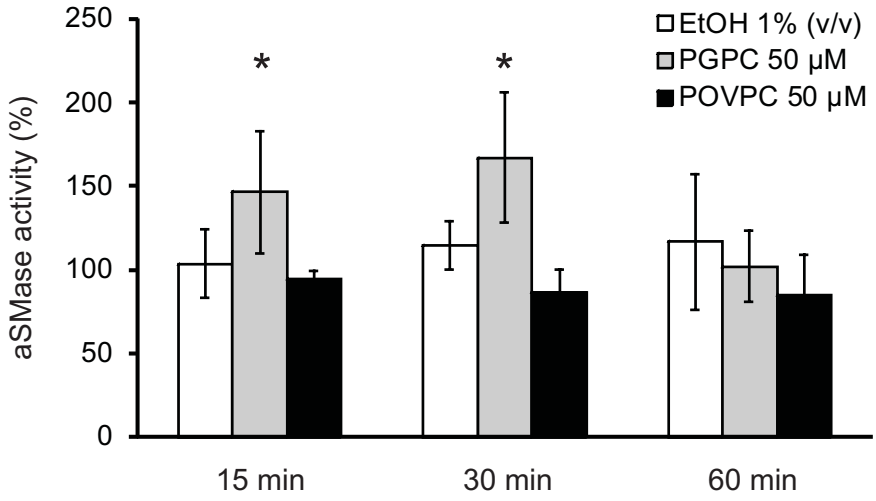

Figure 4.8. Effect of oxPL on acid sphingomyelinase activity in SCC13 cells

*SCC13 cells were incubated with RPMI-1640 media containing 50 µM oxPL or 1% EtOH (v/v) as negative control. Cells were harvested, lysed and acid sphingomyelinase activities were determined as previously described (Loidl et al., 2002). Data are expressed as % activity of unstimulated cells. Stimulation of aSMase by PGPC is significantly increased between 15 and 30 min, whereas POVPC shows hardly any effect. Values are expressed as means ± SD. * $P < 0.05$ compared with control ($n \geq 3$)*

4.4.7 Influence of oxPL on migration of HaCaT and SCC13 cells

Cancer cells spread from the initial site of tumor growth into the surrounding tissue and eventually form metastatic tumors far distant from the primary lesion. Prevention of this spread represents an ultimate therapeutic approach in cancer treatment.

OxLDL, which contains significant amounts of PGPC and POVPC, is known to induce different responses (proliferation or cell death) in cells depending on concentration, incubation time and extent of particle oxidation (Han *et al.*, 1999). We found that B16-BL6 mouse melanoma cells under the influence of oxPL show different tendencies to migrate into a cell free zone. PGPC stimulated migration of B16-BL6 cells whereas POVPC significantly inhibited migration (Ramprecht, Britz *et al.*, unpublished data).

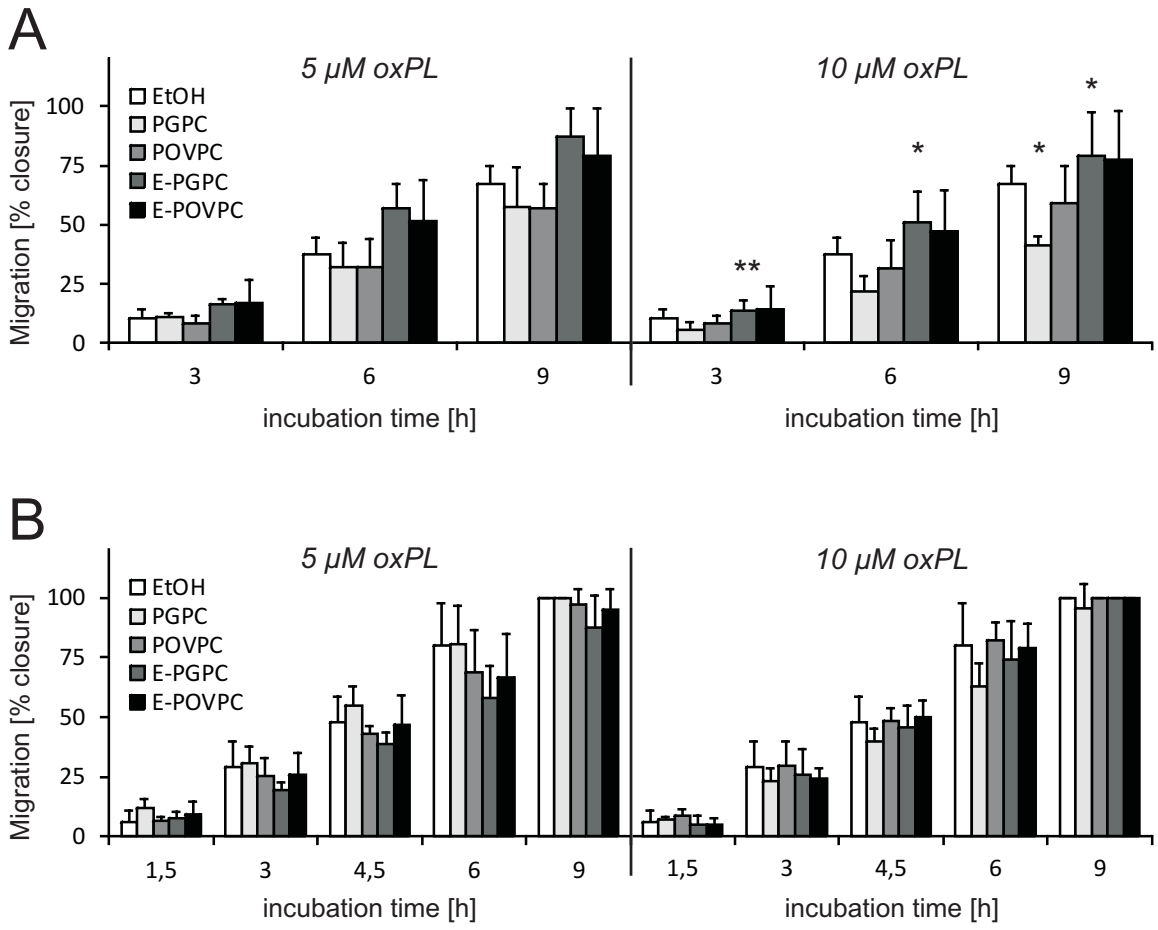

Figure 4.9. Influence of oxPL on migration of HaCaT cells and SCC13 cells

Cultured HaCaT keratinocytes ***(Panel A)*** *and SCC13 carcinoma cells* ***(Panel B)*** *were analyzed for their potential to migrate into a cell-free zone under the influence of oxPL (see Experimental Procedures). For this purpose, cells were incubated with 5 or 10 µM oxPL and microscopic images were taken from identical areas within one well after the indicated incubation times. The width of the cell-free zone was measured using ImageJ software and the extent of migration was calculated as percentage of the initial width of the gap. Results represent means ± SD ($n \geq 3$).*

In this study we determined the effects of 5 µM and 10 µM oxPL on proliferation and migration of HaCaT keratinocytes and SCC13 carcinoma cells. Figure 4.9 summarizes the results. Typically, cells were incubated with oxPL and their migration into a cell-free zone was determined over 9 hours until closure of the cell-free zone was detectable. 5 µM oxPL does not significantly change migration of both cell types. A slightly faster migration of keratinocytes is observed when the cells are exposed to the ether phospholipids. Much faster migration of HaCaT keratinocytes is seen after pre-treatment with 10 µM E-PGPC. In contrast, migration of SCC13 cells is not altered by oxPL. Migration effects due to Edelfosine could not be analyzed. Under the described experimental conditions, this lipid is so toxic that SCC13 and HaCaT cells died, showing cell shrinkage, membrane blebbing and detachment from the plate surface (data not shown).

4.4.8 Concentration-dependent formation of BY-POVPE-protein Schiff bases in SCC13 cells

POVPC contains a chemically reactive aldehyde group at the *sn*-2 position. As a consequence, this lipid can undergo Schiff base formation with NH_2 groups of proteins and aminophospholipids, thus forming lipid-protein and lipid-lipid adducts with distinct properties (Stemmer and Hermetter, 2012). These adducts are unstable and cannot be isolated directly without prior reduction of the Schiff bases with $NaCNBH_3$ to the respective amines.

Former studies by Stemmer *et al.* showed, that the formation of the lipid-protein adducts in RAW 264.7 macrophages is concentration-independent and highly selective, therefore only affecting a defined subset of the whole cell's proteome (Stemmer

et al., 2012). The data presented in our study provides evidence that Schiff base formation in cancer cells is a selective process as well. SCC13 cells were incubated with various concentrations (1, 5, 10 µM) of fluorescently labelled BY-POVPE, followed by protein isolation, chemical reduction of the formed Schiff bases and protein separation by 1-D gel electrophoresis (Figure 4.10). Panels A and B show fluorescently labelled lipid-protein adducts and the full proteome stained with Sypro Ruby, respectively. Multiple fluorescent bands can be detected, but the number of stained lipid-protein bands is much smaller compared to the full protein stain indicating that only a defined subset of proteins is affected by Schiff base formation with BY-POVPE. In addition, fluorescence patterns of proteins from cells stimulated with different concentrations of BY-POVPE are very similar. Thus we conclude that protein tagging by BY-POVPE in SCC13 cancer cells is rather a selective than a random process, comparable to the findings in RAW 264.7 macrophages. However, it has to be emphasized that the fluorescent protein pattern in SCC13 cells is much more complex compared to RAW 264.7 macrophages.

4.4.9 Identification of protein targets of BY-POVPE in SCC13 cells

For identification of BY-POVPE protein targets in SCC13 cells, labelled proteins were subjected to 1-D SDS electrophoresis or 2-D PAGE. Protein bands and spots were excised and tryptically digested followed by MS/MS analysis of the peptides as described in Experimental Procedures. Supplementary Tables 1 and 2 summarize the identified proteins in the 1-D and 2-D gels, respectively. Identified proteins were annotated and functionally clustered using DAVID software (for details see Experimental Procedures).

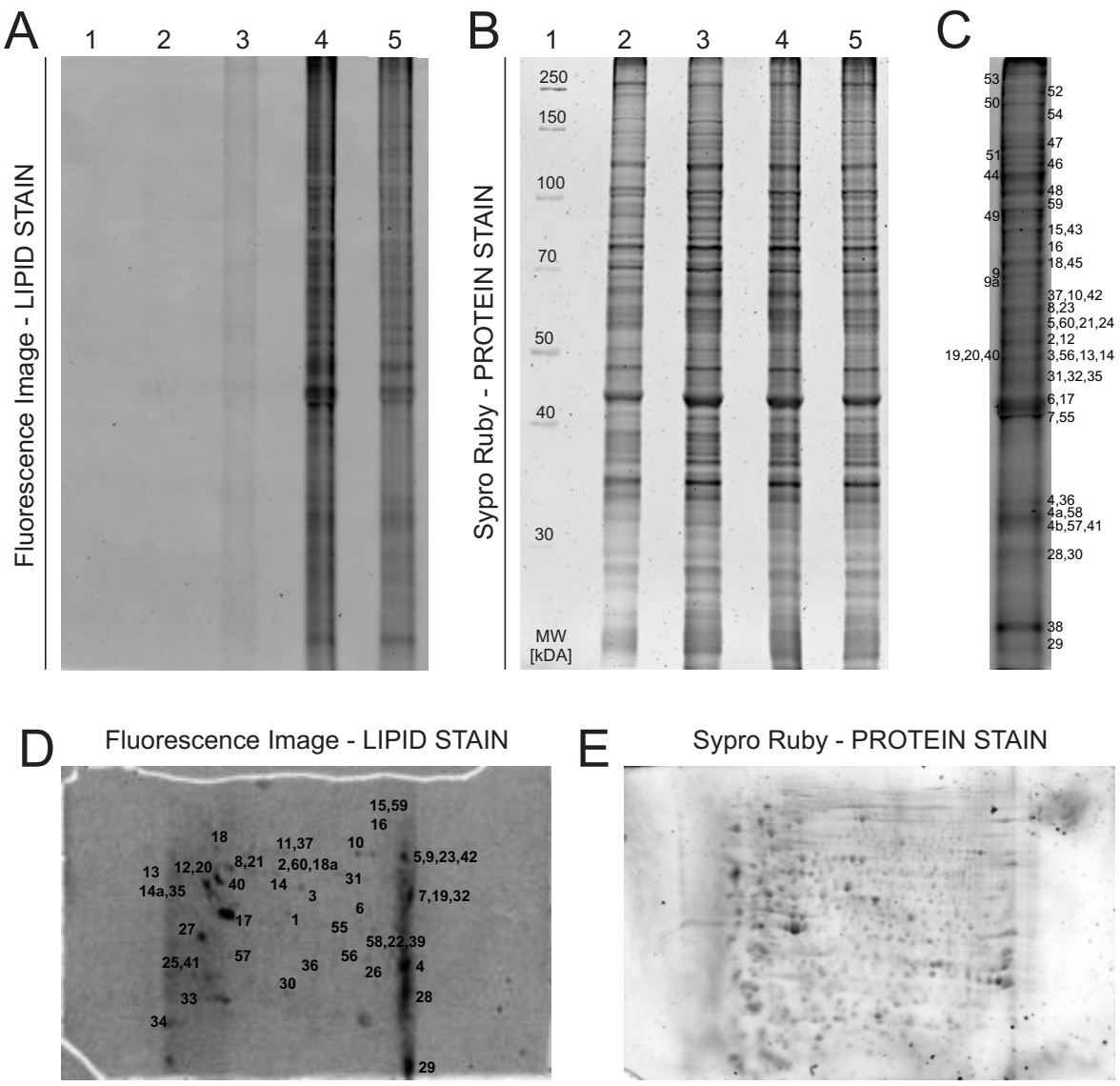

Figure 4.10. Protein targets of fluorescent BY-POVPE in SCC13 cells

Panels A and B: *Cells were incubated with different concentrations of fluorescent BY-POVPE for 30 minutes. After lysis of the cells, proteins were precipitated and 100 µg sample protein per lane were separated by 1-D gel electrophoresis as described in Experimental Procedures. All steps following the incubation were performed under reductive conditions to stabilize formed Schiff bases. Fluorescent protein bands were imaged using a fluorescence laser scanner (BioRad). The lipid stain* ***(A)*** *represents proteins that are covalently bound by BY-POVPE, the SYPRO Ruby protein stain* ***(B)*** *represents the full proteome of the same gel. 1: protein standard; 2: negative control (incubation with 1% (v/v) EtOH in incubation medium for 30 min); 3-5: incubation of cells with 1 µM / 10 µM / 5 µM BY-POVPE for 30 min. The staining of the proteins by BY-POVPE is a selective process. The amount of BY-POVPE does not influence the selectivity of the lipid-protein interaction thus leading to the same fluorescence patterns irrespective of lipid concentrations.*

Continued on the following page

Panel C: *BY-labelled protein bands isolated for MS/MS analysis. The labelled bands were excised, tryptically digested and proteins identified. Results of MS/MS analysis are summarized in Supplementary Table 1.* ***Panels D and E:*** *Two-dimensional gel electrophoresis of fluorescent lipid-protein adducts after incubation of cells with 10 μM BY-POVPE* ***(D)*** *and total protein stain of the same gel with Sypro ruby* ***(E)****. Spots were excised, tryptically digested and identified by MS/MS analysis. Results are summarized in Supplementary Table 2.*

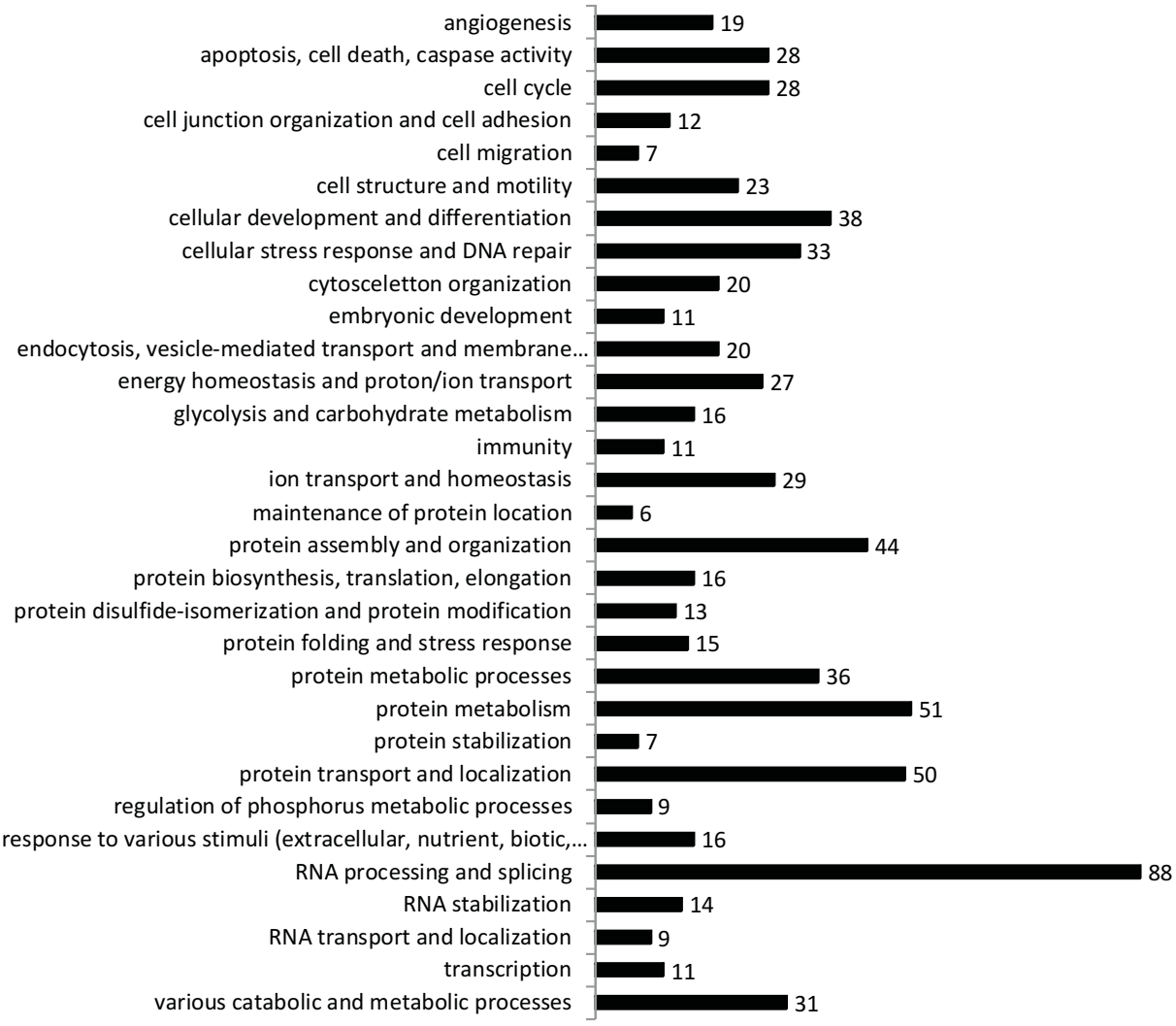

Table 4.3. Functional annotation clustering of identified BY-POVPE protein targets

Functions of BY-POVPE-tagged proteins were analyzed using DAVID (Database for Annotation, Visualization, and Integrated Discovery). An annotation term clustering with annotation terms referred to biological processes of tagged proteins was performed and biological processes were classified by applying analytical steps described in Experimental Procedures.

According to this functional classification (Figure 4.3), protein targets of BY-POVPE are involved in RNA processing and splicing (e.g. splicing factors, heterogeneous nuclear ribonucleoproteins, ribosomal proteins), membrane transport (e.g. VDAC), cellular stress response (e.g. heat shock proteins), apoptosis (e.g. Diablo homolog), cell migration, cell structure and mobility (e.g. myosin, integrin) as well as other processes.

4.5 Discussion

In the present study, we report on the cytotoxicity of oxidized phospholipids and their ether analogues in non-melanoma skin cancer cell lines. We found that these compounds induce cell death in squamous carcinoma cells, whereas healthy keratinocytes are almost unaffected. Fluorescent analogues of PGPC and POVPC are rapidly internalized by cancer cells but not by keratinocytes and localize to an ER near region. OxPL-induced cell death in SCC13 cells is associated with lipid-dependent activation of acid sphingomyelinase and the formation of the second messenger ceramide. In addition, we were able to identify primary protein targets of POVPC, which forms covalent Schiff bases with selected proteins. The respective targets are involved in various cellular processes including cell death, RNA processing, migration and cellular stress response.

Microscopy screenings of squamous carcinoma cell lines (SCC12, SCC13) and keratinocytes (HaCaT) showed that the oxPL influence cell morphology and integrity of tumor cells (Figure 4.2). High oxPL concentrations ($\geq$ 100 µM) lead to lysis of tumor cells. In keratinocytes, the same lipid concentrations only affect cell morphology, but

do not lyse them. To identify the mode of cell death, we examined and compared the toxic effects of the oxidized phospholipids PGPC and POVPC as well as their ether analogues E-PGPC and E-POVPC SCC13 tumor cells and in HaCaT keratinocytes. We also included Edelfosine as a cytotoxic reference in this study. The latter compound is known to selectively induce apoptosis in various tumor cell lines (Ruiter *et al.*, 2001) by modulating membrane properties and activating pro-apoptotic signaling pathways (Gajate and Mollinedo, 2007). Edelfosine triggers an ER-dependent stress response which results in the activation of the mitochondrial apoptosis pathway, the perturbation of the outer mitochondrial membrane, cytochrome c release and the activation of caspase-3 (Huang *et al.*, 2011; Mollinedo *et al.*, 2011).

Our studies showed that oxPL as well as their ether analogues (50 µM) preferentially induce apoptosis but not necrosis in SCC13 cells. Exposure of HaCaT cells to this lipid concentration leads to a slight increase in the fraction of necrotic cells (Figure 4.6). The toxic effects of oxidized phospholipids in non-melanoma skin cancer cells are in line with results from our laboratory obtained with human and murine melanoma cell lines (Ramprecht *et al.*, unpublished data, Ramprecht, Britz *et al.*, unpublished data). It is interesting to note that the ether analogues E-PGPC and E-POVPC exhibit similar toxicities as compared to their diacyl counterparts. This confirms the assumption of Subbanagounder *et al.* that the biological activities of truncated phospholipids are mainly determined by the structure of the polar *sn*-2 acyl chain and to a much lesser extent by the structure of the polar headgroup (Subbanagounder *et al.*, 2000). The synthetic lipid Edelfosine induces necrosis in keratinocytes and SCC13 cells under all experimental conditions in our study.

Selective and efficient uptake of a drug into a cancer cell is a prerequisite for its cellular activity. We used fluorescent PGPC and POVPC analogues to investigate the uptake and intracellular localization in HaCaT keratinocytes and SCC13 cells. In previous studies, we found that the uptake of various oxPL labelled with different fluorophores always led to the same fluorescence pattern irrespective of the attached fluorophore indicating that the label does not affect lipid properties. This assumption is supported by the observation, that unlabelled and labelled lipids elicit the same cellular responses in VSMCs (Moumtzi *et al.*, 2007). BY-POVPE localizes to the plasma membrane of RAW 264.7 macrophages (Stemmer *et al.*, 2012) and VSMCs (Moumtzi *et al.*, 2007) as a consequence of covalent Schiff base formation with NH_2 groups of proteins and phospholipids. In contrast, BY-PGPE was rapidly internalized by both cell lines. Surprisingly, both lipids stained the plasma membrane in HaCaT keratinocytes (Figure 4.3). To date it is unclear, why BY-PGPE is not internalized by these cells. In contrast both lipids were rapidly internalized by SCC13 tumor cells without retention in the plasma membrane, finally localizing in part to the endoplasmic reticulum (Figure 4.4). This finding is in line with previous studies in our laboratory where similar uptake patterns were observed in human and murine melanoma cell lines (Ramprecht *et al.*, unpublished data, Ramprecht, Britz *et al.*, unpublished data). We speculate that this fast and efficient uptake into cancer cells is in part responsible for the more toxic effects elicited by oxPL in tumor cells as compared to keratinocytes.

In contrast to healthy cells, the surface of cancer cells contains unusually high amounts of phosphatidylserine. According to Riedl *et al.*, the malignancy of tumor cells correlates with the amount of PS exposed on the cell surface (Riedl *et al.*, 2011). Why and how cancer cells expose phosphatidylserine, which is enriched in the inner plasma

membrane leaflet in healthy cells (Zwaal *et al.*, 2005), is currently unknown. The aminophospholipids PE and PS may be considered potential targets of oxPL, especially of POVPC, which is capable of forming covalent lipid-lipid adducts (Stemmer *et al.*, 2012). Such compounds would contain three hydrophobic chains and a relatively small headgroup. Molecular dynamics studies by Khandelia and collaborators demonstrated that accumulation of such a lipid condensation product leads to breakdown of phosphatidylcholine bilayers (H. Khandelia, personal communication) (Stemmer and Hermetter, 2012). In addition, high amounts of PS in the outer plasma membrane leaflet of cancer cells may change membrane polarity, thus facilitating internalization of the oxPL. It may be speculated that the particular membrane lipid composition of tumor cells contributes to the fast uptake of oxPL in these cells.

OxPL-induced apoptosis is associated with activation of acid sphingomyelinase and formation of the second messenger ceramide in VSMCs (Loidl *et al.*, 2003), RAW 264.7 macrophages (Stemmer *et al.*, 2012), murine B16-BL6 melanoma cells (Ramprecht, Britz *et al.*, unpublished data) and some human melanoma cell lines (Ramprecht *et al.*, unpublished data). Increased ceramide concentrations have also been observed in tumor cells as a consequence of treatment with chemotherapeutic agents (Senchenkov *et al.*, 2001). The reported drugs induced ceramide formation by *de novo* synthesis, activation of sphingomyelinases and/or by blocking glucosylceramide formation. Ceramide-based therapies that stimulate the generation of ceramide and inhibit ceramide catabolism or modification have been discussed as potential cancer therapies (Reynolds *et al.*, 2004). In this context, preclinical studies suggest that induction of ceramide formation and inhibition of ceramide degradation might be a useful new approach for killing cancer cells with tolerable toxicity to normal healthy cells.

Therefore ceramide has also been termed a“tumor suppressor lipid” (Hannun and Linardic, 1993).

Here we provide evidence that the oxPL-dependent cell death in SCC13 cells is associated with activation of acid sphingomyelinase and the formation of ceramide. Interestingly, PGPC and POVPC stimulate different ceramide responses, although both lead to the same endpoint, namely apoptosis. PGPC triggers a fast activation of aSMase for at least 30 minutes (Figure 4.8), but ceramide and sphingomyelin levels are not affected even after 6 hours (Figure 4.7). However, it has to be noted that degradation of sphingomyelin by aSMase and formation of ceramide in the plasma membrane are small compared to the total cellular lipid amounts and may escape detection in a total lipid extract. Already minor changes in ceramide content, e.g. by activation of aSMase, may exert profound effects on various cellular processes. This lipid is involved in apoptosis (Pettus *et al.*, 2002), cell aging (Venable *et al.*, 1995), cell growth arrest (Jayadev *et al.*, 1995) and differentiation (Bielawska *et al.*, 1992) depending on stimulus and cell type. Additionally, it represents a critical membrane component since it may modulate membrane protein activities by influencing lateral membrane organization and curvature (Schenck *et al.*, 2007).

POVPC does not influence aSMase activity in SCC13 cells at all (Figure 4.7). Despite this fact, ceramide levels in POVPC treated cells are elevated after 6 hours (Figure 4.8), demonstrating that other ceramide forming pathways, e.g. the *de novo* pathway or sphingosine recycling may be responsible for this effect. We have evidence that such a pathway is responsible for ceramide formation in cultured macrophages under the influence of oxPL for several hours (L. Marlingapla Halasiddappa *et al.*, unpublished

data). The involvement of *de novo* ceramide synthesis in oxPL-induced SCC13 cell death would be in line with the subcellular localization of the POVPC in the endoplasmic reticulum (Figure 4.4) which is the organelle accommodating the enzymes of the *de novo* ceramide synthesis.

Toxic effects of oxidized phospholipids may also depend on their biophysical properties. The structural differences between PGPC and POVPC are only small but their biological activities differ to a large extent. It was reported that the polar phospholipid headgroup are likely to play only a minor role in oxPL activity (Subbanagounder *et al.*, 2000), which is mainly influenced by the truncated acyl chain at the *sn*-2 position. OxPL can specifically interact with other biomolecules within the cell membrane, modulate physical membrane properties such as membrane organization and curvature, affect membrane-associated molecules and therefore lead to fundamental consequences for cellular signaling networks (Stemmer and Hermetter, 2012). The key functional difference between PGPC and POVPC structure is due to the chemical reactivity of POVPC (see above). This lipid is able to form covalent Schiff bases with amino groups of proteins and aminophospholipids due to its aldehyde group at the ω-position of the truncated *sn*-2 fatty acyl chain (Stemmer and Hermetter, 2012). Covalent modification of those biomolecules can trigger downstream signaling cascades and therefore represent primary signaling platforms. In contrast, PGPC can only physically interact with target molecules on the cell surface and within the cell.

In this study, we screened SCC13 tumor cells for primary protein targets of a fluorescent POVPC analogue and compared the results with earlier findings by Stemmer *et al.* for RAW 264.7 macrophages (Stemmer *et al.*, 2012). Covalent protein modification

by BY-POVPE was a highly selective process in both cell types, affecting only a defined subset of cellular proteins (Figure 4.10, Panels A and B). Similar results were found using biotin-tagged probes for lipid target identification (Gugiu *et al.*, 2008). A detailed analysis of the found targets in SCC13 cells led to the identification of proteins involved in cell death and survival, protein folding and cellular stress response, RNA processing, stabilization and splicing, cell migration and mobility, protein transport and localization and others (Figure 4.3). There is some overlap between the protein targets identified in cancer cells and the protein targets detected in RAW 264.7 macrophages (Stemmer *et al.*, 2012) and endothelial cells (Gugiu *et al.*, 2008). However, the number of identified protein targets in SCC13 cells is much higher compared to the results obtained in other studies. Further investigations will aim at confirming selected protein targets as functional components and signaling platforms of oxPL toxicity. For this purpose, gain and loss of function experiments will be performed to provide additional information about functional consequences of covalent protein modification by POVPC and to exclude false positive hits.

In summary, the oxidized phospholipids PGPC and POVPC as well as their ether analogues E-PGPC and E-POVPC selectively induce cell death in squamous carcinoma cell lines but not in keratinocytes. Lipid toxicity in skin cancer cells seems to be related to efficient uptake of oxPL, formation of ceramide and covalent modification of proteins and lipids (by POVPC). The unusual high PS content of the cancer cell surface could play a particular role in this scenario. The results obtained in this study will be the basis for further experiments to exploit the potential of oxidized phospholipids for the topic treatment of skin tumors and to understand the mechanisms of their activities.

4.6 Acknowledgements

We gratefully acknowledge financial support of the PhD thesis of Claudia Ramprecht by TU Graz .

Supplementary Table S 4.4. Protein targets of BY-POVPE (1-D PAGE)

Cells were incubated with BY-POVPE (10 µM) in serum-free medium for 30 min followed by isolation and 1-D SDS gel electrophoresis of the labelled proteins. Protein bands (Figure 4.3, panel C) were excised and tryptically digested. Subsequently, peptides were analyzed by MS/MS and targets were identified by database search (SwissProt).

Spot (#)	Group (#)	Spectra (#)	Distinct Peptides (#)	Disinct Summed MS/MS Search Score	AA Coverage [%]	Protein MW [DA]	Protein pI	Database ID Accession GI (#)	Protein Name
1	8	8	5	80,58	12	50317,6	7,05	Q9P2R7,3	Succinyl-CoA ligase [ADP-forming] subunit beta, mitochondrial
1	13	11	5	75,88	22	44740,1	5,85	Q13148,1	TAR DNA-binding protein 43
2	1	257	34	595,37	63	56782,7	5,99	P30101,4	Protein disulfide-isomerase A3
2	7	22	10	174,19	30	56501,0	5,57	P21281,3	V-type proton ATPase subunit B, brain isoform
3	8	90	14	229,40	40	49229,7	5,89	P31943,4	Heterogeneous nuclear ribonucleoprotein H
3	25	12	5	80,37	21	50436,0	5,85	Q07960,1	Rho GTPase-activating protein 1
4	2	110	14	260,89	41	38746,8	9,17	P09651,5	Heterogeneous nuclear ribonucleoprotein A1
4	4	70	14	237,19	54	33296,5	9,83	Q99623,2	Prohibitin-2
4	6	48	10	183,57	38	36688,9	8,44	P00338,2	L-lactate dehydrogenase A chain
4	7	54	11	180,35	56	30772,7	8,62	P21796,2	Voltage-dependent anion-selective channel protein 1
4	13	30	7	128,73	41	30840,8	9,34	Q13151,1	Heterogeneous nuclear ribonucleoprotein A0
4	21	17	5	98,14	19	36092,1	9,23	Q15717,2	ELAV-like protein 1
4	29	7	3	57,40	11	36249,9	9,01	P53597,4	Succinyl-CoA ligase [ADP/GDP-forming] subunit alpha, mitochondrial
4a	6	21	10	165,74	42	34833,1	8,67	Q00403,1	Transcription initiation factor IIB
4a	9	40	10	154,98	36	35619,6	9,22	Q9H9B4,4	Sideroflexin-1
4a	10	33	10	150,61	33	33934,6	8,17	Q16831,1	Uridine phosphorylase 1
4a	19	26	7	108,74	31	31566,7	7,50	P45880,2	Voltage-dependent anion-selective channel protein 2
4a	20	22	7	107,21	25	32996,2	9,23	P36542,1	ATP synthase subunit gamma, mitochondrial
4a	23	26	7	99,62	22	37429,9	8,97	P22626,2	Heterogeneous nuclear ribonucleoproteins A2/B1
4a	28	23	7	90,95	23	36067,9	9,35	Q16698,1	2,4-dienoyl-CoA reductase, mitochondrial
4a	47	4	3	40,38	9	32004,6	8,88	Q96HS1,2	Serine/threonine-protein phosphatase PGAM5, mitochondrial
4a	53	5	2	31,34	7	35351,1	9,14	Q9BRJ2,2	39S ribosomal protein L45, mitochondrial

4a	63	5	2	21,68	9	33172,2	9,05	Q9Y314,1	Nitric oxide synthase-interacting protein
4b	1	82	17	272,87	74	26688,5	9,68	P23396,2	40S ribosomal protein S3
5	4	57	18	307,21	43	57924,6	7,96	P50991,4	T-complex protein 1 subunit delta
5	6	40	15	272,93	43	57937,2	7,95	P14618,4	Pyruvate kinase isozymes M1/M2
5	7	46	16	269,68	43	59367,0	7,55	Q99832,2	T-complex protein 1 subunit eta
5	14	16	5	93,46	13	58449,5	7,05	O43172,2	U4/U6 small nuclear ribonucleoprotein Prp4
5	25	4	3	50,12	7	63705,4	5,99	O00425,2	Insulin-like growth factor 2 mRNA-binding protein 3
5	28	5	3	43,23	7	56084,8	9,02	Q0P258,2	Protein RCC2
5	38	3	2	21,86	3	63945,5	8,55	Q96HC4,5	PDZ and LIM domain protein 5
6	2	66	19	311,43	52	49541,8	7,26	P49411,2	Elongation factor Tu, mitochondrial
7	3	70	8	153,27	43	32854,2	4,79	P08865,4	40S ribosomal protein SA
7	16	11	4	72,72	10	51712,7	8,45	O75390,2	Citrate synthase, mitochondrial
8	2	62	18	340,93	43	61055,0	5,70	P10809,2	60 kDa heat shock protein, mitochondrial
9	2	83	26	449,81	46	70898,4	5,38	P11142,1	Heat shock cognate 71 kDa protein
9	3	91	27	426,76	40	77516,1	8,85	P52272,3	Heterogeneous nuclear ribonucleoprotein M
9	6	56	17	275,88	32	67560,7	7,18	Q96AE4,3	Far upstream element-binding protein 1
9	13	17	9	134,05	14	80272,9	8,53	Q92841,2	Probable ATP-dependent RNA helicase DDX17
9	31	6	3	49,88	6	70671,3	9,51	P11940,2	Polyadenylate-binding protein 1
9a	12	22	10	169,35	24	72912,2	6,99	O00425,2	Alkyldihydroxyacetonephosphate synthase, peroxisomal
9a	27	10	4	63,23	9	68330,3	9,08	Q15637,4	Splicing factor 1
10	12	17	6	107,75	17	72691,9	7,06	P31040,2	Succinate dehydrogenase [ubiquinone] flavoprotein subunit, mitochondrial
10	34	3	2	33,10	5	66452,9	6,11	Q15833,2	Syntaxin-binding protein 2
12	8	41	9	168,15	26	43476,3	5,51	Q6NZI2,1	Polymerase I and transcript release factor
12	27	9	3	56,49	9	48207,5	5,02	Q9UJU6,1	Drebrin-like protein
13	5	57	16	281,12	55	49831,3	4,79	P68371,1	Tubulin beta-4B chain
14	2	61	16	296,53	46	56560,2	5,26	P06576,3	ATP synthase subunit beta, mitochondrial
14	18	16	8	122,18	22	52878,8	5,66	Q96KP4,2	Cytosolic non-specific dipeptidase
14	15	11	7	110,73	16	48991,6	5,44	Q13838,1	Spliceosome RNA helicase DDX39B
14	34	9	3	53,97	10	84121,6	4,95	Q15084,1	Protein disulfide-isomerase A6
15	3	70	10	154,69	19	95338,7	6,41	P13639,4	Elongation factor 2
16	5	61	17	299,14	32	73115,7	6,85	Q92945,4	Far upstream element-binding protein 2
17	11	18	9	139,88	25	46154,2	5,32	P60842,1	Eukaryotic initiation factor 4A-I
17	25	10	4	72,89	17	40573,0	4,99	Q9UNZ2,2	NSFL1 cofactor p47
17	15	5	2	36,19	8	45672,1	5,38	P52597,3	Heterogeneous nuclear ribonucleoprotein F
18	1	211	33	619,87	51	72333,3	5,07	P11021,2	78 kDa glucose-regulated protein
18	2	153	37	606,55	57	72932,8	4,96	P13667,2	Protein disulfide-isomerase A4

18	3	156	31	539,09	52	74139,8	6,57	P02545,1	Prelamin-A/C
19	1	180	26	449,56	56	59750,9	9,16	P25705,1	ATP synthase subunit alpha, mitochondrial
19	4	82	17	285,61	44	55993,3	8,76	P34897,3	Serine hydroxymethyltransferase, mitochondrial
20	3	91	16	292,44	49	49895,6	4,96	Q9BQE3,1	Tubulin alpha-1C chain
21	8	22	9	162,58	24	58849,2	5,27	Q12874,1	Splicing factor 3A subunit 3
23	7	42	12	207,65	26	64133,1	8,46	P14866,2	Heterogeneous nuclear ribonucleoprotein L
c	21	8	4	52,40	11	61640,7	8,60	Q96I24,2	Far upstream element-binding protein 3
23	23	7	4	48,53	9	51556,9	9,94	P08621,2	U1 small nuclear ribonucleoprotein 70 kDa
24	5	93	16	279,52	58	48141,8	4,29	P27797,1	Calreticulin
28	8	33	9	139,31	38	28415,7	8,71	P09661,2	U2 small nuclear ribonucleoprotein A'
28	10	22	7	123,83	33	25176,9	9,29	Q00688,1	Peptidyl-prolyl cis-trans isomerase FKBP3
28	22	25	6	69,64	26	26477,9	7,67	P54819,2	Adenylate kinase 2, mitochondrial
28	30	7	3	54,19	14	24893,9	5,61	P09429,3	High mobility group protein B1
29	6	29	7	119,32	24	27131,0	5,68	Q9NR28,1	Diablo homolog, mitochondrial
29	7	36	7	98,39	40	19329,7	11,7	P84103,1	Serine/arginine-rich splicing factor 3
29	9	21	6	89,80	36	20776,8	8,71	O96000,3	NADH dehydrogenase [ubiquinone] 1 beta subcomplex subunit 10
29	10	32	6	88,81	34	20762,5	10,7	Q02543,2	60S ribosomal protein L18a
29	12	27	5	80,26	27	21539,2	8,67	Q9NVJ2,1	ADP-ribosylation factor-like protein 8B
29	15	28	5	78,35	26	19889,1	5,50	Q9Y5S9,1	RNA-binding protein 8A
29	18	15	5	71,36	22	23742,7	9,42	P23284,2	Peptidyl-prolyl cis-trans isomerase B
29	19	12	5	67,40	23	21379,0	8,43	P60763,1	Ras-related C3 botulinum toxin substrate 3
29	43	5	2	34,18	18	14787,1	9,21	P35268,2	60S ribosomal protein L22
30	9	29	7	126,23	35	28993,6	6,77	P30040,4	Endoplasmic reticulum resident protein 29
31	9	28	10	170,42	30	46837,3	6,68	P05455,2	Lupus La protein
32	4	140	17	277,97	54	50185,3	9,15	Q5VTE0,1	Putative elongation factor 1-alpha-like 3
32	23	14	6	79,46	18	50680,2	8,77	Q16181,2	Septin-7
32	41	3	2	31,78	8	50646,8	9,18	Q9H0S4,1	Probable ATP-dependent RNA helicase DDX47
35	10	53	10	163,48	31	49203,8	5,13	P17980,3	26S protease regulatory subunit 6A
35	17	15	6	103,00	26	47366,5	5,09	P43686,2	26S protease regulatory subunit 6B
35	26	6	5	64,53	10	47629,1	5,63	Q8NBS9.2	Thioredoxin domain-containing protein 5
35	31	5	3	56,30	12	44468,6	5,17	Q16543,1	Hsp90 co-chaperone Cdc37
36	31	8	3	56,57	13	36984,0	6,12	P36873,1	Serine/threonine-protein phosphatase PP1-gamma catalytic subunit
37	3	54	18	303,26	29	67689,1	5,28	Q03252,3	Lamin-B2
37	5	35	13	231,64	27	70811,4	5,41	P13797,4	Plastin-3
37	35	3	3	29,80	10	54235,1	5,61	Q9BR76,1	Coronin-1B

38	1	87	15	263,40	70	23489,9	6,39	P51149,1	Ras-related protein Rab-7a
38	4	36	10	185,67	56	23545,7	6,08	P61019,1	Ras-related protein Rab-2A
38	5	35	10	174,15	62	23277,4	9,97	P48047,1	ATP synthase subunit O, mitochondrial
38	8	41	9	143,97	28	22591,5	10,7	P46781,3	40S ribosomal protein S9
38	9	48	8	142,39	30	28480,4	6,43	P28074,3	Proteasome subunit beta type-5
38	14	64	7	117,42	35	21634,6	11,7	Q07020,2	60S ribosomal protein L18
38	15	24	7	112,78	27	24722,2	8,34	P04179,2	Superoxide dismutase [Mn], mitochondrial
38	17	39	7	105,79	26	22876,5	9,73	P46782,4	40S ribosomal protein S5
40	51	3	2	21,91	8	53126,3	5,83	Q12849,3	G-rich sequence factor 1
41	52	12	2	30,40	9	26269,6	4,47	A6NL28,2	Putative tropomyosin alpha-3 chain-like protein
42	1	60	20	341,94	46	67878,0	7,58	P29401,3	Transketolase
43	1	266	65	1082,49	57	157906,0	5,81	P42704,3	Leucine-rich PPR motif-containing protein, mitochondrial
43	1	459	31	495,50	43	84660,2	4,94	P07900,5	Heat shock protein HSP 90-alpha
43	2	70	24	408,64	35	90933,3	7,12	O43143,2	Putative pre-mRNA-splicing factor ATP-dependent RNA helicase DHX15
43	3	65	22	370,94	36	93488,8	5,50	Q8N1F7,2	Nuclear pore complex protein Nup93
43	4	78	24	367,86	39	91918,0	8,97	Q13724,5	Mannosyl-oligosaccharide glucosidase
43	5	80	20	325,77	27	95338,9	8,85	Q12906,3	Interleukin enhancer-binding factor 3
43	8	40	18	266,28	27	89595,7	6,34	O94874,2	E3 UFM1-protein ligase 1
43	10	60	15	233,60	27	81075,2	6,45	Q08945,1	FACT complex subunit SSRP1
43	13	33	13	190,49	22	76614,7	4,60	P19338,3	Nucleolin
43	14	19	10	158,68	19	83678,3	6,08	Q16891,1	Mitochondrial inner membrane protein
44	4	72	20	315,11	23	126633,0	6,39	P23229,4	Integrin alpha-6
44	6	44	18	273,85	18	123800,0	5,50	P18206,4	Vinculin
44	7	35	18	263,67	18	131986,0	9,43	O43795,3	Unconventional myosin-Ib
45	4	50	16	276,37	32	73243,8	6,73	O00571,3	ATP-dependent RNA helicase DDX3X
45	5	42	13	206,45	23	80420,6	8,65	Q95573,3	Long-chain-fatty-acid--CoA ligase 3
45	9	27	10	182,91	20	83000,1	9,16	P40939,2	Trifunctional enzyme subunit alpha, mitochondrial
45	10	25	11	178,85	24	76690,1	5,37	P16435,2	NADPH--cytochrome P450 reductase
45	11	35	10	176,99	21	69603,0	8,68	O60506,2	Heterogeneous nuclear ribonucleoprotein Q
45	13	33	9	155,73	20	69492,0	9,68	Q96PK6,2	RNA-binding protein 14
45	14	22	9	130,59	12	90584,9	5,76	Q00839,6	Heterogeneous nuclear ribonucleoprotein U
46	2	162	39	689,75	37	140959,0	6,41	Q08211,4	ATP-dependent RNA helicase A
46	4	118	33	573,09	31	141542,0	6,77	Q9UQE7,2	Structural maintenance of chromosomes protein 3
46	3	134	31	537,58	33	135578,0	5,13	Q15393,4	Splicing factor 3B subunit 3
46	6	47	15	244,57	18	139440,0	5,51	Q5JPE7,1	Nodal modulator 2
46	7	30	15	243,65	16	133897,0	6,44	P30876,1	DNA-directed RNA polymerase II subunit RPB2

46	8	40	15	227,33	17	128303,0	5,33	Q93009,2	Ubiquitin carboxyl-terminal hydrolase 7
47	1	131	42	709,76	40	143234,0	7,51	Q14683,2	Structural maintenance of chromosomes protein 1A
47	2	124	36	604,48	36	145831,0	6,65	O75533,3	Splicing factor 3B subunit 1
47	3	69	31	460,54	27	156276,0	5,52	Q86UP2,1	Kinectin
47	5	92	25	399,24	29	129296,0	5,16	P17301,1	Integrin alpha-2
47	4	80	21	324,24	21	141456,0	6,43	Q00341,2	Vigilin
48	2	85	26	438,36	35	102487,0	6,36	P19367,3	Hexokinase-1
48	3	90	26	428,87	31	106926,0	8,49	O94906,1	Pre-mRNA-processing factor 6
48	2	96	26	415,72	35	101998,0	6,74	Q7KZF4,1	Staphylococcal nuclease domain-containing protein 1
48	4	91	21	335,82	28	95338,9	8,85	Q12906,3	Interleukin enhancer-binding factor 3
48	5	63	23	319,92	27	106875,0	5,73	Q14697,3	Neutral alpha-glucosidase AB
48	5	64	18	318,25	34	88550,2	5,52	Q13263,5	Transcription intermediary factor 1-beta
48	13	40	17	247,00	24	90981,3	5,53	P25205,3	DNA replication licensing factor MCM3
49	1	302	57	1050,55	67	104855,0	5,27	O43707,2	Alpha-actinin-4
49	2	189	37	630,12	49	92469,3	4,76	P14625,1	Endoplasmin
49	3	90	34	552,62	58	100072,0	5,95	P35221,1	Catenin alpha-1
49	8	35	14	228,44	17	112897,0	5,33	P05023,1	Sodium/potassium-transporting ATPase subunit alpha-1
50	1	398	83	1514,61	46	226533,0	5,50	P35579,4	Myosin-9
50	3	95	38	615,26	24	234710,0	5,84	Q9NZM1,1	Myoferlin
50	4	82	37	603,86	20	278165,0	5,47	O75369,2	Filamin-B
50	10	12	7	115,98	5	195460,0	6,24	Q07157,3	Tight junction protein ZO-1
51	1	246	46	808,86	42	140959,0	6,41	Q08211,4	ATP-dependent RNA helicase A
51	15	20	9	118,43	9	132822,0	5,57	Q8IX12,2	Cell division cycle and apoptosis regulator protein 1
52	1	349	94	1632,22	51	280740,0	5,71	P21333,4	Filamin-A
52	2	286	83	1285,25	44	273602,0	8,95	Q6P2Q9,2	Pre-mRNA-processing-splicing factor 8
52	3	174	69	1151,61	37	284541,0	5,22	Q13813,3	Spectrin alpha chain, non-erythrocytic 1
52	5	154	53	911,29	28	274611,0	5,39	Q01082,2	Spectrin beta chain, non-erythrocytic 1
53	1	534	107	1898,76	60	278165,0	5,47	O75369,2	Filamin-B
53	6	31	14	242,22	8	274377,0	5,64	P11717,3	Cation-independent mannose-6-phosphate receptor
54	1	263	60	1060,08	43	189253,0	6,08	P46940,1	Ras GTPase-activating-like protein IQGAP1
55	8	23	7	117,77	31	41487,7	6,15	Q15019,1	Septin-2
56	46	23	2	26,99	8	36926,7	6,37	P31942,2	Heterogeneous nuclear ribonucleoprotein H3
57	41	4	2	41,79	14	26922,9	5,09	O00299,4	Chloride intracellular channel protein 1
58	2	66	14	255,85	56	35503,5	8,92	P40926,3	Malate dehydrogenase, mitochondrial
59	14	12	5	86,18	7	101560,0	6,89	P11586,3	C-1-tetrahydrofolate synthase, cytoplasmic
59	20	6	4	63,20	5	89814,4	7,66	Q96T88,1	E3 ubiquitin-protein ligase UHRF1
59	35	2	2	21,64	2	97396,0	8,74	Q9NTZ6,1	RNA-binding protein 12
60	15	20	6	77,43	12	60131,0	5,60	Q75131,1	Copine-3

Supplementary Table S 4.5. Protein targets of BY-POVPE (2-D PAGE)

Cells were incubated with BY-POVPE (10 µM) in serum-free medium for 30 min followed by isolation and 1-D SDS gel electrophoresis of the labelled proteins. Protein bands (Figure 4.3, panel C) were excised and tryptically digested. Subsequently, peptides were analyzed by MS/MS and targets were identified by database search (SwissProt).

Spot (#)	Group (#)	Spectra (#)	Distinct Peptides (#)	Disinct Summed MS/MS Search Score	AA Coverage [%]	Protein MW [DA]	Protein pI	Database ID Accession GI (#)	Protein Name
1	2	31	8	106,13	17	44740,1	5,85	Q13148,1	TAR DNA-binding protein 43
1	1	9	3	37,50	6	50317,6	7,05	Q9P2R7,3	Succinyl-CoA ligase [ADP-forming] subunit beta, mitochondrial
2	1	79	13	194,11	25	56782,7	5,99	P30101,4	Protein disulfide-isomerase A3
2	3	20	2	34,44	4	56501,0	5,57	P21281,3	V-type proton ATPase subunit B, brain isoform
3	1	25	7	103,65	19	49229,7	5,89	P31943,4	Heterogeneous nuclear ribonucleoprotein H
3	7	4	2	19,59	4	50436,0	5,85	Q07960,1	Rho GTPase-activating protein 1
4	1	137	16	278,91	50	38746,8	9,17	P09651,5	Heterogeneous nuclear ribonucleoprotein A1
4	2	115	13	219,48	45	37429,9	8,97	P22626,2	Heterogeneous nuclear ribonucleoproteins A2/B1
4	2	27	7	125,96	30	36092,1	9,23	Q15717,2	ELAV-like protein 1
4	5	24	8	116,36	31	34833,1	8,67	Q00403,1	Transcription initiation factor IIB
4	6	23	7	95,35	27	30772,7	8,62	P21796,2	Voltage-dependent anion-selective channel protein 1
4	3	28	5	90,72	26	26688,5	9,68	P23396,2	40S ribosomal protein S3
4	4	15	4	69,90	15	30840,8	9,34	Q13151,1	Heterogeneous nuclear ribonucleoprotein A0
4	5	19	5	67,88	22	33296,5	9,83	Q99623,2	Prohibitin-2
4	9	14	4	63,99	15	32996,2	9,23	P36542,1	ATP synthase subunit gamma, mitochondrial
4	10	8	5	62,08	19	36067,9	9,35	Q16698,1	2,4-dienoyl-CoA reductase, mitochondrial
4	11	24	3	52,99	9	36688,9	8,44	P00338,2	L-lactate dehydrogenase A chain
4	10	9	3	44,86	12	35619,6	9,22	Q9H9B4,4	Sideroflexin-1
4	8	17	3	43,30	11	36249,9	9,01	P53597,4	Succinyl-CoA ligase [ADP/GDP-forming] subunit alpha, mitochondrial
4	8	8	3	37,17	13	31566,7	7,50	Q9H9B4,4	Voltage-dependent anion-selective channel protein 2
4	11	4	3	33,45	11	33172,2	9,05	Q9Y314,1	Nitric oxide synthase-interacting protein
4	14	8	3	30,86	10	32204,6	8,88	Q96HS1,2	Serine/threonine-protein phosphatase PGAM5, mitochondrial

4	17	4	2	23,33	5	33934,6	8,17	Q16831,1	Uridine phosphorylase 1
4	18	4	2	22,60	10	35351,1	9,14	Q9BRJ2,2	39S ribosomal protein L45, mitochondrial
5	1	99	16	243,06	31	57937,2	7,95	P14618,4	Pyruvate kinase isozymes M1/M2
5	5	19	9	135,94	22	58449,5	7,05	O43172,2	U4/U6 small nuclear ribonucleoprotein Prp4
5	6	54	9	133,74	17	59347,0	7,55	Q99832,2	T-complex protein 1 subunit eta
5	7	18	8	125,27	14	57924,6	7,96	P50991,4	T-complex protein 1 subunit delta
5	4	24	8	104,83	16	63705,4	8,99	O00425,2	Insulin-like growth factor 2 mRNA-binding protein 3
5	8	4	4	53,90	9	63945,5	8,55	Q96HC4,5	PDZ and LIM domain protein 5
5	14	6	4	47,49	9	56084,8	9,02	Q0P258,2	Protein RCC2
6	1	15	2	37,55	4	49541,8	7,26	P49411,2	Elongation factor Tu, mitochondrial
6	2	11	3	30,99	4	43295,9	8,35	P08559,3	Pyruvate dehydrogenase E1 component subunit alpha, somatic form, mitochondrial
7	10	4	2	29,63	4	51712,7	8,45	O75390,2	Citrate synthase, mitochondrial
7	6	2	2	24,71	8	32854,2	4,79	P08865,4	40S ribosomal protein SA
8	1	45	13	186,58	27	61055,0	5,70	P10809,2	60 kDa heat shock protein, mitochondrial
9	1	160	23	346,51	37	77516,1	8,85	P52272,3	Heterogeneous nuclear ribonucleoprotein M
9	2	85	19	285,11	28	80272,9	8,53	Q92841,2	Probable ATP-dependent RNA helicase DDX17
9	15	10	5	94,71	14	72912,2	6,99	O00425,2	Alkyldihydroxyacetonephosphate synthase, peroxisomal
9	5	11	6	83,31	10	70671,3	9,51	P11940,2	Polyadenylate-binding protein 1
9	6	17	5	71,24	10	48227,6	8,72	Q07666,1	KH domain-containing, RNA-binding, signal transduction-associated protein 1
9	7	9	4	59,22	6	68330,3	9,08	Q15637,4	Splicing factor 1
9	13	6	3	37,97	6	67560,7	7,18	Q96AE4,3	Far upstream element-binding protein 1
9	14	4	3	37,18	5	70898,4	5,38	P11142,1	Heat shock cognate 71 kDa protein
10	1	8	4	36,00	5	72691,9	7,06	P31040,2	Succinate dehydrogenase [ubiquinone] flavoprotein subunit, mitochondrial
10	2	6	3	27,32	5	66452,9	6,11	Q15833,2	Syntaxin-binding protein 2
11	1	14	5	65,42	7	69367,1	5,92	P02768,2	Serum albumin
12	3	13	5	62,10	13	48207,5	5,02	Q9UJU6,1	Drebrin-like protein
12	5	12	2	32,24	7	43476,3	5,51	Q6NZI2,1	Polymerase I and transcript release factor
13	1	146	11	165,86	23	49831,3	4,79	P68371,1	Tubulin beta-4B chain
14a	2	49	7	113,28	16	84121,6	4,95	Q15084,1	Protein disulfide-isomerase A6
14a	7	23	2	42,21	5	56560,2	5,26	P06576,3	ATP synthase subunit beta, mitochondrial
14	1	9	3	32,64	6	52878,8	5,66	Q96KP4,2	Cytosolic non-specific dipeptidase
14	5	4	2	19,45	4	48991,6	5,44	Q13838,1	Spliceosome RNA helicase DDX39B
15	1	17	5	63,96	6	95338,7	6,41	P13639,4	Elongation factor 2

16	1	54	13	159,90	23	73115,7	6,85	Q92945,4	Far upstream element-binding protein 2
17	1	38	8	131,95	21	45672,1	5,38	P52597,3	Heterogeneous nuclear ribonucleoprotein F
17	2	18	7	105,50	19	46154,2	5,32	P60842,1	Eukaryotic initiation factor 4A-I
17	4	5	3	43,82	10	40573,0	4,99	Q9UNZ2,2	NSFL1 cofactor p47
18	1	93	20	346,70	35	72333,3	5,07	P11021,2	78 kDa glucose-regulated protein
18	2	28	9	124,56	14	72932,8	4,96	P13667,2	Protein disulfide-isomerase A4
18a	1	23	7	86,83	12	74139,8	6,57	P02545,1	Prelamin-A/C
19	2	15	7	84,65	13	55993,3	8,76	P34897,3	Serine hydroxymethyltransferase, mitochondrial
19	3	20	6	77,58	12	59750,9	9,16	P25705,1	ATP synthase subunit alpha, mitochondrial
20	1	100	17	268,57	41	49895,6	4,96	Q9BQE3,1	Tubulin alpha-1C chain
21	8	3	2	25,80	3	58849,2	5,27	Q12874,1	Splicing factor 3A subunit 3
22	1	100	18	268,05	51	38604,2	7,58	P07355,2	Annexin A2
23	3	65	10	152,51	17	64133,1	8,46	P14866,2	Heterogeneous nuclear ribonucleoprotein L
23	7	29	8	126,95	17	61640,7	8,60	Q96I24,2	Far upstream element-binding protein 3
23	9	31	10	123,97	24	51556,9	9,94	P08621,2	U1 small nuclear ribonucleoprotein 70 kDa
25	3	13	4	48,79	11	29174,1	4,63	P62258,1	14-3-3 protein epsilon
26	5	7	3	43,65	13	33697,3	6,94	Q99439,4	Calponin-2
27	4	57	8	116,30	21	32575,2	4,64	P06748,2	Nucleophosmin
27	6	22	4	60,36	21	31122,0	4,9,0	P29692,5	Elongation factor 1-delta
28	2	12	6	92,33	27	24893,9	5,61	P09429,3	High mobility group protein B1
28	3	12	8	86,79	23	28415,7	8,71	P09661,2	U2 small nuclear ribonucleoprotein A'
28	4	13	4	52,29	20	26477,9	7,67	P54819,2	Adenylate kinase 2, mitochondrial
28	8	7	3	43,34	13	25176,9	9,29	Q00688,1	Peptidyl-prolyl cis-trans isomerase FKBP3
29	5	7	5	62,53	30	14787,1	9,21	P35268,2	60S ribosomal protein L22
30	1	9	3	44,35	14	28993,6	6,77	P30040,4	Endoplasmic reticulum resident protein 29
31	1	5	2	22,44	4	46837,3	6,68	P05455,2	Lupus La protein
32	1	36	8	99,34	15	50185,3	9,15	Q5VTE0,1	Putative elongation factor 1-alpha-like 3
32	5	18	3	46,84	8	50680,2	8,77	Q16181,2	Septin-7
32	7	3	2	32,36	5	50646,8	9,18	Q9H0S4,1	Probable ATP-dependent RNA helicase DDX47
33	1	24	2	35,98	9	28315,9	5,05	P04632,1	Calpain small subunit 1
34	5	7	2	25,43	22	11283,9	6,09	P81605,2	Dermcidin
35	3	12	6	62,09	14	49203,8	5,13	P17980,3	26S protease regulatory subunit 6A
35	4	9	5	52,77	9	47366,5	5,09	P43686,2	26S protease regulatory subunit 6B
35	5	9	3	45,72	7	47629,1	5,63	Q8NBS9.2	Thioredoxin domain-containing protein 5

35	8	9	3	41,58	7	44468,6	5,17	Q16543,1	Hsp90 co-chaperone Cdc37
36	2	12	4	54,73	13	36984,0	6,12	P36873,1	Serine/threonine-protein phosphatase PP1-gamma catalytic subunit
37	2	7	4	54,41	8	54235,1	5,61	Q9BR76,1	Coronin-1B
37	6	7	2	30,94	3	70811,4	5,41	P13797,4	Plastin-3
37	9	3	2	18,29	3	67689,1	5,28	Q03252,3	Lamin-B2
39	1	7	2	28,45	6	36225	8,21	Q99729,2	Heterogeneous nuclear ribonucleoprotein A/B
40	5	12	2	31,49	4	53126,3	5,83	Q12849,3	G-rich sequence factor 1
41	2	13	4	57,55	14	26269,6	4,47	A6NL28,2	Putative tropomyosin alpha-3 chain-like protein
42	5	22	5	70,60	10	67878,0	7,58	P29401,3	Transketolase
55	2	2	2	21,15	6	41487,7	6,15	Q15019,1	Septin-2
56	3	6	2	27,89	7	36926,7	6,37	P31942,2	Heterogeneous nuclear ribonucleoprotein H3
57	1	23	3	42,83	14	26922,9	5,09	O00299,4	Chloride intracellular channel protein 1
58	3	52	10	151,46	39	35503,5	8,92	P40926,3	Malate dehydrogenase, mitochondrial
59	2	11	2	29,71	2	97396,0	8,74	Q9NTZ6,1	RNA-binding protein 12
59	3	3	3	29,60	3	101560,0	6,89	P11586,3	C-1-tetrahydrofolate synthase, cytoplasmic
59	4	2	2	20,47	3	89814,4	7,66	Q96T88,1	E3 ubiquitin-protein ligase UHRF1
60	2	7	5	53,78	9	60131,0	5,60	Q75131,1	Copine-3

References Chapter IV

Abràmoff, M., P. Magalhães, and S. Ram (2004). Image processing with imagej. *Biophotonics international 11*(7), 36–42.

Batzri, S. and E. Korn (1973). Single bilayer liposomes prepared without sonication. *Biochimica et Biophysica Acta 298*(4), 1015–1019.

Berliner, J., N. Leitinger, and S. Tsimikas (2009). The role of oxidized phospholipids in atherosclerosis. *Journal of lipid research 50*(Supplement), S207–S212.

Berridge, M., P. Herst, and A. Tan (2005). Tetrazolium dyes as tools in cell biology: new insights into their cellular reduction. *Biotechnology annual review 11*, 127–152.

Berridge, M., A. Tan, *et al.* (1993). Characterization of the cellular reduction of 3-(4, 5-dimethylthiazol-2-yl)-2, 5-diphenyltetrazolium bromide (mtt): subcellular localization, substrate dependence, and involvement of mitochondrial electron transport in mtt reduction. *Archives of Biochemistry and Biophysics 303*(2), 474.

Bielawska, A., C. Linardic, and Y. Hannun (1992). Modulation of cell growth and differentiation by ceramide. *FEBS letters 307*(2), 211–214.

Birner-Gruenberger, R. and A. Hermetter (2007). Activity-based proteomics of lipolytic enzymes. *Current Drug Discovery Technologies 4*(1), 1–11.

Bochkov, V., O. Oskolkova, K. Birukov, A. Levonen, C. Binder, and J. Stöckl (2010). Generation and biological activities of oxidized phospholipids. *Antioxidants & redox signaling 12*(8), 1009–1059.

Boukamp, P., R. Petrussevska, D. Breitkreutz, J. Hornung, A. Markham, and

N. Fusenig (1988). Normal keratinization in a spontaneously immortalized aneuploid human keratinocyte cell line. *The Journal of cell biology 106*(3), 761–771.

Bradford, M. (1976). A rapid and sensitive method for the quantization of microgram quantities of protein utilizing the principle of protein-dye binding. *Anal Biochem 72*(1-2), 248–54.

Carr, S., R. Aebersold, M. Baldwin, A. Burlingame, K. Clauser, and A. Nesvizhskii (2004). The need for guidelines in publication of peptide and protein identification data working group on publication guidelines for peptide and protein identification data. *Molecular & Cellular Proteomics 3*(6), 531–533.

Diepgen, T., M. Fartasch, H. Drexler, and J. Schmitt (2012). Occupational skin cancer induced by ultraviolet radiation and its prevention. *British Journal of Dermatology 167*(s2), 76–84.

Fling, S. and D. Gregerson (1986). Peptide and protein molecular weight determination by electrophoresis using a high-molarity tris buffer system without urea. *Analytical biochemistry 155*(1), 83–88.

Fruhwirth, G. and A. Hermetter (2008). Mediation of apoptosis by oxidized phospholipids. *Lipids in Health and Disease 49*, 351–367.

Fruhwirth, G., A. Loidl, and A. Hermetter (2007). Oxidized phospholipids: from molecular properties to disease. *Biochimica et Biophysica Acta (BBA)-Molecular Basis of Disease 1772*(7), 718–736.

Fruhwirth, G., A. Moumtzi, A. Loidl, E. Ingolic, and A. Hermetter (2006). The oxidized phospholipids povpc and pgpc inhibit growth and induce apoptosis in vascular smooth muscle cells. *Biochimica et Biophysica Acta (BBA)-Molecular and Cell Biology of Lipids 1761*(9), 1060–1069.

Gajate, C. and F. Mollinedo (2002). Biological activities, mechanisms of action and biomedical prospect of the antitumor ether phospholipid et-18-och3 (edelfosine), a proapoptotic agent in tumor cells. *Current drug metabolism 3*(5), 491–525.

Gajate, C. and F. Mollinedo (2007). Edelfosine and perifosine induce selective apoptosis in multiple myeloma by recruitment of death receptors and downstream signaling molecules into lipid rafts. *Blood 109*(2), 711–719.

Gajate, C., A. Santos-Beneit, A. Macho, M. Lazaro, A. Hernandez-De Rojas, M. Modolell, E. Muñoz, and F. Mollinedo (2000). Involvement of mitochondria and caspase-3 in et-18-och3-induced apoptosis of human leukemic cells. *International journal of cancer 86*(2), 208–218.

Görg, A., W. Postel, and S. Günther (2005). Two-dimensional electrophoresis. the current state of two-dimensional electrophoresis with immobilized ph gradients. *Electrophoresis 9*(9), 531–546.

Greenberg, M., X. Li, B. Gugiu, X. Gu, J. Qin, R. Salomon, and S. Hazen (2008). The lipid whisker model of the structure of oxidized cell membranes. *Journal of Biological Chemistry 283*(4), 2385.

Gugiu, B., K. Mouillesseaux, V. Duong, T. Herzog, A. Hekimian, L. Koroniak, T. Vondriska, and A. Watson (2008). Protein targets of oxidized phospholipids in endothelial cells. *Journal of lipid research 49*(3), 510–520.

Han, C., Y. Pak, *et al.* (1999). Oxidation-dependent effects of oxidized ldl: proliferation or cell death. *Exp Mol Med 31*(4), 165–173.

Hannun, Y. and C. Linardic (1993). Sphingolipid breakdown products: anti-proliferative and tumor-suppressor lipids. *Biochimica et Biophysica Acta-Biomembranes-Including Reviews on Biomembranes 1154*(3), 223–236.

Hartler, J., M. Trötzmüller, C. Chitraju, F. Spener, H. Köfeler, and G. Thallinger (2011). Lipid data analyzer: unattended identification and quantitation of lipids in lc-ms data. *Bioinformatics 27*(4), 572–577.

Hermetter, A., H. Stütz, R. Franzmair, and F. Paltauf (1989). 1-o-trityl-sn-glycero-3-phosphocholine: a new intermediate for the facile preparation of mixed-acid 1, 2-diacylglycerophosphocholines. *Chemistry and physics of lipids 50*(1), 57–62.

Housman, T., S. Feldman, P. Williford, A. Fleischer, N. Goldman, J. Acostamadiedo, and G. Chen (2003). Skin cancer is among the most costly of all cancers to treat for the medicare population. *Journal of the American Academy of Dermatology 48*(3), 425–429.

Huang, W., C. Chen, Y. Lin, and C. Lin (2011). Apoptotic sphingolipid ceramide in cancer therapy. *Journal of lipids 2011*.

Jayadev, S., B. Liu, A. Bielawska, J. Lee, F. Nazaire, M. Pushkareva, L. Obeid, and Y. Hannun (1995). Role for ceramide in cell cycle arrest. *Journal of Biological Chemistry 270*(5), 2047–2052.

Loidl, A., R. Claus, H. Deigner, and A. Hermetter (2002). High-precision fluorescence assay for sphingomyelinase activity of isolated enzymes and cell lysates. *Journal of lipid research 43*(5), 815–823.

Loidl, A., R. Claus, E. Ingolic, H. Deigner, and A. Hermetter (2004). Role of ceramide in activation of stress-associated map kinases by minimally modified ldl in vascular smooth muscle cells. *Biochimica et Biophysica Acta (BBA)-Molecular Basis of Disease 1690*(2), 150–158.

Loidl, A., E. Sevcsik, G. Riesenhuber, H. Deigner, and A. Hermetter (2003). Oxidized phospholipids in mmldl induce apoptotic signaling via activation of acid sphingomyelinase in arterial smooth muscle cells. *Journal of Biological Chemistry 278*(35), 32921.

Madan, V., J. Lear, and R. Szeimies (2010). Non-melanoma skin cancer. *The Lancet 375*(9715), 673–685.

Marathe, G., K. Harrison, R. Murphy, S. Prescott, G. Zimmerman, T. McIntyre, *et al.* (2000). Bioactive phospholipid oxidation products. *Free radical biology & medicine 28*(12), 1762.

Mollinedo, F., M. Fernández, V. Hornillos, J. Delgado, F. Amat-Guerri, A. Acuña, T. Nieto-Miguel, J. Villa-Pulgarín, C. González-García, V. Ceña, *et al.* (2011). Involvement of lipid rafts in the localization and dysfunction effect of the antitu-

mor ether phospholipid edelfosine in mitochondria. *Cell Death & Disease 2*(5), e158.

Moumtzi, A., M. Trenker, K. Flicker, E. Zenzmaier, R. Saf, and A. Hermetter (2007). Import and fate of fluorescent analogs of oxidized phospholipids in vascular smooth muscle cells. *Journal of lipid research 48*(3), 565–582.

Pettus, B., C. Chalfant, and Y. Hannun (2002). Ceramide in apoptosis: an overview and current perspectives. *Biochimica et Biophysica Acta (BBA)-Molecular and Cell Biology of Lipids 1585*(2), 114–125.

Reynolds, C., B. Maurer, and R. Kolesnick (2004). Ceramide synthesis and metabolism as a target for cancer therapy. *Cancer letters 206*(2), 169–180.

Rheinwald, J. and M. Beckett (1981). Tumorigenic keratinocyte lines requiring anchorage and fibroblast support cultured from human squamous cell carcinomas. *Cancer research 41*(5), 1657–1663.

Riedl, S., B. Rinner, M. Asslaber, H. Schaider, S. Walzer, A. Novak, K. Lohner, and D. Zweytick (2011). In search of a novel target–phosphatidylserine exposed by non-apoptotic tumor cells and metastases of malignancies with poor treatment efficacy. *Biochimica et Biophysica Acta (BBA)-Biomembranes 1808*(11), 2638–2645.

Ruiter, G., M. Verheij, S. Zerp, and W. van Blitterswijk (2001). Alkyl-lysophospholipids as anticancer agents and enhancers of radiation-induced apoptosis. *International Journal of Radiation Oncology* Biology* Physics 49*(2), 415–419.

Schenck, M., A. Carpinteiro, H. Grassmé, F. Lang, and E. Gulbins (2007). Ceramide: physiological and pathophysiological aspects. *Archives of biochemistry and biophysics 462*(2), 171–175.

Schmid, H. and T. Takahashi (1968). The alk-i-enyl ether and alkyl ether lipids of bovine heart muscle. *Biochimica et Biophysica Acta (BBA)-Lipids and Lipid Metabolism 164*(2), 141–147.

Senchenkov, A., D. Litvak, and M. Cabot (2001). Targeting ceramide metabolism -

a strategy for overcoming drug resistance. *Journal of the National Cancer Institute 93*(5), 347–357.

Sherman, B., R. Lempicki, *et al.* (2009). Bioinformatics enrichment tools: paths toward the comprehensive functional analysis of large gene lists. *Nucleic acids research 37*(1), 1–13.

Shevchenko, A., M. Wilm, O. Vorm, and M. Mann (1996). Mass spectrometric sequencing of proteins from silver-stained polyacrylamide gels. *Analytical chemistry 68*(5), 850–858.

Stemmer, U., Z. Dunai, D. Koller, G. Pürstinger, E. Zenzmaier, H. Deigner, E. Aflaki, D. Kratky, and A. Hermetter (2012). Toxicity of oxidized phospholipids in cultured macrophages. *Lipids in Health and Disease 11*(1), 110.

Stemmer, U. and A. Hermetter (2012). Protein modification by aldehydophospholipids and its functional consequences. *Biochimica et Biophysica Acta (BBA)-Biomembranes*.

Stemmer, U., C. Ramprecht, E. Zenzmaier, B. Stojčić, G. Rechberger, M. Kollroser, and A. Hermetter (2012). Uptake and protein targeting of fluorescent oxidized phospholipids in cultured raw 264.7 macrophages. *Biochimica et Biophysica Acta (BBA)-Molecular and Cell Biology of Lipids*.

Subbanagounder, G., N. Leitinger, D. Schwenke, J. Wong, H. Lee, C. Rizza, A. Watson, K. Faull, A. Fogelman, and J. Berliner (2000). Determinants of bioactivity of oxidized phospholipids specific oxidized fatty acyl groups at the sn-2 position. *Arteriosclerosis, thrombosis, and vascular biology 20*(10), 2248–2254.

Trakatelli, M., C. Ulrich, V. Del Marmol, S. Euvrard, E. Stockfleth, and D. Abeni (2007). Epidemiology of nonmelanoma skin cancer (nmsc) in europe: accurate and comparable data are needed for effective public health monitoring and interventions. *British Journal of Dermatology 156*(s3), 1–7.

Venable, M., J. Lee, M. Smyth, A. Bielawska, and L. Obeid (1995). Role of ceramide in cellular senescence. *Journal of Biological Chemistry 270*(51), 30701–30708.

Zwaal, R., P. Comfurius, and E. Bevers (2005). Surface exposure of phosphatidylserine in pathological cells. *Cellular and molecular life sciences 62*(9), 971–988.

Appendix A

Abbreviations

AK	actinic keratosis
aSMase	acid sphingomyelinase
BCC	basal cell carcinoma
BODIPY	4,4-difluoro-4-bora-3a,4a-diaza-s-indacene
BY	BODIPY
BY-PGPE	N-BODIPY-1-palmitoyl-2-glutaroyl-*sn*-glycero-3-phosphoethanolamine
BY-POVPE	N-BODIPY-1-palmitoyl-2-(5-oxovaleroyl)-*sn*-glycero-3-phosphoethanolamine
cer	ceramide
CTL	cytotoxic T-lymphocyte
DMEM	Dulbecco's modified Eagle medium
DTIC	dacarbazine
Edelfosine	1-octadecyl-2-O-methyl-*sn*-glycero-3-phosphocholine
E-PGPC	1-O-hexadecyl-2-glutaroyl-*sn*-glycero-3-phosphocholine
E-POVPC	1-O-hexadecyl-2-(5-oxovaleroyl)-*sn*-glycero-3-phosphocholine

ER	endoplasmic reticulum
EtOH	Ethanol
FACS	fluorescence activated cell sorting
FCS	fetal calf serum
HaCaT keratinocytes	human adult low calcium high temperature keratinocytes
HPLC	high-performance liquid chromatography
HPV	human papilloma virus
IFN	interferon
IL	interleukin
JNK	c-Jun N-terminal kinase
KA	keratoacanthoma
LDL	low density lipoprotein
MAPK	mitogen-activated protein kinase
mmLDL	minimally modified low density lipoprotein
MMS	Mohs micrographic surgery
MTT	3-(4,5-Dimethylthiazol-2-yl)-2,5-diphenyltetrazolium bromide
NBD	*N*-7-nitrobenz-2-oxa-1,3-diazol
NBD-Cer	*N*-7-nitrobenz-2-oxa-1,3-diazol-ceramide
NBD-SM	*N*-7-nitrobenz-2-oxa-1,3-diazol-sphingomyelin
oxLDL	oxidized low density lipoprotein
oxPL	oxidized phospholipid
PAF	Platelet activating factor
PAF-AH	Platelet activating factor acetyl hydrolase
PAPC	1-palmitoyl-2-arachidonoyl-*sn*-glycero-3-phosphocholine
PBS	phosphate buffered saline

PDGF	platelet-derived growth factor
PE	phosphatidylethanolamine
PGPC	1-palmitoyl-2-glutaroyl-*sn*-glycero-3-phosphocholine
PI	propidium iodide
PLPC	1-palmitoyl-*sn*-glycero-3-phosphocholine
PM	plasma membrane
POPC	1-palmitoyl-2-oleoyl-*sn*-glycero-3-phosphocholine
POVPC	1-palmitoyl-2-(5-oxovaleroyl)-*sn*-glycero-3-phosphocholine
PS	phosphatidylserine
PUFA	poly unsaturated fatty acid
RGP	radial growth phase
ROS	reactive oxygen species
RPMI-1640 medium	Roswell Park Memorial Institute medium
RT	room temperature
SCC	squamous cell carcinoma
SFM	serum-free medium
SHH	sonic hedgehog
SM	sphingomyelin
STS	staurosporine
TLC	thin layer chromatography
UV	ultraviolet
VEGF	vascular endothelial growth factor
VGP	vertical growth phase
VSMC	vascular smooth muscle cell